

Development and application of a high-throughput biophysical approach to
study transmembrane protein interactions with small molecules

By

Manuel A. Castro

Dissertation

Submitted to the Faculty of the
Graduate School of Vanderbilt University
in partial fulfillment of the requirements

for the degree of

DOCTOR OF PHILOSOPHY

in

Biochemistry

June 30th, 2022

Nashville, Tennessee

Approved:

Kevin L. Schey, Ph.D., Committee Chair

Charles R. Sanders, Ph.D., Advisor

Tina M. Iverson, Ph.D.

Stephen W. Fesik, Ph.D.

Adrian Olivares, Ph.D.

Rich Breyer, Ph.D.

Copyright © 2022 by Manuel Castro

All Rights Reserved

Dedication

I dedicate this dissertation to my family.

A special thanks to my mother, Julie, who never doubted my potential and made all this possible through her selfless sacrifices that opened doors in my life. There has been no time for which I could not rely on her unrelenting support. She truly is my champion, has paved the way for my successes in life, and I could not have done this without her. I also thank my father, Rafael, who endowed upon me, among many other things, a unique, multicultural life that has allowed me to connect and empathize with people of all creeds and colors; to see them for who they are on the inside and not judge. I admire him for his complete lack of materialism and autonomic drive for helping others, even at his own expense. My brother, Hernan, also deserves mention. He is quite possibly the most curious person I have met; a citizen scientist by nature and a true lover of biology. Throughout my life, our conversations, trips into nature, and general shenanigans have had a direct impact on my passion for natural philosophy. The final family members that warrant dedications are my grandmother Sue and late grandfather Mick, who have been my guiding beacons during this long journey of pursuing education higher. They have always challenged me to do my best and given me some of the best advice, even if it wasn't solicited. Both directly and indirectly, they nurtured my scientific passion and helped hone my confidence in myself. Their prescribed wisdom has helped me to make some of the best decisions in my life, and their lessons function as pillars in my thoughts and behaviors. In many ways, they were my first mentors, and I will always look up to them.

Acknowledgements

First and foremost, I would like to acknowledge my first scientific mentor, Dr. Wade Van Horn. In 2013, a simple conversation over some physical labor turned into the single greatest opportunity in my life: my first research experience. It is also imperative that I acknowledge my graduate advisor and mentor, Dr. Charles R. Sanders (Chuck). He has been the best mentor I could have asked for and allowed me to pursue a thesis project that was tailored to my interests, skillset, and long-term goals. He has shared my passion for pushing the boundaries of science and taught me how to be creative in my interpretation and dissemination of data. What fire Wade ignited in me; Chuck has fueled. I intend to embody their mentoring styles no matter where I go in life.

I also acknowledge my thesis committee who have honed me into an independent and confident thinker that invites challenge. Their scientific advice over the years has consistently helped me choose the right research paths and avoid unnecessary rabbit holes. Their collective support and consultation helped make this project successful, and it could not have been done without each one of them.

Another group of people that deserves mention are my many scientific collaborators both within and without Vanderbilt University. There have been many, and they all played unique and important roles in my success.

I would like to acknowledge my friends. From my experience in graduate school, I have concluded that becoming successful scientist and leader is about more

than collecting data and publishing papers; it is also essential that one builds bridges and does not burn them. Creating long-lasting and healthy friendships is an embodiment of this concept, as it is hard to predict the successes one's friends may have and how those will come back to bring you success as well. I can argue that the friends I've made in my scientific journey are far more valuable than any of the academic feathers I have put in my cap, although I do not discredit the value that the feathers can have. Rather, I view the fellowship with my friends as the 'other side of the coin' of education; that is, education would not have been as enjoyable or successful if I did not have these great people beside me.

Finally, I acknowledge my partner and fellow scientist, Abigail. She played a direct role in fostering my success in graduate school by fervently supporting me, listening to my scientific ideas, issues, and qualms, and being generally inspiring. Even at my worst of times, she has made my scientific journey a positive experience. It can be argued that the single best decision I made in graduate school was to ask her to marry me, and the luckiest moment when she said 'yes'.

Table of Contents

DEDICATION.....	iii
ACKNOWLEDGEMENTS.....	iv
TABLE OF CONTENTS.....	vi
LIST OF FIGURES.....	ix
LIST OF ABBREVIATIONS.....	xi
CHAPTER 1: INTRODUCTION TO THE AMYLOIDOGENIC PATHWAY.....	1
<i>Preface.....</i>	<i>1</i>
<i>The vexing complexity of the amyloidogenic pathway.....</i>	<i>4</i>
<i>Overview of Alzheimer’s disease (AD).....</i>	<i>4</i>
<i>Components of the amyloidogenic pathway.....</i>	<i>8</i>
<i>Amyloid-β is not always generated at the cell surface and does not always end up the extracellular milieu.....</i>	<i>15</i>
<i>The mechanisms by which FAD mutations promote the etiology of Alzheimer’s disease may be more complex than previously appreciated.....</i>	<i>17</i>
<i>Is full length APP sometimes toxic?.....</i>	<i>24</i>
<i>Is C99 sometimes toxic?.....</i>	<i>25</i>
<i>The first direct genetic evidence for the role of the amyloidogenic pathways in late-onset AD.....</i>	<i>28</i>
CHAPTER 2: INTRODUCTION TO DRUG DISCOVERY, NMR, AND SPTMRs.....	36
<i>Single-pass transmembrane receptors (SPTMRs).....</i>	<i>36</i>
<i>Biochemistry and biophysics of protein-small molecule interactions.....</i>	<i>39</i>
<i>Probing small molecule-protein interactions using NMR.....</i>	<i>45</i>
<i>Biological NMR spectroscopy.....</i>	<i>46</i>
<i>Observing protein-small molecule interactions by NMR.....</i>	<i>52</i>
<i>C99 and Notch-1 as disease-relevant models for probing SPTMR-small molecule interactions.....</i>	<i>55</i>
CHAPTER 3: DEVELOPMENT OF AN NMR-BASED HIGH-THROUGHPUT SCREEN AMENABLE TO SINGLE-SPAN TRANSMEMBRANE PROTEINS.....	59
<i>Introduction.....</i>	<i>59</i>
<i>Results.....</i>	<i>60</i>
<i>Yield and NMR parameter optimization for C99 screening.....</i>	<i>60</i>
<i>Results of an initial test screen using a Fesik Fragment Library mixture plate.....</i>	<i>66</i>
<i>Discussion.....</i>	<i>68</i>
CHAPTER 4: FDA-APPROVED DRUG VERTEPORFIN IS A SUBSTRATE-SELECTIVE γ-SECRETASE INHIBITOR THAT BINDS THE AMYLOID PRECURSOR PROTEIN TRANSMEMBRANE DOMAIN.....	71
<i>Introduction.....</i>	<i>71</i>
<i>Results.....</i>	<i>74</i>
<i>Summary of NMR screen of 1,200 FDA-approved drugs.....</i>	<i>74</i>

<i>Verteporfin binds C99 with a 17 μM K_D in model membranes, sparing Notch-1</i>	76
<i>Verteporfin associated with membrane mimetics</i>	80
$^1\text{H}, ^1\text{H}$ -NOESY confirms direct contact between verteporfin and C99	83
<i>Mutations in C99 reduce affinity of verteporfin for C99</i>	84
<i>Native ion mobility-mass spectrometry and chemical cross-linking indicate that verteporfin binds to the monomeric form of C99 and does not induce homodimerization</i>	85
<i>Verteporfin inhibits γ-secretase with a preference for C99 over Notch-1</i>	90
<i>Experimentally restrained Rosetta modelling of C99-verteporfin complex</i>	92
<i>Discussion</i>	93
CHAPTER 5: PAINS IN THE MEMBRANE: DISCOVERY OF SMALL MOLECULE FRAGMENTS THAT WEAKLY AND NON-SPECIFICALLY BIND TRANSMEMBRANE PROTEINS IN LMPG MICELLES	98
<i>Introduction</i>	98
<i>Results</i>	100
<i>Summary of NMR screen of 15,000 small molecule fragments</i>	100
<i>Discovery and characterization of putative membrane pan-assay interference compounds (PAINS)</i>	101
<i>Discussion</i>	112
CHAPTER 6: CONCLUDING DISCUSSIONS AND FUTURE DIRECTIONS	115
MATERIALS AND METHODS	130
<i>Reagents and Buffers</i>	130
<i>Protein Expression and Purification</i>	131
<i>C99 I109W</i>	131
<i>C99 NT2 (His-cleavable) and mutants</i>	132
<i>C55 and C74</i>	133
<i>Notch-1 TM/JM (residues 1721-1771)</i>	133
<i>KCNQ1-VSD</i>	134
<i>High-throughput Screening</i>	135
<i>Compound Sourcing</i>	135
<i>Compound Distribution</i>	135
<i>Compound Storage</i>	135
<i>Sample Preparation and Mixing for Screening</i>	136
<i>NMR spectroscopy</i>	136
<i>High-throughput NMR Screening of C99</i>	136
<i>Fitting of NMR Binding Data</i>	136
<i>1D ^1H Data Acquisition and Processing Parameters</i>	137
<i>2D ^1H-^{15}N CLEANEX-HSQC Acquisition and Processing Parameters</i>	137
<i>^1H-^1H NOESY Acquisition and Processing Parameters</i>	138
<i>Other Methods</i>	138
<i>Glutaraldehyde Crosslinking</i>	138
<i>Ion Mobility Mass Spectrometry</i>	139

<i>γ</i> -secretase Assays.....	139
<i>IC</i> ₅₀ Measurements	140
<i>Dynamic Light Scattering</i>	140
<i>Molecular Modeling and Docking</i>	140
<i>Preparation of Protein Structures for Docking</i>	140
<i>Preparation of Verteporfin Conformers for Docking</i>	140
<i>Local Docking of Verteporfin to C99</i>	141
<i>Model Evaluation and RMSD Analysis</i>	141

List of Figures

Figure 1. *Self-diagnosis of Alzheimer's disease by Charles R. Sanders Sr.*

Figure 2. *'Jack plot' illustrating the appearance of AD biomarkers with aging that can be used to measure and predict the development of AD.*

Figure 3. *Canonical processing of the amyloid precursor protein.*

Figure 4. *Competing processive γ -secretase cleavage reaction pathways.*

Figure 5. *Locations of FAD mutation sites in presenilin 1 cryo-EM structure.*

Figure 6. *Model for gencDNA formation and expression in neurons based on the work of the Chun lab*

Figure 7. *Example of a well-drugged SPTMR: activation of the Thrombopoietin receptor (TPoR)*

Figure 8. *Example of protein-ligand binding.*

Figure 9. *Example of protein thermal stabilization upon ligand binding.*

Figure 10. *Pulse program optimization for C99 screening.*

Figure 11. *LMPG and DMSO concentration optimization for C99 screening.*

Figure 12. *1st hit compound: the discovery that VU0410776 is a C99 binder.*

Figure 13. *The amyloidogenic pathway and our screening workflow for compounds that bind to the C99 protein.*

Figure 14. *TROSY NMR spectral overlays of representative initial hit spectra from primary screen.*

Figure 15. *Verteporfin binds C99 in LMPG micelles and does not bind to the Notch-1 TM/JM.*

Figure 16. *Verteporfin binds C99 in D6PC/DMPC ($q=0.33$) bicelles with an observed K_D of $17 \pm 4 \mu\text{M}$, whereas verteporfin does not bind the Notch-1 TM/JM.*

Figure 17. *Verteporfin binds untagged C99 in DDMB micelles with a K_D of $45 \pm 22 \mu\text{M}$ and does not bind the Notch-1 TM/JM domain.*

Figure 18. *Verteporfin binds to LMPG micelles, which suppress its aggregation in aqueous solution.*

Figure 19. *$^1\text{H}, ^1\text{H}$ -NOESY of the C99-verteporfin complex.*

Figure 20. *C99 point mutations that ablate affinity for verteporfin.*

Figure 21. *Glutaraldehyde crosslinking of C99 reveals no change in oligomeric state in response to verteporfin.*

Figure 22. *IM-MS indicates that verteporfin does not alter C99 mass or induce dimerization.*

Figure 23. *Verteporfin inhibits γ -secretase cleavage of C100-Flag more potently than for Notch-1.*

Figure 24. *Verteporfin inhibits γ -secretase cleavage of C100-Flag (C99) in low enzyme and substrate conditions.*

Figure 25. *Most favorably scoring model from experimentally restrained Rosetta modeling of the micellar verteporfin-C99 complex.*

Figure 26. *High throughput screening strategy used to discover small molecule binders of C99 in LMPG micelles.*

Figure 27. *Structures and properties of hits from the Fesik Fragment Library.*

Figure 28. *NMR titrations of C99 in LMPG with five of the six fragment hits*

Figure 29. *VUx95 non-specifically perturbs C99 and Notch-1 NMR spectra in LMPG and does not saturate binding.*

Figure 30. *CLEANEX (Clean Exchange) HSQC (non-TROSY) NMR spectral overlaps of C99 with or without 10 mM VUx95 fragment.*

Figure 31. *Titration of empty LMPG micelles with VUx95 indicates that the micelle size is unchanged, but that LMPG methylene dynamics likely have.*

Figure 32. *Titration of VUx95 against KCNQ1-VSD protein in LMPG and against C99 in DHPC/DMPC bicelles confirms the fragment's non-specificity and LMPG-dependance, respectively*

Figure 33. *SAR by catalog of VUx95 did not significantly enhance the binding affinity for C99 in LMPG*

Figure 34. *Calmodulin titration with VUx95, with or without pH control.*

Figure 35. *pH-controlled titration of C99 with VUx95.*

Figure 36. *SAR by Catalog optimization of VU0410776 analogs reveals tighter and weaker binding analogs.*

Figure 37. *Discovery that VU0410776 is a C99 binder.*

Figure 38. *Discovery that VUx76 analog VU0412456 is a tighter and more specific C99 binder than its parent.*

Figure 39. *C99 L723A mutant loses all affinity for VUx76 and VUx56 fragments, confirming binding site.*

List of Abbreviations

A β : Amyloid Beta peptide

AD: Alzheimer's disease

AICD: Amyloid intracellular domain

APP: Amyloid Precursor Protein

CLEANEX: Clean-exchange HSQC NMR spectroscopy

CSP: Chemical Shift Perturbation

C99: C-terminal 99 amino acid transmembrane fragment of the amyloid precursor

DDMB: β -dodecylmelibioside detergent

DMSO: Dimethyl sulfoxide

EOAD: Early onset Alzheimer's disease

FAD: Familial Alzheimer's disease

FBDD: Fragment-based drug discovery

GA: Glutaraldehyde

GS: γ -secretase

GSI: γ -secretase inhibitor

GSM: γ -secretase modulator

HSQC: Heteronuclear single quantum coherence spectroscopy

HTS: High-throughput screening

IM-MS: Ion-mobility mass spectrometry

LMPG: lyso-myristoylphosphatidylglycerol detergent

LOAD: Late onset Alzheimer's disease

NMR: Nuclear magnetic resonance

NOESY: Nuclear Overhauser effect spectroscopy

PAINS: Pan-assay interference compounds

SAR: Structure-activity relationships

SPTMR: Single-pass transmembrane protein

TM/JM: Transmembrane and juxtamembrane domain construct

TROSY: Transverse relaxation HSQC spectroscopy

VU0XXXXXX: Code numbers for compounds based on their VU-ID numbers, typically VU0 followed by a six-digit number such as VU0021995

VUxXX: Shorthand for VU-ID numbers, such as VUx95 instead of VU0021995

Chapter 1

Introduction to the Amyloidogenic Pathway

Preface

In 1850, the person who would formally become 'patient 0' for Alzheimer's disease (AD), Mrs. Auguste Deter, was born in Cassel, Germany. For the most part, she lived a relatively normal life with her husband near the river Main in Frankfurt. In 1901, at the ripe age of 51, her husband brought her to a psychiatric clinic, reporting that he noticed progressive changes in her personality, a rapidly weakening memory, and worsening psychosocial state. She was admitted there and remained in in-patient care for the remainder of her life. As her condition worsened, she became apathetic, confused, and generally unintelligible. In 1906, at the age of 55, Auguste sadly succumbed to septicemia because of an ulcer, but her name and story would be immortalized by a rising young physician name Dr. Alois Alzheimer. ¹

Dr. Alzheimer was a senior assistant at the Frankfurt Psychiatric Hospital where Auguste was first admitted in 1901. He was notably fascinated by her condition, and he documented her case in detail from the time he first met her. Eventually, their paths would split as Auguste was transferred to the Community Psychiatric Hospital in Frankfurt and Alois went on to continue his practice in Munich. The physical distance between them, however, had no effect on his interest in her case. Upon her death, Alois requested her brain and medical records for further, posthumous examination. Using

histology, he discovered the presence of large plaques and neurofibrillary tangles in the brain, hallmarks that we now associate with AD. These discoveries appeared incite little enthusiasm in the medical community when he initially presented them, but that did little to hold back Alois' continued research. ¹⁻²

In the years to come, Dr. Alzheimer would continue to present his work and had a successful career studying psychiatric illnesses. In his later years, in addition to studying psychotic mental diseases, he started a scientific journal and was eventually appointed Chair of Psychiatry at the University of Breslau. It was not long after his appointment in Breslau that he died in 1915 after a successful, acclaimed career. Today, Dr. Alzheimer's name is a household staple, ironically not due to his success as a late-career physician, but rather his early fascination with Auguste Deter and his little-appreciated discoveries in her brain.

Dr. Alzheimer was a medical scientist who was interested in correlating neuropathological changes in the brain to psychological changes in behavior. His discoveries and his well-documented passion for his work are inspiring to me. Specifically, to pursue a career in basic, discovery science, where the fruits of one's work may not be immediately realized and even perhaps ignored. When my PhD mentor, Dr. Charles R. Sanders (Chuck) proposed a thesis project aimed at building off the plaque observation that Dr. Alzheimer made over 100 years ago, I was beaming with passion and enthusiasm. Much progress has been made with regard to understanding the molecular and genetic hallmarks of AD, and the plaques, which are made up primarily of a peptide called amyloid- β (A β), continue to be a central feature of AD pathology and research.

I want to start this thesis by making it clear that my thesis work was not intended to develop a cure or treatment of AD, but rather to use the AD-implicated amyloid precursor protein (APP), which is eventually turned over into the amyloid peptides that seed the plaques that Dr. Alzheimer discovered, as a model for investigating how drugs interact with proteins of its family. APP belongs to a large family of proteins called single-pass transmembrane proteins (SPMTRs), which are highly represented in the human genome and are often involved in human health and disease. SPTMRs are infamously recalcitrant biochemical systems to work with, so we repurposed previously successful approaches used on other types of recalcitrant proteins to further our understanding of how they interact with other molecules. The primary methodology used for my dissertation was high throughput screening (HTS) by nuclear magnetic resonance (NMR) spectroscopy, which is particularly amenable to investigating these types of systems. This document will walk the reader through the rationale for this project, elaborate on the methodologies that it has developed or advanced, describe molecules of interest that may help AD research, and importantly, highlight issues and pitfalls that can be mitigated by future scientists pursuing this type of project.

Although I find it unlikely that the compounds presented in this thesis will be useful for treating Alzheimer's disease, I do have hope that this work will provide lessons that help the reader understand the biophysical and biochemical issues that hinder membrane protein disease drug discovery and development. At the very least, this document will serve as a useful reference for developing NMR-based HTS strategies for recalcitrant membrane protein systems, inclusive to and beyond those involved in Alzheimer's disease.

The Vexing Complexity of the Amyloidogenic Pathway¹

An Overview of Alzheimer's Disease

The role of the amyloidogenic pathway in the etiology of Alzheimer's disease (AD), particularly the common sporadic late onset forms of the disease, is controversial. To some degree, this is a consequence of the failure of drug and therapeutic antibody trials based either on targeting the proteases in this pathway or its amyloid end products. Here, we explore the formidable complexity of the biochemistry and cell biology associated with this pathway. For example, we review evidence that the immediate precursor of amyloid- β , the C99 domain of the amyloid precursor protein (APP), may itself be toxic. We also review important new results that appear to finally establish a direct genetic link between mutations in APP and the sporadic forms of AD. Based on the complexity of amyloidogenesis, it seems possible that a major contributor to the failure of related drug trials is that we have an incomplete understanding of this pathway and how it is linked to Alzheimer's pathogenesis. If so, this highlights a need for further characterization of this pathway, not its abandonment.

Alzheimer's disease (AD) is a progressive neurodegenerative disorder with no cure or disease-modifying therapies. There are both rare familial (inherited) forms (FAD or early AD [LOAD]) forms of this disorder. There are presently roughly 50 million AD patients

¹ This work is published in: Castro, M. A., Hadziselimovic, A. and Sanders, C. R. (2019). The vexing complexity of the amyloidogenic pathway. *Protein Science* **28**(7), 1177-1193.

onset AD [EOAD]) and much more common sporadic (SAD or late onset worldwide—5.7 million in the United States alone, with the number expected to increase two to fourfold by mid-century, depending on the country- by mid-century, depending on the country. The Alzheimer's association has documented these trends on their disease fact and figures sheet here: <https://www.alz.org/media/documents/alzheimers-facts-and-figures.pdf>. The cost to the U.S. economy of compensated and uncompensated care of AD patients is currently on the order of half a trillion dollars. 10% of men and 20% of women are expected to succumb to AD, which is inevitably fatal. Currently approved pharmacological treatments are limited to marginally effective management of early-stage disease symptoms. LOAD patients typically survive for 4–8 years following initial diagnosis, but there is considerable heterogeneity in disease progression. Classically, patients with Alzheimer's initially present with short-term memory problems and other mental deficits (some outlined in **Figure 1**), with the disease progressing to expunge all memory, both short and long term. AD results in significant reductions in brain mass and, eventually, loss of organ functions and increased susceptibility to secondary disorders such as pneumonia. Brain tissues in patients who have died from AD or its complications usually exhibit the presence of extracellular amyloid plaques under the conditions of histological staining with Congo red, as viewed under a polarizing microscope. Except for the age of onset (usually much earlier for FAD than for LOAD), the symptoms and progression are similar for FAD and LOAD. In addition to amyloid- β deposition, other cellular and biochemical changes in brain tissue occur in AD, including hyper-phosphorylation of the

tau protein and consequent formation of intraneuronal neurofibrillary tangles, increased glutamatergic signaling, neuroinflammation, and decreases in cholinergic signaling.

The notion that the production and neurotoxicity of the amyloid- β (A β) polypeptides is central to the etiology and pathology of AD—the “amyloid hypothesis” or

CHARLES R SANDERS 4-27-07

Difficulty remembering recent events
what did I (we) do yesterday, last week?
... today?

Difficulty remembering names and faces
especially new acquaintances
also some people I've known a long time

Difficulty remembering directions while driving
especially routes recently learned.
Remember routes I've known a long time

Witness - calendar book - blank days unlikely to
be filled. filled.

Medication (pills) taken twice daily - if I
remember, I am now assisted by an
alarm wrist watch, (Suggested by Mr Klaus)

Some slow motion finding, where some tools are
when working in basement work area.

Processing fast talk is difficult. A phrase or
sentence may block out subsequent talk.

Figure 1. Self-diagnosis of Alzheimer's disease by Charles R. Sanders Sr. This handwritten letter is the self-diagnosis of Charles R. Sanders Sr., father of my PhD advisor Dr. Chuck Sanders. These symptoms describe what would eventually be proved to be late-onset AD. Charles R. Sanders Sr. eventually succumbed to disease 10 years after this was written, in 2017 at the age of 87.

“amyloid cascade hypothesis”—has been enormously influential over the past 30 years.³ However, in part due to the failure of a series of well-publicized clinical trials designed around drugs or antibodies that target either A β aggregates or the biochemical pathway responsible for amyloid production, the “amyloidogenic pathway,” considerable skepticism has developed that amyloidogenesis is truly central to most forms of AD, particularly for the common sporadic late-onset forms of this fell disorder.⁴⁻⁶ The genetic linkage of the amyloidogenic pathway to FAD is unquestioned.⁷⁻¹² However, while a number of gene variations have now been documented to be risk factors for the sporadic

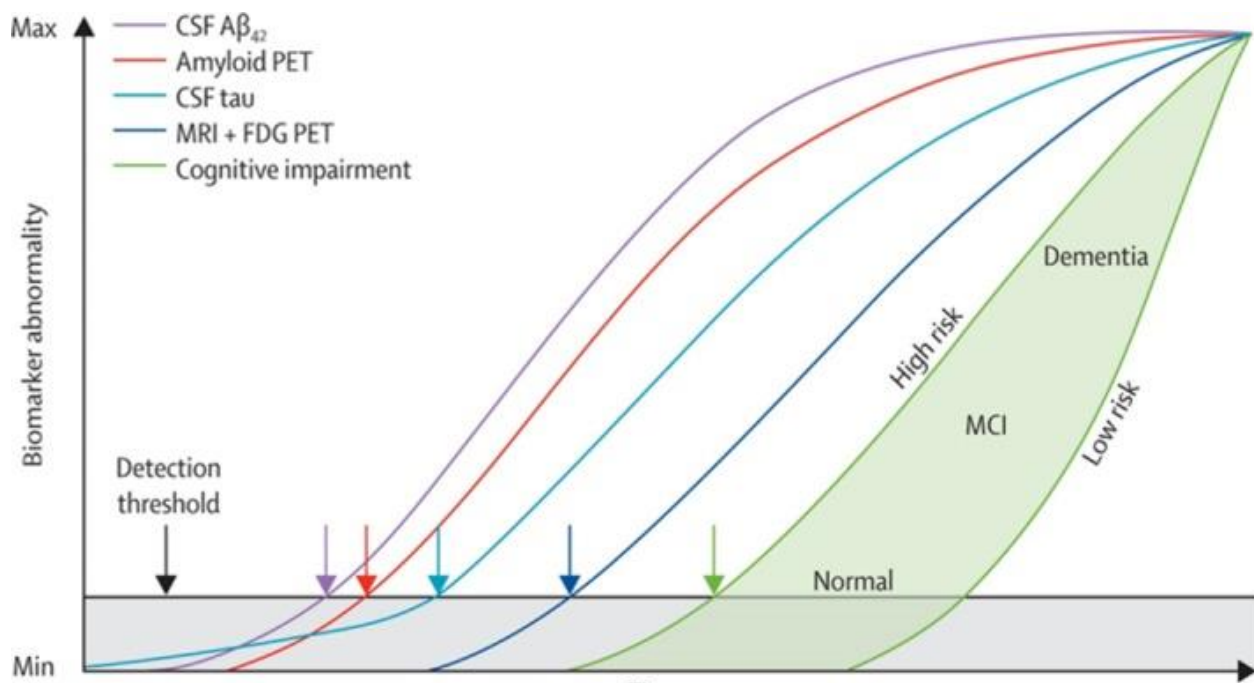


Figure 2. ‘Jack plot’ illustrating the appearance of AD biomarkers with aging that can be used to measure and predict the development of AD. The earliest predictor of AD is the detection of long form A β in CSF, as collected via spinal tap. This is followed by the detection of amyloid plaques in the brain through the binding of ¹⁸F-labelled compounds and positron emission tomography (PET). The next predictor is the elevation of the tau protein in CSF and then the detection by magnetic resonance imaging of changes in the brain morphology, along with detection by PET of problem with energy metabolism in the brain. Only after these biomarkers appear to early signs of memory loss and other relatively minor problems arise as “mild cognitive impairment”, which finally progresses to full-blown AD. While not discussed elsewhere in this review, we suggest a significant additional layer of complexity for the amyloidogenic pathway as a target for AD therapeutics is the fact that A β production, deposition, and accumulation takes place over period of decades. The conundrum of how to target a decades-long process with a potential therapeutic in a drug trial of short duration represent yet another vexing problem. This figure was reproduced in my first-authored review titled ‘The vexing complexity of the amyloidogenic pathway’ with permission from *The Lancet Neurology* (Elsevier).

LOAD form of the disease, it has been a puzzling fact that the growing roster of risk factors has not included variations impacting genes that have an obvious role in the amyloidogenic pathway.¹³⁻¹⁵ Moreover, amyloid plaques are found in the brains of many who never develop AD symptoms.¹⁶ Conversely, there are rare AD patients who have few amyloid plaques or neurofibrillary tangles in their brains.¹⁷ These factors are probably part of the reason why the fraction of the US National Institute of Aging grant budget devoted to A β -related research has decreased from 27% in 2007 to 18% in 2017.¹⁸ Doubts about the centrality of the amyloidogenic pathway in AD persist even though LOAD can now be diagnosed in living patients based on the detection of A β in the cerebrospinal fluid (CSF) and of A β plaques in the brain (**Figure 2**).

It is not the goal here to conduct a comprehensive review of the evidence for or against a central role for A β production in the pathogenesis of AD, excellent examples of which are published elsewhere.¹⁹⁻²⁰ Rather, we provide some examples of how very *complex* the amyloidogenic pathway is. We argue that this complexity represents a confounding factor in efforts to treat or prevent AD by targeting either the biochemistry of this pathway or the toxic oligomer/aggregate forms of A β . We also highlight a recent breakthrough study that appears to, at last, establish a genetic link between the amyloidogenic pathway and LOAD.

Components of the Amyloidogenic Pathway

Our understanding of the role of the amyloidogenic pathway is closely linked to the genetics of the familial (inherited) form of AD. FAD is epidemiologically characterized by having an early onset (before 65 years of age) and nearly 100%

penetrance throughout families that harbor pathogenic mutations or duplications in specific protein-coding genes.⁷⁻⁸ The first identified FAD gene was *APP* (chromosome 21; location: 21q21.3), which codes for the conserved, ubiquitously expressed single-pass transmembrane amyloid- β precursor protein (APP).^{9-10, 12, 21} Full-length APP has 770 residues with a large ectodomain, a single transmembrane span, and a modest (ca. 45 residue) intracellular domain. The most common neuronal splice variant of *APP* encodes 695 residues. The role of the APP in the adult brain has not been fully elucidated; however, it may be important for proper neurological development during gestation, on top of playing roles in neuroplasticity, synaptic function, and homeostasis throughout life.²² The complete knock-out of *APP* leads to small, slow, vacuous mice.²³ Only when the *ALP1* and *ALP2* genes are also deleted is deletion of *APP* embryonic-lethal.²³ As of February 2019, some 18 different sites, all located in or proximal to the C-terminal 99 residues of APP (C99), are known to be subject to mutations that cause FAD (see compilation at Alzforum.org/mutations/app).

One APP mutation is known to protect humans from AD: the “Icelandic mutation,” A673T.²⁴⁻²⁵ Along these same lines is a fascinating case study of a Down syndrome (DS) patient who escaped from the usual early onset (30–40 years old) Alzheimer's neurodegeneration that normally accompanies DS.²⁶⁻²⁸ People with DS have an extra copy of chromosome 21 (trisomy-21) and consequently, an extra copy of APP.^{11, 29} The presence of an extra copy of *APP* is thought to cause EOAD by increasing total expression of the APP protein, resulting in increased total A β .^{26, 30} A DS patient was recently identified who exhibited incomplete trisomy of chromosome 21 in which the APP locus was not duplicated, but most other genes of that chromosome were.³⁰ This

individual, who was studied extensively between ages 66 and 72, presented with the mild intellectual disability characteristic of DS. However, he did not exhibit the cognitive decline that normally accompanies DS, nor was dementia evident and only low levels of A β deposition were detected by amyloid positron emission tomography (PET) imaging. While these findings are not without dispute, this patient seems to provide a compelling example of how APP is linked to Alzheimer's. ^{26, 30-31}

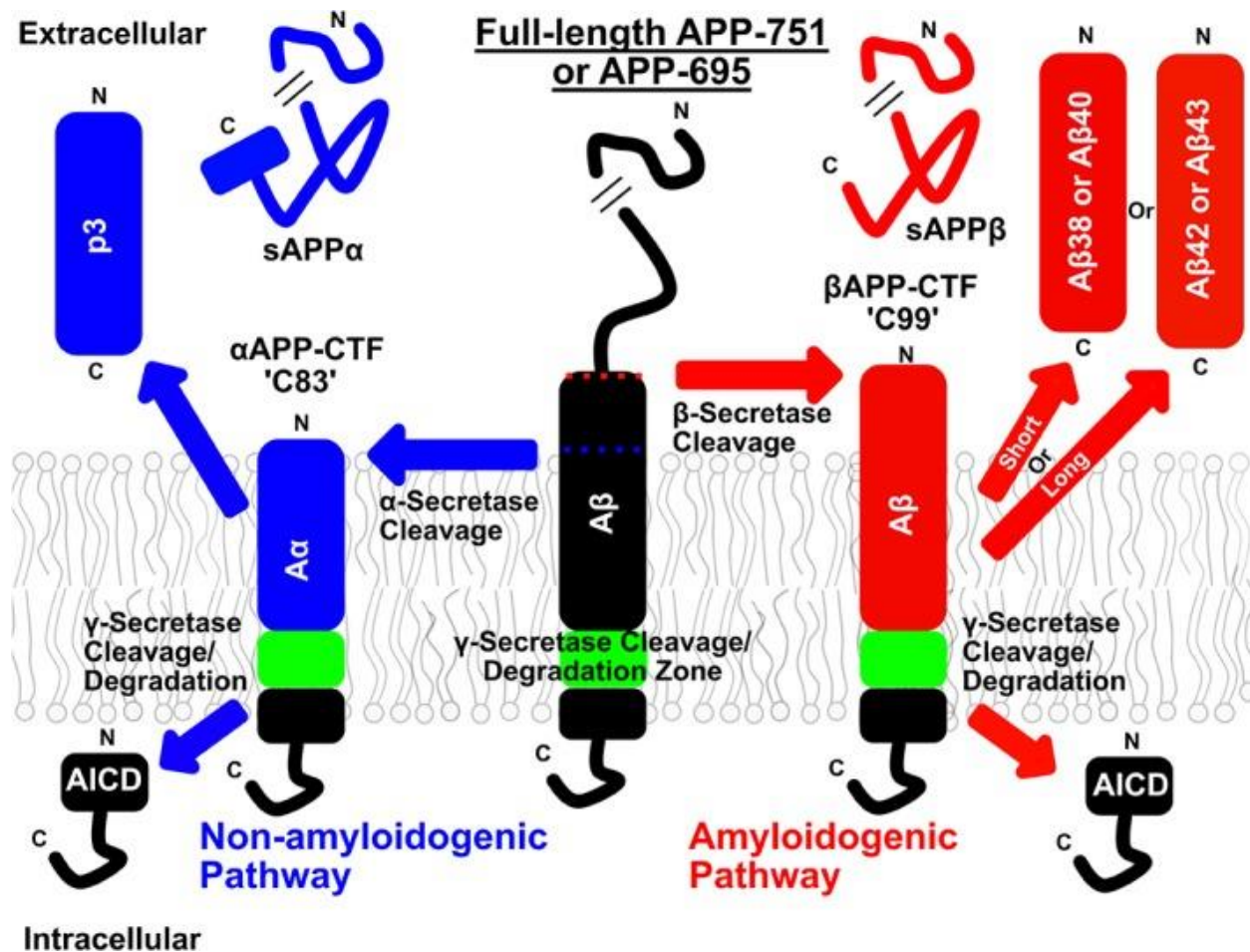


Figure 3. *Canonical processing of the amyloid precursor protein.* Full-length APP (either neuronal 751- or 695-residue isoform) is shown in the middle in black. On the right (red arrows) is the amyloidogenic proteolytic cascade that is initiated by β -secretase and generates sAPP β and β APP-CTF (C99). This cleavage is followed by a subsequent cleavage of C99 by γ -secretase to liberate AICD and A β . On the left (blue arrows) is the nonamyloidogenic proteolysis pathway that is initiated by α -secretase (ADAM10) and generates sAPP α and α APP-CTF (C83). Cleavage of C83 is then finalized by γ -secretase to liberate p3 and AICD.

Also causative of FAD is pathogenic dominant familial mutation in either *PSEN1* and *PSEN2*, which code for the two isoforms of presenilin, the catalytic subunit of the heterotetrameric γ -secretase protease.³²⁻³³ γ -secretase cleaves a wide range of single span membrane proteins in their transmembrane domains, the most studied of which are APP and the Notch receptor, the latter being a master regulator of cell and tissue differentiation and development.³⁴⁻³⁷

The amyloidogenic processing of APP to A β involves cleavage by the β -secretase (BACE1) and γ -secretase proteases that successively hydrolyze APP in the juxtamembrane extracellular domain and then in the transmembrane domains, respectively (**Figure 3**).³⁸ BACE1 cleavage releases the large soluble extracellular N-terminal fragment, sAPP β , leaving the 99 residue transmembrane C-terminal fragment of APP behind: C99 (also known as β APP-CTF). Liberated sAPP β may have important roles such as stimulating increased axonal outgrowth, decreased cell adhesion, neural differentiation of human stem cells, and stimulation of GABA receptors to alter synaptic transmission.³⁹⁻⁴⁰

The C99 domain of the APP has a single transmembrane span and a propensity both for homodimerization and cholesterol binding.⁴¹⁻⁴³ In the amyloidogenic pathway, C99 is engaged by the heterotetrameric γ -secretase complex, which binds C99 monomers and initially cuts C99 at either of two possible “epsilon cleavage” sites in the membrane near the cytosol, resulting the in the release of the amyloid intracellular domain (AICD). The function of AICD is controversial, with some evidence suggesting that it plays a role in regulating transcription of certain genes.⁴⁴⁻⁵⁷ Intriguingly, some of the these genes encode proteins clearly related to the amyloidogenic pathway or to tau

hyperphosphorylation and fibrillization. ^{49-50, 53, 55-56, 58} However, at least some of these studies have been challenged. ⁵⁹⁻⁶⁰ Painstaking research has shown that the remaining and still membrane-anchored N-terminus of C99 is not then released by γ -secretase, but rather is subjected to processive cleavage in which tripeptides or tetrapeptides are successively released from the C-terminal end of the transmembrane domain (TMD) domain until all that is left of C99 is either the long form of A β (mostly A β_{42}) or the short form (mostly A β_{40}) (**Figure 4**). ⁶¹ A β then dissociates from γ -secretase and potentially from the membrane. Recent evidence suggests that β - and γ -secretases sometimes form a complex in brain tissue that processively catalyzes the sequential cleavage of full-length

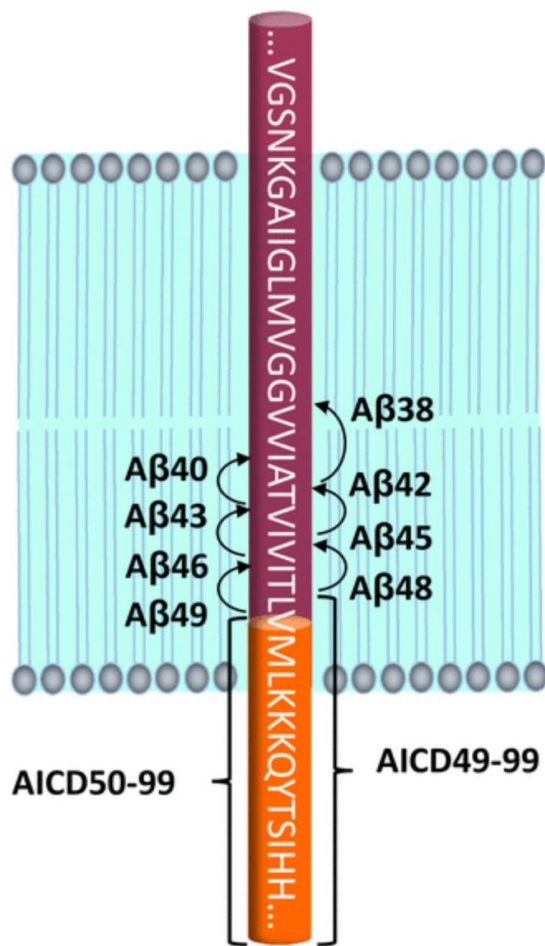


Figure 4. *Competing processive γ -secretase cleavage reaction pathways.* Γ -secretase can cleave C99 via two distinct pathways: one that generates A β_{40} and AICD₅₀₋₉₉ or the other that generates A β_{38} or A β_{42} and AICD₄₉₋₉₉.

APP to A β .⁶²⁻⁶³ A β represents a polypeptide that contains half of what was originally a transmembrane domain. It is therefore unsurprising that it retains considerable affinity for membranes and has a high propensity to form aggregates in solution—particularly the longer A β_{42} form.⁶⁴ Conventionally, it has generally been thought that release of A β occurs mainly at the outer leaflet of the plasma membrane, with the peptide being released into the extracellular milieu. A β then forms toxic oligomers that go on to form cross-beta fibrils that eventually become entangled with other molecules to form mature amyloid plaques in brain tissue.⁶⁵⁻⁶⁶ The toxicity of extracellular A β may be related to its ability to self-assemble at the membrane surface to form ion channels and/or to stimulate any one or more of a number of candidate receptors at the cell surface.⁶⁷⁻⁷² One or more of these events are thought to then trigger ill-defined pathways that lead to hyperphosphorylation and fibrillization of tau, ultimately resulting in intraneuronal neurofibrillary tangles and cell death.⁷³ The exact nature of the physiological toxic A β oligomers is a matter of mystery. Numerous different forms of A β oligomers have been examined under laboratory conditions, but establishing which ones, if any, are pathophysiologically relevant has been elusive.²⁰ While the toxicity of amyloid plaques was once questioned, there now seems to be little question that they are toxic because they trigger chronic inflammation in the brain.⁷⁴⁻⁷⁵ They also likely serve as a reservoir of toxic A β oligomers, which can dissociate from the plaques to re-enter solution.⁷⁶⁻⁷⁷

Competing with the amyloidogenic pathway for processing of APP is a major “nonamyloidogenic” pathway that is initiated when the extracellular matrix-metalloprotease α -secretase (usually ADAM10, but sometimes ADAM9 or ADAM 17) cleaves full-length APP, as is illustrated in the left half of **Figure 3**.^{38, 78-79} Full-length APP

is clipped by α -secretase at an extracellular site closer to the membrane than the β -secretase cleavage site to release the transmembrane C83 fragment, which is then further processed by γ -secretase in a manner analogous to C99 processing. The resulting APP fragments are the large extracellular sAPP α ectodomain, AICD, and P3 (a nonamyloidogenic fragment of A β , sometimes referred to as A α). α -secretase competes with β -secretase for the initial cleavage of APP. Any factor that shifts the balance toward β -secretase cleavage is expected to increase the total A β generated, potentially contributing to the pathogenesis in AD.⁸⁰ Conversely, activation of α -secretase cleavage is expected to reduce A β production. α -Secretase also has other important substrates and is believed to be involved in maintaining synaptic health, neurogenesis, and neuronal homeostasis.⁸⁰⁻⁸¹ A fascinating emerging area of biology is how ADAM proteases are modulated by members of the iRhom (noncatalytic rhomboid homologs) and tetraspanin families of multispan membrane proteins.⁸²

One confounding factor in efforts to develop agents that reduce amyloid- β levels that act by inhibiting γ -secretase and β -secretase or by activating α -secretase is the fact that all three of these proteases have multiple substrates besides APP, some of which are of great importance in their own right.^{36, 83-84} For example, both γ -secretase and α -secretase play critical signaling roles when they cleave the Notch receptor, a master regulator of cell development. Inhibition of γ -secretase activity is associated with severe toxicity when Notch cleavage is inhibited, disrupting Notch signaling.⁸⁵⁻⁸⁷ This has led to a search for “ γ -secretase modulator” compounds that do not alter Notch receptor cleavage, but that perturb γ -secretase cleavage of C99 to tip the A β ₄₂:40 production ratio

toward production of the shorter and less toxic forms. ⁸⁸⁻⁹⁰ Whether compounds of this class will eventually be therapeutically useful remains to be seen.

Finally, it should be noted that in addition to the classical amyloidogenic and nonamyloidogenic pathways summarized above, there appear to be yet other proteolytic cleavage events that release other APP fragments encompassing all or part of A β . ⁹¹⁻⁹⁵ In some cases, products may be due to rare alternative cleavage events by one of the canonical secretases, but sometimes other proteases are involved. Whether some of these alternative APP-derived peptides might contribute to AD is not yet clear.

Amyloid- β is not always generated at the cell surface and does not always end up in the extracellular milieu

Another source of complexity in the amyloidogenic pathway lies in the fact that there are two forms of γ -secretase: one with presenilin 1 (PSEN1) and another with presenilin 2 (PSEN2) as the catalytic substrate. Familial AD mutations are found in both PSEN isoforms but are much more common in PSEN1. One of the other subunits of the γ -secretase complex, Aph1, also has two isoforms, Aph1a and Aph1b. Moreover, Aph1a is found in two common splice variant forms: Aph1aL and Aph1aS. Some of the different forms of γ -secretase, based on the various possible combinations of subunits, appear to have different catalytic properties. ⁹⁶

In terms of the cellular location of amyloid formation, conventional thinking is that most PSEN1 cleavage of C99 occurs at the plasma membrane, leading to direct

release of A β into the extracellular milieu. PSEN2 cleavage is generally thought to occur mostly in endosomes, with A β being released into the lumen.⁹⁷ Whether this endosome-luminal population of A β is secreted from cells via exocytosis, traffics on to lysosomes, or has a different trafficking itinerary is not well established. However, endocytosis of extracellular A β and subsequent lysosomal membrane “leakiness” (into the cytosol) was first reported over two decades ago.⁹⁸⁻¹⁰⁰ There are also many reports of C99 cleavage taking place in other organelles, with the resulting A β being reported in the lumen of these compartments, as well as in the cytosol¹⁰¹⁻¹⁰⁸ The trafficking pathways that lead to the presence of A β in some of these locations are by no means always clear. It has not been ruled out that some of the toxicity of A β is generated by its intracellular population. Could it be that it is intracellular A β that triggers hyperphosphorylation of tau and formation of neurofibrillary tangles? We decline to weigh in on this question but note hypotheses have been published that raise this possibility.¹⁰⁹⁻¹¹²

It should also be pointed out that not all extracellular amyloids are deposited in amyloid plaques located in the extracellular milieu of brain tissue. In the case of cerebral amyloid angiopathy (CAA), central nervous system amyloid deposits are formed in the walls of cortical and leptomeningeal arteries, arterioles, and, sometimes, capillaries and veins. CAA pathogenesis, like AD, is often associated with age. Similar to AD, accumulation of A β is thought to cause CAA and therapeutics are limited.¹¹³ Indeed, CAA often accompanies AD.¹¹⁴

While it may be unrelated to Alzheimer's, we point out a remarkable study documenting the accumulation of A β in the placentae of women afflicted with

preeclampsia, raising the possibility that this often tragic condition is also linked to amyloidogenesis.¹¹⁵

The Mechanisms by Which FAD Mutations Promote the Etiology of AD May Be More Complex than Previously Appreciated

Inherited point mutations at any one of 18 residues of APP result in early onset FAD.^{7, 116} Nearly all the AD-related pathogenic single nucleotide polymorphisms cluster around the α -, β -, or γ -secretase cleavage sites located in the transmembrane and extracellular juxtamembrane domain (TM/JM) of APP-C99.

It has generally been thought that there are several mechanisms by which FAD mutant forms of APP promote AD pathogenesis. These include increasing the A β _{42:40} production ratio, increasing the aggregation propensity of the released A β , and/or increasing total A β production.¹¹⁷⁻¹¹⁸ Yet another mechanism seems to be reflected by the K687N mutation adjacent to the α -secretase site, which results in decreased nonamyloidogenic cleavage by that protease, likely tipping the balance of APP processing toward increased β -secretase cleavage, as well as altering the biophysical properties of the consequent mutant form of A β .¹¹⁹ Along the same lines, the K670N/M671L (Swedish) APP double-mutant, in which the mutation sites are immediately N-terminal to the β -secretase cleavage site, is associated with increased β -secretase cleavage and increased total A β production.¹²⁰⁻¹²⁶ In some cases, a single mutation is associated with more than one disease phenotype, such as the D694N (Iowa) mutant that

is associated with both FAD and CAA. This mutation is thought to alter the biophysical properties of the A β peptides, resulting in increased fibrillization and toxicity.¹²⁷⁻¹³⁰ As noted previously, the AD-protective Icelandic APP A673T mutation proximal to the β -secretase cleavage site is associated with *defective* β -secretase cleavage and lower levels of A β .^{24-25, 131}

The mutations mentioned above are all located in the extracellular/juxtamembrane region of the APP, however most FAD-associated mutations are at sites in the transmembrane domain, where it has long been thought that they cause FAD by altering γ -secretase processing to elevate in the A β 42:40 production ratio.¹³²⁻¹³⁶ However, in a recent cell-based study, Xu et al. reported that while most FAD-associated APP mutations at sites located in the cytosolic end of the APP TM domain are indeed associated with an increased A β 42:40 production ratio, these mutants are also partially *resistant* to cleavage, thereby reducing total A β cleavage.¹³⁷⁻¹³⁸ This is a surprising result, but is consistent with the recently determined landmark structure of the complex of the APP C83 domain and presenilin 1, which supports the notion that some APP mutations are likely to reduce the affinity of γ -secretase for C99, which would lower physiological A β production.¹³⁹ Is it possible that that *reduced* cleavage of APP-C99 could also contribute to the etiology of AD? If so, then we might expect to see that the other class of FAD mutations—those that alter the sequences of PSEN1 and PSEN2—might sometimes be γ -secretase *loss of function* mutations.

The Mechanisms by Which Presenilin Mutations Promote the Etiology of AD May Be More Complex than Previously Appreciated

Presenilin-1 and its presenilin-2 isozymes are multispan membrane proteins that are ubiquitously expressed throughout the body, including the nervous system.^{34, 140} In general, γ -secretase complexes have a diverse range of biological functions that involve regulating synaptic plasticity, learning and memory, as well as neuronal survival and homeostasis.^{34, 37, 140} The presenilin-1 protein (PSEN1; coded by the *PSEN1* gene) harbors over 180 documented human FAD-causing missense mutations affecting about 130 amino acid sites (Alzforum.org). There are at least 39 FAD mutations in presenilin-2 (PSEN2; the product of the *PSEN2* gene), which impacts 17 different sites. Together, mutations in *PSEN1* and *PSEN2* account for 90% of the known autosomal dominant FAD gene mutations.^{35, 140-141} It is interesting to note that frameshift or nonsense mutations in the PSEN1 gene have not yet been linked to AD, but instead result in a skin disorder, acne inversa, most likely because of a resulting reduction in Notch cleavage.¹⁴²⁻¹⁴³

γ -secretase is composed of a heterotetrameric (1:1:1:1) complex of presenilin, anterior pharynx-defective 1 (APH1), presenilin enhancer 2 (PEN2), and nicastrin (NCT).³⁴ There is also evidence that γ -secretase may sometimes function as a multimer of heterotetramers.¹⁴⁴ The primary biochemical role of γ -secretase is to catalyze the intramembrane proteolysis of Type 1 (N-terminal extracellular single span) transmembrane proteins such as APP-C99; however, at least 90 protein substrates (such

as Notch receptors, integrins, cadherins, etc.) have been reported, earning it the pseudonym “the proteasome of the membrane.”³⁴⁻³⁶ As noted earlier and illustrated in **Figure 4**, γ -secretase cleavage of C99 involves competing multistep cleavage pathways that lead primarily to A β 42 or A β 40.

In recent years, several studies have suggested that many FAD mutations in PSEN1 are partial or total loss-of-function (LOF) mutations. Cacquevel et al. noticed a drastic LOF of purified γ -secretase containing FAD-mutant forms of PSEN1 (PSEN1^{Mut}), with other groups describing similar LOF phenomena for FAD-associated PSEN mutants.^{145 146-147} Sun et al. later published findings based on studying purified γ -secretases harboring pathogenic PSEN1 mutants and assaying C99 cleavage *in vitro*, as well as in a cell-based assay.¹⁴⁸ In a wide range of biochemical conditions, they found that about 90% of tested FAD-associated PSEN1^{Mut}-containing γ -secretases exhibited catalytic LOF in the presence of PSEN1^{WT}-containing γ -secretase and did so in a dominant negative manner. Indeed, PSEN1^{Mut} γ -secretases behaved analogously to pharmacological antagonists of wild type (WT) γ -secretase activity, such that titration of PSEN1^{Mut} γ -secretase into solution containing PSEN1^{WT} γ -secretase induced LOF of WT at ratios as low as 2:1 (mutant:WT γ -secretase).¹⁴⁴ This interesting result can be rationalized based on direct dominant negative interactions between WT and mutant forms of γ -secretase (see additional discussion below).^{51, 62, 144}

For most FAD mutants that induced partial LOF, it has also usually been seen that the A β 42:40 production ratios for the residual activity were significantly

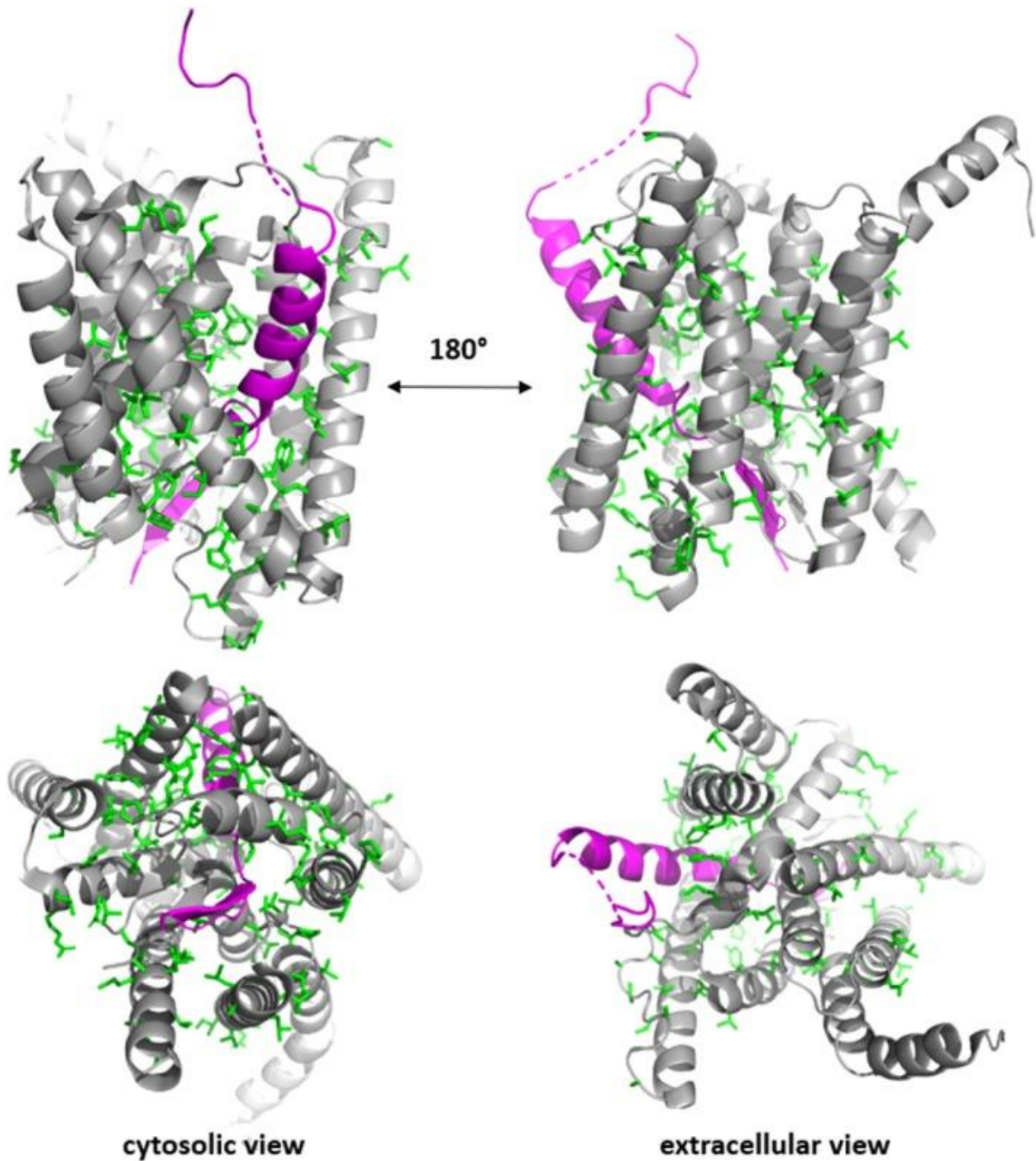


Figure 5. *Locations of FAD mutation sites in presenilin 1 cryo-EM structure.* Known FAD disease mutation sites are highlighted in green (WT residue side chains are shown). The magenta protein is a substrate, α APP-CTF or C83, bound to the active site of presenilin 1, with the C-terminal end of its TM unraveled in preparation for cleavage.

increased (although a *decreased* A β 42:40 ratio was observed for 10% of mutants). One might expect that reduced total A β production by γ -secretase would be *protective* against AD, although the increased A β 42:40 for the residual activity could conceivably be the dominant effect, promoting disease pathogenesis. However, arguing against this possibility was the observation that the age of onset of FAD from mutation to mutation did not inversely correlate with the corresponding change in the A β 42:40 ratio. ¹⁴⁸

Before further discussing whether γ -secretase LOF could sometimes contribute to the development of AD, we highlight additional evidence that FAD mutations in PSEN1 may often induce LOF. **Figure 5** illustrates the locations of disease mutations sites in the structure of the protease (PSEN1) in complex with one of its substrates, the APP-C83 protein (C83 being the product of α -secretase cleavage of full-length APP, see **Fig. 3**). ¹³⁹ We make two observations about the distribution of the FAD mutants in this structure. First, the disease mutations are most highly localized around the substrate-binding interface. It is not hard to imagine how some of these mutations might interfere with substrate recognition or the catalytic mechanism (in either case leading to reduced catalytic activity) and/or that they alter the distribution of cleavage sites leading to an increased A β 42:40 ratio. However, mutations sites are also well distributed throughout entire presenilin structure, with many sites not located near the substrate interface. This widespread distribution of disease mutation sites is akin to what is seen for retinitis pigmentosa (RP) mutations in rhodopsin (see fig. 23 in ¹⁴⁹) and for a number of other disease-linked membrane proteins, including the cystic fibrosis transmembrane regulator protein (see fig. 3 in Reference ¹⁵⁰). What is known for RP/rhodopsin and several other disease mutation/membrane protein relationships is that there are at least two

(nonexclusive) mechanisms by which mutations can result in disease pathogenesis. Some mutations are located at ligand or substrate binding sites and directly induce dysfunction of the protein. However, other mutations—particularly those located distal from the functional site—cause LOF by inducing misfolding. The misfolded protein is often degraded by endoplasmic reticulum protein folding quality control, although the misfolded protein in some cases escapes degradation to form toxic aggregates that may further contribute to disease pathogenesis. The fact that the distribution of presenilin mutations conform to what is now a well-established pattern for a number of other disease-linked membrane proteins is fully consistent with the notion that some presenilin mutations result in LOF due to misfolding of the protein, with FAD being promoted by the resulting loss of catalytic function and/or by toxicity of the misfolded presenilin.¹⁴⁹⁻¹⁵⁰ The dominant negative nature of these mutations possibly may be explained by a model in which the folding-defective γ -secretase is still able to form higher ordered oligomers with WT, with the consequence being that both mutant and WT are targeted for degradation when the mutant form is recognized as folding defective by endoplasmic reticulum (ER) quality control.¹⁴⁴ A similar phenomenon has previously been documented for peripheral myelin protein 22, a tetraspan membrane protein for which dominant mutations that induce misfolding of one allele result in mistrafficking of both the mutant protein and associated WT PMP22.¹⁵¹ To summarize, the structure of the presenilin/C83 complex is consistent with the notion that mutation-induced loss of γ -secretase function may be a factor that colludes with an increased A β 42:40 production ratio to trigger pathogenesis of FAD.

The possibility that loss of γ -secretase catalytic function could contribute to AD pathogenesis was further suggested by results of clinical trials for γ -secretase

inhibitors Semagecestat, and Avagecestat, which despite achieving the desired significant reduction in total A β , exhibited a lack of efficacy coupled to toxicity and worsening of AD symptoms.¹⁵²⁻¹⁵⁴ This prompted the cessation of the related drug trials. In general, nearly every disease-modifying drug candidate that targets the amyloidogenic pathway has thus far been unsuccessful due to issues with toxicity, lack of efficacy, or both.^{4-5, 155}

It seems possible that γ -secretase LOF may contribute to some phenotypes of FAD. If so, there must be associated mechanisms contributing to disease pathogenesis in some patients that are not yet well recognized. These etiological mechanisms would possibly act in collusion with an increased A β ₄₂:40 production ratio. In the next sections, we discuss possible mechanisms by which γ -secretase LOF could contribute to the etiology of AD.

Is Full Length APP Sometimes Toxic?

As noted above, the relationship between APP processing and FAD appears to be more complex than simply being based on total A β levels and the A β ₄₂:40 ratio. Consistent with this thinking are findings from studies of transgenic mice expressing a BRI-A β fusion protein that was designed to be processed such that extracellular A β ₄₀ and A β ₄₂ are generated independent of either full-length APP or its C99 fragment. Interestingly, the mice developed amyloid deposits resembling those seen in humans; however, at all ages tested, the mice did not show cognitive or behavioral deficits.

¹⁵⁶ Similarly, Hamm et al. reported that early (pre-plaque) neurodegenerative symptoms observed in TgCRND8 AD mouse models were A β independent, as indicated by the *promotion* of AD phenotypes using β - or γ -secretase inhibitors. ¹⁵⁷ Accumulation of full-length APP in mitochondria has been observed in several AD patients but not in age-matched controls. ¹⁵⁸ Along these same lines, full-length APP was found to aggregate within dystrophic and degenerative neurons (but not glial cells or astrocytes) in humans with AD, leading some groups to posit that accumulation of full-length APP precedes A β accumulation as a contributing factor to disease progression. ¹⁵⁹ The concept that full-length APP could actively contribute to AD, independent of its role in amyloidogenesis is suggested by the results summarized above, but the evidence is not yet strong. Moreover, the lack of β -secretase mutations as a cause or risk factor for AD is unsupportive of this idea. On the other hand, support for a possible role for the APP C99 domain as a toxic agent in some forms of AD is stronger and is consistent with evidence that many FAD mutations induce full or partial γ -secretase LOF, leading to accumulation of APP-C99 and/or APP-C83, which could be toxic under some conditions. ¹⁶⁰ Additional evidence for such toxicity is presented in the following section.

Is C99 Sometimes Toxic?

The transgenic mouse strain (3xTg: APP^{swe}, M146V presenilin 1, TauP301L) is associated with enhanced C99 accumulation and the absence of tau hyperphosphorylation. In a recent study, 3xTg was compared to the corresponding 2xTg

strain lacking the presenilin mutation, such that amyloid- β production is unimpeded. It was seen that the 3xTg mice developed more severe AD-like symptoms including apathetic behavior (an early behavioral symptom of AD), decreased long-term potentiation, and decreased spontaneous locomotor activity.¹⁶¹ In the same 3xTg mouse strain, it was found that C99 accumulation was the primary contributor to hippocampal lesions.¹⁶² It has also been reported that C99 accumulation in J20 AD-model mice is associated with alterations in the early brain network, a process that could be reversed by treatment with β -secretase inhibitors.¹⁶³ In a familial Danish dementia mouse model, in which a deficiency in the protein BRI2 resulted in increased total APP levels, only pharmacological inhibition of β -secretase processing of APP (and not γ -secretase) rescued memory and deficits in long term potentiation (LTP), implicating C99 as the pathogenic agent.¹⁶⁴ Lauritzen et al. demonstrated in two separate mouse models that C99 accumulation induced defects in lysosomal-autophagic function, another early hallmark of AD neuropathology, and that the defects were not observed in β -secretase-inhibitor treated mice.¹⁶⁵ In okadaic acid-treated mice (in which tau hyperphosphorylation is induced), total levels of C99 increase and accumulate primarily in axons, suggesting C99 redistribution (on top of accumulation) may also play a role in AD-related pathogenesis.¹⁶⁶

Cellular studies have also provided evidence for toxicity of C99. Pera et al. showed that C99 build-up in the mitochondria-associated endoplasmic reticulum membranes (MAMs) of AD model cells resulted in altered lipid metabolism/composition in the MAMs and in mitochondrial membranes.¹⁰⁷ These changes, unobserved in wild-type cells, interfered with the assembly and activity of mitochondrial respiratory

complexes, offering a possible explanation for the bioenergetic shortfalls associated with AD. Primary cells from DS patients showed endocytic abnormalities that were reversible by reducing expression of either full-length APP or β -secretase.¹⁶⁷ The group also found that γ -secretase inhibition was sufficient to induce endocytic defects in healthy fibroblasts and worsened endosomal pathology in DS fibroblasts, suggesting that the abnormalities were derived at least in part from C99 accumulation but not A β .¹⁶⁷ Neuronally differentiated induced pluripotent stem cells derived from two FAD and two LOAD patients (which displayed elevated levels of the AD biomarkers A β , phosphorylated-tau, and active GSK-3 β) exhibited reductions in phosphorylated-tau and active GSK-3 β after treatment with β -secretase inhibitors but not γ -secretase inhibitors, suggesting that AD-promoting GSK-3 β activation and tau hyperphosphorylation are more closely linked to C99 production than to A β .¹⁶⁸

While it is premature to declare that toxicity from accumulation of C99 contributes directly to AD pathogenesis, the studies summarized above suggest that C99 does appear sometimes to be toxic. Further investigation will be required to rigorously test whether FAD mutation-induced γ -secretase LOF results in C99 accumulation in brain tissue and, if so, whether this accumulation contributes to the etiology of the related phenotypes of FAD. If this was proved to be the case, it would fundamentally alter our understanding of the relationship of the amyloidogenic pathway to AD, providing new insight into the failures of previous drug trials and perhaps pointing to promising future therapeutic strategies.

The First Direct Genetic Evidence for the Role of the Amyloidogenic Pathway in Late-Onset AD

While it is clear that genetically dominant mutations in APP, PSEN1, or PSEN2 cause FAD, *one of the mysteries of the amyloid hypothesis is why incompletely penetrant mutations in these proteins have not been discovered as risk factors for sporadic LOAD*. This is despite the fact that variations in many other protein-coding genes have been identified as risk factors for LOAD (e.g. *APOE4*, *TREM2*, and *COBL*).¹³⁻¹⁵ Of course, for most cases of LOAD, it may be that a combination of nongenetic factors leads to accumulation of toxic forms of A β . Such factors could include chemical modification of A β (e.g. by reactive oxygen species or ROS by-products), decreased transport of A β out of the brain, or decreased proteolytic cleavage of A β . Moreover, a number of the known genetic risk factors for LOAD do have linkages to the amyloid pathway, likely being involved in APP trafficking (e.g. *SORL1*, A β transport [e.g. *APOE* or *PICALM*¹⁷³]), inflammatory response to formation of amyloid plaques (*TREM2* or *ABCA7*), or combinations of several pathways (e.g. *BIN1*).¹⁶⁹⁻¹⁷⁴

In what may eventually prove to be a major breakthrough in AD research, new data have been published by the Jerold Chun group at the Burnham Institute that describe a nonclassical genetic mechanism that brings mutations in APP into play as risk factors for LOAD.¹⁷⁵⁻¹⁷⁶ This work was based on the fact that genomic heterogeneity exists within complex multicellular organisms such as humans, a phenomenon termed *genomic mosaicism*. The authors uncovered a novel phenomenon by which APP-specific gene recombination events lead to the expression of genomically integrated

mutant *APP* genes, and the hyper-accumulation of these mutant *APP* genes correlates with disease in sporadic LOAD patient-derived neurons. Both healthy- and LOAD-derived neurons underwent *APP*-specific gene recombination events, resulting in new mutant genomic *APP* sequences (referred to as *gencDNAs*). Many of these *gencDNAs* were transcribed into mRNAs and presumably translated into the mutant *APP* proteins. While this phenomenon was observed even in age-matched non-diseased controls, neurons from LOAD patients contained a roughly 10X greater number of unique *APP* *gencDNA* sequences, and it was demonstrated that *APP* *gencDNA* accumulation correlated with LOAD progression in J20 AD-model mice. We summarize this fascinating work here in

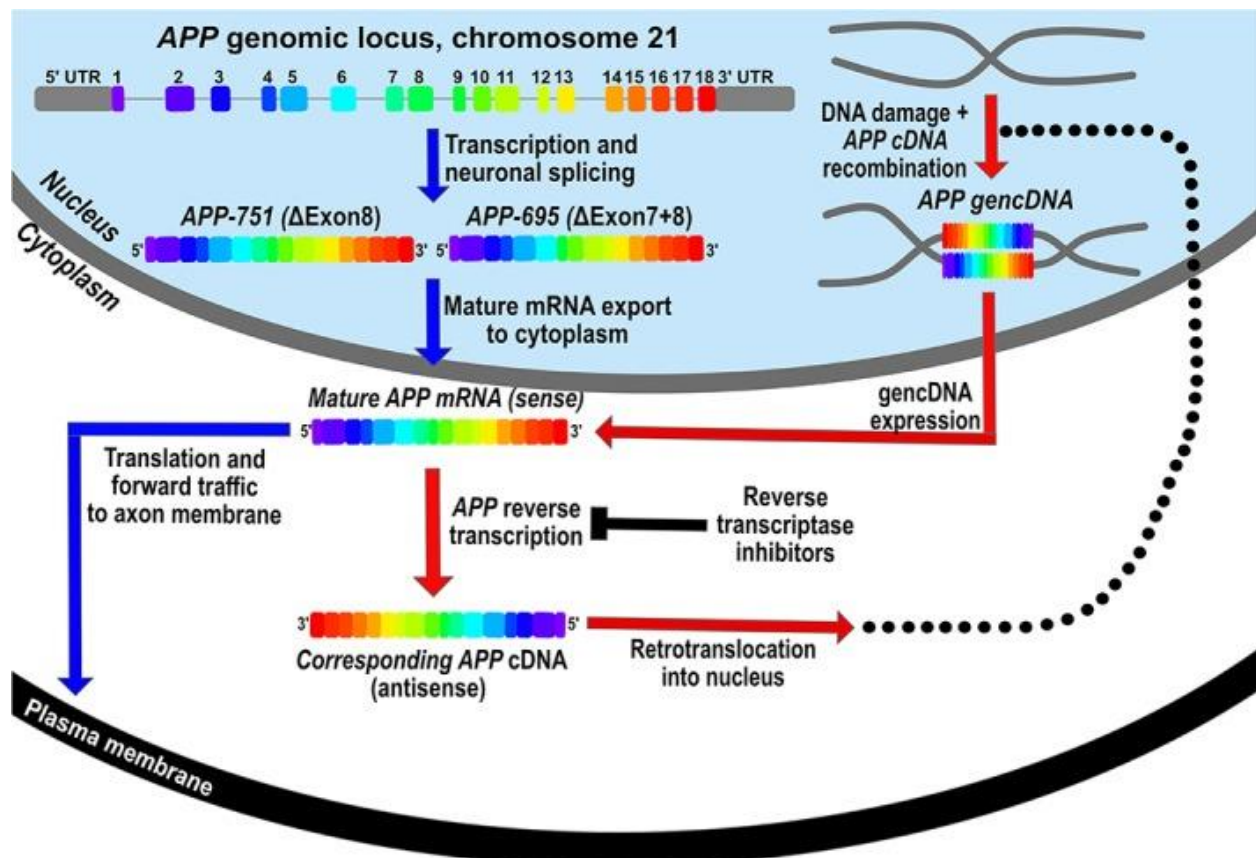


Figure 6. Model for *gencDNA* formation and expression in neurons based on the work of the Chun lab. Illustrated by blue arrows is the canonical gene expression program for neuronal *APP* splice variants *APP*-751 and *APP*-695. The *gencDNA* creation pathway, illustrated by red arrows, is considered to be initiated by *APP* reverse transcription followed by translocation and recombination back into chromosomal DNA following DNA damage. Newly formed *APP gencDNAs* can be expressed and fed into the typical gene expression program in blue.

Figure 6. This study was made possible by the donation of brains from both control and LOAD patients.

For diseases such as LOAD, where a single cause of disease is difficult to pinpoint, a directed interrogation of the diseased-cell transcripts can be a useful way to fingerprint the disease biological state. The prefrontal cortices (an area of the brain involved in cognition, personality, and behavior) for six non-AD individuals (ages 80–94; three females, three males) and for seven with verified LOAD (ages 72–88; six females, one male) were sectioned and prepared for an intensive genomic and transcriptomic analysis. Using flow cytometry to separate neurons from other brain cells, the Chun lab was able to analyze the transcriptomic state of small populations (50 at a time) of primary neurons from control and LOAD brain tissue. Using the reverse transcriptase-based polymerase chain reaction (RT-PCR) and Southern blot, they found transcripts that represented not only the APP-751 and APP-695 neuronal splice variants, but also lower molecular weight transcripts that were verified to be *APP* mutants using ³²P antisense probes. The smaller, mutant transcripts were present both in healthy and LOAD neurons, however, the disease neurons expressed a roughly 10X greater fraction of unique reads, suggesting this process is out of balance in LOAD. They then sequenced the transcripts.

In addition to detecting the normal neuronal APP splice variants (APP-751 or APP-695, which contain all 18 APP exons except for 8 or 7–8, respectively), the group identified several unique *APP* sequences that map back to noncanonical inter-exon junctions (IEJs). Over-represented among these sequences were *APP* variants that joined exons from early in the APP locus (exons 1, 2, 3, or 6) to those toward the end of the locus (exons 11, 14, 16, 17, or 18), skipping a large a portion of the central exons.

Using RNA *in situ* hybridization, the group detected the transcripts in the cytoplasm, indicating they were exported out of the nucleus as mature mRNAs. They also demonstrated that non-neurons from the same individuals did not express mutant *APP* transcripts, nor were mutant *PSEN1* transcripts expressed. A dangling question was whether these strange *APP* transcripts reflected a malfunction in gene splicing or if expression was genomic of nature. To verify whether the transcripts found in their previous experiment were expressed from the WT *APP* locus, Chun and colleagues developed a DNA *in situ* hybridization (DISH) strategy that would target only genomic loci with IEJs (absent of intron sequences in between them). They identified several mutant genomic IEJs (gencDNA) in both healthy and LOAD neurons that were absent in other cell types; however, *APP* gencDNA sequences were greatly overrepresented in LOAD neurons. Using fluorescently labeled DISH probes and sequence-specific restriction enzyme digests, it was verified that the gencDNA sequences were indeed chromosomal and that they did not colocalize with the WT *APP* locus.

Sequencing of the gencDNAs revealed a pattern of insertions, deletions, and missense mutations that clustered around the 3' (exons 1, 2, and 3) and 5' (exons 16, 17, and 18) ends of the *APP* open reading frame. Exons 16, 17, and 18 include the sequence for the *APP* C-terminal C99 domain. It was found that some LOAD cell populations also contained gencDNAs that encoded mutations *corresponding to known FAD APP mutations*, which were totally absent in non-diseased neurons. It was also verified that some mutant *APP* gencDNAs were expressed into proteins. Moreover, expression of one such construct caused significant reduction of cell viability in

culture. *This discovery points to a somatic mechanism by which mutant forms of APP are generated and can come into play in the etiology of LOAD.*

Although it was not tested, it seems reasonable that some of the identified mutant APP gencDNAs present in LOAD neurons would be toxic via the same mechanisms by which inherited mutations in APP promote FAD. For example, one identified gencDNA (D3/16) coded for an APP variant that harbored three previously known FAD pathogenic point mutations: A673V (known to increase relative β -secretase cleavage of APP and increase aggregation potential of A β), as well as V715M (French) and V717F (Indiana), which are thought to be pathogenic due to increasing the A β ₄₂:A β ₄₀ production ratio. If *APP* gencDNAs containing known FAD mutations are expressed into the corresponding protein, it would help to explain why the hallmarks of LOAD are so similar to FAD. This concept is further supported by lack of any detected FAD mutant *APP* gencDNA in neurons from healthy brain tissue. To summarize, the evidence points to a newly discovered mechanism by which the *APP* gene is selectively retrotranscribed (inferred by the lack of genomic introns in the mutant genes and detected *PSEN1* gencDNA sequences) and integrated into the genome by homologous recombination.

How does gencDNA form *in situ*? Chun et al. hypothesized that the *APP* recombination event was mediated by endogenous reverse transcriptase (RT) activity coupled to DNA damage. To test this, gencDNA formation in Chinese hamster ovary (CHO) cells was induced and the relative levels of endogenous RT activity was measured in brain samples, in CHO cells, and following purification of RT *in vitro*. It was shown that the formation of novel *APP* gencDNAs could be induced using hydrogen

peroxide (H₂O₂), which introduces single- and double-stranded DNA breaks. In contrast, gencDNA did not form when the cells were treated with abacavir and azidothymidine, commonly prescribed RT inhibitors used to treat HIV infection. While the RT activity was observed in the brain cells was modest (ca. 100,000X less activity than in CHO cells), that it would be detected at all points to the possibility that this process could happen in neurons *in vivo*. To further validate this, a J20 sporadic AD model mouse (which develops amyloid plaques in an aging-dependent manner) was examined, confirming that the number of neuronal (contrary to other brain cell types) *APP* gencDNA loci also increases with age, correlating with the development of the AD-like state in the mouse model.

The question remains as to where the “endogenous” RT activity found in neurons comes from. RT enzymes are a common tool of viruses for integrating their genes into the host genome, however, the brain is an immune-privileged organ with several barriers and potent immune responses to infection. Nonetheless, certain viruses are able to enter the central nervous system (such as alpha-herpes, rabies, HIV, and polioviruses) through various routes.¹⁷⁷⁻¹⁷⁸ The authors postulated that DNA damaging events linked to AD, such as head injuries, may further assist gencDNA formation in the context of active RT. Could it be that *APP* recombination is what connects familial AD with some phenotypes of LOAD? While this study was conducted with only a small set of human subjects, if confirmed in future studies, it may point to new direction for disease-modifying therapeutics that act through very different mechanisms than previously investigated. It also stands to reason that genomic restructuring events such as these could promote the progression or onset of neurodegenerative disorders beyond sporadic AD.

Final Perspectives

In this first chapter of my thesis, I have provided a selective overview of the complexity of the amyloidogenic pathway. We have also highlighted a couple of recent studies that provide fresh evidence that the amyloidogenic pathway is not a red herring in the pursuit of potential Alzheimer's therapeutics. Indeed, the studies featured in this review suggest that it is partly the complexity of this pathway that has confounded early efforts to target it or its amyloid products in order to prevent or treat AD. We conclude by respectfully suggesting that continued research on the amyloidogenic pathway is well merited as the only route to eventually ascertaining whether this pathway is druggable for preventing or treating AD.

It was remarked by John Hardy, an early adopter of the amyloid cascade hypothesis, that Alzheimer's disease is a disease of the membrane. While it is clear the dominant AD mutations in *APP*, *PSEN1*, and *PSEN2* are disease-causing likely via an amyloid-centric mechanism, it appears that many of AD risk factor genes are involved lipid metabolism and immune-response following amyloid burden. Specifically, genes including but not limited to *ABCA7* (a lipid transporter), *TREM2* (a lipid receptor and immune regulator), *PLCG2* (a phospholipase), and *APOE* (a lipid transporter) all have functions related to membrane homeostasis and their expressions are increased in response to amyloid damage. Considering the main topic of this thesis involves a drug screening effort against the transmembrane domain of APP (C99), that the next

subchapter will focus on developing the reader's understanding of the general complexity of membranes and membrane proteins before circling back to C99.

CHAPTER 2

INTRODUCTION TO DRUG DISCOVERY, NMR, AND SPTMRs

Single-pass Transmembrane Receptors (SPTMRs) and Human Disease

Approximately 6% of all human proteins, and about 25% of all membrane proteins, code for single-pass transmembrane receptor proteins. As the name suggests, they have a single transmembrane domain, flanked by water-exposed intra- and extracellular domains. While the percentage of genes that code for ion channel and transporter proteins is relatively consistent across distant organisms (4-5% of all protein-coding genes), the percentage of SPTMRs goes up exponentially with organismal complexity. These proteins have a diverse set of often-essential functions including but not limited to signal transduction, regulating cell growth, adhesion, and catalysis. Their biological roles in these areas, coupled to the growing repertoire of disease-causing mutations found in them, make certain SPTMR proteins genetically validated drug targets. Examples of some of these proteins include receptor tyrosine kinases (RTKs), cytokine receptors, integrins, and the main topics of this dissertation, the amyloid precursor protein and Notch receptors. Collectively, their overrepresentation in the human genome suggests they are important units of biology; however, they are difficult to work with in reconstituted systems and remain markedly underrepresented among the structures deposited in the Protein Data Bank. Historically, structure determination for SPTMRs has usually been exclusive to their water-soluble domains and seldom includes the structures

of their transmembrane segments. While cryo-EM will likely make structure determination for SPMTRs more streamlined going forward, our understanding of how these proteins can structurally transduce their signals across the membrane remains largely unknown with a few exceptions. In summary, there are significant gaps in knowledge with regards to the structure-function relationships for proteins in this class.¹⁷⁹

While it is advantageous to have 3D structures of a protein target to guide drug discovery efforts, it is not always essential. This is true for the case of eltrombopag (ETP), an FDA-approved drug for the treatment of thrombocytopenia that engages the SPTMR called the thrombopoietin receptor (TPoR; **Figure 7**). Thrombocytopenia is a blood disease that manifests as excessive bleeding due to low platelet count, often because of improper activation of the TPoR and its downstream signaling cascade. In 2005, scientists from GlaxoSmithKline Pharmaceuticals published revealed their compound, SB394725 (ETP), that functions as a selective TPoR agonist with a 200 nM EC₅₀.¹⁸⁰ It was later found using mutagenesis that ETP activity was due to a direct interaction with the transmembrane domain of the TPoR, which stabilized the receptor in the active, dimeric state. ETP remains one of the few known small molecules that elicit their activity by binding the transmembrane domain of an SPTMR.¹⁸¹ It is remarkable that these discoveries were made using well-defined biological assays without any structural knowledge of the transmembrane domain of the protein, which suggests that phenotypic screens such as these may be the future for SPTMR drug discovery pipelines. However, the ETP case study also confirms that it is feasible to find compounds that bind the transmembrane domain of an SPTMR.

When I started my thesis project, I had no knowledge of ETP, TPoR, or thrombocytopenia in general. What I knew was that Dr. Sanders had the idea that, given his lab's previous determination of the C99 structure by NMR, we could use NMR to investigate how C99 interacts with small molecules in model membranes, with the intention of discovering tight C99 binders. Like the TPoR, C99 is a SPTMR, however it is not yet known to have a well-defined downstream signaling pathway that could be used for phenotypic screening in cells. C99 does have a biochemical role that could be used to investigate interactions; that is, it is the immediate precursor via its proteolytic cleavage to the amyloid- β peptides that are involved in Alzheimer's disease.

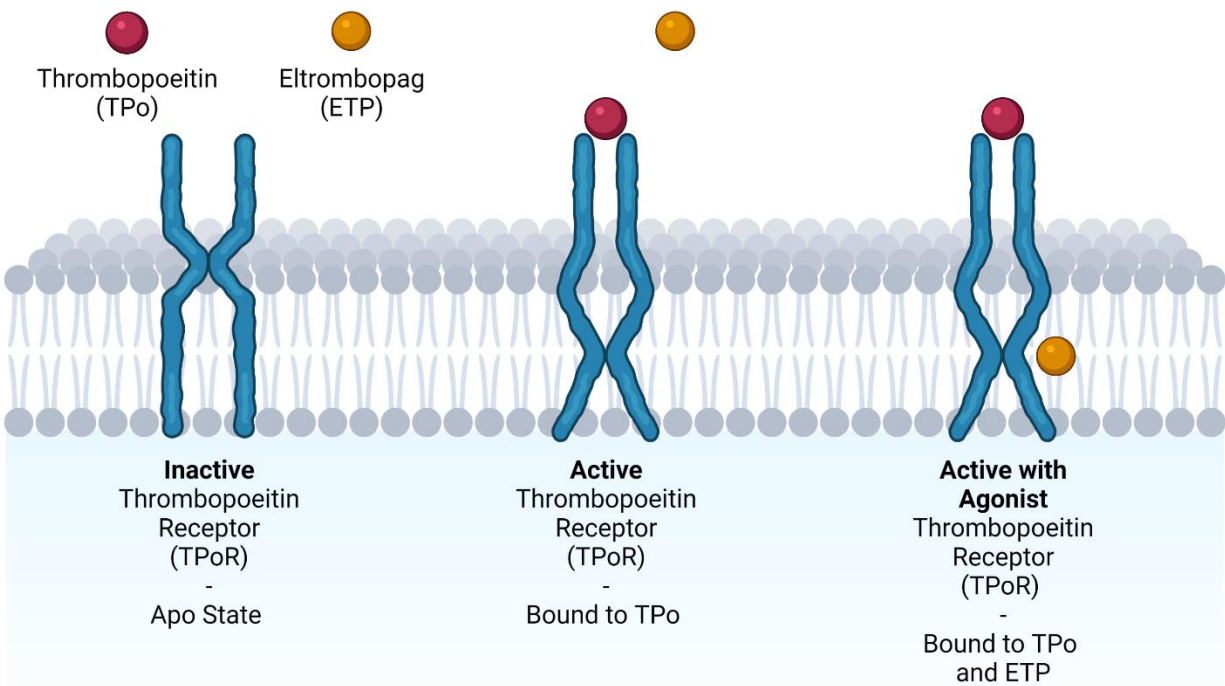


Figure 7. Example of a well-drugged SPTMR: activation of the Thrombopoietin receptor (TPoR). TPoR is a single-pass transmembrane protein involved in blood platelet formation. Upon binding the endogenous ligand, Thrombopoietin (TPo), it undergoes a conformational change that results in signal transduction leading to platelet formation. Eltrombopag (ETP) is a TPoR agonist that stimulates the active ligand-bound TPoR by binding it in the transmembrane domain, further stabilizing the active state of the receptor and increasing signal output. This figure created with BioRender.com.

The Biochemistry and Biophysics of Small Molecule-Protein Interactions

Most single-domain proteins fold spontaneously, with the folded state being thermodynamically favored. Many of the molecular forces responsible for protein folding, such as hydrogen bonding, van der Waals interactions, and the hydrophobic effect, also are integral to driving protein-protein or protein-small molecule interactions. Many folded proteins will have pockets or crevasses on the surface of the folded structure that are accessible and complimentary in shape to certain small molecules, loosely analogous to how a key fits a lock. In general, these interfaces are typically where drug development projects focus their effects, as they can offer significant molecular area that can contribute to binding energy. These sites on a protein can be categorized into two main types: orthosteric and allosteric sites. Orthosteric sites are defined as a protein interface where cognate molecular interactions and functions are observed, sometimes referred to as an 'active site'. Examples of these include regions such as an ATP-binding site for a kinase, a 5-hydroxytryptamine (5-HT; serotonin) binding site on a serotonin receptor, or the heme binding site on the oxygen carrying protein hemoglobin. As such, compounds that target orthosteric sites will commonly be analogs of (and compete with) the orthosteric ligand. By contrast, allosteric sites are regions on a protein that are not the active site but can alter the structure or activity of the protein when bound by a compound. Both ortho- and allosteric drug discovery strategies are commonplace, with unique advantages and disadvantages.

Regardless of the mode of the protein-small molecule interaction, upon binding, there is a change in enthalpy (ΔH) called the enthalpy of binding. Furthermore,

protein pockets may have coordinated water molecules when in the apo (unbound) state, such that a small molecule can displace them and change the entropy (ΔS) of the system, similar to a micelle excluding water from the hydrophobic core. Together, the changes in the enthalpy and entropy of the system drive the potency of the interaction, which is typically measured as dissociation constant (K_D). As with protein folding, the more negative the ΔH and positive ΔS at a given absolute temperature in Kelvin (T), the more negative the free energy (ΔG) is associated with the interaction, such that we consider it thermodynamically favored according to the classic Gibbs' free energy equation, shown in Equation 1.

$$\text{Equation 1: } \Delta G = \Delta H - T\Delta S$$

A process with a negative ΔG value is considered favorable, and the magnitude of the ΔG value is logarithmically proportional to the K_D , as shown in Equation 2, where R is the ideal gas constant of $8.312 \frac{J}{mol \cdot K}$, and K_D is the equilibrium dissociation constant.

$$\text{Equation 2: } \Delta G = RT \ln K_D$$

These equations can be rearranged to show more clearly show the relationship Equation 1 and Equation 2 as follows:

$$\text{Equation 3: } \Delta H - T\Delta S = RT \ln K_D$$

Equation 3 more clearly shows how linear changes the free energy (ΔG) from enthalpic and entropic contributions are logarithmically related to changes in K_D . For

our purposes in this document, K_D values inform on the two-state process of a protein and ligand forming a complex. Imagine a situation where a molecular complex is formed between a ligand [L] and a protein [P], to form the complex [LP], which are at equilibrium. The K_D of the complex can be mathematically depicted by Equation 4 where [L], [P], and [LP] are all in molar units. This concept is also graphically portrayed in **Figure 8**.

$$\text{Equation 4: } K_D = \frac{[L][P]}{[LP]} = \frac{\text{off-rate}}{\text{on-rate}}$$

The dissociation constant K_D refers to the ligand concentration [L] at which half of the protein [P] is bound, or in other words, the concentration where the complex [LP] is equal to the uncomplexed protein [P]. Furthermore, a K_D value is proportional to the off-rate over the on-rate of the complex. At equilibrium, the rate of [P] and [L] associating to form [LP] is equal to the rate of [LP] dissociating to [L] and [P]. Complexes with small K_D values, such as $\leq 10^{-6}$ M (≤ 1 μ M), are considered relatively strong interactions, such that complexes form in relatively dilute conditions of [P] and [L] to form complex [LP]. Weaker interactions are reflected by K_D values of $\geq 10^{-6}$ M (≥ 1 μ M), which require higher concentrations of [P] and [L] to form the complex [LP]. It should be clarified

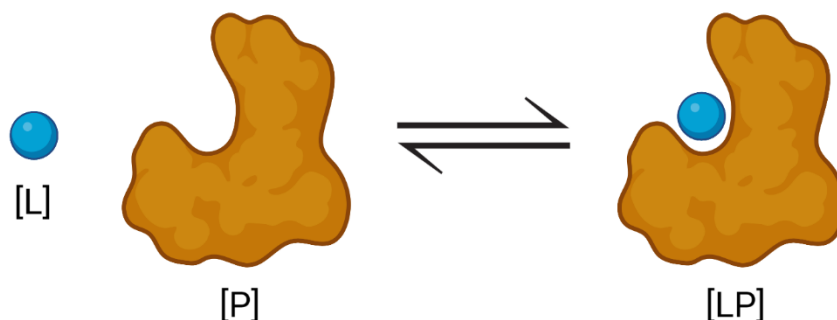


Figure 8. *Example of protein-ligand binding.* Here, I show an arbitrary protein [P] with a crevasse that the ligand [L] can bind to. Upon binding, the two molecules form a complex [LP], which is reversible and in equilibrium with the uncomplexed [L] and [P]. When the concentration of [L] is equal to that of [LP] at equilibrium, that is the K_D of the complex. This figure created with BioRender.com.

that while in this document I use the aforementioned K_D values as the cutoffs for ‘strong’ or ‘weak’ binding, these limits are arbitrary. These cutoffs were set for the purposes of this document with regards to protein-drug interactions, where $K_D \geq 1 \mu\text{M}$ is typically considered weak.¹⁸²

K_D values are central to the fields of chemistry, biochemistry, and drug discovery. They are the primary unit used to discuss the potency of a protein-protein or protein-ligand interaction, and modern drug discovery efforts are typically focused on achieving tight affinities ($K_D = 0.1\text{-}1 \text{ nM}$) for their target, meanwhile sparing affinities for off-targets. K_D values are notoriously sensitive to changes in solution, such as pH, salt concentrations, and temperature.¹⁸³ For more complicated systems, such as the membrane protein system that will be discussed in this thesis, the type of membrane mimetic that envelops the protein target can impact the observed K_D .¹⁸⁴

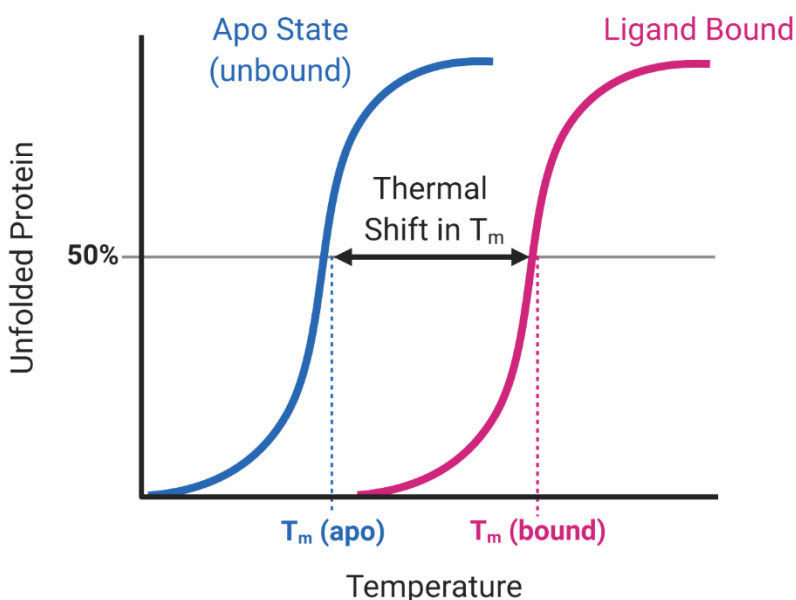


Figure 9. *Example of protein thermal stabilization upon ligand binding.* When the arbitrary protein is heated, it unfolds to reveal a melting temperature (T_m apo; blue curve), which is where half of the protein is folded, and the other half unfolded. Upon ligand binding, the protein is thermostabilized and the melting temperature of the protein is right shifted (pink curve) to reveal a new T_m (T_m bound). This figure created with BioRender.com.

The free energy of ligand binding to a protein often results in thermodynamic stabilization of the protein. Very often, the thermal stability correlates with thermodynamic stability. Thermal stability is often determined by varying the temperature and using some method sensitive to the state of folding to determine the denaturation temperature (T_m) of the protein. Ligand binding therefore often shifts the T_m for that protein to higher value.

Methods to measure T_m include differential scanning calorimetry and differential scanning fluorimetry, where the temperature of the system is slowly increased until the protein is unfolded thermally. For example, if an arbitrary protein's T_m is 50°C without ligand, one would expect the ligand-bound protein to 'right-shift' the T_m such that it would be $\geq 50^\circ\text{C}$, which is graphically shown in **Figure 13**. The shift in T_m is typically proportional to the energy contributed to the system from ligand binding since both the intermolecular protein-ligand and intramolecular protein-protein interactions must be broken to unfold (melt) the protein. For that reason, thermal shift assays (TSAs) that measure the changes in T_m upon ligand binding are often used to verify a direct interaction between a protein and a ligand.

It should be mentioned that nature has evolved some fascinating protein-ligand interactions that serve as apparent upper limits for binding energy and affinity. Indeed, the interaction between the protein streptavidin from the bacteria *S. avidinii* and the small molecule biotin (vitamin B7) is so tight ($K_D = 10^{-14}$ M; 10 fM; 0.00001 nM) that the complex is extremely long-lived (very low off-rate) and resembles a covalent bond.¹⁸⁵ The absolute free energy of binding for this system has been calculated to be -20.4

kcal/mol, which results in a thermal shift for the streptavidin T_m from 75°C when unbound to 112°C upon saturating biotin binding.¹⁸⁶ This is regarded to be one of the strongest non-covalent interactions observed in nature and has been heavily repurposed for use in biotechnology (protein purification, nanoparticles, immunoassays).

In drug discovery, protein-drug interactions can be very strong but only rarely approach the affinity of the biotin-streptavidin complex. Still, some remarkable affinities between small molecules and proteins have been observed, including those for transmembrane proteins. GPCRs are remarkably amenable to drug development, with some small molecule ligands reported to bind in the pico-to-nanomolar K_D ranges. For example, LSD-25 (LSD) was synthesized by Dr. Albert Hoffman in 1938 and was determined by him in 1943 to have uniquely potent and long-lasting psychoactive effects (an effective dose of less than 100 µg, with effects lasting 6-15 hours). Until very recently, the reason for its potency was highly speculative, but research for Dr. Bryan Roth's group at UNC Chapel Hill has helped elucidate the mechanisms of these features. Although it was previously found that LSD effects were mediated primarily by serotonergic GPCRs, in 2017, Wacker, Wang, and McCorvy *et al.* from the Roth group published the first co-crystal structure of the 5-HT_{2B} GPCR in complex with LSD among other relevant pharmacological information. Interestingly, the group found that the 5-HT_{2B} receptor underwent a conformational change upon LSD binding that effectively enclosed the LSD molecule in the binding site. They determined that the K_D of the interaction was approximately 0.33 nM, with an extremely long residence time of 221 minutes in the receptor. Together, these results explain both LSD potency and lifetime and serve as a model for potency of a synthetic drug to a protein.¹⁸⁷

Considering it was discovered in a time before biochemical receptors were identified and appreciated, I consider the discovery of a drug as potent as LSD serendipitous and unsophisticated relative to today's standards. Modern drug discovery is far more targeted and multidisciplinary, using a combination of genetics, biochemistry, cell biology, and medicinal chemistry to design and validate highly potent small molecules for a validated biological target. While this section focused primarily on the basic thermodynamics and kinetics of protein-small molecule interactions, using the streptavidin-biotin and LSD-5-HT_{2B} complexes as examples, the next section will focus on more recent advancements in small molecule drug discovery, including a central topic of this thesis: examining drug binding by NMR. Furthermore, I will discuss a new frontier for targeted small molecule drug discovery: single-pass transmembrane domain protein targets.

Probing protein-small molecule interactions by NMR

There are several techniques available to investigate how proteins interact with small molecules, some of which were discussed in the previous section. The bulk of the work discussed in this thesis was conducted using biomolecular NMR spectroscopy, which is remarkably sensitive to chemical exchange (binding events) and can give structural information about them at atomic resolution. This subsection will focus on introducing the reader to NMR as a technique, and how it can be used to probe protein-

small molecule interactions. Furthermore, I will discuss previous work conducted by my predecessors in the Sanders lab, who paved the way for this project by both determining the 3D structure of C99 in detergent micelles and by discovering that it binds cholesterol using NMR.

Biological NMR spectroscopy

Nuclear magnetic resonance (NMR) spectroscopy is now commonly used by chemists, physicists, and biochemists alike. It takes advantages of a quantum physical property called nuclear spin, which is the intrinsic angular momentum of elementary particles such as atomic nuclei. Specifically, when nuclei with a particular spin value (spin $\frac{1}{2}$ or $-\frac{1}{2}$ most commonly) are in a magnetic field, they can align with the field and begin to precess (angular momentum) at a given frequency, which depends on the atom. At that point, the direction of the nuclei's precession can be perturbed using energy (such as radiofrequency or magnetism), sending it out of magnetic alignment into a higher energy state. When the energy is then removed from the system, the nuclei will begin to relax back to their lower energy state in alignment with the magnetic field. The intensity, timeline, and 'timbre' of the relaxation produces a complex wave referred to as a free induction decay (FID) and is the raw data obtained from a modern Fourier transform NMR spectrometer. Because the raw FID data is complex and difficult to analyze in any meaningful way, NMR data is often converted into usable spectra using a mathematical

principle called Fourier transform (FT). The result of the FID-FT is what is most seen of NMR data: resolved, sharp peaks (resonances) on a standardized frequency scale (PPM units) that is immediately informative about the sample and useful for comparison between samples and spectrometers. In the contents of this thesis, all NMR data is plotted in PPM units, as is the standard in modern NMR use. ¹⁸⁸

NMR today is in a greatly advanced state that is almost 90 years in the making. The first attempt to observe this fundamental property of matter was published in 1936 by Cornelis J. Gorter in the journal *Physica*, where he described the negative results of a calorimetric experiment using lithium fluoride and alum. Two years later, Isidor Rabi was the first to accurately detect nuclear magnetic moments, and approximately 8 years after that in 1945-46, two scientific groups, led by Felix Bloch and Edward Purcell, respectively, independently reported their detection of NMR signals from water and paraffin. The latter three would go on to win Nobel prizes in Physics, however C.J. Gorter's work, although highly impactful, would not be recognized by the Nobel society because his results were negative. ¹⁸⁹

In the early days of NMR, the advancements were primarily made by physicists, such as those at the Varian Associates company that developed the first 'NMR machine' (now a subsidiary of Siemens Co.). Over the decades, the early NMR machines evolved into what we now recognize as NMR spectrometers, which have a wide variety of uses across fields including chemistry, physics, and biology. NMR spectrometers also paved the way for the use of MRI machines in medicine, which were developed heavily in the 1970s and recognized by the Nobel prize in Physiology and Medicine in 2003. ¹⁹⁰

The impact of the field of magnetic resonance field is broad, and it is easy to take for granted the notable progress made by the giants before my time. Today, it is common for academic research institutions and industrial entities alike to have one or many NMR spectrometers. NMR is an important tool for chemists, who typically use it to analyze the structures, dynamics, and purities of small molecules. However, despite being essential for modern chemical, chemists were relatively 'late adopters' of NMR technology. Even later than the chemists were the biochemists/biophysicists, who pushed the boundaries of NMR spectroscopy in the late 1970s, 1980s and 90s and brought NMR to bear onto macromolecules such as proteins. Considering that proteins are large, polymeric biomolecules, NMR is useful for probing similar features for them as were already commonplace for small molecules, including molecular structure and dynamics. The first NMR-determined 3D structure of a protein was reported by the lab of Kurt Wüthrich in 1985, who would later go on to win a shared Nobel prize in 2002 for his pioneering work.¹⁹¹ It should be noted that on top of Wüthrich, there are many scientists across the world who made significant contributions to protein NMR, who collectively made it a practical, simplified tool that requires minimal understanding of the physics of NMR to generate and analyze NMR data.¹⁹⁰

NMR spectroscopy is an inherently low-sensitivity experiment, and as mentioned previously, requires specific NMR-active nuclei to be observed. Biochemical tricks can be used to make an NMR sample that can give way to a useful NMR signal. Except for the proton (^1H ; hydrogen), which is the most common nucleus of a hydrogen atom and the 2nd most NMR-sensitive nucleus (after tritium), other NMR-active nuclei that are central to biomolecular NMR (namely carbon-13, and ^{15}N nitrogen-15) give relatively

weak NMR signals and are also in relatively low abundance in nature.¹⁹² This makes NMR signals from these nuclei very weak when they are measured using natural abundance. Major advancements in isotopic enrichment of NMR-active nuclei in biomolecules were also made in the '80s and '90s with the advent of recombinant gene expression technologies. For example, it is highly uncommon today for a human protein to be extracted from human tissue due to ethical and practical limitations. Furthermore, it is impractical to feed humans or other animals on a diet where the food is enriched in ¹³C and ¹⁵N. To get around these combined issues, most modern NMR research and biochemical research in general is based on recombinant production of proteins, using other model organisms such as the bacteria *E. coli* or the yeast *Pichia pastoris* to produce the biomolecules of interest.¹⁸⁸

E. coli and *P. pastoris* are both fantastically amenable to genetic modification and recombinant manipulation, such that one can express a gene of interest by providing the microbes with recombinant DNA. Typically, the recombinant genes are associated with 'overexpression promoters', which are genetic elements that drive the overexpression of the protein far beyond the levels that are seen in the native organism. Both *E. coli* and *P. pastoris* are chemoheterotrophic, meaning they must eat other biological material to create their own biomolecules. This feature can be manipulated by feeding them isotopically enriched nutrients (such as ¹³C-labelled glucose or ¹⁵N-labelled ammonia) that they will ingest and incorporate into their proteins, DNA, etc. The biomolecules of interest can then be extracted from the organisms following cell lysis (breaking) and enriched or purified using biochemical chromatography techniques. At the end of the process, a biochemist can obtain large amounts of pure, isotopically enriched

biomolecules that can give way to strong NMR signals without the need for human tissue samples.

Recombinant protein expression and isotopic enrichment is one side of the coin for obtaining high-quality NMR spectra with good signal. The other side of the coin is the requirement for very strong and uniform magnetic fields (typically 6-18 Tesla). Modern NMR spectrometers can achieve magnetic fields of greater than (tesla; unit of magnetic field strength), which is approximately 300,000-1,000,000 times stronger the Earth's magnetic field (25-65 μT). These remarkably high magnetic field strengths are achieved using miles of supercooled coils of metal wires that are tightly wrapped within the device. The supercooled coils can then conduct impressive amounts of electricity, which results in the generation of a magnetic field in the center of the coil system. NMR samples can then be dropped into the core of the coil system where the magnetic field is the strongest and homogenous, and then electronic radio transmitters can be used to deliver the radiofrequency energies that excite and manipulate the magnetized nuclei. In short, NMR spectrometers are magnificent feats of electrical engineering consisting of hardware (coils and other physical parts) and electronic components (radio transmitters and detectors).¹⁹⁰

Stronger magnets have helped extend the practical uses of NMR to lower sensitivity systems such as larger proteins, but protein NMR was also made possible by the development of sophisticated radiofrequency programs, called pulse programs, that manipulate nuclear spin physics by perturbing the system using radiofrequency pulses, delays, and gradients. A robust understanding of spin physics is required to understand

or develop pulse programs, and their development has allowed NMR users to ask new questions and extract new types of information from their samples. For example, proteins are large biopolymeric molecules that have too many resonances in a 1-dimensional (1D) spectrum to discern which resonances belong to which atoms in the molecule. Therefore, 2-dimensional (2D) and multidimensional (nD, where n is usually 3 or 4) NMR experiments, such as those pioneered by Wüthrich *et al*, allow the user to deconvolute the p numerous and poorly dispersed resonances in a 1D protein NMR spectrum by splitting it into additional dimensions. A commonly used protein NMR experiment is a 2-dimensional heteronuclear single quantum coherence (2D HSQC) experiment, which manipulates how spins between two different covalently bonded nuclei (^1H - ^{15}N or ^1H - ^{13}C most commonly) to show only the resonances from the atomic pair of interest. In contrast to 1D NMR, where the x-axis is the PPM scale of a particular nucleus and the y-axis is the resonance intensity, HSQC NMR data typically shows one nucleus on the x-axis (such as ^1H) and the other nucleus (such as ^{15}N) on the y-axis, with the peak intensity shown on the z-axis as a topographical contour. The data presents as contour peaks, and in the case of a ^1H - ^{15}N HSQC experiment, each peak typically corresponds to a specific amino acid amide (N-H) on the protein backbone. In other words, a 100 amino acid protein would be expected to have approximately 100 peaks on the 2D ^1H - ^{15}N HSQC spectrum, with some exceptions. Although not a central issue for the topics of this thesis, it should be noted that as proteins get larger (more amino acids per protein), even 2D spectra become convoluted with overlapping peaks, such that more complicated multidimensional NMR experiments are required to resolve peaks.

The process of discerning which peaks correspond to which amino acids in a protein ^1H - ^{15}N HSQC is called 'resonance assignment'. Assigning a protein NMR spectrum can be an arduous task and can require several complicated multidimensional NMR experiments to accurately complete. Although I was formally trained in this process as a young graduate student, the NMR studies I will present in this thesis on C99, Notch, and other proteins were carried out with the benefit of having access to previously completed NMR spectral assignments that I inherited from my predecessors in the Sanders lab or obtained from the literature. Similarly, I want to acknowledge that all the NMR pulse programs that I used in my research were developed by others, and that my research would not have been possible without the giants upon whose shoulders I stood.

Observing protein-small molecule interactions by NMR

NMR spectroscopy is particularly well suited for probing thermodynamic and kinetic properties of molecular systems. Protein-small molecule interactions, as discussed in previous sections, are one of those types of systems for which NMR can provide useful insight. When chemical exchange (binding/unbinding) occurs between a protein and a ligand, NMR can provide information on the potency (K_D) and kinetics (off-rates vs. on-rates) of the molecular system. Furthermore, if the protein's NMR spectrum is assigned, binding events can be pinpointed to specific amino acid residues or structural regions of the protein involved in the interaction and/or conformational changes that result

from ligand binding. The ability of NMR to provide thermodynamic, kinetic, and structural information about chemical exchange makes it a highly desired technique for studying protein-small molecule interactions, as is central to drug discovery.

When a protein binds a ligand in a strong way (K_D is small, off-rate is low), the occupancy time of the ligand on the protein is long relative to the difference in free and bound resonance frequencies. When this happens, the NMR binding data is presented as 'slow exchange', such that both the free- and bound-resonances of the molecules are directly observed in the NMR spectrum (example shown later in **Figure 16**). As more ligand is added to the protein, the bound-state resonance increases in intensity and the free-state resonance decreases in a corresponding way until saturation (when all the proteins are fully bound by ligand). In contrast, if the binding is weak (typically microseconds or lesser occupancy times), chemical exchange is fast, such that the exchange rate is higher than the difference between the free and bound peak resonance frequencies. This results in what is known as 'fast exchange' on the NMR timescale, which results in peak averaging between the free- and bound-states of the protein (Example shown below in **Figure 15A**). This means that when a protein is titrated with a ligand, the observer can immediately gain insight on whether the molecular interaction is weak ($> 10 \mu\text{M } K_D$) or strong ($< 10 \mu\text{M } K_D$).

K_D values can be determined by NMR titrating in ligands against a constant concentration of protein (in which case it is usually the protein resonances that are monitored) or the reverse (where protein is varied; in which case it is often the ligand peaks that are observed). When ligand is added to the protein sample, in the case of fast

exchange conditions some or all the protein's NMR peaks will shift in response to complex formation (referred to as chemical shift perturbations or CSPs). For slow exchange, K_D values can be determined by monitoring the emergence of the bound-state peak or disappearance of the free-state, typically by calculating the peak integral (peak volume) or the peak height (peak maxima). For fast exchange binding, K_D values can be determined by monitoring a shift in the peak's resonance frequency as a function of the ligand titration. In either case, these perturbations in the NMR spectra are plotted as a function of ligand concentration. In an ideal 1:1 stoichiometric binding event, the curve will fit to a hyperbolic binding isotherm, where the concentration at which half of the protein is saturated with ligand corresponds to the K_D .

Another key structural experiment that can be used to confirm binding is the nuclear Overhauser effect spectroscopy (NOESY), which can detect through-space $1H-1H$ distances up to approximately 5Å (0.5 nm). When two nuclei are located within this distance range limit, the two produce a 'cross-peak' resonance. It is uncommon to use such an experiment to discover new ligands because it has intrinsically low sensitivity and experimental time is long (hours to days). However, this experiment is powerful for verifying an interaction between two molecules and can offer more structural information to add to HSQC-derived data. These types of data will also be presented in the data sections of this dissertation and will be further explained as they come.

This section elaborated on some of the NMR experiments and data types that will be presented in this document. NMR can be used to answer structural and thermodynamic questions for an array of recombinant proteins; however, where it really

fills a niche is for smaller proteins that are recalcitrant to other structural techniques such as X-ray crystallography. As discussed in previous sections, single-pass transmembrane receptors (SPTMRs) are protein candidates of this class, particularly for their transmembrane/juxtamembrane domains. The SPTMRs that are central to this thesis, such as C99 and Notch-1, are well-validated drug targets that I employ in my studies as models to study how small molecules interact with transmembrane domains and their enveloping membrane mimetics. The following section will focus on discussing how NMR has been used to investigate molecular interactions between small molecules and C99 and highlight the gaps in knowledge that that I tried to answer in my PhD studies.

C99 and Notch-1 are disease-relevant models for probing SPTMR-small molecule interactions

Chapter 1 of this document focused on the complexity of Alzheimer's disease and some of the key factors at play during disease progression. Specifically, I extensively discussed the roles that proteins such as the Amyloid Precursor Protein (APP), its C-terminal transmembrane 99-residue fragment (C99), the transmembrane protease complex γ -secretase (GS), and the plaque-forming product of C99 proteolysis by γ -secretase amyloid- β ($A\beta$) play in AD pathology, and how off-target effects of early generation γ -secretase inhibitors on Notch signaling was partially responsible for some clinical failures. This subchapter focused on discussing membrane systems, such as

detergent micelles and lipid bilayers, some of the transmembrane proteins that have been studied within them, and how they can be involved in human disease and targeted by drugs. The third subchapter was intended to briefly explain the NMR methodology that is central to the contents of this thesis and justify the use of NMR to answer the scientific questions that provoked this work. This final subchapter of the introduction will amalgamate the topics discussed so far and explain the gaps in knowledge that this work was designed to fill.

Regarding Alzheimer's disease, the relationship between amyloidogenesis and disease progression is subject to ongoing investigation. Drugs targeting A β generation by inhibiting β and γ -secretase, or anti-amyloid- β drugs targeting A β oligomerization and aggregation, have marked effects on reducing amyloid burden in the brain. However, despite their potent effects on clearing amyloid, these drugs typically have failed due to off-target effects, a lack of efficacy, or both. These results suggest that there is still more to the amyloidogenic pathway than we currently understand, such that novel ways to probe it are needed to help drive further scientific understanding.

The transmembrane C99 fragment of APP would be a useful amyloidogenic intermediate to target, as it is the immediate precursor to A β and is associated with a growing literature supporting its involvement in AD pathology (see Chapter 1). Furthermore, it belongs to the SPTMR class of proteins, which is a large family containing several proteins of pharmacological interest. For that reason, the focus of the studies presented in this dissertation are investigating what types of molecules can bind a single-pass transmembrane C99 domain, and with what potencies and specificities they do so.

This work was made possible by important advancements made by my predecessors in the Sanders lab, who in 2012, published the NMR-determined 3D structure of C99 in lysomyristoylphosphatidylglycerol (LMPG) micelles in the journal *Science*. Coupled to the structure, they determined that certain residues in the transmembrane domain of C99 are involved in forming a direct 1:1 complex with cholesterol, proving the concept that this protein could associate with small molecules. There is significant evidence that cholesterol promotes amyloidogenic processing of APP. Beyond the discovery that C99 binds cholesterol, other work carried out by predecessors in the lab produced preliminary evidence that C99 bound to other sterol analogs, although that data has not yet been published. These observations begged a new question: could other small molecules bind C99 and perhaps shift it away from amyloidogenic processing by, for example, occluding it from the γ -secretase active site or another mechanism? Taken together, these studies and these concepts were foundational for establishing the early question of this thesis, which was: “can we discover small molecules that could bind C99 and function as substrate-selective inhibitor of γ -secretase, sparing the proteolysis of other known γ -secretase substrates?”

To start answering this question, we first had to design a high throughput pipeline to screen small molecule libraries. To do this, we optimized an NMR-based high-throughput screening program that produced high quality and reproducible C99 NMR spectra in very short times. The process of optimizing this pipeline is the theme of Chapter 3 of this document. Upon screening a library of FDA-approved small molecules, I discovered that a small molecule called verteporfin binds C99. We also rigorously tested the strength, breadth, and specificity of the compound and biochemical effects it had on

γ -secretase processing of C99 and Notch, which are the general theme of Chapter 4. Chapter 5 describes the findings from a high throughput screen of the locally curated Fesik Fragment Library, which is a structurally diverse library of small molecule fragments. From this screen, we discovered several classes of small molecules that non-specifically bind transmembrane proteins in the screening detergent, LMPG. Ongoing investigations are presented in Chapter 6 in the Future Directions and Preliminary Results subsections.

Chapter 3

Development of an NMR-based high-throughput screen amenable to single-pass transmembrane proteins

Introduction

Previous work from the Sanders lab left the C99 project in a good position for high throughput development. Modeled off pioneering work from our scientific collaborator Dr. Stephen W. Fesik, who uses high throughput NMR to discover small molecule ligands bind to water-soluble proteins, we began to optimize an analogous screen amenable to recalcitrant single-pass transmembrane proteins using C99 as a model. The Fesik Fragment library is a small molecule repository of approximately 15,000 small molecule fragments that are available at Vanderbilt University. These compounds are 'rule of three' compliant, meaning they have drug-like pharmacological properties and serve as building blocks for larger drug-like molecules. The Fesik lab at Vanderbilt specializes in a technique called Fragment-based Drug Discovery (FBDD), which uses small drug-like fragments to thoroughly screen through chemical space using a relatively small number of structurally diverse molecules.

In the classical FBDD approach, one would screen through the library in search of at least two binders that occupy close but distinct pockets on the protein target. While it does help if the binders have strong affinities for the target, it is not essential because their affinities will be optimized and partially summed using medicinal chemistry

and combinatorial chemistry to link them. As discussed in a classic review written in part by Dr. Fesik, FBDD coupled to medicinal and combinatorial chemistry has had a strong record of developing relatively weak ligands ($>100 \mu\text{M } K_D$) into highly potent drug like molecules with orders of magnitude tighter affinity for the target.¹⁹³ Notably, Venetoclax, an FDA-approved small molecule for treatment of certain blood cancers, is a product of an initial fragment discovered in an NMR-based FBDD screen. Due to the advanced state of C99 NMR studies in the Sanders lab, and availability of both the Fesik Fragment Library and of Dr. Fesik himself here at Vanderbilt, beginning our screens with this type of library seemed a logical first step into the drug discovery targeting single-pass TM proteins.

This chapter focuses on the repurposing of protocols established by the Fesik lab and further development for our specific purposes on C99. This work was achievable by significant consultation with Kelvin Luong, who was a graduate student in the Fesik lab. In general, this methods development chapter can be split into two main sections: 1) optimizing C99 expression/purification protocols and NMR parameters for screening, and 2) running an initial test run of 1,152 small molecules from a Fesik Fragment Library plate to verify the protocol was working. Here, I describe the methodology we optimized and the results from the preliminary verification screen.

Results

Yield and NMR parameter optimization for C99 screening

I inherited a relatively advanced protocol for C99 expression and purification

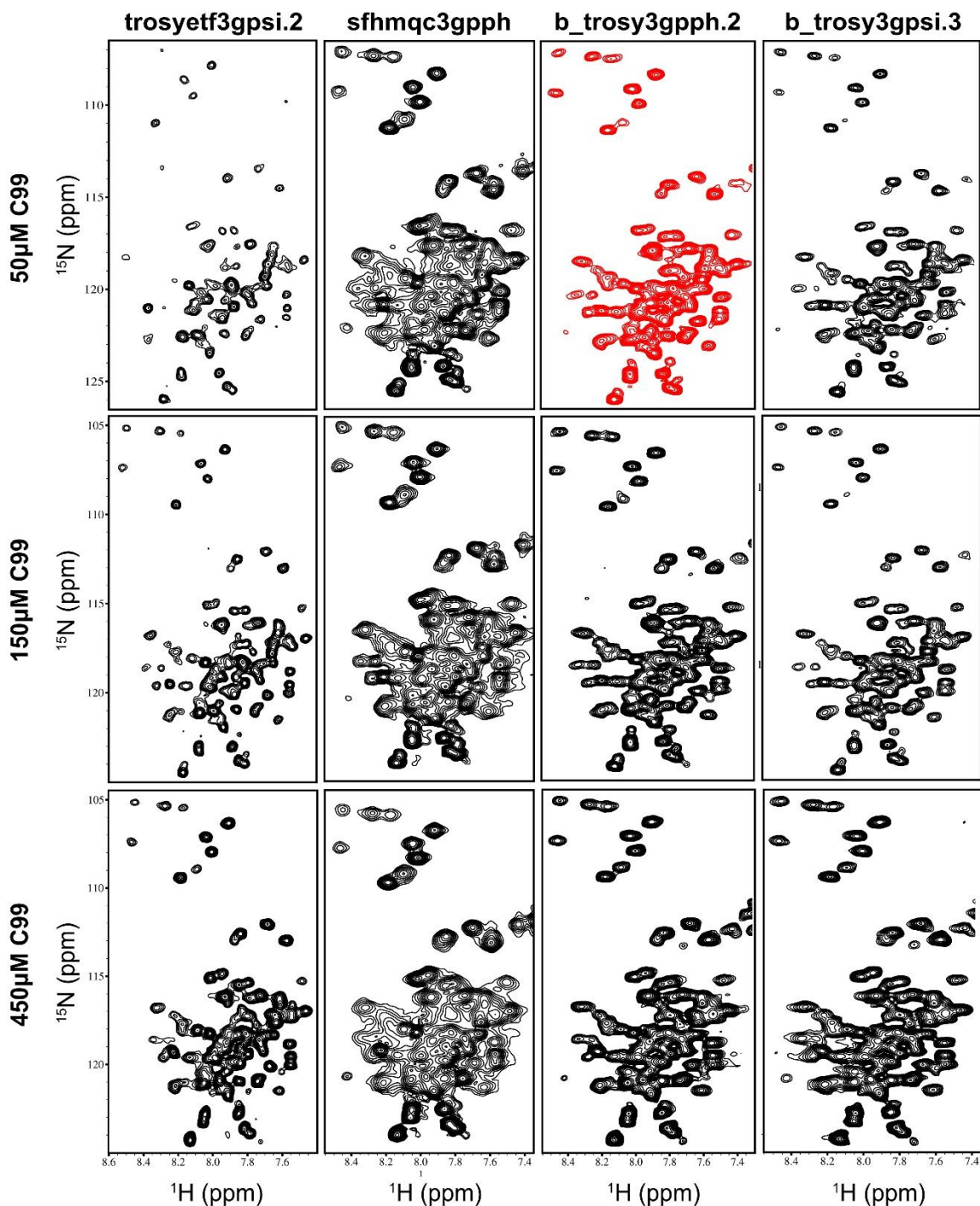


Figure 10. *Pulse program optimization for C99 screening.* Shown here are ^{15}N -labelled C99 spectra in LMPG using four different pulse programs and 3 different protein concentrations. At the 50 μM point, the BEST-TROSY-2 (b_trosy3gpph.2; in red) program gave way to the best signal-to-noise and resolution at the low concentration. For most of the work presented in thesis, that concentration and program will be used.

from recombinant *E. coli* culture, which was used to purify the C99 used in several of the previous manuscripts from the Sanders lab. That protocol was revamped by me and my colleague J. M. Hutchison to increase the inclusion body extraction efficiency, which resulted in higher final yields of purified protein. Details of this protocol are in the methods section below. Generally, yields were between 5-10 mg of >95% pure C99 per liter of isotopically labelled (^{15}N) M9 minimal media culture. To maintain simplicity and consistency with past C99 work, we continued using imidazole NMR buffer (IMD NMR Buffer) with LMPG detergent as the membrane mimetic. This sample condition was suitable for collection of high-quality NMR spectra in previous years and C99 was stable for weeks in this condition with no visible signs of aggregation or precipitation.

High throughput screening pipelines require a maximally efficient data quality to data acquisition time ratio. To find this optimized point, we tested several expedited 2D ^{15}N - ^1H NMR experiments at matched acquisition times to evaluate which would give the highest quality HSQC spectrum of C99. These included a SOFAST-HMQC program (sfmhqcf3gpqh), two BEST-TROSY programs (b_trosetf3gpsi.3 and b_trosetf3gpqh.2), and the canonical TROSY-HSQC program (trosetf3gpsi.2) that is commonly used in the Sanders lab. During equal acquisition times, the traditional TROSY-HSQC by-in-large produced the worst NMR spectra over the course of the 30-minute experiment, with markedly inadequate signal-to-noise. The SOFAST-HMQC produced the highest signal-to-noise data during the same experiment time, however it lacked in spectral resolution leading to broad peaks with significant overlap and making it difficult to use. BEST-TROSY-2 (b_trosetf3gpqh.2) was a happy medium of useful signal-to-noise and spectral resolution compared to the other three, so we continued optimizing

conditions for this experiment. (**Figure 10**). To optimize for screening of thousands of high throughput samples, we had to produce the best NMR spectra with the least amount of protein possible. We tested several C99 concentrations from 50-450 μM C99 at constant 20% w/v LMPG to identify the lowest necessary protein molarity to produce a sufficiently strong NMR spectrum. Remarkably, we found that the signal-to-noise at 50 μM was satisfactory during a total experiment time of 30 minutes. (**Figure 10**). Impressively, 50 μM C99 samples would allow us to create approximately an entire screen plate worth (96) of 200 μL NMR samples from 12 L worth of M9 *E. coli* cell pellet. Considering the spectral quality was sufficient and the need for manual labor (such as protein expression and purification) would be reduced, we proceeded with this concentration.

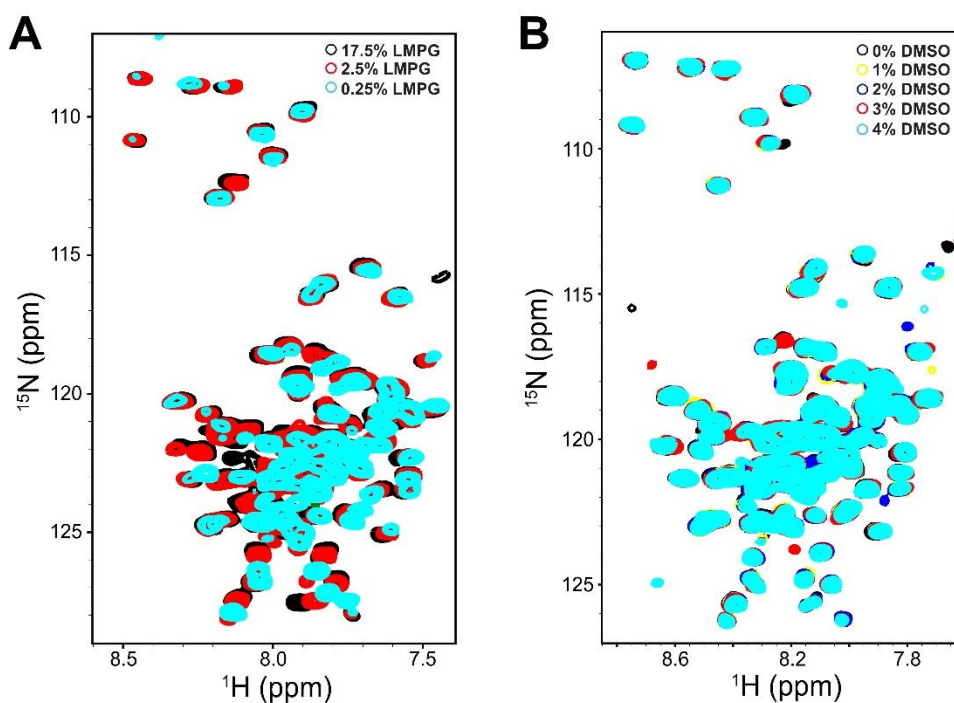


Figure 11. *LMPG and DMSO concentration optimization for C99 screening.* **A)** Three overlaid spectra of ^{15}N -labelled C99 at different LMPG concentrations. Overall, C99 spectra looked similar at 2.5% w/v and 17.5% w/v concentrations, but looks markedly worse at the lower 0.25% w/v point. This suggested that higher levels of detergent would provide higher quality NMR spectra than lower. **B)** Five overlaid C99 spectra at DMSO concentrations ranging from 0% to 4% v/v. Overall, DMSO had very little effect on C99 spectral quality, suggesting it was resistant to the 'DMSO effect'.

We next sought to minimize the LPMG (detergent) concentration to characterize what minimum concentration of LPMG would be sufficient to avoid the cohabitation (forced colocalization) of multiple C99 molecules in one LPMG micelle. This is a feature common to membrane proteins when protein:micelle ratios are high and they have intrinsic properties of self-oligomerization (as C99 does). Considering that we wanted to screen against the monomer form of C99, we had to have a sufficiently high C99:micelle ratio, so we tested LPMG bulk concentrations of 0.25% w/v (approximately 5.2 mM bulk detergent; 0.08 mM micelle), 2.5% w/v (approximately 52 mM bulk detergent; 0.8 mM micelle), and 17.5% w/v (approximately 364 mM bulk detergent; 5.6 mM micelle). The micelle concentration was determined using the published LPMG aggregation number of 65 molecules per micelle.¹⁹⁴ NMR spectral quality was relatively poor at 0.25% LPMG, but was significantly improved by 2.5%, and remained largely identical to the 2.5% sample at 17.5% (**Figure 11A**). Since 2.5% LPMG meant we had approximately 0.8 mM (800 μ M) micelles and our working concentration of protein was 50 μ M, the protein:micelle ratio would be 1:16. Taken together, the NMR spectra of C99 was sufficient at 50 μ M and the protein:micelle ratio at 2.5% LPMG was high enough that C99 molecules would usually not cohabitate micelles with other C99 molecules. We therefore used these conditions for most of the high throughput screens discussed later.

The final condition we wanted to explore was the limit of acceptable DMSO concentrations before C99 spectra were perturbed. Most of the compounds screened in this thesis were dissolved in a DMSO vehicle, and we wanted to eliminate any spectral effects that would arise from the 'DMSO effect'. We tested DMSO concentrations from 0% to 4% v/v at the constant C99:LPMG micelle ratio discussed previously. We found

that C99 was quite tolerant to DMSO up to 4% v/v, with only marginal shifts observed, primarily for peaks from solvent-exposed parts of the protein (**Figure 11B**). At a constant DMSO concentration (4% v/v), three replicate samples revealed that C99 spectra were reproducible and suggested DMSO would not be a problem vehicle during screening. With that reasoning in mind, we continued to attempt our first try at a screen plate using the discussed conditions.

Another point that should be covered regarding the screening conditions was the type and concentration of buffer. All the early screens that I conducted, were carried out in imidazole NMR buffer, which contained 25 mM Imidazole, 100 mM NaCl, and 0.5 mM EDTA at pH 6.5. While imidazole is a good buffer at that pH, peak overlap from its protons even at 25 mM with protein amide resonances at high concentration provide problematic. This was particularly true for the Fesik Fragment Library, where the relatively high concentrations of fragments with acidic or basic groups could significantly alter the pH of the sample with only 25 mM buffer. This led to me eventually swap from using imidazole to PIPES buffer (50 mM PIPES, 100 mM NaCl, and 0.5 mM EDTA at pH 6.5). PIPES enabled use of a sufficient buffer concentration without introducing peaks that overlap with key C99 resonances. The final point I want to cover in this section is that this screening protocol is amenable to use for either 3 mm or 5 mm NMR tubes, which use 200 μ L or 500 μ L of sample volume, respectively. This is important because tubes could be selected based on the protein/compound requirement to achieve the desired final concentrations or the distribution layout of the prospective compound library. For example, the entire FDA-approved drug library was screened using 3 mm NMR tubes because we could only access 1 μ L of 10 mM FDA-approved drug and we wanted to

maximize drug concentration by using lower total sample volumes. Inversely, the entire Fesik Fragment library was screened using 5 mm NMR tubes because the fragments were effectively unlimited for our purposes, and 5 mm NMR tubes produced C99 NMR spectra with significantly higher signal-to-noise. The major advantage to using 3 mm tubes was they used less total sample volume, such that approximately 0.14 mg of C99 (2.5 times less protein than 5 mm tubes) was required to achieve the desired 50 μ M final concentration at 200 μ L final sample volume and still produced usable signal-to-noise, albeit the intensity of C99 resonances was markedly lower. On the contrary, 50 μ M protein in a 5 mm tube required 0.35 mg of C99 in 500 μ L but produced significantly stronger NMR signal intensities due to the increased number of total molecules (N) present in the spectrometer window. For our C99 system, either tube was suitable because protein quantity was not a rate limiting step for the screening. However, should protein quantity be the rate limiter in a prospective screening project, I would suggest using 3 mm tubes.

Results of an initial test screen using a Fesik Fragment Library mixture plate

The initial plate we screened was from the Fesik Fragment Library, mixture plate 2 (for plate barcodes and compound identifiers, refer to Materials and Methods). This plate contained 96 wells of compound mixtures, with 12 compounds per well for a total of 1152 compounds in the plate. Most of the wells did not have any obvious signs of C99 spectral perturbation; however, one well gave rise to obvious shifts in C99 transmembrane residues A713-L723 (**Figure 12A/B**). This mixture well was then deconvoluted into mixtures of three, then individual compounds to reveal the causative agent. The compound producing these shifts was found to be 2-(4-fluorophenyl)-5-propyl-4*H*-pyrazol-3-one, designated VU0410776 (VUx76 for short; shown in insert in **Figure 12A**). Interestingly, this compound demonstrated a slow-exchange binding on the NMR timescale, suggesting that the complex with C99 was tight and long-lived. However,

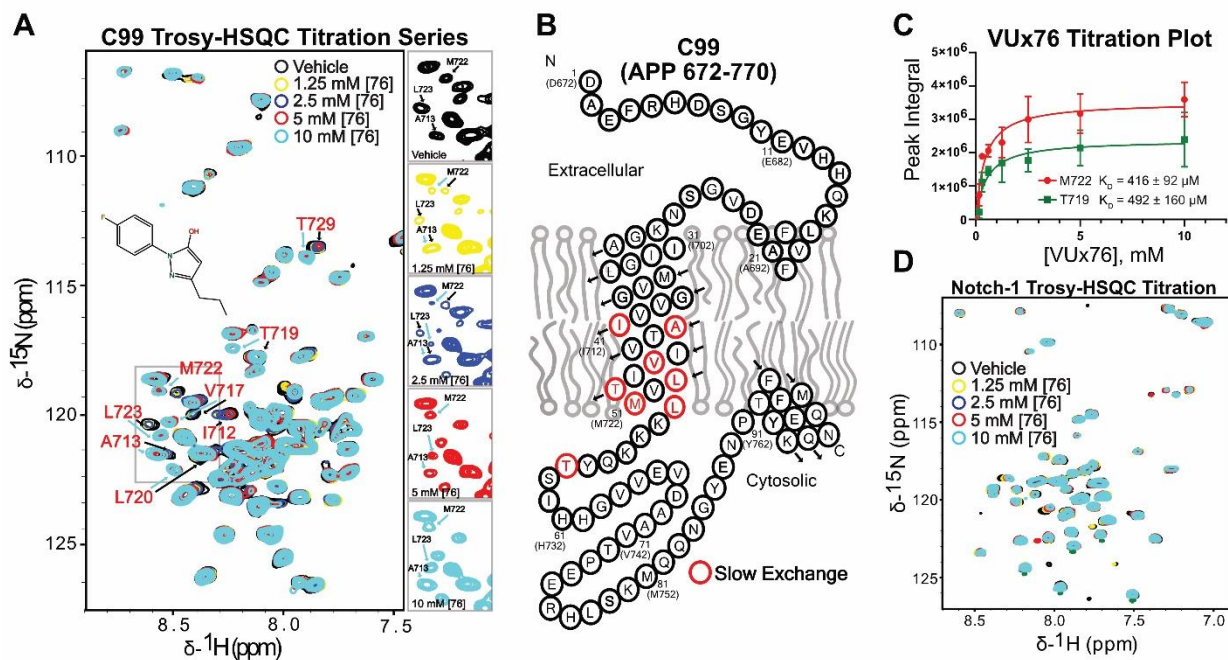


Figure 12. *1st hit compound: the discovery that VU0410776 is a C99 binder.* **A)** Five overlaid ^{15}N -C99 spectra at varying [VU0410776] concentrations reveals slow exchanging peaks upon compound addition. **B)** Shifting peaks map to C-terminal transmembrane/juxtamembrane region of C99 sequence. **C)** Binding isotherm of the emerging peak integral of the C99 bound-state vs. [VU0410776] concentration. **D)** Notch-1 TM/JM titration with [VU0410776] reveals non-specific, fast-exchange interactions that do not saturate.

titration of this compound revealed only modest K_D values of $\sim 400 \mu\text{M}$ when monitoring the peak volume of the emerging bound-state resonance (**Figure 12C**). We then also tested this compound for non-specific binding against Notch-1 TM/JM in the same conditions (**Figure 12D**). We found that while this compound did indeed shift some Notch resonances, they were in the fast-exchange timescale and did not saturate binding, confirming that the interaction with Notch was much weaker than for C99 and likely non-specific. On top of confirming that this screening method would likely discover some C99 binders, it was foreboding that we would also find several non-specific membrane binders that appear to interact non-specifically with the Notch-1 control embedded in the membrane mimetic. The discovery of such molecules and characterizing their properties is the major thesis of Chapter 4 in this dissertation.

Beyond this one compound, VUx76, it seemed notable that the rest of the wells examined in our preliminary study (1152 total compounds) did not give rise to titratable hit compounds. This meant that the hit-rate for a screen of this type, if extrapolated from this sample, would produce 1 hit compound out of 1152, or an approximate 0.1% hit rate. While this rate appeared low, it suggested that any hits that would be found by further screening were likely true positives. This established the precedent for the potential success of this work, providing my first evidence that non-sterol/non-lipid small molecules could form specific, titratable interactions with a single-pass transmembrane domain such as C99.

Discussion

The initial screen of a single Fesik Fragment Library plate (1152 compounds) revealed a small molecule fragment that bound C99 in its transmembrane/jxtamembrane region with 400 μM K_D . The weak K_D value, which was calculated by measuring the peak volume of the bound-state resonance, was surprising for a slow-exchanging event. As explained in the introduction of the thesis, slow exchange on the NMR timescale is typical for tight binding ($<10 \mu\text{M}$ K_D), and it puzzles me as to why it was seen for an observed K_D values of 400 μM . However, this type of phenomenon is not entirely unexpected for a membrane system, as the interaction could be diffusion limited due to membrane binding, resulting in slow-exchange behavior. I am still currently attempting to parse out why this phenomenon was observed, so the deconvolution of this problem, which includes SAR by NMR, protein mutagenesis, and mass spectrometry, is presented in greater detail in the Future Directions of this thesis under the Exploration of the Phenazone Fragment subsection.

Regardless of the exchange phenomenon, it was clear that this method would be able to detect C99 binders and we had estimated a preliminary hit rate of 0.1%. After these initial experiments, the project temporarily shifted direction towards screening an entirely different library of small molecules. We postulated that the fragments were unlikely to result in tight binders since they were so-called molecular fragments offering limited chemical contacts and would likely require significant medicinal chemistry to develop further. Before returning to complete screening of the FBDD library (see Chapter

5), we decided to screen the available SelleckChem library of FDA-approved drugs. This library harbored approximately 1,200 small molecules that were approved as of 2018, meaning they were both efficacious for treating their respective ailments and importantly, safe for use in preclinical and clinical settings. The next chapter of this document will describe the minor alterations of this high throughput pipeline to adapt it for that library, and the discovery of a macrocyclic small molecule verteporfin that specifically bound C99 and was a Notch-1 sparing γ -secretase inhibitor. We then will return to the FBDD fragment library.

Chapter 4

The FDA-approved drug verтеporfin is a substrate-selective γ -secretase inhibitor that binds the Amyloid Precursor Protein transmembrane domain²

Introduction

The *APP* gene encodes the amyloid precursor protein (APP), a single-span membrane protein implicated in neurological development, axon guidance, learning and memory, and general neuronal homeostasis.^{22-23, 195} Heritable mutations affecting the *APP* gene were the first to be discovered to cause Alzheimer's disease (AD).^{10, 21, 196} Gene-duplication of *APP* as well as a number of missense mutations in *APP* found in and around the region encoding the amyloid- β (A β) domain are associated with inherited forms of AD.^{28, 30, 195, 197-198}

Historically, these associations between genetics and AD have been thought to be the consequences of toxic oligomer and amyloid fibril formation by A β polypeptides released after successive proteolysis of APP by the β - and γ -secretase proteases (**Figure 13A**).^{197, 199-200} These proteolytic events and the subsequent aggregation of A β —referred to as “the amyloidogenic pathway”—have been extensively targeted pharmacologically.^{5, 201} However, previous clinical trials of inhibitors of γ -

² This work is published in: Castro, M. A., *et al.* (2022). Verтеporfin is a substrate-selective γ -secretase inhibitor that binds the Amyloid Precursor Protein transmembrane domain. *Journal of Biological Chemistry*, Article 101792

secretase have failed, in large part due to toxicity associated with lack of substrate-specific inhibition of γ -secretase, which has many dozens of substrates.^{36, 202} Particularly notable is toxicity resulting from inhibition of Notch-1 cleavage, which disrupts essential signaling from this receptor.^{155, 203} In this paper, we describe our efforts to find compounds that act as substrate-selective γ -secretase inhibitors. Specifically, we sought to discover compounds that inhibit cleavage of C99—the product of APP cleavage by β -secretase and the immediate precursor of A β , while at the same time allowing Notch cleavage by γ -secretase to proceed uninhibited.

In addition to their potential utility in reducing A β production, compounds that inhibit C99 cleavage would be valuable tool compounds for studying C99 biology. Intact C99 may be directly involved in some of the cellular pathologies associated with

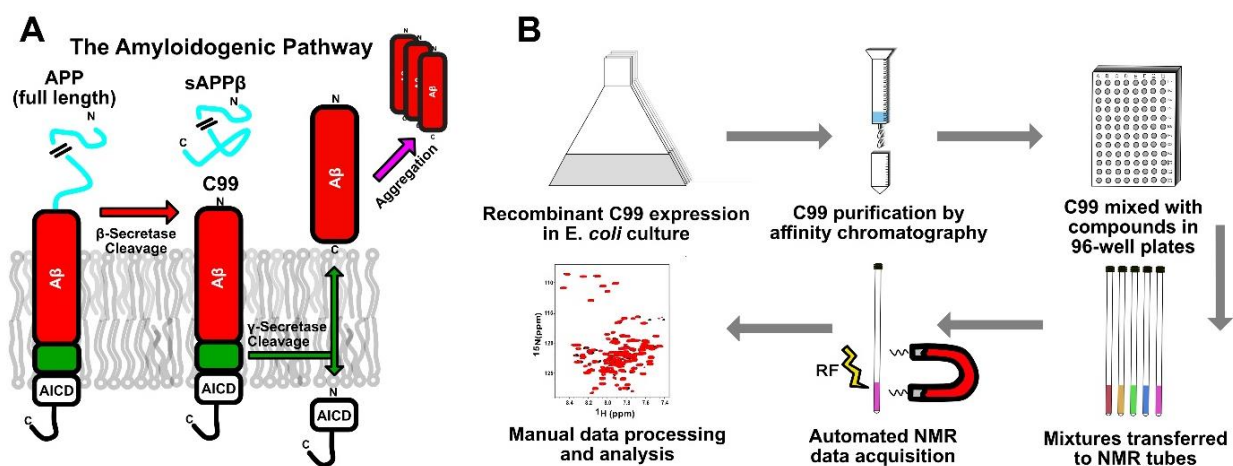


Figure 13. *The amyloidogenic pathway and our screening workflow for compounds that bind to the C99 protein.* **A**) A β amyloidogenesis begins with proteolysis of the full-length amyloid precursor protein (APP) by β -secretase, liberating the soluble extracellular domain (sAPP β) and the transmembrane 99 residue C-terminal (C99) domain. C99 is then further proteolyzed by the γ -secretase complex in its transmembrane domain, generating both the amyloid intracellular domain (AICD) and A β , the latter of which can then go on to form A β oligomers and amyloid plaques. **B**) For high-throughput C99 screening, C99 is expressed in *E. coli* cultured in ^{15}N isotopically-enriched media and purified from cells by affinity chromatography into detergent micelle solutions suitable for solution NMR spectroscopy. The protein in NMR conditions is then mixed with small molecule binding candidates (in DMSO) in 96-well plates and transferred to an NMR tube. NMR data is collected and then processed and analyzed. Standard NMR sample conditions are: 200 μl of 50 μM C99 in 2.5% w/w LMPG, 50 mM PIPES, 100 mM NaCl, 0.5 mM EDTA, pH 6.5, 318 $^\circ\text{K}$ (45 $^\circ\text{C}$) and 50 μM of the test compound, all in a 3 mm NMR tube.

AD, such as defects in mitophagy, autophagy, mitochondrial structure, bioenergetics, lipid homeostasis, and AD-model animal behavior.^{107, 158, 161-162, 165, 204-205} These discoveries suggest that C99 is itself directly involved in AD pathogenesis. Thus, a C99-specific binder that selectively inhibits its degradation would be a useful tool for further investigating the relationship between C99 and AD.

We are not the first to consider the concept of substrate-selective modulators of amyloidogenesis.²⁰⁶⁻²⁰⁹ Indeed, “Notch-sparing” modulators of γ -secretase that bind directly to the enzyme have been reported in the literature, with one entering clinical trials.²¹⁰ This compound, however, possessed questionable selectivity for C99²¹¹ and caused toxicities due to suppression of Notch cleavage at higher doses.¹⁵⁴ Moreover, some compounds initially reported to selectively modulate C99 cleavage by binding free C99²⁰⁶ were later shown NOT to bind free C99, but instead act by interacting directly with γ -secretase, perhaps cooperatively with C99-dependent binding.²¹²⁻²¹⁶ Another group reported the discovery of benzofuran compounds that appear to bind full-length APP and inhibited its proteolysis by γ -secretase.²⁰⁹ Studies such as these motivated this study to further explore this substrate-directed inhibitory approach.

Here, we report the results of our search for compounds that act by specifically binding to the C99 substrate rather than by targeting the protease itself. We describe the discovery that the porphyrin-based drug verteporfin directly binds C99 in model membranes to form a 1:1 complex with a K_D of ca. 17 μ M. Moreover, verteporfin inhibits γ -secretase cleavage of C99 at concentrations where it does not inhibit Notch cleavage.

RESULTS

Optimization of conditions for screening for small molecules that bind C99. We previously determined the 3D structure of monodisperse C99 in model membranes using solution nuclear magnetic resonance (NMR) spectroscopy (PDB: 2LP1).²¹⁷ Previous studies from our lab established that NMR can be used to detect and characterize the interactions of C99 both with small molecules such as cholesterol and with other proteins.^{212, 217-220} We therefore set out to screen a library of 1184 FDA-approved drugs using NMR to detect C99-binders and then to exhaustively validate binding and to determine the binding affinity, as outlined in **Figure 13**.

Before initiation of the screen, various NMR conditions such as the C99 protein concentration, detergent concentration, tolerable concentration of DMSO (vehicle), and NMR pulse programs/parameters were explored. While several conditions produced high-quality NMR spectra, we settled on screening conditions consisting of 50 μ M C99 in 2.5% w/v (52 mM) lyso-myristoylphosphatidylglycerol (LMPG) micelles at pH 6.5, with NMR spectra being acquired using the BEST-TROSY pulse sequence.²²¹⁻²²² These conditions were similar those used in our previous determination of the structure of C99.²¹⁷ Nearly all C99 resonances exhibited satisfactory signal-to-noise even at 50 μ M protein concentration and using a short data acquisition time (35 minutes, **Figure 14A**).

This approach enabled the screening of all 1184 samples in 36 days with the assistance of a Bruker SampleJet automated sample changer.

Initial Hits from FDA-approved Drug Screen

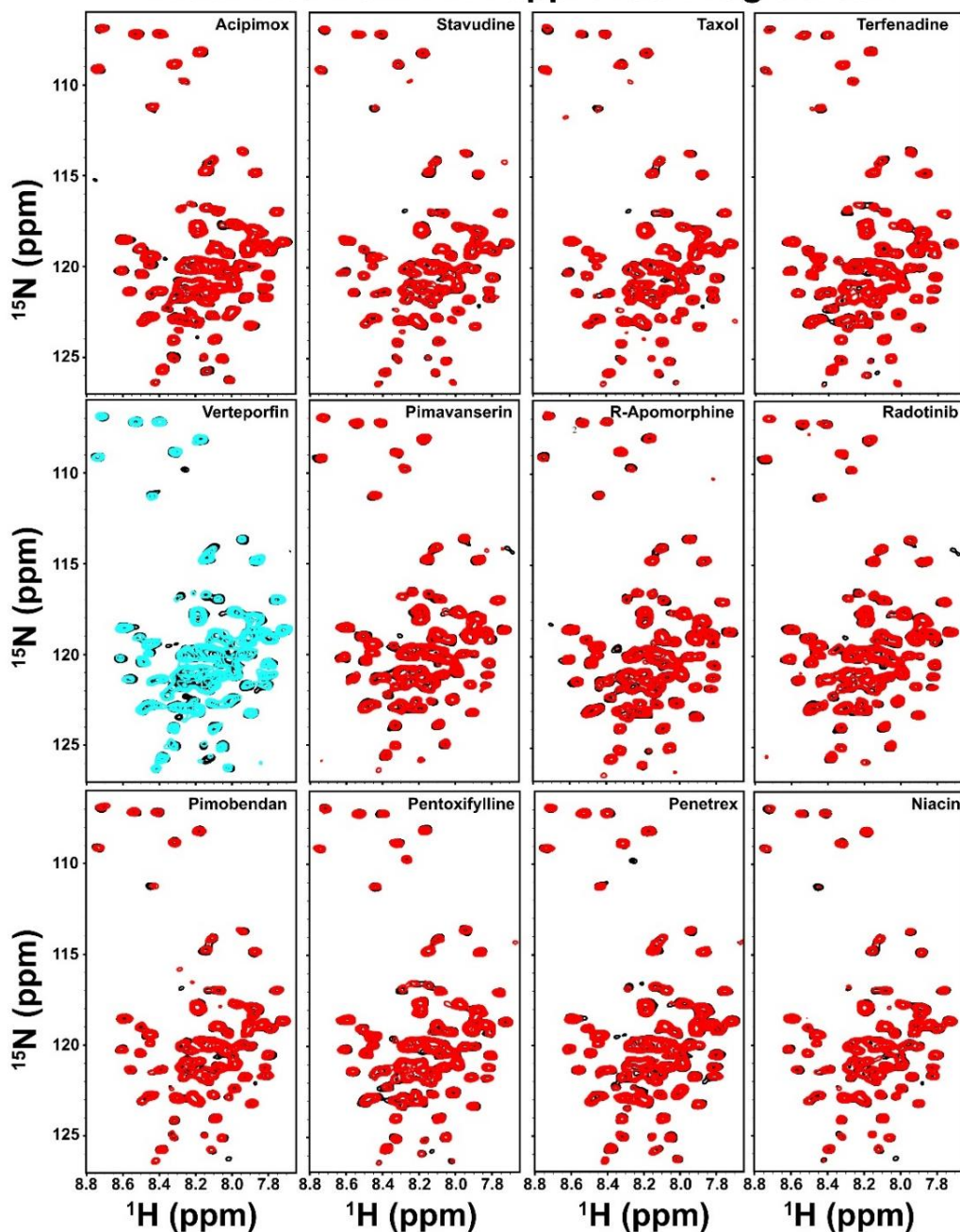


Figure 14. TROSY NMR spectral overlays of representative initial hit spectra from primary screen. Spectra for hit compound-containing samples are shown in red, overlaid onto the vehicle control (DMSO) spectrum in black. Initial hits were recognized based on chemical shift perturbations at one or several C99 residues. The initial NMR screen of approximately 1,200 compounds produced 20 hits that were followed-up on (12 shown here). Verteporfin (cyan spectrum) was seen to induce spectral

Verteporfin binds C99 avidly, but not Notch-1. Using the optimized conditions described above, we completed a screen of the available SelleckChemical library of FDA-approved drugs. We identified 20 compounds as potential hits based on the observation that 50 μM concentrations of these compounds perturbed the resonances of 50 μM C99 (**Figure 14**). Of these 20 compounds only verteporfin yielded results that stood out when C99 was subjected to a titration by each compound. Specifically, only verteporfin led to changes in the positions of C99 peaks during titration that were seen to saturate at sub-millimolar concentrations. Chemical shift perturbations were observed in TROSY amide backbone NH resonances from multiple C99 peaks, most arising from sites in and around

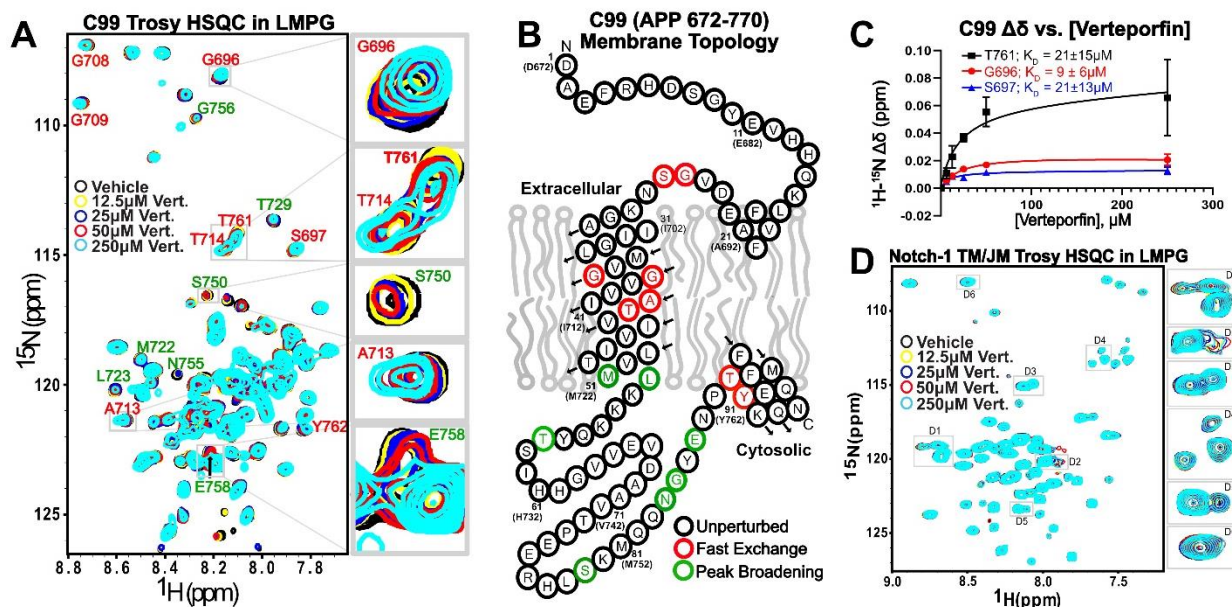


Figure 15. *Verteporfin binds C99 in LMPG micelles and does not bind to the Notch-1 TM/JM.* **A)** Five overlaid C99 TROSY NMR spectra of C99 with varying concentrations of verteporfin. **B)** C99 topology diagram highlighting residues that undergo perturbations in response to verteporfin binding. Sample conditions: 50 μM C99 in 50 mM PIPES buffer, 100 mM NaCl, 0.5 mM EDTA, 2.5% w/v LMPG, pH 6.5, 318 K, 3 mm NMR tube. **C)** Plotted chemical shift perturbations for the titration summarized in panel A. The average result of three replicate experiments were fit by a 1:1 binding model. Error bars indicate the standard error of the mean (SEM). **D)** TROSY spectral overlay for the Notch-1 TM/JM domain at varying concentrations of verteporfin. For more direct comparison with selected peaks in the C99 data (insets to panel A), peaks are highlighted in insets D1-D6, showing the minimal spectral perturbations seen for Notch in response to verteporfin treatment. The data shown in D have also been collected in 3 technical replicates.

the transmembrane domain and amphipathic C-helix (**Figure 15A** and **15B**). For experiments in LMPG micelles, fits of the 1:1 binding model to the titration traces from multiple different peaks (**Figure 15C**) led to determination of an average dissociation constant (K_D) of $17 \pm 11 \mu\text{M}$ across multiple residues in and around the TM domain. The presence of both fast and slow-exchanging resonances is consistent with the determined micromolar K_D value. Peaks that undergo large changes in resonance frequency upon complex formation fall in the slow exchange regime, where both complexed and free protein peaks are directly observed. Peaks that undergo smaller changes in frequency upon complex formation were in the fast exchange regime, where only a single peak is observed at a population-weighted average frequency between the free and fully complexed peak frequency limits.

We have previously used NMR to characterize the structure of the Notch-1 transmembrane domain flanked by its juxtamembrane segments (residues 1721-1771, "Notch-1 TM/JM").²²³ Titration of Notch-1 TM/JM by verteporfin in LMPG micelles under the same conditions as used for the titration of C99 revealed only minor perturbations of Notch resonances in response to increasing levels of verteporfin (**Figure 15D**). That there are minor verteporfin-induced shifts that are small and must less extensively seen than for C99 is not surprising in light of data shown below that verteporfin does bind non-specifically to micelles. Overall, these NMR titration results indicate that verteporfin binds C99 but not Notch-1.

Verteporfin binds to C99 in other membrane mimetics. To confirm that binding of verteporfin to C99 is not highly dependent on the nature of the membrane mimetic in which C99 is solubilized, we repeated TROSY-monitored titrations of C99 in two model membrane systems that differ in important ways from anionic LMPG micelles: (1) *zwitterionic* bicelles composed of 3:1 (mol:mol, $q = 0.33$) dihexanoylphosphatidylcholine (D6PC):dimyristoylphosphatidylcholine (DMPC) and (2) *non-ionic* beta-dodecylmelibiose (DDMB) micelles. NMR titration of C99 in D6PC-DMPC bicelles by verteporfin revealed

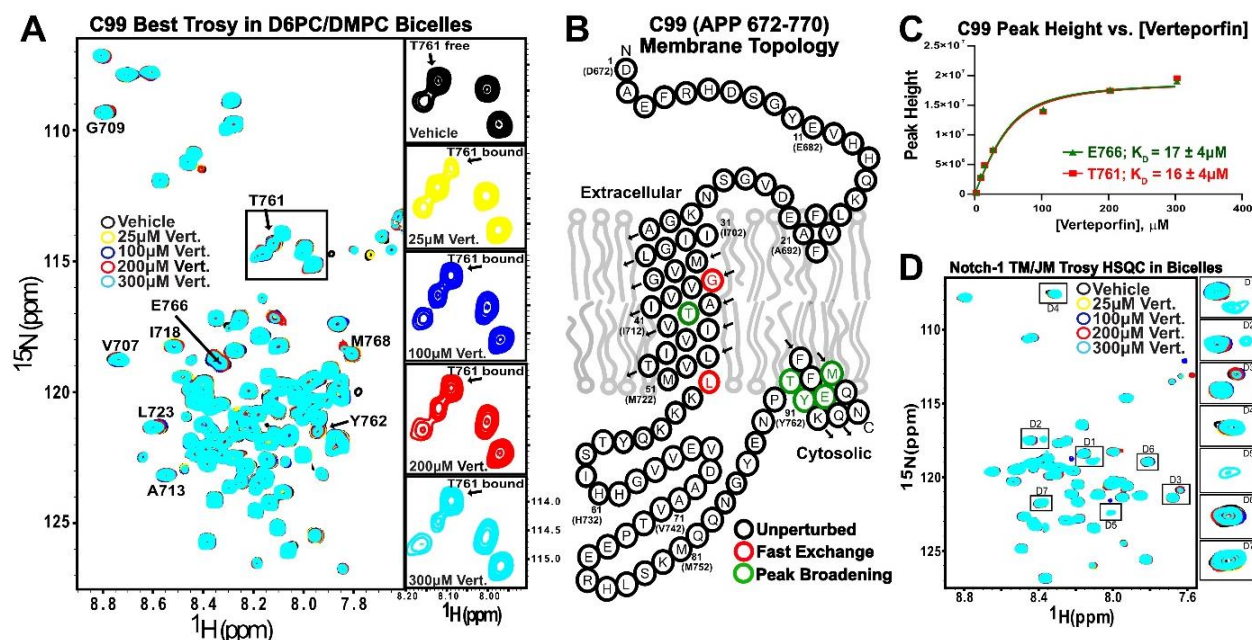


Figure 16. *Verteporfin binds C99 in D6PC/DMPC ($q=0.33$) bicelles with an observed K_D of $17 \pm 4 \mu\text{M}$, whereas verteporfin does not bind the Notch-1 TM/JM.* **A)** Five overlaid C99 TROSY NMR spectra of C99 at varying concentrations of verteporfin. The central insert zooms in on the boxed region near T761, and shows a new peak appearing in response to increasing verteporfin concentrations. The sub-panels to the right illustrate the individual spectra of the T761 peak from the titration series. The free (0 M verteporfin) resonance of T761 disappears as the new bound state T761 resonance appears nearby in a verteporfin-dependent manner. **B)** Topology plot for C99, highlighting sites for which verteporfin binding induced either gradual (fast exchange) changes in peak positions or the slow exchange disappearance of free protein peaks in concert with the appearance of the corresponding complexed-protein peaks. **C)** Plotted chemical shift perturbations for two peaks from the titration shown in panel A. K_D values were derived from fitting these data to the 1-site binding model, where error values were derived from the error of the fit. **D)** TROSY spectral overlay for the Notch-1 TM/JM at varying concentrations of verteporfin in bicelles, indicating that verteporfin does not bind to Notch-1. It is worth noting that spectral perturbations are noticeable at 300 μM verteporfin, which are shown as insets D1-D7. However, these weak effects are likely due to non-specific perturbation of the membrane mimetic. Data shown in this figure are $n=1$, and the error shown in panel C are the errors of the fit.

both fast- and slow-exchange perturbations, similar to what was observed in LMPG (Figure 16A). The perturbed residues (regardless of NMR exchange regime) mainly mapped to the transmembrane and amphipathic C-helix residues (Figure 16B). Fitting of two of the titration curves revealed K_D of $17 \pm 4 \mu\text{M}$ and K_D of $16 \pm 4 \mu\text{M}$, corroborating well with what was seen in LMPG micelles (Figure 16C). A corresponding titration of the Notch-1 juxtamembrane/transmembrane domain in micelles by verteporfin again revealed only minor spectral changes at very high concentrations that are much less extensive than seen for C99 and likely arise from effects related to non-specific binding of verteporfin to the protein-containing micelles and bicelles (Figure 16D).

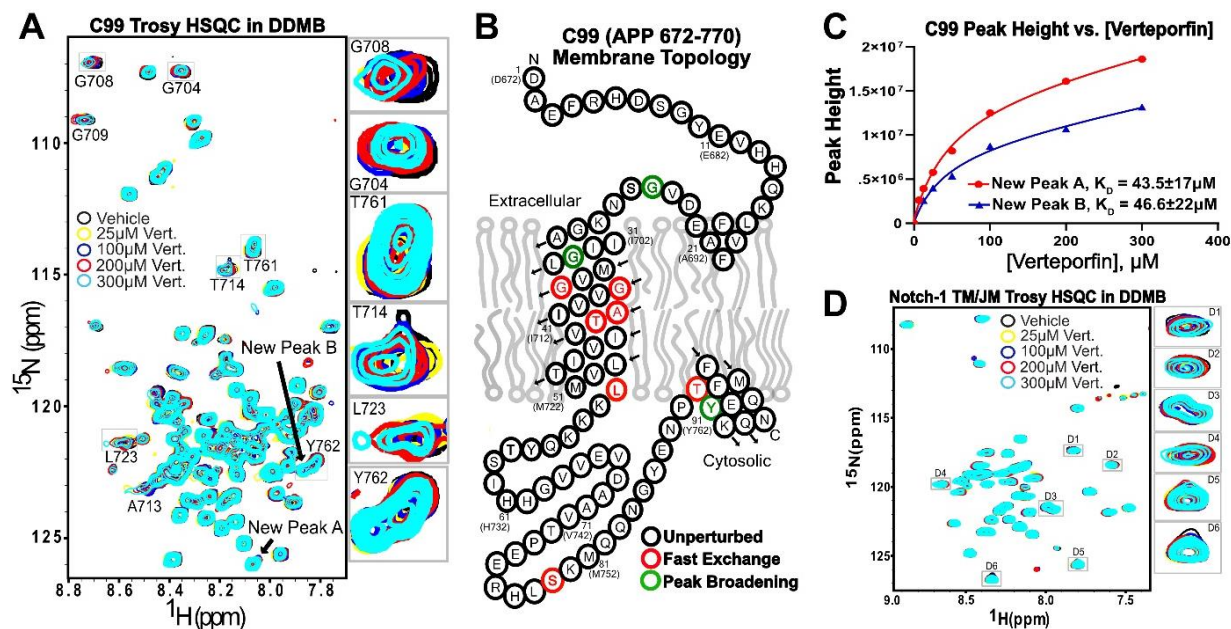


Figure 17. Verteporfin binds untagged C99 in DDMB micelles with a K_D of $45 \pm 22 \mu\text{M}$ and does not bind the Notch-1 TM/JM domain. **A)** Five overlaid C99 TROSY NMR spectra at varying concentrations of verteporfin. **B)** C99 topology diagram highlighting residues that undergo perturbations in response to addition of verteporfin. **C)** Chemical shift perturbations from the verteporfin titration shown in panel A. **D)** Notch-1 TM/JM TROSY spectral overlay at varying concentrations of verteporfin. Insets D1-D6 highlight minor spectra changes observed in Notch-1 spectra at high concentrations of verteporfin, likely arising from non-specific membrane perturbations. These data are $n=1$, where the uncertainties for the K_D in C are the error of the fit.

Verteporfin titration of C99 in non-ionic DDMB micelles confirmed binding in this medium as well, with fitting of the data for two different peaks yielding K_D of $43 \pm 17 \mu\text{M}$ and $47 \pm 22 \mu\text{M}$, a little weaker than seen for LMPG micelles and DHPC-DMPC bicelles (**Figure 171A-C**). Again, the peaks that shifted were mostly located in the transmembrane domain and amphipathic C-helix. Verteporfin titration of Notch-1 in DDMB revealed little change in the spectrum of Notch-1 until a concentration of $300 \mu\text{M}$ (**Figure 17D**), consistent with interactions between Verteporfin and Notch-1 that are only very weak and/or non-specific.

The DHPC-DMPC bicelle and DDMB micelle results corroborate the LMPG micelle results to show that verteporfin binds C99 in a wide range of membrane-like conditions and that the affinity exhibits only modest variation (K_D in the range of $15\text{-}47 \mu\text{M}$) across multiple different classes of model membranes.

Verteporfin associates with membrane mimetics. We tested to see if verteporfin interacts with LMPG micelles in the absence of protein to investigate the possibility that verteporfin interactions with C99 might be modulated by the intrinsic affinity of verteporfin for membranes. We therefore titrated empty LMPG micelles with verteporfin, as monitored by examining the 1-D ^1H NMR spectra of LMPG as a function of verteporfin concentration. Concentration-dependent changes in the position of the LMPG acyl chain methylene peak envelope revealed that their resonance frequencies were shifted by increasing verteporfin concentrations (**Figure 18A**). A fit of the 1 verteporfin binding to 1 detergent micelle binding model to these changes yielded a reasonably good fit and a K_D of $53 \pm 21 \mu\text{M}$ (**Figure 18B**). Dynamic light scattering (DLS) measurements revealed that

verteporfin had only modest effects on micelle particle size over a range of concentrations from 0-200 μM (**Figure 18C**).

We also carried out a reciprocal titration in which the ^1H NMR resonances from constant 100 μM verteporfin resonances were monitored as LMPG was titrated up through and far beyond its critical micelle concentration (CMC), which is ca. 0.2-0.5 mM at neutral pH values.²²⁴ Verteporfin resonances were very broad at LMPG concentrations below CMC (**Figure 18D**), indicating aggregate formation by verteporfin in micelle-free aqueous solutions. Above CMC the quality of its spectrum increased gradually as the

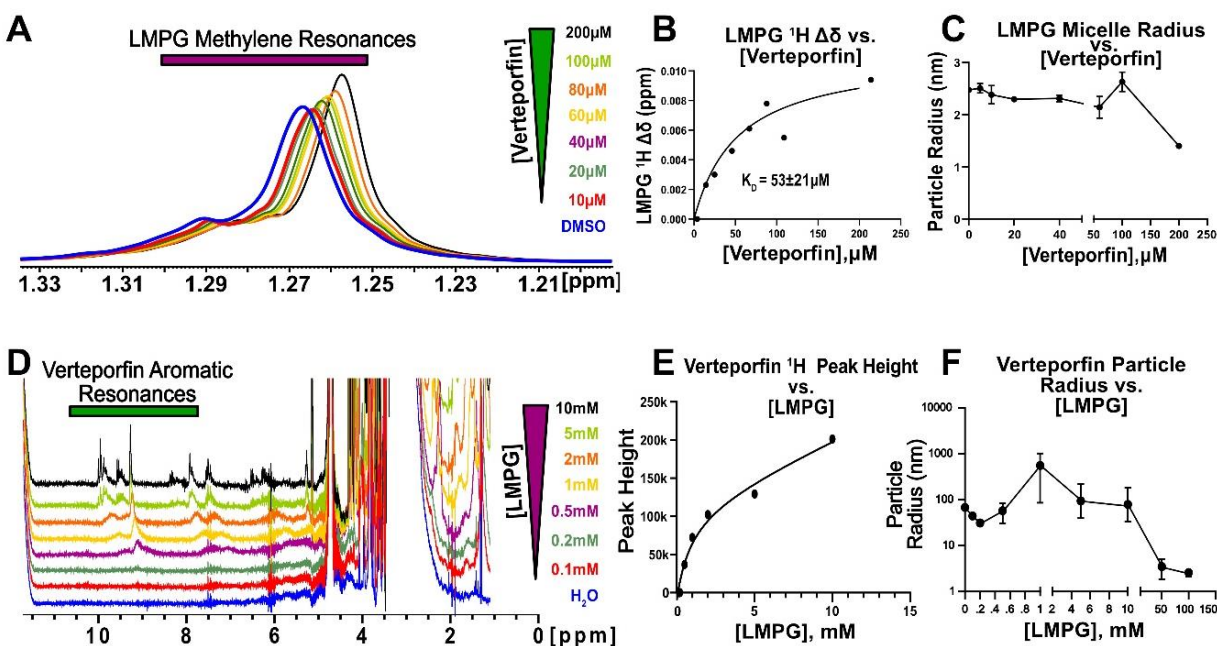


Figure 18. Verteporfin binds to LMPG micelles, which suppress its aggregation in aqueous solution. **A)** Overlaid 1D ^1H NMR spectra showing the LMPG methylene resonances from empty LMPG micelles as verteporfin is titrated in. Sample conditions: 200 μl of 2.5% LMPG in 50 mM PIPES buffer, 100 mM NaCl, 0.5 mM EDTA, pH 6.5, 318 $^\circ\text{K}$, 3 mm NMR tube. **B)** LMPG micelle acyl chain methylene peak resonance chemical shift perturbations reveal binding of verteporfin to LMPG micelles. Data is $n=1$. **C)** DLS measurements show that the size of the LMPG micelles under the same conditions as **A** is insensitive to verteporfin concentrations in the 0-200 μM range. Data is $n=3$. **D)** Overlaid 1D ^1H NMR spectra of constant 100 μM verteporfin in NMR buffer with increasing concentrations of LMPG. 100 μM verteporfin in 50 mM PIPES buffer, 100 mM NaCl, 0.5 mM EDTA, pH 6.5, 318 $^\circ\text{K}$, 3 mm NMR tube. **E)** The peak heights of verteporfin aromatic resonances are increased (due to line-narrowing) in response to increasing LMPG concentration. Data is $n=1$. **F)** DLS reveals that as 100 μM verteporfin is titrated with LMPG that soluble aggregates of verteporfin are fully dispersed by the point where the LMPG concentration reaches 50 mM. Data represents $n=3$ technical replicates. For panels C and F, error bars reflect the SEM of triplicate experiments.

LMPG concentration were increased to 10 mM, suggesting dispersal of the constant population of verteporfin from interacting with a small number of micelles at LMPG concentrations near the CMC to interactions at higher LMPG levels in which each micelle has fewer associated verteporfin molecules (**Figure 18E**). DLS measurements further illuminate that even in the mixture of 10 mM LMPG and 100 μ M verteporfin, there is a persistence of large verteporfin aggregates, which are fully dissolved only near the point at which the LMPG concentration approaches that present in NMR screening conditions (50 mM) (**Figure 18F**). This indicates that micelle formation is required to disperse the verteporfin aggregates and that the concentration of the micelles needs to be high enough to ensure that multiple molecules of verteporfin do not interact with same micelle.

Taken together, our results indicate that verteporfin binds to LMPG micelles, which suppresses verteporfin aggregation at higher micelle concentrations. The results also indicate that verteporfin does not significantly alter the size or structure of the micelles with which it associates, provided that there are a sufficient number of micelles present. We conclude that verteporfin's membrane affinity helps bring this compound in contact with C99 by solubilizing the drug and by providing the model membrane environment in which these two molecules can encounter each other. However, it is notable that under identical conditions Notch-1 in LMPG micelles does not exhibit interactions with verteporfin, indicating that micelle binding by verteporfin alone is not the determinant of C99-verteporfin interaction.

$^1\text{H},^1\text{H}$ -NOESY confirms direct contact between verteporfin and C99. To verify that that complex formation between verteporfin and C99 truly involves direct intermolecular contact, we recorded a 2D $^1\text{H},^1\text{H}$ -NOESY spectrum for a 1:1 mixture of verteporfin and C99 in 2.5% d_{27} -LMPG (deuterated acyl chains) micelles to see if cross-peaks can be observed between well-resolved verteporfin and C99 resonances. **Figure 19** documents the unambiguous presence of at least two such cross-peaks, which confirms direct

A $^1\text{H},^1\text{H}$ -NOESY of Verteporfin and C99

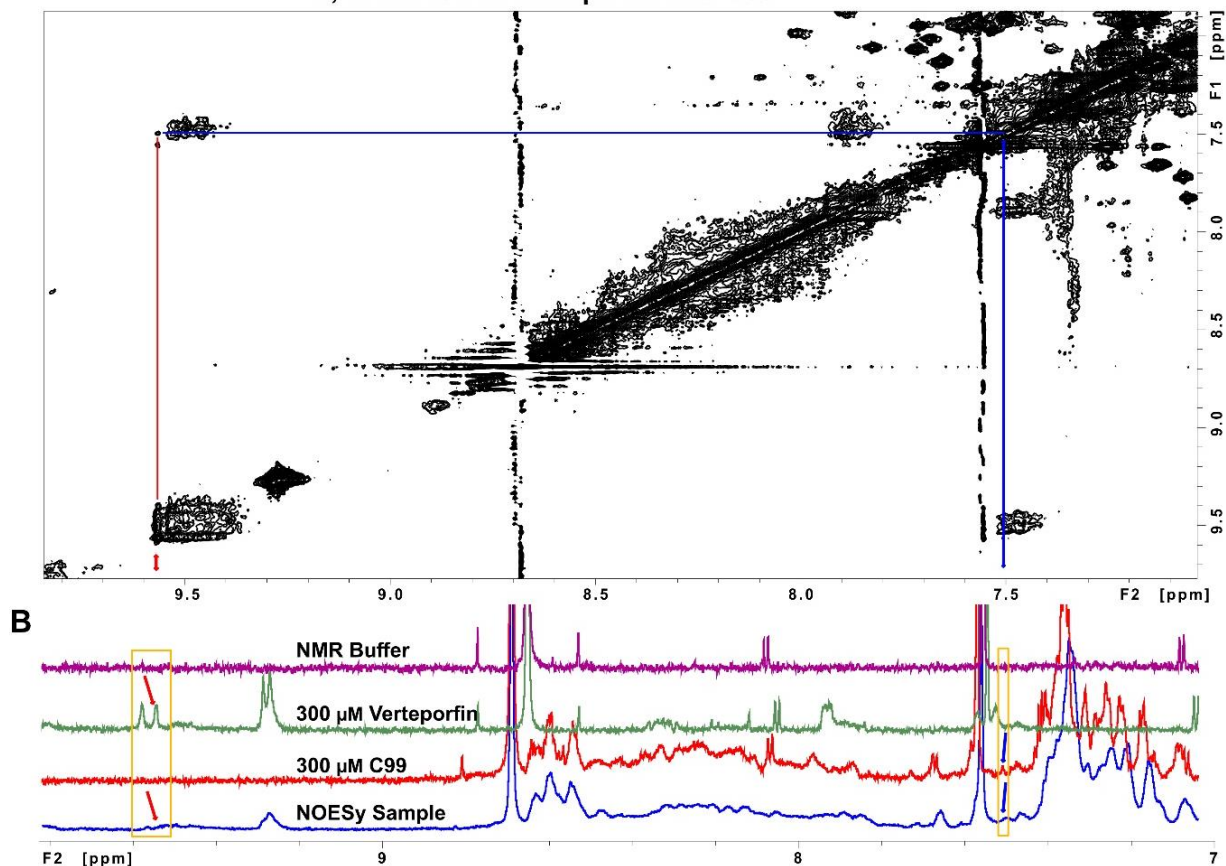


Figure 19. $^1\text{H},^1\text{H}$ -NOESY of the C99-verteporfin complex. **A**) 2D $^1\text{H},^1\text{H}$ -NOESY experiment applied to a sample containing 300 μM C99 and 300 μM verteporfin revealed cross-peaks between well-resolved aromatic verteporfin and C99 resonances. **B**) ^1H spectra of four samples containing either NMR buffer only (purple spectrum), 300 μM verteporfin in NMR buffer (green spectrum), 300 μM C99 in NMR buffer (red spectrum), and the NOESY sample containing both verteporfin and C99 (blue). The verteporfin inner-ring proton resonance (green spectrum, orange box, 9.55 ppm) exhibits an NOE interaction with a C99 amide resonance (red spectrum, orange box, 7.5 ppm). The corresponding resonances in the NOESY sample (blue spectrum) are broadened due to intermediate exchange, similar to what was seen for some C99 residues in the corresponding TROSY NMR spectra. These data were only collected once.

binding of verteporfin to C99. Other verteporfin-C99 cross-peaks were also likely present but are difficult to unambiguously assign due to peak overlap with the intense resonances from the nondeuterated glycerol backbone of d_{27} -LMPG. These data confirmed direct verteporfin-C99 interactions.

Mutations in C99 reduce the affinity of verteporfin for C99. We tested to see if verteporfin binding to C99 could be attenuated or eliminated by mutations in the protein.

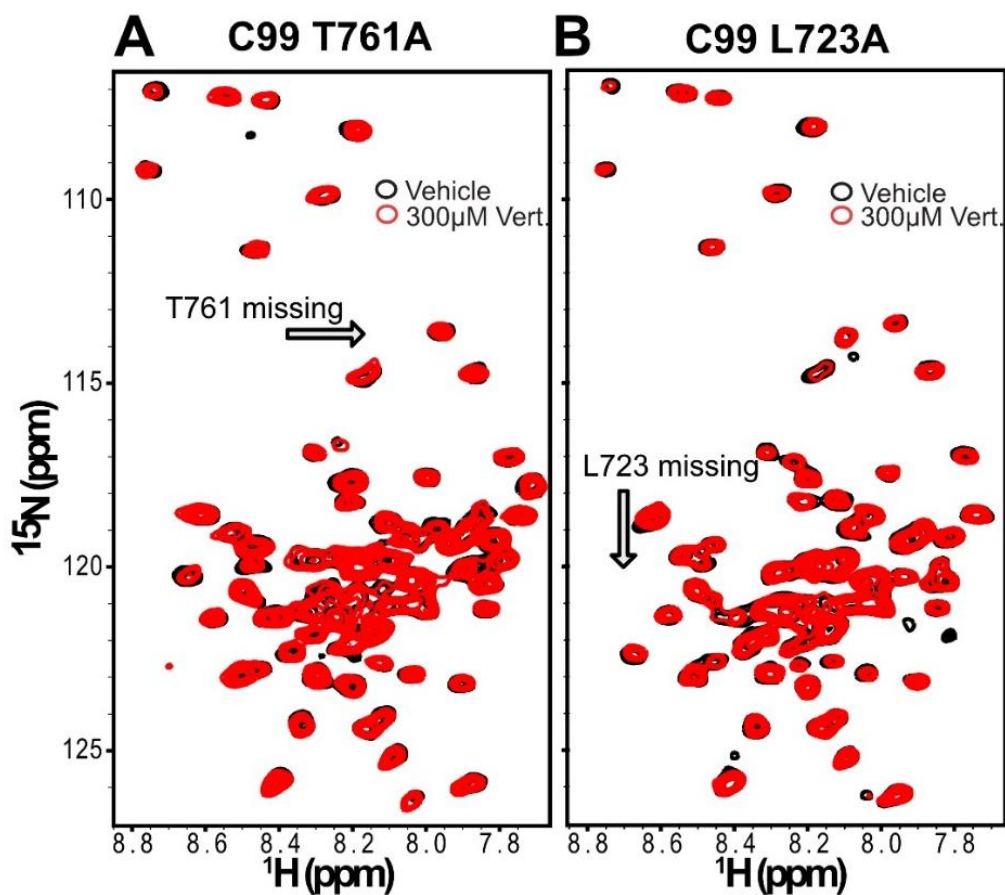


Figure 20. *C99 point mutations that ablate affinity for verteporfin.* **A)** Two NMR spectra of C99 T761A with vehicle-treated in black overlaid by spectra for samples containing 300 μM verteporfin in red. There were no chemical shift perturbations seen at any concentrations for this mutant, suggesting complete lack of binding. **B)** Two NMR spectra of C99 L723A, with vehicle-treated in black overlaid by the red spectrum representing the 300 μM verteporfin condition. There were only noisy shifts seen for this construct when treated with verteporfin, suggesting a nearly complete lack of binding. These data are representative spectra taken from the highest and lowest (zero) titration point from the series. The titrations were done once ($n=1$) per mutant.

The single-site mutations L723A, and T761A were chosen both because we observed chemical shift perturbations for these residues in one or all the previously discussed model membrane conditions and because of their dispersal across the C99 primary sequence. As shown in **Figure 20**, we observed that binding was disrupted by both mutations and that peak shifts were either non-existent or weak as a function of verteporfin concentration and could not be fit by binding isotherms, indicating that these residues played critical roles in mediating interactions between C99 and verteporfin. It is worth noting that peaks from transmembrane residues such as G708, G709, and A713 continued to undergo small shifts or broadening in the spectra from these mutants, likely reflecting the residual effects of verteporfin's affinity for detergent micelles and forced cohabitation of verteporfin with C99 molecules at high verteporfin concentrations, as was also seen for Notch-1, but only at high verteporfin concentrations.

Native ion mobility-mass spectrometry and chemical cross-linking indicate verteporfin binds to the monomeric form of C99 and does not induce homodimerization. We sought to determine whether verteporfin binds to the monomeric form of C99 and if binding of verteporfin induces a change in the oligomeric state of C99. C99 is known to form monomers or dimers depending on concentration, lipid composition, and model membrane type, or mutation.²²⁵⁻²²⁷ Glutaraldehyde (GA) crosslinking of verteporfin-C99 mixtures in LMPG micelles in NMR-like conditions showed no increase in higher-order C99 species upon increasing GA concentration when compared to the DMSO-only treated control (**Figure 21**). This finding was confirmed by showing no change in oligomeric state when the GA concentration was maintained constant and

verteporfin was increased. These results indicated both that verteporfin binds to monomeric C99 and that binding of verteporfin does not induce protein dimerization.

Native ion mobility-mass spectrometry (IM-MS) has proven to be a useful structural biology tool capable of interrogating complex mixtures. With the use of membrane mimetics, the native conformation of membrane proteins can be retained and studied

C99 Glutaraldehyde Crosslinking Experiments

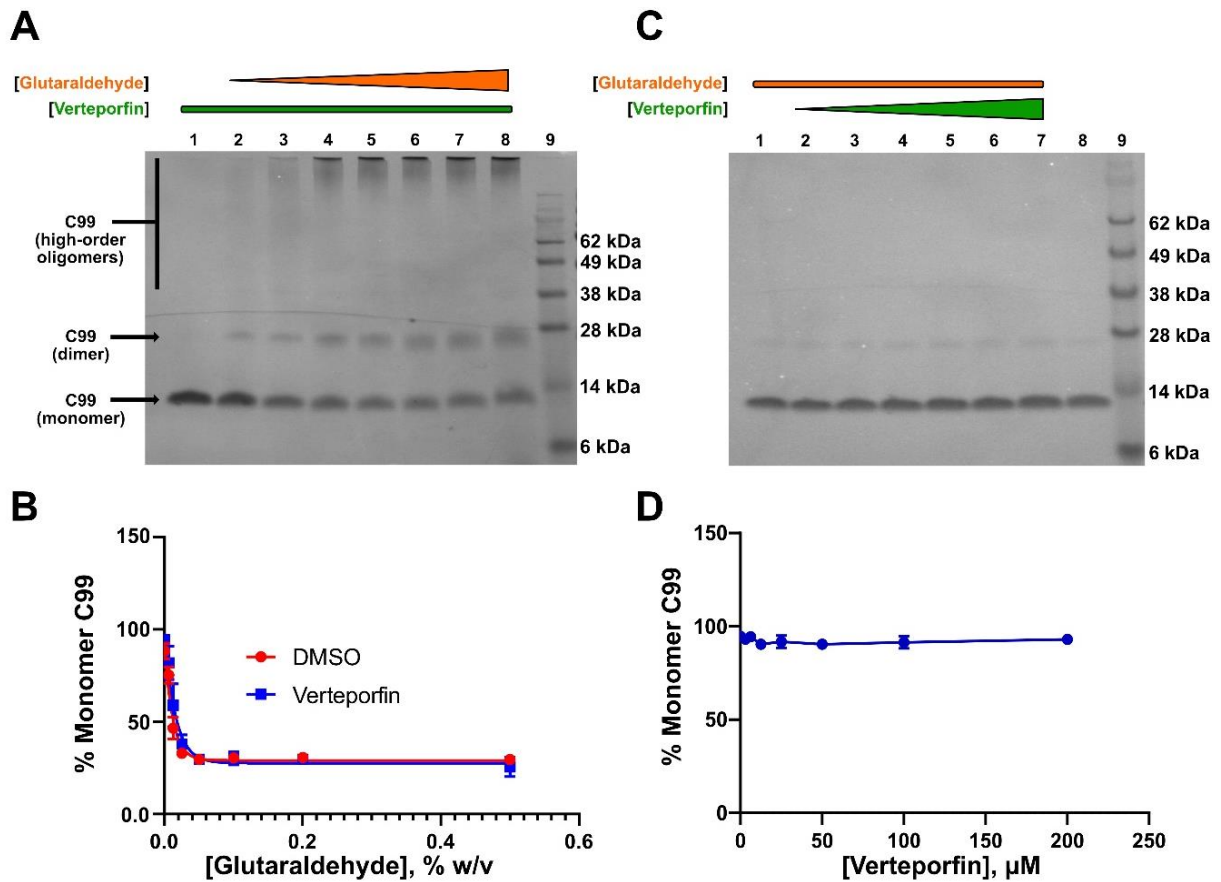


Figure 21. *Glutaraldehyde crosslinking of C99 reveals no change in oligomeric state in response to verteporfin.* **A)** SDS-PAGE gel of crosslinking experiment at constant 100 μM verteporfin and treatment with increasing levels of glutaraldehyde from 0-0.5% w/v at final dilution. **B)** Quantified C99 band intensities from gel shown in A, indicating no changes of the oligomeric state of C99 in response to verteporfin treatment when compared to the DMSO treated control. **C)** SDS-PAGE gel of crosslinking experiment with C99 being treated with increasing amounts of verteporfin at a constant low concentration (0.0064% w/v) of glutaraldehyde, where basal levels of dimer crosslinking can be seen. **D)** Quantification of the gel from B also verifies that C99 remains a robust monomer in response to titration with verteporfin. All data shown here are representative of n=3 technical replicate experiments, which were quantified by densitometry using ImageJ, where the error bars denote the standard deviation of the replicate values.

using IM-MS.²²⁸⁻²³³ IM separates the ions based on their size, shape, and charge. In

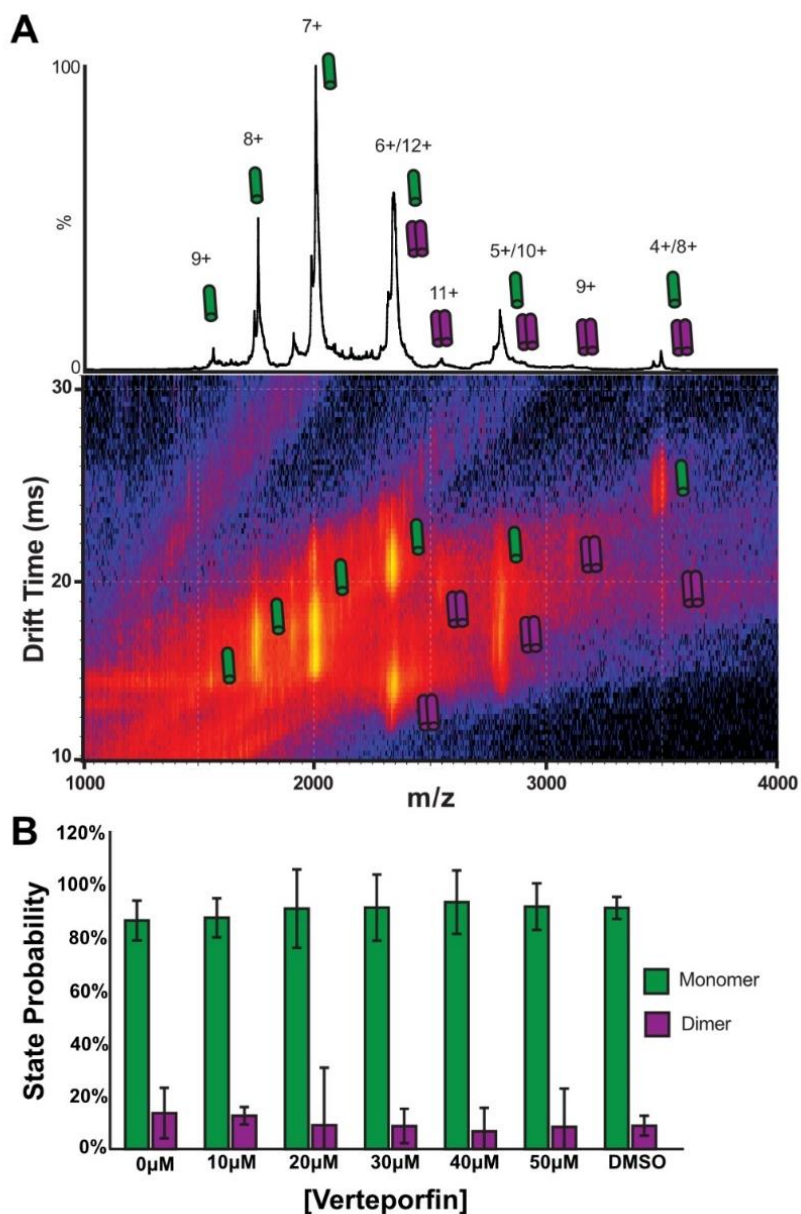


Figure 22. *IM-MS* indicates that verteporfin does not alter C99 mass or induce dimerization. **A**) A representative mass spectrum (top) and *IM-MS* spectrum (bottom) showing the various states of C99 oligomerization. Native C99 monomer charge states (4-9+) are denoted by a single green cylinder, and dimer charge states (8-12+) are shown as two purple cylinders. No changes in C99 mass were observed, suggesting that no chemical modifications were made to the protein in response to drug treatment. **B**) The relative intensities of each species were used to calculate the percent of each oligomeric species for C99 at 0 μM , 10 μM , 20 μM , 30 μM , 40 μM , 50 μM verteporfin, respectively. To avoid overlapping monomer/dimer peaks, monomer charge states 9-11+ and dimer charge states 9+ and 11+ were included in analysis. Quantification of the *IM-MS* data indicates that C99 does not undergo any significant change in oligomeric state upon addition of Verteporfin, indicating that Verteporfin interacts with the C99 monomer. Data is $n=3$, where error bars indicate the standard deviation of three technical replicate experiments.

native IM-MS experiments, we can separate different conformations and oligomeric states of membrane protein ions.²³⁴⁻²³⁸ All IM-MS data were collected using a Synapt G2 HDMS IM-Q-ToF mass spectrometer (Waters, Milford, MA), with a direct infusion nESI source set to positive ion mode. Instrument settings were tuned to dissociate detergent micelles, with minimal perturbation of protein structure prior to the IM separator. Arrival time distributions of charge states that were known to be uniquely monomer or dimer, as indicated in **Figure 22**, were extracted using a text-based format using TWIMExtract.²³⁹ IM-MS of C99-verteporfin mixtures in LMPG and DDMB micelles revealed that verteporfin causes only a marginal increase in the population of dimeric C99 in low detergent conditions (high protein-to-detergent ratio), which indicates verteporfin-induced dimerization would be insignificant at the much higher detergent concentrations (and lower C99-to-detergent ratios) of our NMR-based binding experiments. We note that verteporfin was not detected in complex with C99 by IM-MS experiments, and this may be due to the dissociation of verteporfin with the surrounding detergent molecules during collision-induced dissociation.

The IM-MS data also revealed that the mass of C99 remained intact following complex formation with verteporfin, indicating no covalent modification of the protein by verteporfin or induced oxidation (**Fig. 22A**). This is a significant observation as verteporfin is a photoactivatable molecule that can stimulate the production of radical oxygen species (ROS) in the presence of ambient light and O₂.²⁴⁰ Stringent precautions were taken throughout these studies to ensure that verteporfin-containing samples were

maintained in the dark. The IM-MS data confirmed that our observations are unrelated to potential photoactivation of verteporfin.

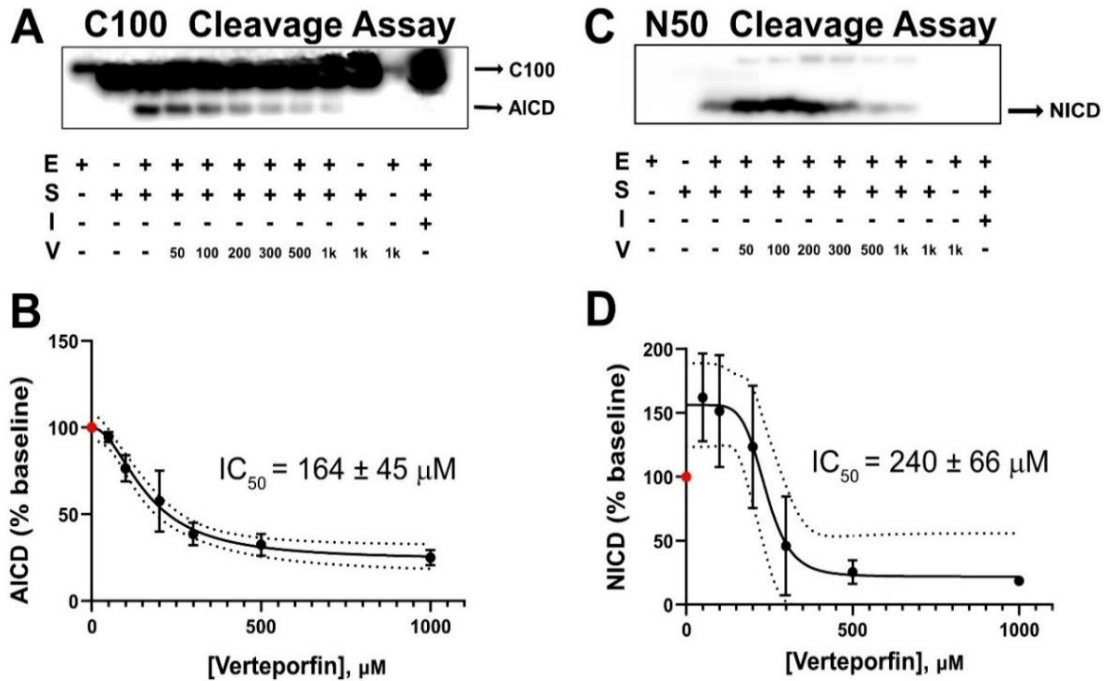


Figure 23. *Verteporfin inhibits γ -secretase cleavage of C100-Flag more potently than than for Notch-1.* **A)** Anti-Flag tag Western blot of verteporfin inhibition of C100-Flag cleavage by 30 nM purified γ -secretase at different levels of verteporfin. The legend below the blot denotes the added components: **E is enzyme** (γ -secretase), **S is substrate** (C100), **I is inhibitor** (30nM LY411,575), and **V is verteporfin** in micromolar units. Top band: C100-Flag substrate; bottom band; AICD-Flag (intracellular domain product of γ -secretase cleavage of C100-Flag). The presence of both enzyme and substrate produces the amyloid intracellular domain (AICD) band, indicating C100 cleavage. Upon addition of increasing amounts of verteporfin, the cleavage efficiency is greatly reduced in a concentration-dependent manner. The AICD band intensities were quantified using densitometry using ImageJ, as shown in the next panel (3 replicates). **B)** Quantitation of the data for verteporfin inhibition of AICD production from panel A (plus replicates). “% Baseline” refers to the amount of AICD that is observed relative to the 0 verteporfin conditions. These data indicate an IC_{50} of $164 \pm 45 \mu\text{M}$ ($n=3$, technical replicates). **C)** Western blot of the γ -secretase assay showing cleavage of Notch-1 TM/JM to release NICD, as detected using an antibody against the V1744 neopeptide. Notch-1 TM/JM is recombinant Notch-1 transmembrane/juxtamembrane construct (residues 1721-1771). The legend below the blot denotes the added components: **E is enzyme** (γ -secretase), **S is substrate** (Notch-1 TM/JM), **I is inhibitor** (30 nM LY411,575), and **V is verteporfin** in micromolar units. The presence of both enzyme and substrate produces the Notch Intracellular Domain (NICD) band, indicating Notch cleavage. It is seen in these data that verteporfin first activates then inhibits γ -secretase cleavage of Notch-1. The AICD band intensities were quantified using densitometry (plus results for two additional replicates) using ImageJ, as shown in the next panel. **D)** Quantitation of the ($n=3$) data for verteporfin inhibition of NICD production from panel C. “% baseline” refers to the amount of NICD that is observed relative to the 0 verteporfin conditions. The error for the dataset was propagated using the standard deviation of three technical replicates. Upon addition of increasing amounts of verteporfin, it is seen that Notch-1 cleavage is bi-phasic: cleavage is first activated by verteporfin until a concentration of 200 μM , then inhibited at higher concentrations, with an estimated IC_{50} of $240 \pm 66 \mu\text{M}$ ($n=3$).

Verteporfin inhibits γ -secretase cleavage of C99 with an approximate two-fold selectivity over Notch-1. We tested whether formation of the C99-verteporfin complex resulted in inhibition of C99 cleavage by γ -secretase. γ -Secretase assays were conducted *in vitro* for both C100 (C99 with an N-terminal start methionine) and Notch-1 TM/JM as substrates (**Figures 23A,B** and **23C,D**, respectively). Verteporfin induced dose-dependent inhibition of γ -secretase-catalyzed production of the amyloid intracellular domain (AICD), with an IC_{50} of $164 \pm 45 \mu M$ under these assay conditions. (**Figure 23B**) The degree of inhibition levels off at approximately 75%, with some residual cleavage activity being observed even at apparently saturating levels of verteporfin. In another condition, where the enzyme concentration was much lower, verteporfin exhibited a $15 \pm 1 \mu M$ IC_{50} for γ -secretase cleavage of C99 (**Figure 24**) which correlated well with the observed K_D values between verteporfin and C99 (Figures 19, 20, 21). The lower IC_{50} observed in this experiment relative to that of **Figure 23A,B** reflects the lower concentration of γ -secretase: With less enzyme in competition for C99 binding, verteporfin can more effectively protect C99 from proteolytic processing.

For Notch-1 (Notch-1 TM/JM), concentrations of verteporfin below $200 \mu M$ actually *enhanced* Notch-1 cleavage by γ -secretase relative to 0 verteporfin conditions (**Figure 23C,D**). However, at higher concentrations verteporfin inhibited γ -secretase cleavage of Notch-1 with an IC_{50} of $240 \pm 66 \mu M$. As for C99, saturating concentrations of verteporfin reduced cleavage by approximately 75%.

Taken together, these data indicate that at lower concentrations verteporfin binding to C99 shields the protein from γ -secretase cleavage without inhibiting γ -secretase cleavage of Notch. For example, when the concentration of verteporfin is at the IC_{50} of 164 μ M, there is 50% maximal inhibition of C99 cleavage, but no inhibition of Notch-1 cleavage (**Figure 23**). Moreover, the fact that verteporfin was not seen by NMR to bind to Notch under three different sets of model membrane conditions, but can nevertheless inhibit Notch cleavage at higher concentrations, suggests that inhibition is likely be the consequence of interactions of high levels of verteporfin with γ -secretase and/or with the model membranes employed in the γ -secretase assays.

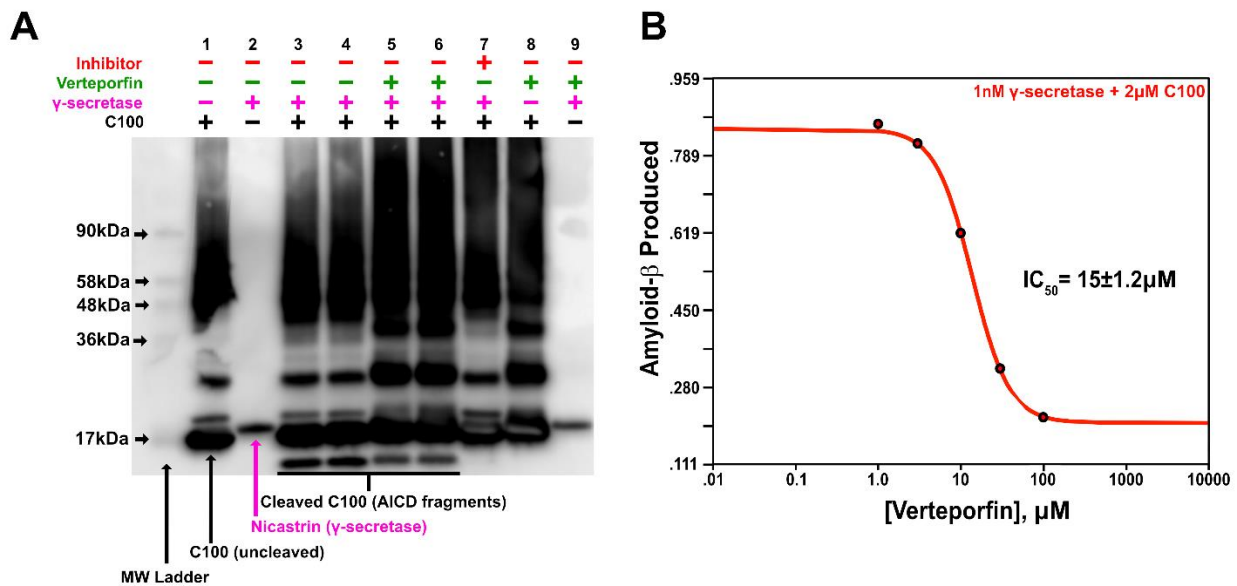


Figure 24. *Verteporfin inhibits γ -secretase cleavage of C100-Flag (C99) in low enzyme and substrate conditions.* C100-Flag is recombinant C99 with an N-terminal start methionine and a C-terminal Flag epitope tag. **A**) Anti-Flag tag Western blot of 2 μ M C100-Flag cleavage by 1 nM purified γ -secretase. Cleavage of C100-Flag proceeds as expected in lanes 3 and 4 (bottom band; AICD-Flag = intracellular domain product of C100-Flag cleavage by γ -secretase). However, upon addition of 100 μ M verteporfin, the cleavage efficiency is greatly reduced (lanes 5 and 6), but not as fully as seen in lane 7, which contained 30 nM of the potent γ -secretase-inhibitor, LY411,575. **B**) Sandwich ELISA of A β 40 production from C100-Flag cleavage by purified γ -secretase performed as in panel A. Inhibition by verteporfin is concentration-dependent. Curve fitting reveals a half-maximal inhibitory constant (IC_{50}) of $15 \pm 1 \mu$ M verteporfin. These data are from single n=1 experiment, and the error was interpolated from the error of the fit.

Modelling the C99-verteporfin complex. Although verteporfin induced spectral perturbations across many regions of C99, the focal points were primarily in and around the transmembrane domain and amphipathic C-helix. We sought to use experimentally restrained Rosetta modeling to generate structural insight on how the complex may look and to illuminate possible mechanisms of γ -secretase inhibition. Using our previously published C99 structure (PDB: 2LP1) as a template, we generated models of the complex showing that verteporfin localizes to the transmembrane domain (**Figure 25**). In the top-scoring model, verteporfin is seen to adopt a binding pose in which its planar macrocyclic ring is in contact with transmembrane C99 residues near the TM kink. The semi-polar

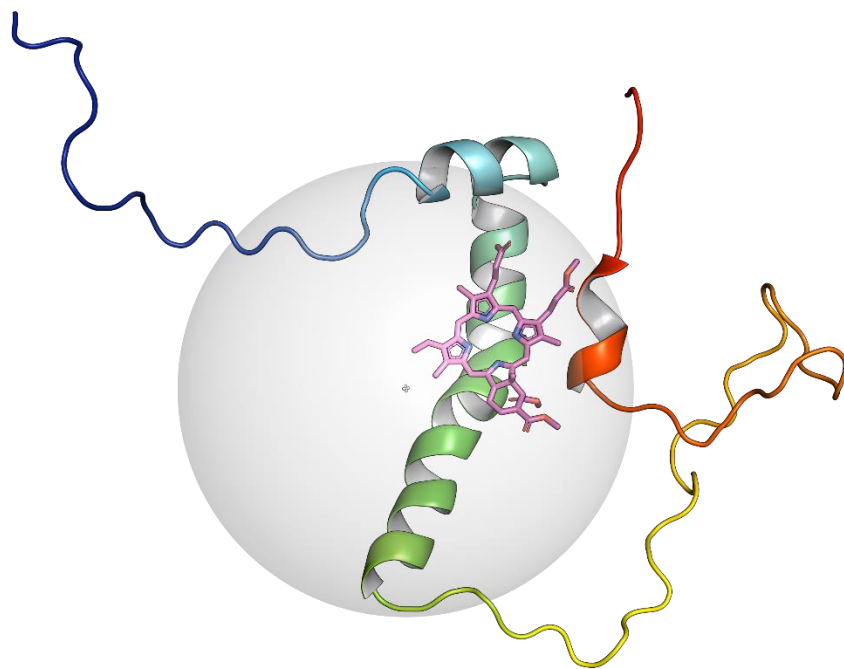


Figure 25. *Most favorably scoring model from experimentally restrained Rosetta modeling of the micellar verteporfin-C99 complex.* Experimentally restrained Rosetta suggests that the planar face of verteporfin interacts with the transmembrane domain. It appears the entire macrocycle of the compound is embedded in the micellar model membrane and contacts transmembrane residues near the transmembrane kink. The positions of the semi-polar methyl ester chains generally point towards the solvent-membrane interface and form contacts with the N- and C-terminal amphipathic helices. The grey sphere represents a detergent micelle.

verteporfin methyl ester arms extend toward the surface of the membrane and may be responsible for the chemical shift perturbations seen in the amphipathic N- and C-helices.

DISCUSSION

APP can be classified as a member of the single-pass transmembrane receptors (SPTMRs), a collection of membrane proteins that make up approximately 6% of the human protein-coding genome and play critical roles in essential biological processes such as cell growth, adhesion, metabolism, and immunity.¹⁷⁹ The close relationship between SPTMRs and human health and disease suggests that many proteins of this class may be viable drug targets; however their transmembrane domains have been thought to lack the druggable pockets that are associated with multi-span membrane or water-soluble proteins.²⁴¹ Nevertheless, at least one drug does indeed target the transmembrane domain of an SPTMR. Eltrombopag is an FDA-approved thrombopoietin receptor (TPoR) agonist that activates the receptor by binding to its transmembrane domain.²⁴²⁻²⁴⁴ The present study was inspired, in part, by the hope that the paradigm in molecular recognition established by the Eltrombopag/TPoR interaction could be extended to the discovery of molecules that specifically bind to the transmembrane C99 domain of the human APP.

Our study establishes verteporfin binds specifically to monomeric C99 with an affinity in the 10-50 μ M range under a variety of model membrane conditions. verteporfin does not induce dimerization of C99. Future work will be required to determine if a medicinal chemistry campaign can identify verteporfin analogs or derivatives with an even higher affinity for C99. Binding of verteporfin to C99 is facilitated by the intrinsic

affinity of this compound for membranes, which increases the local concentration of this compound in the vicinity C99. NMR NOE measurements confirmed that the C99-verteporfin interaction is direct. Moreover, the fact that NOEs were seen between verteporfin and *both* C99 and detergent under conditions in which the vast majority of verteporfin was C99-associated strongly suggests the C99-verteporfin interactions are at the detergent-protein interface. The fact that verteporfin binds C99 with similar affinity in LMPG micelles (anionic), dodecylmelibioside micelles (non-ionic), and DHPC-DMPC bicelles (zwitterionic) indicates that binding of verteporfin to C99 is independent the detailed chemistry and structure of the molecules comprising the membrane mimetic. At the same time, interfacial binding of verteporfin to C99 is structurally specific: it is saturable, and affinity can be reduced by mutating specific residues in C99. Moreover, verteporfin was shown not to bind to another single span membrane protein, the Notch 1 receptor.

Verteporfin was found to inhibit cleavage of C99 by γ -secretase, with an IC_{50} that ranged from 15 μ M (near K_D) to 164 μ M, depending on the exact conditions. For γ -secretase, IC_{50} —the concentration of compound that inhibits 50% of product formation from an enzyme reaction—will vary with enzyme and substrate concentrations and other assay conditions. In this case, verteporfin was seen to compete with γ -secretase for C99, binding much more effectively in the presence of 1 nM enzyme (IC_{50} 15 \pm 1 μ M) than in the presence of 30 nM enzyme (IC_{50} 164 \pm 45 μ M).

Under the same conditions where IC_{50} for inhibition of C99 cleavage was 164 \pm 45 μ M, verteporfin was seen to stimulate Notch-1 cleavage at concentrations of up to ca. 200 μ M, above which verteporfin inhibits cleavage with an IC_{50} value of 240 \pm 66

μM , depending on the specific Notch-1 substrate used. In light of our results that verteporfin does not bind directly to Notch-1 and that verteporfin exhibits membrane-disrupting effects at concentrations above 200 μM , we think it is likely that both activation and inhibition of Notch-1 cleavage by different concentrations of verteporfin are the consequence of verteporfin perturbation of the membrane mimetic used in the cleavage assays. This is consistent with previous results showing that the activity of purified γ -secretase is sensitive to membrane conditions, such as phospholipid composition and cholesterol content, as well as to solubilizing detergent type and concentration.²⁴⁵⁻²⁴⁷

Our results suggest the feasibility of finding compounds that bind even more tightly to C99 without binding to Notch-1. This would be a welcome development, as inhibition of Notch-1 receptor cleavage by γ -secretase inhibitors causes severe toxicity that has thwarted efforts to explore these inhibitors as potential Alzheimer's therapeutics.^{86-87, 154, 248}

Verteporfin is a porphyrin-based molecule that is FDA-approved for subfoveal choroidal neovascularization, typically derived from age-related macular degeneration. Commonly sold under the trademark Visudyne®, verteporfin is administered intravenously and is absorbed by retinal blood vessels behind the eyes. The patient's eyes are then irradiated with red light (689 nm), which causes verteporfin to produce radical oxygen species that cause local damage to the blood vessels and enhance their clearance. Beyond its FDA-approved use, verteporfin has several other reported biological effects. For example, when exposed to ambient light, verteporfin can induce cross-linking of proteins in cells, leading to cell death.²⁴⁹ Other effects include but are not limited to inhibition of cellular autophagy²⁵⁰ and inhibition of cell growth by

modulating the Hippo pathway.²⁵¹⁻²⁵² The photochemistry of verteporfin combined with these cytotoxic properties and likely problems with bioavailability dictate that verteporfin cannot be regarded as a promising clinical candidate as an inhibitor of C99 cleavage by γ -secretase, much less as a possible Alzheimer's therapeutic. Moreover, our results also show that while verteporfin does not directly bind Notch-1, it nevertheless does perturb its cleavage at high concentrations. Despite these obvious flaws in verteporfin as a drug lead or even as a tool compound, our discovery does confirm a previous study²⁰⁹ that molecules can be found that inhibit γ -secretase cleavage of C99 through direct interaction with this substrate. It can be expected that high-throughput screening of much larger compound collections than the library of FDA-approved drugs will lead to the discovery of other C99-specific binders that have more attractive chemical, pharmaceutical, and pharmacological properties. It is hoped that the results of this study will motivate future studies to identify and develop molecules of this class. Such molecules may provide potent tools for sorting out the great complexity of the amyloidogenic pathway, the C99 protein fragment, and its relationship to Alzheimer's disease.¹⁹⁵ Finally, we note our hope that the power of using NMR spectroscopy as a primary tool for detecting molecules that bind to C99 is evident from this work.

Conclusion

Here we show findings from an NMR-based high-throughput screen that the FDA-approved porphyrin molecule, verteporfin, forms a direct 1:1 complex with the transmembrane domain of the human amyloid precursor protein, C99. It was the only compound out of 1,200 molecules that reproducibly bound during titration. The complex is robust and detectable across a variety of membrane conditions and does not bind to

the Notch-1 transmembrane domain. Certain mutations in C99 disrupt complex formation. Verteporfin was seen to behave as a selective inhibitor of C99 proteolysis. We think these data further validate the proof-of-concept that substrate-specific modulators of single-pass transmembrane proteins such as C99 can be discovered by coupling NMR-based high throughput screening to rigorous validation experiments.

Chapter 5

PAINS in the membrane: discovery of small molecule fragments that non-specifically bind membrane proteins in membrane mimetics³

Introduction

Drug discovery against transmembrane (TM) proteins is an emerging field of interest for academic and pharmaceutical interests alike, and certain TM proteins can be validated drug targets due to their roles in human health and disease. There is little known about what hit rates to expect when conducting small molecule screens or what types of molecules may present themselves as false positives during screening. Specifically, there remains a significant gap in knowledge pertaining to what types of artifacts may arise when screening TM proteins in detergent-solubilized conditions or how small molecules may interact directly with the detergent. In this study, some of these knowledge gaps were addressed by screening small molecule fragments against the Alzheimer's disease (AD) implicated C99¹⁹⁵ protein in anionic lyso-myristoylphosphatidylglycerol (LMPG) micelles using NMR spectroscopy.

The Vanderbilt University curated Fesik Fragment Library contains approximately 15,000 small molecule fragments that are optimized for fragment-based

³ This work is in preparation. Putative title: Castro, M. A., *et al.* (2022). PAINS in the membrane: discovery of small-molecule fragments that non-specifically bind membrane proteins in membrane mimetics. Journal TBD.

drug discovery (FBDD). FBDD has the advantage of expediting early drug discovery by allowing for quick sampling through chemical space using fragments of drug-like molecules (typically (< 300 Da)).¹⁹³ Fragment hits can then be used to drive lead-optimization to create highly potent and specific ligands for a given biomolecular target. However, fragment libraries and small molecule libraries more generally may also contain PAINS compounds that can mislead and derail drug discovery efforts by leading to false positives via a number of mechanisms.²⁵³ PAINS compounds are typically small molecules that lead to false positive activity assays (such as binding assays, receptor activation assays, etc) by indirect phenomena including colloidal aggregation, non-specific covalent modification of the target, pH-changing effects, or membrane disruption. There are many reports describing the structures of common PAINS compounds that have proven useful for certain formats of small molecule discovery.²⁵³⁻²⁵⁴ However, little is known about what types of compounds may be PAINS for detergent-solubilized protein systems and how different types of detergents or membrane mimetics may influence small molecule-protein interactions. In this manuscript, we describe the results of an NMR-based screen of the entire Fesik Fragment Library against C99 solubilized by anionic LMPG micelles. We present the discovery of six initial hit compounds that turned out to be putative membrane protein PAINS that should be cautiously explored if appearing to be hits in future screens of this sort. Furthermore, we detail our hit-to-PAINS deconvolution strategy using one such compound, 2,5-dimethyl-N-(pyridine-2-ylmethyl)aniline, as an example.

Results

Our strategy for screening the fragment library is detailed in Figure 26. It is important to note that the LMPG screening condition was chosen because it stabilizes monomeric C99, which has an assigned HSQC NMR spectrum and a published 3D structure (PDB: 2LP1).²¹⁷ Several screening conditions, such as tolerable DMSO and LMPG concentrations, as well as 2D NMR pulse programs were explored to maximize reproducibility and signal-to-noise before screening. The fragment library screen was expedited using fragment mixtures, which contained 12 compounds per well dissolved in DMSO. Mixtures that perturbed C99 TROSY-HSQC NMR spectra relative to the vehicle-only (DMSO) treated control were considered hits. Hit mixtures were then deconvoluted using mixtures of 3 compounds then single compounds. Isolated hit compounds were then subjected to titration against C99 to reveal observed dissociation constants (K_D) if

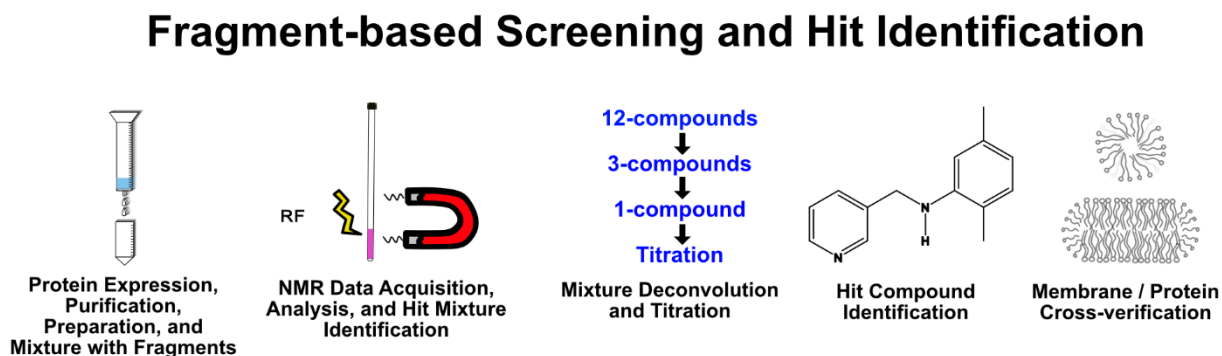


Figure 26. *High throughput screening strategy used to discover small molecule binders of C99 in LMPG micelles.* Like the protocol discussed in Chapter 4, C99 was purified from *E. coli* culture and combined with fragment mixtures (12 per well) in 96-well plates. Samples are transferred to NMR tubes and screened using BEST-TROSY NMR experiments. Upon discovering a hit, the mixture is deconvoluted to reveal the causative single compound. Individual hit compounds are then titrated and subjected to a myriad of validation experiments including titrations against of other proteins, titrations in other model membranes, and SAR by catalog.

saturable. Overall, it took approximately 36 days of 600 MHz NMR time and 400 mg of ^{15}N -labelled C99 to screen the entire fragment library using a Bruker

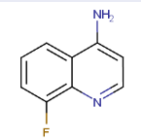
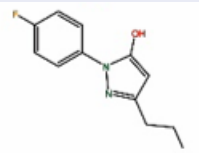
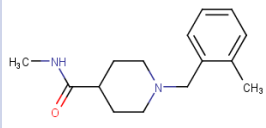
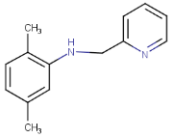
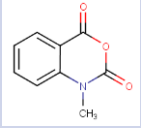
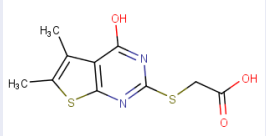
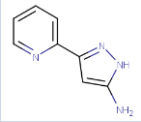
Compound (VUID)	Structure	K_D for C99 (LMPG)	Perturbs C99 in Bicelle?	Perturbs other TM proteins in LMPG?
VU0408786		>10 mM (linear shifts)	Yes	Yes
VU0410776		450 μM (slow-exchange)	No	Yes, but only to a minor degree
VU0408483		4-9 mM (linear shifts)	Yes	Yes
VU0021995		>10 mM (linear shifts)	Yes	Yes
VU0421317		2 mM	No	Yes
VU0410688		>10mM (linear shifts)	No	Yes
VU0410488		1.5mM	Yes	Yes

Figure 27. Structures and properties of hits from the Fesik Fragment Library. This table shown the six hits that perturbed C99 spectra in LMPG in a dose-dependent fashion. The left column indicates the VU-ID numbers for these fragments, which can be searched for using the ChemCart or Waveguide software. The corresponding structures are shown in the second column, and their respective K_D values for C99 in LMPG are shown in the third. The fourth column indicates whether the respective compounds perturbed C99 spectra in bicelles (perturb does not necessarily mean saturate binding). And the final column indicates whether the compound non-specifically perturbed other TM proteins, such as Notch-1 or KCNQ1-VSD, in LMPG.

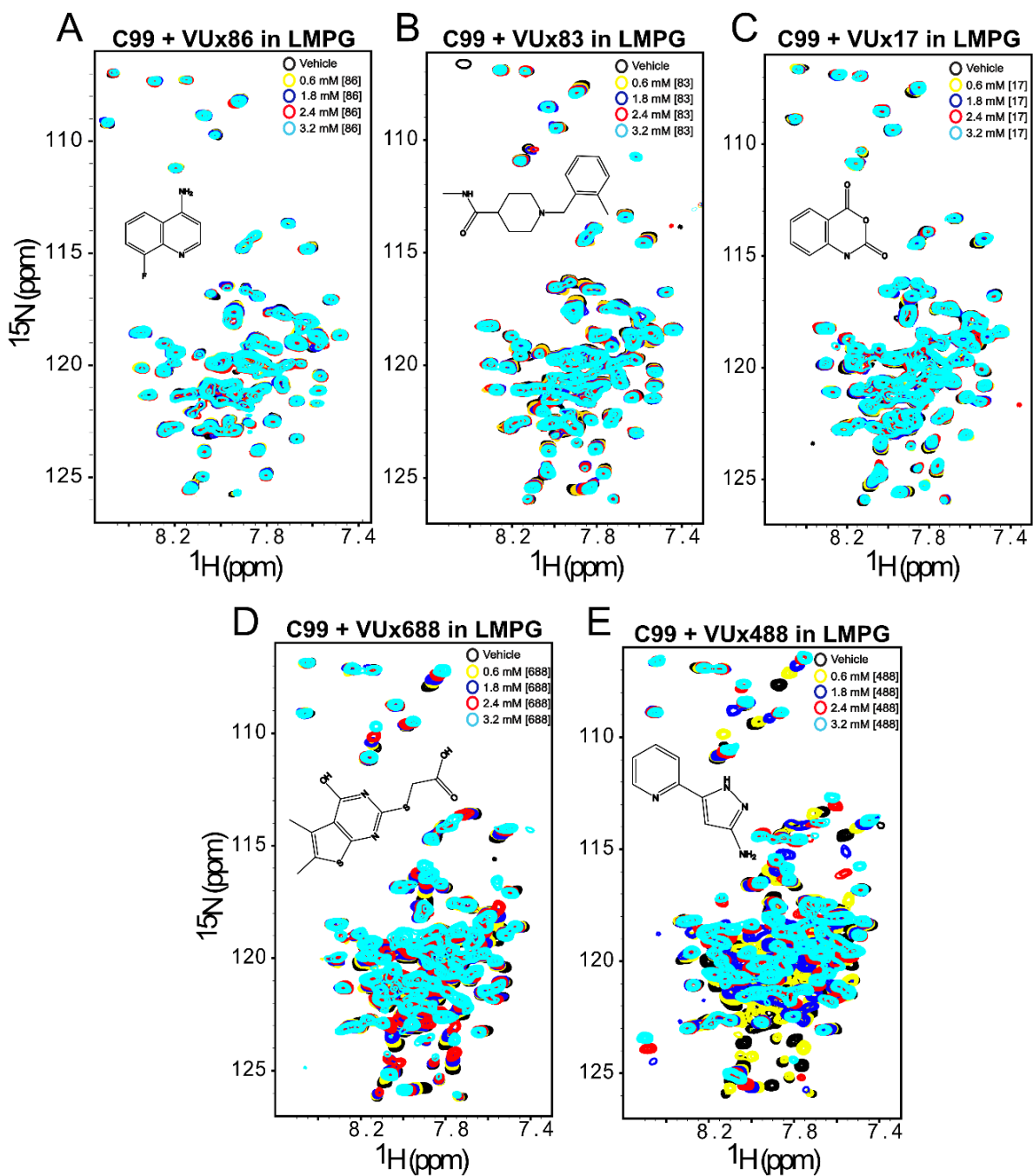


Figure 28. NMR titrations of C99 in LMPG with five of the six fragment hits. **A)** Five NMR spectra of C99 in LMPG at increasing concentrations of VUx86. **B)** Five NMR spectra of C99 in LMPG at increasing concentrations of VUx83. **C)** Five NMR spectra of C99 in LMPG at increasing concentrations of VUx17. **D)** Five NMR spectra of C99 in LMPG at increasing concentrations of VUx688. **E)** Five NMR spectra of C99 in LMPG at increasing concentrations of VUx488. All titrations go from zero (DMSO only) fragment to 3.2 mM. Other titrations were also conducted at concentrations up to 10 mM to verify that perturbations did not saturate (data not shown). The structure of each respective fragment is shown in the corresponding titration series.

SampleJet robotic sample changer.

The library produced seven hit compounds that were followed up with more extensively (**Figure 27 and 28**). As will be seen, only one (VUx76) was a verified C99 binder, as deemed because its binding was avid and saturable and was eliminated by mutagenesis (appendix **Figure 39**). The other 6 compounds were determined to be false-positive PAINS-like molecules due to non-specific interaction effects that were seen for both for C99 and other proteins or effects on sample pH. These PAINS molecules did not saturate their effects at concentrations even up to 5-10 mM, which suggested that their effects were not likely due to stoichiometric complex formation.

Before focusing on a single compound for the rest of this chapter, I will give an explanation about why the other compounds shown in **Figure 27 and 28** were dropped from the discussion. One such compound, VUx86, produced very minor, almost indistinguishable linear shifts (**Figure 28A**) that did not saturate at relevant concentrations. When titrated with empty LMPG micelle, it produced linear CSPs in the methylene envelope, indicating that it is a membrane-binding compound; however, the compound had no notable effect on micelle size as measured by DLS. Furthermore, IM-MS could not detect this compound in complex with C99, furthering the notion that this compound induced perturbations on C99 only indirectly because of membrane binding. However, its effects were reproducible even from commercial sources, confirming its weak membrane-binding properties. It is concluded that this compound was partitioning into the membrane and non-specifically caused spectral changes in both C99 and Notch-1.

VUx83 (**Figure 28B**) produced larger CSPs in C99 and Notch-1, but also did not saturate and were primarily seen for juxtamembrane solvent exposed residues. Again, IM-MS could not detect this compound in complex with C99, suggesting its C99 perturbations were non-specific and not due to true complex. This compound also had no observable effect on membrane size by DLS, and produced linear CSPs on empty LMPG methylene resonances, confirming membrane binding. Overall, this compound displayed similar non-specific properties that are a theme of this chapter.

VUx17 (**Figure 28C**) was more interesting than most because this compound yielded titration curves that exhibited evidence of saturation and to which the 1:1 binding model could be fit, yielding an apparent K_D of 2mM. However, its binding was not specific to C99, with perturbations also seen for Notch-1 in LMPG. Furthermore, VUx17 did not appear to bind to C99 in bicelles, suggesting that the LMPG was playing a direct role in the interaction. However, the most interesting feature of this hit was that it was the only compound detected to be in complex with C99 by IM-MS. This discovery suggested to that this compound, which contains an anhydride group, covalently reacted with C99, as multiple mass shifts (1-3) were observed in C99, indicating that the stoichiometry was certainly not 1:1. Overall, this compound is likely a PAINS due covalent modification, which is still under investigation.

Both VUx688 and VUx488 (**Figure 29D/E**) produced some of the larger chemical shift perturbations that I witnessed in my studies. They appeared to be inducing a dose-dependent conformational shift in C99, particularly in solvent-exposed regions of the protein. However, both compounds bound only with weak affinity (COULD K_d BE DETERMINED?) and were also seen to perturb the NOTCH spectrum. Furthermore, they

exhibited marked reduced affinity for C99 in bicelles, indicating that their effects were likely mediated by the LMPG detergent. However, the most striking thing about these compounds was that four initial results were not reproduced when we repeated experiments using the putatively same compounds from commercial sources. This suggests some problems with these compounds in the original library we employed.

The most remarkable hit that arose from screening and primary example discussed in this chapter was 2,5-dimethyl-N-(pyridine-2-ylmethyl)aniline, which is referred to henceforth as VUx95 (structure shown in **Figure 29A inset**). VUx95 was unique because it induced massive chemical shift perturbations (CSPs) in C99 TROSY-HSQC spectra, suggestive of a binding-induced conformational change (**Figure 29A**). The residues that underwent the most extreme CSPs by [VUx95] titration, such as G696 and S697, as well as G756 and A740, and V736, were the water-soluble loops both N- and C-terminal to the C99 TM domain, respectively (**Figure 29B**). Interestingly, the transmembrane domain was only slightly affected, however smaller CSPs were observed in TM residues including A713, T714, and G700/704. Upon plotting the CSPs at various water-soluble residues, it became clear that the shifts were mostly linear with respect to [VUx95] dose up to 10 mM (**Figure 29C**). The lack of saturability and regiospecificity for the CSPs on C99 suggested that this compound was non-specifically perturbing solvent-exposed residues, which we confirmed by titrating [VUx95] against the topologically similar Notch-1 transmembrane/juxtamembrane (Notch-1 TM/JM) domain (**Figure 29D**).

²²³ We found that, like C99, Notch-1 TM/JM NMR spectra were linearly perturbed primarily

at solvent-exposed residues. Taken together, these data indicate that VUx95 is a weak

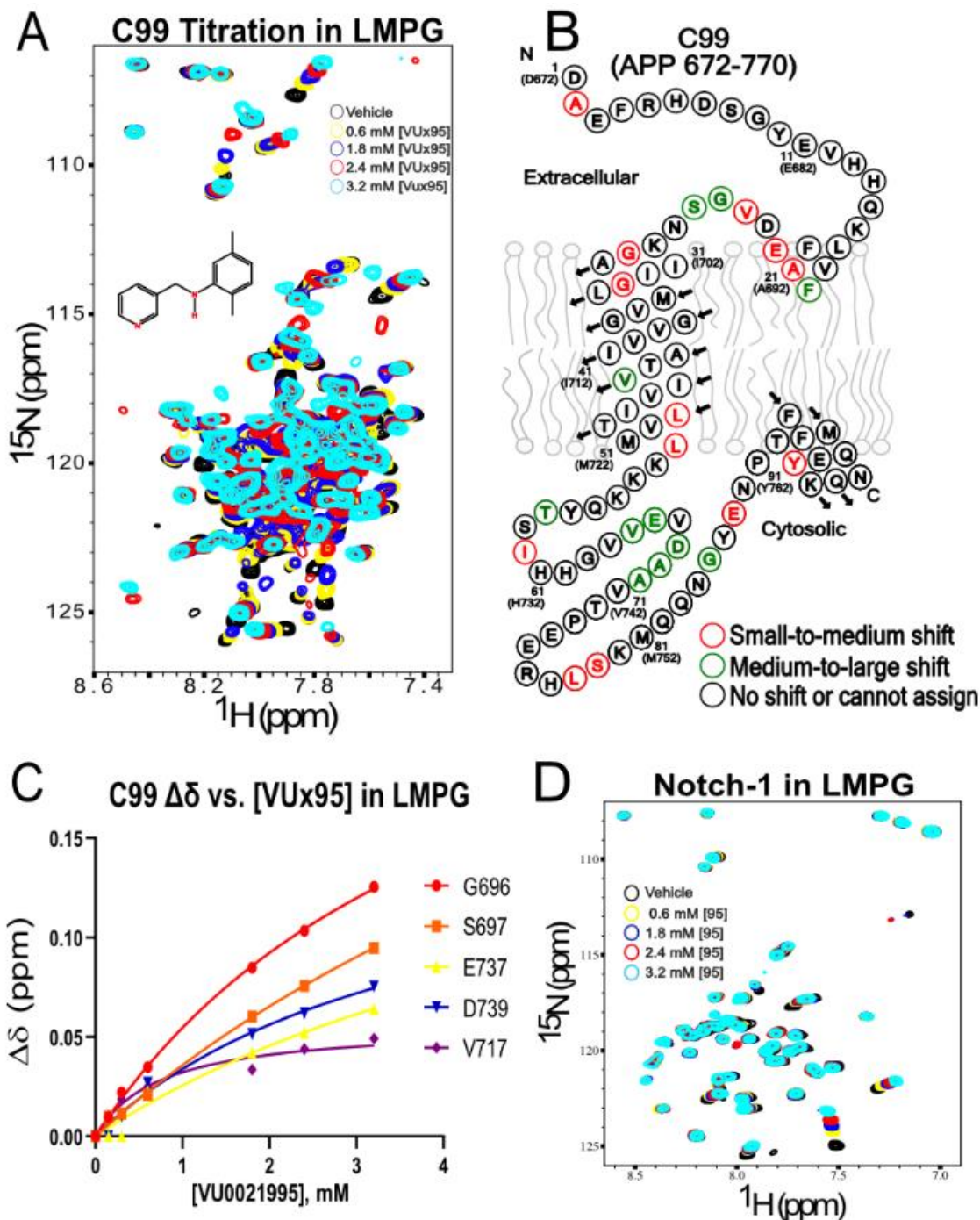


Figure 29. *VUx95 non-specifically perturbs C99 and Notch-1 NMR spectra in LMPG and does not saturate binding.* **A)** NMR titration of C99 in LMPG with VUx95 reveals large, non-saturable shifts in C99 residues, primarily in solvent-exposed regions. **B)** C99 topology map highlighting residues that underwent spectral perturbations in response to [VUx95] dose. **C)** Plot of C99 chemical shift perturbations (CSPs) in response to [VUx95] dose reveals that shifts do not saturate at the tested concentrations, suggesting very weak binding. **D)** NMR titration of Notch-1 in LMPG with VUx95 reveals large, non-saturable shifts in Notch residues, primarily in solvent-exposed regions like C99.

and unspecific membrane protein binder in LMPG micelles.

To confirm that VUx95 was inducing a conformational change in C99, we tested the solvent exchange properties of C99 with and without VUx95 present using a CLEANEX NMR experiment. The presence of a peak in the CLEANEX spectrum indicates

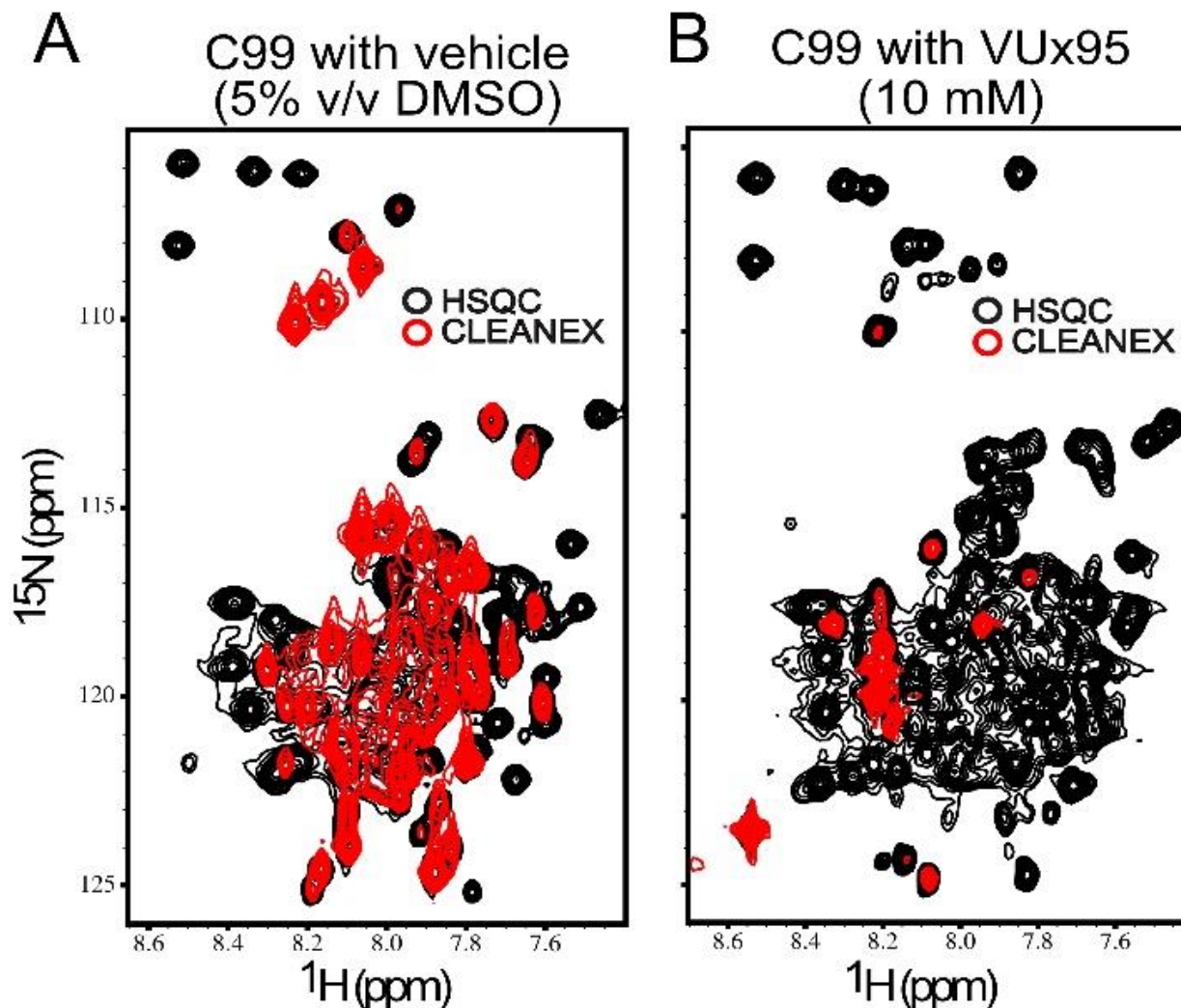


Figure 30. CLEANEX (Clean Exchange) HSQC (non-TROSY) NMR spectral overlaps of C99 with or without 10 mM VUx95 fragment. **A**) 2D CLEANEX-HSQC spectra (red) of C99 overlaid onto the corresponding HSQC (black) shows that the majority of C99 residues are undergoing exchange with the solvent in the absence of VUx95. The majority of C99 residues are solvent-exposed and undergo exchange, with the exception of transmembrane residues (such as the glycines at the top left). **B**) 2D CLEANEX-HSQC spectra (red) of C99 overlaid onto the corresponding HSQC (black) shows that the majority of C99 residues are undergoing exchange with the solvent in the presence of VUx95. VUx95 induces a major structural change in C99 that reduces the solvent-exchange of otherwise solvent-exchanged residues, such as those in the N- and C-loops.

the backbone amide is undergoing chemical exchange with the water solvent that is fast compared to the mixing time of the NMR pulse sequence. The DMSO-only treated C99 CLEANEX presented approximately 50 peaks that arise primarily from the N- and C-loops that underwent solvent exchange, consistent with the known topology of C99 (**Figure 30A**). However, addition of 10 mM VUx95 drastically reduced the solvent accessibility of C99 to only 15 residues, confirming VUx95 was likely altering the global conformation for C99 and subsequently alters its water accessibility in typically water-soluble regions (**Figure 30B**). Importantly, we noted the presence of both intense (rapidly exchanging) and weak (slowly exchanging) CLEANEX peaks in the presence of [VUx95]. This result was critical because it suggested that the changes in amide exchange were not due to

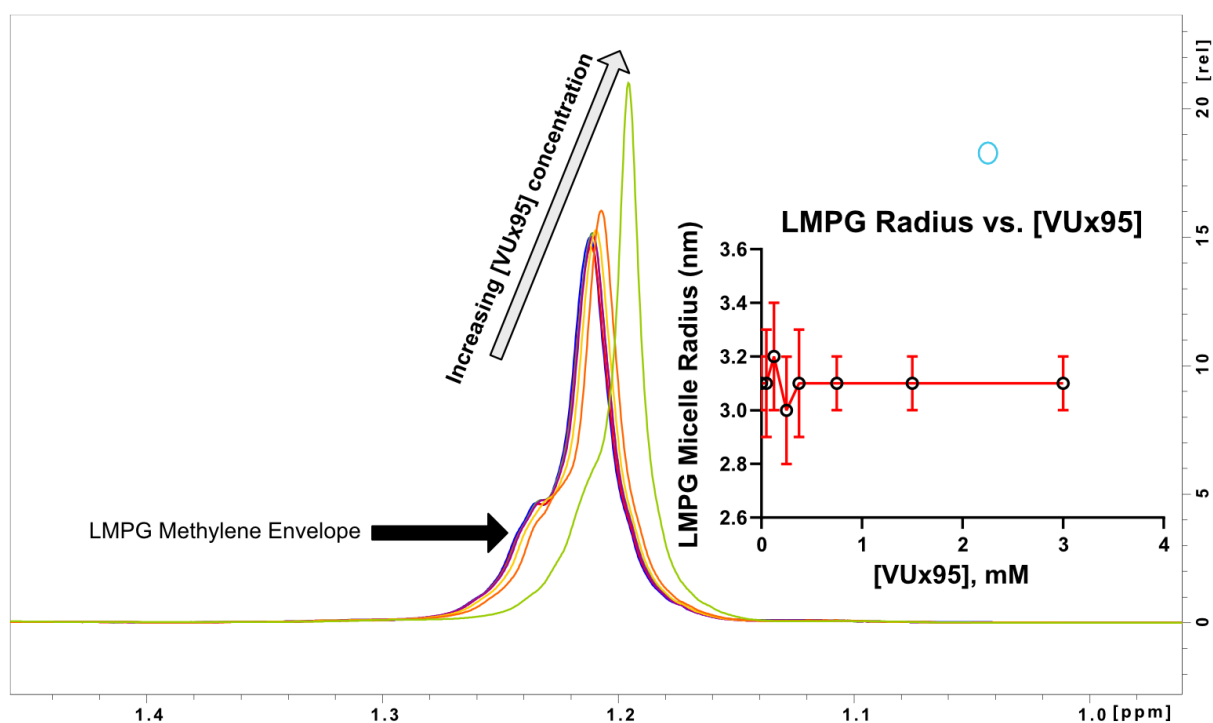


Figure 31. Titration of empty LMPG micelles with VUx95 indicates that the micelle size is unchanged, but that LMPG methylene dynamics likely have. ¹H NMR spectral overlay of the LMPG methylene envelope in response to [VUx95] dose displays a non-saturable line-narrowing of the LMPG peak, suggesting the compound is causing a change in the micellar dynamics. Inset: DLS measurements of the LMPG micelle in response to increasing [VUx95] indicates that the particle size is not changed by VUx95, indicating that the global micellar structure is largely unchanged.

pH shifts in the sample, which would result in global effects on solvent exchange dynamics in C99 amides. In general, we found these NMR data further supportive of an induced conformational change in C99 in response to [VUx95].

We wanted to verify that VUx95 effects were not a consequence of its effects on micellar size. Using dynamic light scattering (DLS), we monitored the size of the LMPG particle as a function of [VUx95] concentration (**Figure 31 inset**). There was no significant effect on LMPG particle size in response to VUx95, implying that this compound was not causing changes in the macrostructure of the micellar aggregate. Furthermore, we monitored the chemical shift of the LMPG methylene envelope without protein using ^1H NMR and found that VUx95 caused dose dependent linear CSPs, indicative of only non-specific interactions of VUx95 with micelles. Moreover, we observed line narrowing of the LMPG peak, possibly indicating a change in the dynamics of the acyl chains (**Figure 31**). Taken together, these data indicated that this compound was interacting with the LMPG micelle and likely altering its organization and without altering the global size of the particle.

It was expected that the shifts this compound induced were far too large and widespread to indicate any sort of sequence specificity against C99, which was corroborated by the initial titration against the Notch-1 TM/JM construct. The non-specific nature of the interacting compound with transmembrane proteins was confirmed by performing titrations in LMPG against the topologically distinct tetraspan transmembrane voltage-sensing domain of the KCNQ1 ion channel (**Figure 32A**).²⁵⁵ These data also showed non-specific and widespread linear CSPs in response to [VUx95] dose, suggesting that VUx95-induced effects were indiscriminate of membrane protein

secondary or tertiary structures and were likely mediated by interactions with the LMPG membrane mimetic. To test that idea, VUx95 was titrated against C99 in zwitterionic bicelles composed of 3:1 (mol:mol, $q = 0.33$) dihexanoylphosphatidylcholine (D6PC):dimyristoylphosphatidylcholine (DMPC), which is both structurally and chemically distinct from anionic LMPG micelles (**Figure 32B**). Interestingly, we found that there were markedly fewer CSPs in C99 in bicelles, with unsaturable shifts observed at only approximately ten residues. Furthermore, the shifts were significantly smaller in magnitude compared to the equivalent titration in LMPG, where massive shifts were documented. Taken together, these data provided initial evidence that the LMPG

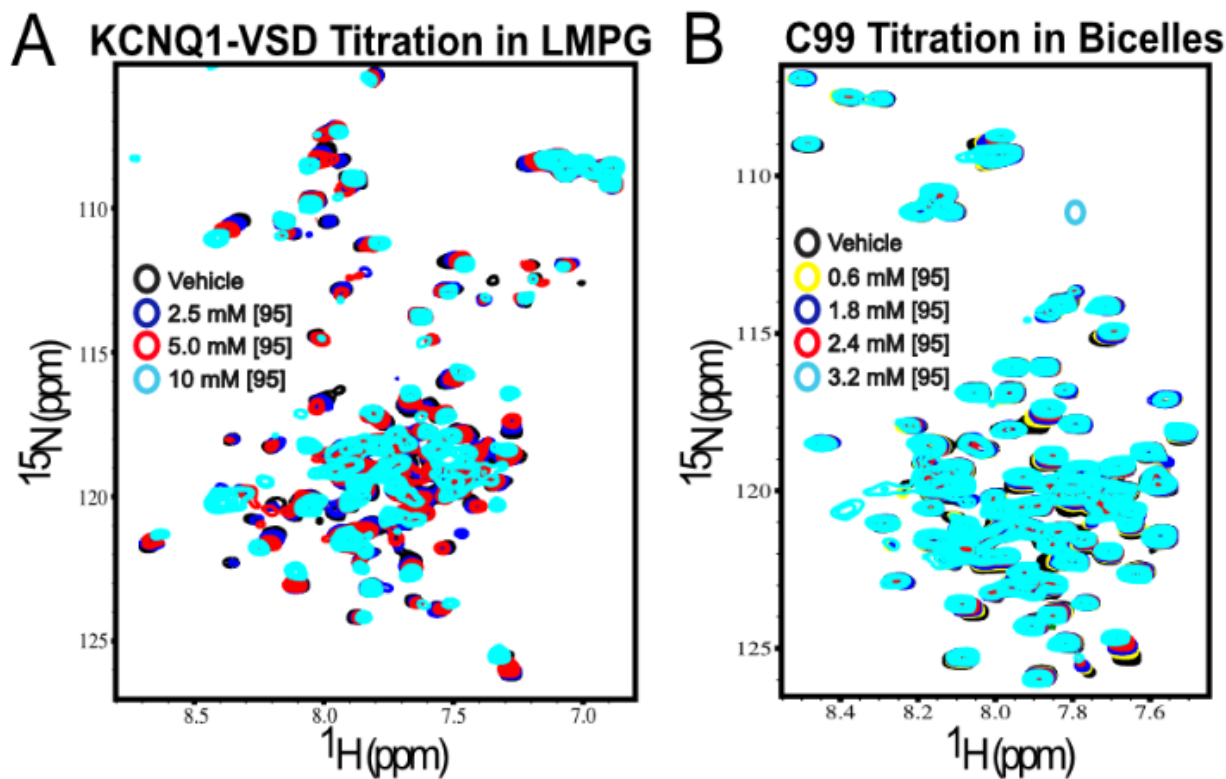


Figure 32. Titration of VUx95 against KCNQ1-VSD protein in LMPG and against C99 in DHPC/DMPC bicelles confirms the fragment's non-specificity and LMPG-dependence, respectively. **A**) NMR spectral overlay of KCNQ1-VSD, a tetraspan integral membrane protein, in LMPG in response to increasing [VUx95] dose confirms that VUx95 non-specifically interacts with membrane proteins in LMPG and is indiscriminate of protein topology. **B**) Titration of bicelle-embedded C99 with increasing amounts of [VUx95] revealed only minor shifts in C99, suggesting that the effects observed in LMPG were LMPG-dependent. However, the fact that shifts are still observed here does suggest that there are direct interactions with VUx95 and C99.

membrane mimetic was playing a critical role in mediating the interaction between membrane proteins and VUx95, although some interaction of this compound with C99 in bicelles was seen.

Up to this point, the evidence was mounting that VUx95 was exhibiting PAIN-like behavior in the LMPG system. We hypothesized that this compound's relatively hydrophilic pyridine lobe was likely driving the interactions with the solvent-exposed regions of C99. We tested this idea by conducting SAR by NMR of VUx95 analogs that altered the chemistry of one or both lobes (**Figure 33**). All analogs except one either entirely lost or reduced the ability to cause CSPs in C99 NMR spectra. However, one analog, VUx95_C, still caused interesting shifts after replacement of both lobes with toluene moieties meanwhile retaining the chemistry of the amine linker. Remarkably, VUx95_C significantly altered the CSP profile of VUx95, such that chemical shifts were observed primarily in TM residues including I712, A713, T714, and N-loop residues including G700, E693, G696, and G697. Similarly, we observed that the C-loop residues were almost entirely unperturbed by this analog, indicating it had a preferred binding region near the N-terminus of the TM domain. However, binding of CX99 by this compound remained weak ($K_D > 10$ mM) and produced non-saturable linear CSPs on C99 spectra, suggesting that it was inducing effects in a non-specific manner, like the

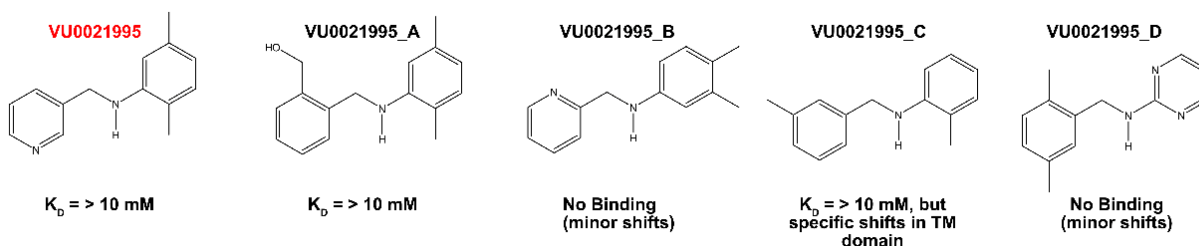


Figure 33. SAR by catalog of VUx95 did not significantly enhance the binding affinity for C99 in LMPG. This figure shows the terse SAR-by-catalog I did to see if VUx95 affinity could be increased by exploring analogs. Overall, the affinities remained the same or were weakened compared to the VUx95 parent.

VUx95 parent fragment. The inability to further advance the specificity or potency of these compounds led us to cease further exploration of its class. These data provided sufficient evidence that these compounds were likely PAINS for detergent-embedded proteins and were likely driven by interactions with hydrophilic headgroups and/or hydrophobic membrane partitioning. Another alternative explanation is that VUx95 is a generally sticky molecule and binds both the micelles and all exposed domains of C99, however the exact mechanism is not entirely clear.

A final control experiment using a soluble protein Calmodulin was done to verify if the VUx95 effects were specific to membrane proteins. Using the same conditions as the other titrations (minus the presence of membrane mimetic), linear perturbations in Calmodulin were observed using NMR (**Figure 34**, left panel). These perturbations appeared like what was seen for C99, Notch-1, and KCNQ1-VSD, and suggested that the

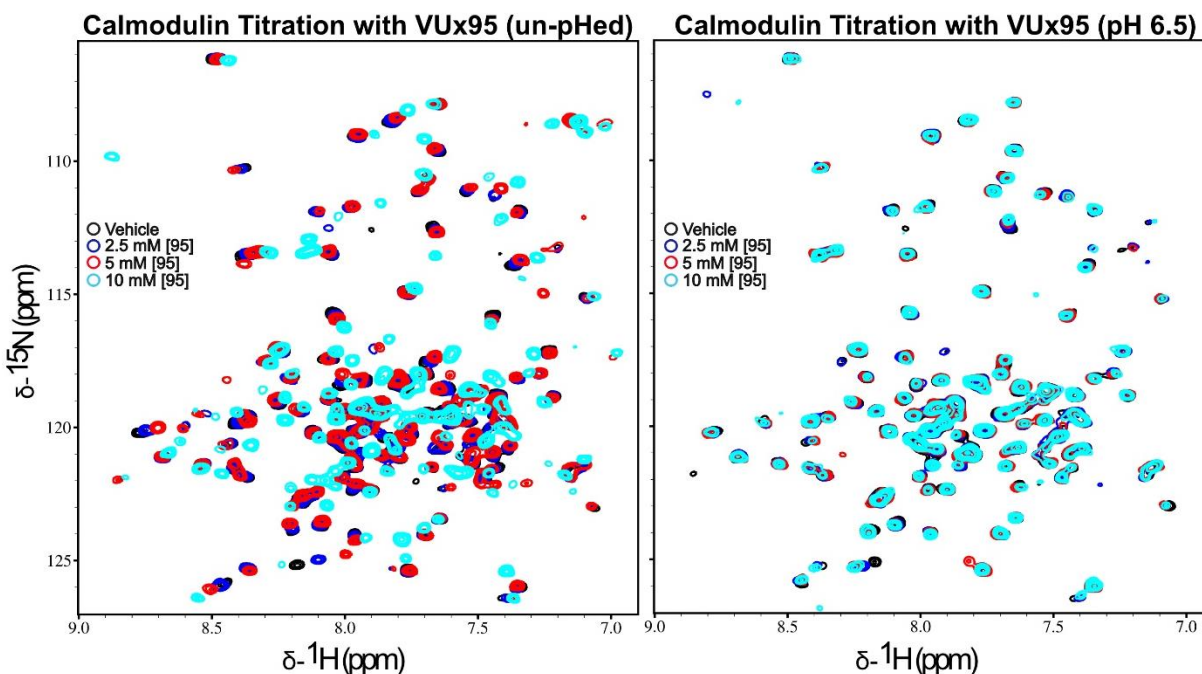


Figure 34. *Calmodulin titration with VUx95, with or without pH control.* Left: NMR-observed titration of water-soluble ^{15}N -Calmodulin with [VUx95] reveals linear, dose-dependent shifts across the protein. Right: After pH adjustment of VUx95-containing samples back to the normal pH of 6.5, the massive shifts are reversed, indicating pH-change was responsible for the massive spectral shifts observed.

linear effects that I observed in all the proteins were entirely independent of the membrane mimetic. It was then hypothesized that VUx95 was changing the properties of the solvent in a global way that was primarily affecting solvent-exposed regions of proteins. It was found that the pKa of the pyridine lobe on VUx95 was approximately 5.1-5.2, so the pH of protein-containing samples were tested after the addition of VUx95. The pH of the samples containing high concentrations (5-10 mM) of [VUx95] were significantly more acidic, having transitioned from pH 6.5-6.6 without compound to pH 5.2 in the presence of 10 mM [VUx95]. This result was unexpected, because the NMR samples contained 50

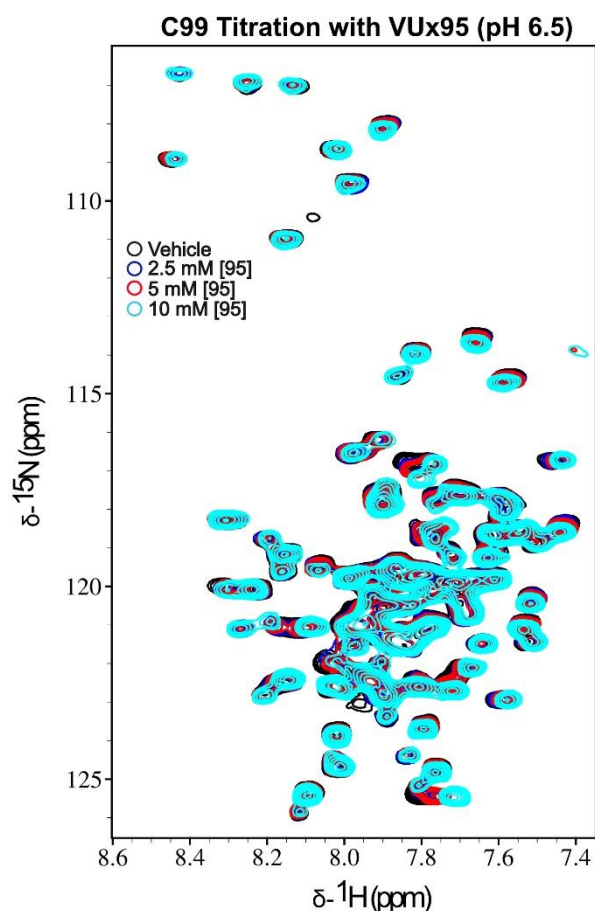


Figure 35. *pH-controlled titration of C99 with VUx95*. This figure depicts the residual spectral perturbations resulting from titration of LMPG-embedded C99 with VUx95. All samples had their pH brought to 6.5-6.6 after addition of VUx95, resulting in the abolishment of the large spectral shifts that were previously observed without pH control. However, weak and linear spectral perturbations were still observed for some transmembrane/juxtamembrane residues (L723, G696, G709, S697, etc), indicating that VUx95 is still a PAINS molecule beyond its pH-changing properties.

mM PIPES, which has strong buffering capacity at neutral pH. It was then clear that the VUx95 that was being used was likely in the acidic salt form, which resulted in linear pH changes with respect to [VUx95] concentration. When the pH of VUx95-containing Calmodulin samples were corrected back to pH 6.5-6.6, the global spectral changes that were observed originally were almost entirely abolished (**Figure 34**, right panel). However, some resonances continued to shift linearly with respect to [VUx95] concentration, suggesting that VUx95 was still likely a PAINS molecule even with proper pH control.

The pH-dependent spectral shifts were confirmed by a pH-corrected titration of VUx95 against C99 in LMPG, where the massive and global spectral changes in solvent-exposed residues were replaced by minor and linear perturbations of both solvent-exposed and some transmembrane residues (**Figure 35**). However, minor linear perturbations in certain transmembrane C99 residues were observed, suggesting that the compound was still behaving like a PAINS molecule, likely by membrane insertion and disruption because no shifts were not observed for Calmodulin after pH correction. These data highlighted the importance of using high concentrations of buffer during high-throughput screening to avoid any pH effects that the small molecules may induce.

Discussion:

The combination of the work described in Chapter 3 with this chapter describes the general methodology used to discover small molecule binders for a transmembrane protein in detergent micelles. Furthermore, this work details useful hit validation experiments that should be employed when conducting such screens to identify and eliminate membrane protein PAINS from unnecessary exploration. Although this

manuscript focuses on the anecdotal discovery and deconvolution of one such compound (VUx95), these types of validation experiments were also conducted for the remaining six mentioned hits from the 15,000-fragment screen (**Figure 27**). All except one (VUx76; see Chapter 6 Future Directions) were determined to be false-positives and likely PAINS due to one or multiple of the following properties: non-specific interactions with membrane proteins and/or detergent micelles, detergent-dependent binding resulting in irreproducibility in other membrane mimetics, or likely reactivity with membrane proteins. Despite providing only a single potentially useful compound for small molecule probe development, these results remain significant as they provide a framework for membrane protein drug discovery and highlight issues that may arise during screening and subsequent hit-to-lead validation.

We previously successfully used this HTS method to discover a more potent ($K_D = 17 \mu\text{M}$) and C99-selective small molecule from a different small molecule library, confirming its usefulness beyond PAINS discovery.²⁵⁶ The original intention for this fragment screening project was to discover and/or develop small molecules that bind C99 selectively and potently by coupling FBDD to medicinal chemistry. However, that goal is not currently feasible because we are confident the six remaining initial hit fragments presented here are exhibiting PAINS-like interactions with C99 rather than forming a stoichiometric complex. Regardless of their properties in our system, it is possible that these compounds may still be useful as building blocks of drug-like molecules without PAINS activity.²⁵⁷ For that reason, we do not intend for this study to prescribe the elimination of these compounds from small molecule libraries. Rather, we suggest that the future re-discovery of such compounds in HTS screens involving membrane proteins

should take these results into account—care should be taken to clarify whether they are *bona fide* hits or not.

The work in the Chapter also highlights the importance of doing upfront control experiments to validate the robustness of the screening system. As shown by Figures 34 and 35, the controls should also include verifying the buffer capacity of the system. While most of the PAINS molecule presented and discussed in this chapter did not have an effect on pH, pH validation should be considered a necessary part of the HTS pipeline, particularly when dealing with compounds in the millimolar or higher range.

Many membrane proteins are well validated drug targets of significant interest for drug development. It is becoming increasingly clear that membranes and membrane mimetics themselves can act as mediators of membrane protein-small molecule interactions, particularly if the binding site is at the protein-membrane interface.²⁵⁸⁻²⁵⁹ We highlight that it is imperative to execute drug discovery screens only after substantial justification is made for the type of membrane mimetic used to solubilize the target protein(s). Furthermore, we illustrate the importance of reproducing binding experiments against an array of membrane proteins and membrane mimetic systems to confirm the breadth and selectivity of hit compounds. We hope this study provides useful insight for small molecule discovery in detergent-solubilized systems, and that these lessons result in reduced time and resources spent following up with PAINS compounds.

Chapter 6

Concluding Discussion and Future Directions

My PhD project was intended to primarily address two objectives: 1) to develop a high throughput screen and hit validation pipeline that is amenable to single span transmembrane proteins; and 2) to use this pipeline to discover small molecule binders of the AD-implicated C99 protein and characterize their effects. Chapter 3 of this document covers the early stage of the project, focused on developing a screen by exploring a myriad of conditions such as sample and NMR parameters. Chapter 4 describes the initial use of the pipeline, where I screened a library of 1,200 FDA-approved small molecules and found one, verteporfin, that bound C99 with low-micromolar (17) K_D and functioned as a substrate-selective inhibitor of γ -secretase. Conversely, Chapter 5 described a later use of the pipeline on a library of 15,000 small molecule fragments, and that produced a single selective binder of C99 plus six PAINS-like compounds that non-specifically perturbed all TM proteins in LMPG, with questionable reproducibility in other model membrane conditions. One of these PAINS, VUx95, was studied in detail. This final chapter will discuss the take-home points from this work and the future directions where it may lead, as well as any outstanding questions and preliminary data that will guide this work moving forward.

Before diving deep into the final discussion, a few personal points that highlight my passion for this work should be reviewed. When I made the decision to join the Sanders lab, my knowledge of the C99 / Alzheimer's disease project was relatively limited. I had an understanding that C99 was the precursor to amyloid- β (A β), an Alzheimer's hallmark and putative disease-causing peptide that was covered several times during my undergraduate biochemistry and biology classes. However, the first time

I had heard the name amyloid- β was when I was 10 years old in the car with my grandfather, who would listen to NPR on his car radio while he drove me to piano lessons. The NPR pundit was interviewing a scientist who was discussing a putative cause of Alzheimer's that developed into the plaque-like substance in the brain. This was one of many radio topics that were covered on his radio over the years, however it is the only one I can remember in such detail. Since then, I have always been interested in the concept of amyloid and my interest in neurodegeneration more globally was certainly enhanced by my grandfather's lost battle with neurodegeneration (ALS).

That radio segment was around circa 2004, and I now understand that was a time where A β was at the center of the Alzheimer's spotlight. The genetic disease evidence from the 1980's and 90's had spurred a widespread interest in A β by doctors, scientists, and pharmaceutical companies alike. A lot of seminal work was accomplished around that time with regards to figuring out the details of how A β is created in the brain, its destructive biological effects, and how it could be destroyed or reduced by pharmacological intervention. However, the laser focus on A β ironically resulted in a significant gap in knowledge in the basic biology of amyloid- β precursor protein (APP) and the immediate precursor to A β , C99. While I admit that gap in knowledge is closing, there is still a lot of work to be done before the scientific community understands just how many ways this protein and its proteolytic products are involved in AD, aging, and human development.

I figured that I could make a small dent in this knowledge gap by studying C99, which is a single-pass TM receptor protein that the Sanders lab had made significant

progress studying over nearly two decades. Dr. Sanders had brought up the concept of trying to develop a drug for the protein in my final lab rotation, and it seemed like an intriguing idea that would give me training that was relevant to my previously honed skills in membrane protein biochemistry/biophysics and my emerging interests in drug discovery. I now understand that the work I would do was unlikely to ever amount to a drug that could be used in humans, much less that it would even amount to a successful drug in preclinical models. However, the principles of the project and the potential implications generated a notable excitement in me. This project would allow me to drive research into a major scientific question: could we find a small drug-like molecule that binds a simple, single-pass transmembrane protein such as C99?

If a C99-specific small molecule binder could be discovered or developed, new aspects of APP biology could be probed chemically and could theoretically further close the gaps in knowledge related to this protein and its biology. However, C99 is a non-ideal drug target for several reasons, including its limited and membrane-embedded druggable surface area. Most “good” drug targets have significant surface area in their binding pockets, and C99 has only a single-span transmembrane domain with floppy flanking loops on either side. However, it does have a limited tertiary structure because of the amphipathic N- and C- helices that partially partition into the membrane and create a concave *pseudo*-pocket in its 3D structure. Indeed, cholesterol binds C99 specifically in the concave pocket between the TM helix and the amphipathic N-helix, and that suggested other molecules, such as cholesterol analogs, lipids, or hydrophobic drugs, could bind C99 in that same pocket or the equivalent between the TM helix and the C-helix. The well-studied interaction between C99 and cholesterol was the original proof-of-

concept suggesting C99 could bind other small molecules, and I wanted to take that feature to the next level by screening the protein against thousands of them.

The first binder that I detected was serendipitously from the first plate of small molecules that I ever tested: plate 2 from the Fesik Fragment Library. The compound, which I refer to as VUx76 and is discussed more heavily future directions section below, appeared to bind C99 specifically in the C-terminal segment of the transmembrane domain. The K_D was a weak $\sim 400 \mu\text{M}$, but it was the initial reinforcement the project needed to suggest that our screening parameters could detect C99 binders. The VUx76 binder, which is initially discussed in Chapter 3 and recapped in Chapter 5, is still under investigation and regarded as a future direction because there are still outstanding questions on that front. Specifically, the questions pertain to reproducibility issues with this compound and its analogs, which I heavily discuss in the Future Directions section. However, the initial discovery of VUx76 propelled this project to switch gears from screening the Fesik Fragment library to a library of FDA-approved drugs in hopes of finding something that could be more immediately useful in cellular and preclinical AD models.

Screening the SelleckChem FDA-approved drug library produced about 20 initial hit compounds that had effects on C99 NMR spectra. Upon reproduction and titration of the hits, only one compound, called verteporfin, convincingly displayed binding properties at relatively potent ($K_D = 17 \mu\text{M}$) concentrations. This affinity was almost 20-times stronger than the original VUx76 fragment compound and remains the tightest binding small molecule for C99 that my studies unearthed. Early on in this project, a

collaboration was started with Dr. Mike Wolfe from the University of Kansas, who is a pioneer of the amyloidogenesis/ γ -secretase field. We sent him and his postdoc, Dr. Ilyas Beg, some verteporfin to see if it had any effect on γ -secretase cleavage of C99. Specifically, they monitored the cleavage of C100 (C99) by γ -secretase as a function of verteporfin concentration in detergent-solubilized assays. Strikingly, they observed the first evidence that verteporfin was inhibiting γ -secretase, with an initial IC_{50} value of ca. 15 μ M. This result was impressive because it matched perfectly with our observed verteporfin K_D for C99 and encouraged us to switch the aims of the project from simply discovering small molecule binders of C99 to discovering small molecule binders of C99 that selectively inhibit γ -secretase proteolysis, which is largely where the project is now.

γ -secretase inhibitors to reduce amyloid burden have been widely explored up through clinical trials but have largely been abandoned as a clinical concept because of off-target effects of early generation γ -secretase inhibitors (GSIs). However, a route that has been only partially explored was to discover and optimize a C99-selective γ -secretase inhibitor, or a compound that targeted the C99 substrate itself and reduced amyloid burden without disrupting γ -secretase cleavage of other essential substrates such as Notch. At that point, the Sanders-Wolfe collaboration hit full gear, as we wanted to explore if verteporfin exhibited C99-selective properties by running the same assays against the Notch-1 substrate, of which proteolytic inhibition is toxic. Overall, we found that verteporfin acted as a γ -secretase inhibitor for both substrates at high concentrations, but at low concentrations where C99 cleavage was inhibited, Notch cleavage was activated. This meant that, with proper dosing, verteporfin was a C99-selective GSI with a 2-3-fold selectivity, depending on the exact Notch substrate used. Considering our

results showed that verteporfin had a negligible affinity for Notch-1 in model membranes, the bi-phasic (activator at low and inhibitor at high verteporfin concentrations) Notch cleavage result suggested that verteporfin was likely affecting its cleavage by non-specific effects such as membrane or γ -secretase perturbation.

To point towards a mechanism of verteporfin-induced γ -secretase inhibition, I extensively studied this interaction in various model membranes using NMR, mass spectrometry, and chemical crosslinking techniques. Our data pointed to the conclusion that verteporfin bound the C99 monomer and had a negligible effect on inducing dimerization of C99. This concept was useful to prove because I had an early hypothesis, based off preliminary ion-mobility mass spectrometry (IM-MS) data, that verteporfin was inducing dimerization of C99. Dimerization of C99 is a known mechanism for reducing amyloid production because γ -secretase can only recognize and proteolyze the monomeric form of C99, such that an induction of dimerization could explain why verteporfin inhibited γ -secretase cleavage of it. However, neither IM-MS nor glutaraldehyde crosslinking of C99 revealed any change in oligomeric state in response to verteporfin dose, indicating verteporfin bound the C99 monomer. This led us to postulate a γ -secretase inhibition mechanism where verteporfin binds the monomeric C99, forming a complex that is inaccessible to the γ -secretase active site and results in reduced C99 proteolysis.

Overall, the verteporfin discovery and characterization manuscript was well received at the *Journal of Biological Chemistry*, requiring no experimental revisions before acceptance. Simultaneous with the completion of the verteporfin project, I was also

concluding my work on the Fesik Fragment Library. The fragment library produced seven initial hit compounds that reproducibly induced dose-dependent NMR spectral perturbations in C99 and were followed up with. However, upon further exploration, it quickly became clear that six of the seven were likely non-specific compounds that bound transmembrane proteins in the LMPG membrane mimetic. I could only confidently assert that one compound, VUx76 (that is still under investigation), was a true C99-specific binder. The six other fragments displayed properties that made them appear to be pan-assay interference compounds (PAINS) for transmembrane proteins in LMPG, which is the main topic of Chapter 5.

PAINS compounds are an increasingly discussed phenomenon in the medicinal chemical and high-throughput screening literature. They are small molecules that typically lead to false-positive hits due to a target-independent sample perturbation.^{253-254, 260} Some mechanisms for PAINS activity include but are not limited to compound aggregation, non-specific covalent modification of the target, and fluorescent assay disruption. As PAINS compounds are identified in the literature, they may be removed from small molecule libraries to avoid future false-positive assay readouts. Most of the PAINS that have been reported produce false positive hits in purified soluble-protein or cellular phenotypic screening experiments. There is a significant gap in knowledge pertaining to what types of molecules may be PAINS for transmembrane proteins in model membranes. Although it was not the intention for the fragment screening project, the PAINS-like compounds I discovered when screening C99 may provide insight into that concept.

Chapter 5 heavily outlined the type of work I did to generate evidence that one such compound (VUx95) was a PAINS, and those types of experiments were mostly done for the remaining five compounds. Unsurprisingly, all the compounds were partially or entirely hydrophobic and aromatic, and likely partitioned into the LMPG micelle or interacted with its negatively charged headgroup. Other than similar degrees of aromaticity, the compounds were all structurally distinct from one another and displayed unique NMR spectral perturbations in C99 that were difficult to compare between them. However, an interesting observation I made was that VUx95 and VUx488 induced quite similar shifts in C99. I posit that the similarity is due to the pyridine moiety present on both compounds, because when I found analogs of VUx95 that replaced the pyridine with a benzene ring, those widespread effects were almost eliminated. SAR was not conducted on VUx488 to confirm this finding for that compound but that I hypothesize it would, and that the pyridine moiety was interacting with the LMPG headgroup.

For a more general perspective, the major take-home message from the fragment screening project was that small molecule fragments may not be the best method of high-throughput screening for this type of protein. I find it more likely that screening of a larger library of larger and more drug-like molecules, such as those in the Vanderbilt Discovery Library, would have produced tighter-binding hit compounds with more desirable pharmacological properties. I started screening a curated subset of the most structurally diverse compounds in that library, which contained approximately 10,000 out of the 150,000 small molecules that are present in the entire library. I was able to screen approximately 3,000 out of the curated 10,000 and saw no evidence of any hits, which resulted in me largely abandoning the project to focus on finishing up the FDA-

approved and Fesik Fragment projects. However, considering my low hit rates (< 0.1%) from the Fesik Fragment or FDA-approved drug libraries, it is likely that there would be C99-binding molecules in that library that may have not been present in the initial 3,000 I screened. Furthermore, the conditions that I used to screen the Discovery library were relatively dilute (20 μM of each compound) compared to the FDA-approved (50 μM) and Fesik Fragment libraries (~600 μM). The Discovery Screen was intentionally designed to be dilute because it would select for tighter binding molecules, however I realize now that may have been a mistake because the screen would also select against possible weak binders that could also have been good starting points for medicinal chemistry. This leads me to draw a major conclusion that NMR-based small molecule screening should likely be done at higher concentrations of small molecule, if possible, to ensure that binding events are saturated enough to be detected in the NMR spectra.

Another major question that drove this work was “how druggable is the C99 protein?”, and more generally, “how druggable are single-pass TM proteins in/around their transmembrane domains?” This question is loaded and may not be entirely answered, but my work has provided some insights. Based on my findings, it appears that C99 is certainly druggable, but it is not an ideal drug target and is unlikely to bind small molecules much tighter than the compounds I present in this thesis. That being said, my screening work was not comprehensive enough to conclude that C99 binders could not be tighter, especially if medicinal chemical SAR optimization was employed. I believe that if the fragment project worked out as we intended it to and gave way to at least two true C99 binders (non-PAINS), we would have had a better shot at generating a tight binder ($K_D < 1 \mu\text{M}$). However, it is not clear that type of work was ever possible for

C99, because it lacks the necessary tertiary structure to have multiple nearby pockets sites for small molecule fragments to bind. Overall, I think the work I present in Chapter 5 of this document is suggestive that FBDD may not be the best route to develop ligands for SPTMR proteins such as C99 in model membranes. However, my work does not eliminate the potential FBDD to work for multipass TM proteins, which offer more druggable surface area as well as internal pockets. A future direction investigating such a concept is currently under works in the Sanders lab, where colleagues of mine are screening the Fesik Fragment Library against a tetraspan membrane protein called PMP22. I find the likelihood of discovering PMP22-binding fragments far more plausible and the discoveries from that project will add to the growing body of knowledge pertaining to the druggability of recalcitrant membrane proteins.

Another major conclusion to draw from my work is that screening membrane proteins in model membranes inherently selects for hydrophobic or amphipathic small molecules. This means that hit compounds will likely have a significant potential to bind proteins at the protein-membrane interface and may lead to a greater degree of non-specificity than a more simple, soluble protein system. Most of the compounds my studies unearthed were hydrophobic molecules that had an affinity for membrane mimetics even in the absence of an integral membrane protein. Furthermore, all the screens discussed in this thesis were done in extremely high levels of detergent (2.5% w/v, 50+ mM). The protocol was intentionally designed this way to ensure a 16-fold excess of detergent micelles relative to protein, with the rationale that it would eliminate potential false positive binders due to forced cohabitation of detergent-partitioning small molecules with C99 by diluting them away. However, my discoveries suggest that this type of design paved the

way for different artifacts by providing sufficient membrane space for hydrophobic molecules to embed into. In other words, I wonder if screening C99 in lower detergent concentrations, such as 1:1 or 1:3 protein:micelle, would have eliminated the selection for these membrane binders. Did having a 1:16 protein:micelle ratio bias towards discovering more hydrophobic, membrane-loving compounds? I think answering that question, which would require rescreening the library at the lower protein:micelle ratio and comparing the hydrophobicity of the hit molecules, would offer great insight for future high-throughput screening strategy. I consider that type of work another future direction for another person, and in some ways, the fragment screening with PMP22 may provide some insights into it. As mentioned, my colleagues are currently screening it against the Fesik Fragment library, and they are doing so at a lower protein:micelle ratio (1:10). Their findings may not directly translate to my system or answer the question, but taken together with my findings, I suspect it will provide insight and help guide future high-throughput screen design for membrane proteins.

Regardless of whether the approach I took to discover C99 binders was the most perfect, I do still think that C99 itself is a validated drug target. I heavily discuss this concept in Chapter 1, and I think the discovery that verteporfin both binds C99 and inhibits amyloid formation is significantly provocative in favor of that assertion. Small molecules fragments may not be the best approach to develop a chemical probe for C99, but I have long wondered if an antibody or nucleotide aptamer targeting the extracellular domain would be a fruitful approach to reduce amyloid burden. Specifically, an antibody or aptamer that could potentially bind the N-loop C99 region would likely occlude C99 from being recognized by γ -secretase and reduce amyloid formation in a highly potent and

specific way. To my knowledge, such a concept has not been fully explored for C99 and may be worth trying if a chemical probe for C99 is still desired in the future.

A major contraindication of the work I conducted in this thesis should be discussed before concluding the document. As I mention in Chapter 1, inhibition of γ -secretase mediated proteolysis of C99 may pose its own deleterious biological consequences, as accumulation of C99 also has implications in AD pathogenesis. I have held that idea in the back of my mind throughout the entire process of my PhD and for that reason, I do not make any bold claims that this route of therapeutic intervention would be useful clinically. Over 400 AD-targeting therapeutics have entered and left clinical trials over the last three decades, many of which have targeted the amyloidogenic pathway in some way and reduced amyloid burden without benefiting cognitive or behavioral impairment. As such, my confidence in amyloid-centric therapeutic intervention is dwindling because it is becoming clearer that amyloid is only part of the AD puzzle and is probably the tip of the iceberg. The recent FDA-approved drug aducanumab, a monoclonal antibody that targets highly toxic soluble amyloid- β oligomers, is a great example of how amyloid burden may be more of a symptom of disease rather than a cause. Aducanumab has a marked effect on reducing amyloid burden in the human brain, however it has a near-negligible effect on stopping or reversing cognitive decline. The early clinical trial evidence of this antibody was not compelling enough to consider it a disease-modifying therapy, at least in my opinion. Nonetheless, the FDA approved aducanumab in the summer of 2021 and spurred significant controversy that brought into question the efficacy of the FDA approval process. Whether this antibody will pan out to

be a useful treatment in the long run will be seen in the coming years, but I do not expect it to last long on the market.

An important future direction of the AD field will be to develop therapeutics that target the APOE- ϵ 4 variant. APOE is an apolipoprotein that functions as the primary lipid transporter of the brain.²⁶¹ There are dozens of APOE variants in the human population but the most well studied are APOE- ϵ 2, - ϵ 3, and - ϵ 4. Significant evidence is having mounted showing that the ϵ 4 allele is the largest genetic risk factor for AD, with ϵ 3 being the wildtype-like normal sequence, and ϵ 2 being protective against AD. The mechanisms by which why these variants play their roles in AD are largely conjecture, but they appear to mediate or perhaps propagate toxicity associated with amyloid oligomers and plaques.²⁶² Early evidence of pharmacological disruption of APOE- ϵ 4 is promising.²⁶³ I predict that APOE- ϵ 4 targeting therapeutics will be a more fruitful approach to AD treatment than amyloid-centric treatments, at least until we understand the amyloidogenic pathway better.

My PhD work was largely amyloid-centric in nature, and I often wonder where my work will leave the field, or if it will be largely forgotten as new discoveries implicate novel targets for Alzheimer's disease intervention and shift the field away from the amyloid cascade hypothesis. Indeed, there are now dozens of therapeutic avenues that are being pursued in the global endeavor to defeat this debilitating and truly horrific disease. Dr. Alzheimer's early discovery of amyloid in Auguste Deter's brain, coupled to the more recent genetic and biological evidence implicating the amyloidogenic pathway in AD, have resulted in a hyperfocus on the amyloid cascade hypothesis. At this point in

history, amyloid-centric therapeutics still have the major market share with regards to scientific and clinical investment, but over the last decade, that share has reduced. If the trend continues and amyloid-targeted therapies proceed to fail on delivering efficacious AD treatments, I can only imagine that the field will shift to other therapeutic avenues such as metabolic and symptomatic management.

I think that my research over the years, both in terms of empirical lab work and literature searching, alludes to a major upcoming shift in the AD field. Specifically, I predict that the future of the AD field will shift away from focusing on AD hallmarks and set its sights on tackling the more general phenomenon of human aging. Indeed the biggest risk factor for AD is age, and a deep understanding of how aging changes the physiology of the brain and body generally may provide insights into how we can slow aging down or reverse it. Furthermore, a deep understanding of aging would likely translate to therapies or changes in lifestyle choices that will also modify the onset and progression of Alzheimer's disease. It is for that reason that the foreseeable future of my scientific career will work on understanding underlying mechanisms of aging and general age-related diseases.

With this final discussion, I conclude the main text of this document. I refer the reader to the contents below for detailed methods and preliminary data that may be revisited in the future by others and/or myself. I believe that I have left the C99 project significantly more advanced than when I inherited it and have made contributions to the way the Sanders lab thinks about drug discovery. The Sanders lab is now pursuing drug discovery projects on membrane proteins from a variety of angles, including NMR-based

drug discovery, which I think is motivated, at least in part, by the precedent that I helped set. More generally, I hope this work shifts how the scientific community thinks about drugging C99 with regards to amyloidogenesis, and perhaps other disease related SPMTRs beyond C99. That may never happen, but I take solace in the idea that my work may not have immediate implications, but may one day it may spark a revolution, just as Dr. Alzheimer's work did 100 years ago.

Materials and Methods

Reagents:

β -n-Dodecyl melibioside (DDMB; Part# ME12) was purchased from Anatrace. 1-myristoyl-2-hydroxy-sn-glycero-3-phospho-(1'-rac-glycerol) (LMPG; CAT# 858120), 1,2-dimyristoyl-sn-glycero-3-phosphocholine (DMPC; CAT# 850345), and 1,2-dihexanoyl-sn-glycero-3-phosphocholine (DHPC; SKU: 850305) were purchased from Avanti Polar Lipids. Imidazole (CAT# I3386), lysozyme (CAT# L6876), RNase (CAT# R4875), and DNase (CAT# DN25) were sourced from Sigma-Aldrich. $^{15}\text{NH}_4\text{Cl}$ (CAT# NLM-467-PK) and 99% D_2O (CAT# DLM-4-PK) was sourced from Cambridge Isotope Labs. Amicon Centrifuge Concentrators 10 kDa molecular weight cut-off (MWCO) spin filters were purchased from Fisher Scientific (CAT# UFC901024). Lauryl betaine (Empigen), 30% solution, was purchased from BOC Sciences (CAT# 66455-29-6). HisPur Ni-NTA resin (CAT# A50591) was purchased from ThermoFisher. Isopropylthiogalactoside (IPTG; CAT# 367-93-1), dithiothreitol (DTT; CAT# 3482-12-3), and HEPES (CAT# H75030-1000) were purchased from Research Products International. Verteporfin was sourced from SelleckChem (CAT# CL 318952), MedChemExpress (CAT# CL 318952), or Sigma-Aldrich (CAT# SML0534). Tris-HCl (J65594) was sourced from Alpha Aesar. PIPES (P6757), Sodium Acetate (S2889), Ammonium Acetate (73594), potassium phosphate monobasic (P0662), and sodium phosphate dibasic (S9763) were all sourced from Sigma-Aldrich. NMR tubes were sourced from WilMad (WG-3000-4-SJ).

Fragment Compounds from VU HTS Core: Most compounds discussed in this document are discussed in terms of their VU IDs. These IDs are denoted as VU0 followed by a 6-digit identifier, such as VU0410776. These compounds can be tracked using web browser-based WaveGuide (BioVIA), which is free to VU users, or the paid-for ChemCart software.

Fragment Compound Reagents (not from VU HTS):

VU0021995 analogs A and B was sourced from Chem-space.com using the IDs CSSS00015312339 and CSSS000000291920, respectively. VU0021995 analogs C and D were sourced from Chem-Space.com using the Chemspace IDs CSSS00000277133 and CSSS00017544602, respectively.

Buffers:

C99 lysis buffer: 25mM Tris, 150mM NaCl, pH 7.8

Notch-1 lysis buffer: 40mM HEPES, 150mM NaCl, pH 7.8

Imidazole NMR buffer: 25mM Imidazole, 100mM NaCl, 0.5mM EDTA, pH 6.5

PIPES NMR buffer: 50mM PIPES, 100mM NaCl, 0.5mM EDTA, pH 6.5

Acetate NMR buffer: 50mM NaOAc, 100mM NaCl, 0.5mM EDTA, pH 4.5

GA X-linking buffer: 250mM Imidazole, 100mM NaCl, pH 7.8

IM-MS buffer: 100mM Ammonium Acetate (AmAc), pH 4.5, 0.5mM EDTA

APOE Lysis Buffer: 20mM NaPi, 300 mM NaCl, pH 8.0, 1 mM TCEP

APOE Ion Exchange (IEx) Buffer A: 20mM NaPi, pH 8.0, 1 mM TCEP

APOE Ion Exchange (IEx) Buffer B: 20mM NaPi, 300 mM NaCl, pH 8.0, 1 mM TCEP

APOE Size Exclusion (SEC) Buffer: 20mM NaPi, 100 mM NaCl, pH 8.0, 1 mM TCEP

APOE NMR Buffer: DPBS, pH 7.4, 10 mM DTT

Expression of C-terminally tagged C99 (C99I109W)

C-terminally hexa-His-tagged C99 with an added tryptophan to increase its light extinction coefficient at 280 nm (I109W C99, was expressed in BL21DE3 strain *E. coli* using a pET21b expression vector system as previously described by Hutchison *et al.* ²³⁷. A freshly transformed colony (or a colony from a freshly prepared glycerol stock) was used to inoculate a 250 ml baffled flask containing 80 ml LB starter culture with 50 µg/ml ampicillin. The starter culture was grown at 30 °C overnight in a shaking incubator at 200 rpm for a total of 18-20 hours. The following morning, 5 ml of the densely grown starter culture was transferred into a 2.8 L baffled flask containing 1 L of ¹⁵N-NH₄Cl-labelled minimal media (M9) enriched with 0.4% dextrose, 1xMEM vitamins (from 100x stock [New England Biolabs]), 1mM MgSO₄, 0.1 mM CaCl₂, and 50ug/ml ampicillin. The M9 culture was grown at 37 °C in an incubated shaker at 220 rpm until an optical density (OD) of 0.6-0.8 (usually about 5 hours after subculture), at which point IPTG was added to a final concentration of 1mM. The incubator temperature was then lowered to 20 °C and tumbled overnight. The following morning, the bacteria were harvested by centrifugation at 10,000x g for 20 minutes using a JLA8.1000 rotor in a Beckman J-20 XP centrifuge. The supernatant was discarded, and cell pellets were collected and stored at -80 °C in 50 mL conical vials until further use.

Purification of C99

C99 pellets were removed from 80 °C and thawed at room temperature for 30 minutes. The thawed pellet was then resuspended in 10 ml of C99 lysis buffer per gram of wet cell, followed by addition of 1mM PMSF from a 0.1M stock in EtOH and 20 µg Lysozyme, 2 µg DNase, and 2 µg RNase from a 500x stock. The sample was then tumbled at 4°C for 1 hour and then sonicated on ice at 60 amps, alternating 5 seconds on /5 seconds off, for a total of 10 minutes. The lysate was then transferred to centrifuge tubes and spun at 50,000g for 20 minutes at 4°C using a JA25.50 rotor in a Beckman J-20 XP centrifuge. The supernatant was discarded, and the C99-containing pellet was dislodged by spatula into 10 ml of C99 Lysis buffer per gram of pellet. The pellet debris was then fully resuspended using a Dounce homogenizer until the solution was cloudy and white in color. The homogenized solution was again sonicated on ice at 60amps, 5 seconds on / 5 seconds off, for a total of 10 minutes, and centrifuged at 50,000x g for 20 minutes at 4 °C. The supernatant was discarded, and the pellet (now mostly inclusion bodies) was Dounce homogenized again in 10ml of C99 Lysis buffer per gram of pellet. The fully resuspended solution was then transferred to 50ml conical vials, at which point Empigen (lauryl betaine) was added to a final concentration of 3% w/v (from 30% stock). The solution was then tumbled at 4 °C overnight to ensure solubilization of the inclusion bodies.

The following morning, the sample was centrifuged at 50,000x g at 4 °C for 20 minutes, keeping the supernatant and discarding the pellet. The supernatant was then tumbled with 1 ml of pre-equilibrated Nickel NTA resin per 50ml of lysate for 1 hour at 4 °C. The resin was then spun down in a table-top centrifuge at 500x g for 5 minutes and transferred

to a column. The column was first washed with 25 column volumes (CV) of C99 lysis buffer + 3% w/v Empigen, then 25 CV of C99 lysis buffer + 1.5% w/v Empigen. Once fully drained, the column was then wash/exchanged into 25 CV of C99 lysis buffer + 0.05% w/v LMPG (14:0 lyso-myristoylphosphatidylglycerol; Avanti 858120) detergent. Then, weakly bound proteins were removed by adding 25 CV of C99 lysis buffer + 0.05% w/v LMPG + 10 mM imidazole. The remaining weakly bound proteins were washed away using 25 CV of C99 Lysis buffer + 0.05% w/v LMPG + 30 mM imidazole, collecting some of the flow-through for an SDS-PAGE sample. *Note that LMPG can be exchanged for any desired membrane mimetics before elution, such as DDMB or D6PC/DMPC bicelles. Finally, the protein was eluted from the column using 5-10 CV of C99 lysis buffer + 0.2% w/v LMPG + 500 mM imidazole. The eluate was then buffer exchanged into NMR Buffer (PIPES or imidazole NMR buffer, depending on the experiment) using an Amicon 10kDa cutoff centrifugal concentrator. When thoroughly buffer exchanged (after at least 3 cycles of concentration then 10x dilution), the C-terminally His-tagged I109W C99 concentration was determined by UV₂₈₀ absorbance using the concentrator flow-through as a blank and the 280 nm extinction coefficient (ϵ) of 11,420 OD units per molar per cm. Typical yields for C99 I109W are approximately 5mg of pure protein per liter of M9 cell growth. The protein was then concentrated to 200 μ M and flash frozen in liquid nitrogen in 250 μ l aliquots and stored at -80°C until further use.

Expression, purification, and thrombin cleavage C99-NT2 (His tag-cleavable)

Thrombin-cleavable N-terminally His-tagged C99 (C99-NT2) was expressed in BL21DE3 strain *E. coli* using a pET21a expression construct follows the same steps as the C-terminally tagged C99 (inclusion body extraction/purification) mentioned above. C99-NT2 pellets were lysed and purified in the same way as mentioned above for C-terminally His-tagged C99. After elution into C99 lysis buffer + 0.2% LMPG + 500 mM imidazole, the sample pH was brought up to 8.0 using NaOH, and 500 units of thrombin protease was added to the eluted solution. The sample was tumbled at room temperature overnight to ensure 100% proteolysis, which was confirmed by SDS-PAGE. After cleavage was verified, the imidazole in the solution was buffer exchanged away by at least 3 cycles of 10x concentration/dilutions into C99 Lysis buffer using an 10kDa-cutoff Amicon centrifugal concentrator. After imidazole was diluted to <1 mM, the sample was passed over a fresh NiNTA column equilibrated with C99 lysis buffer, collecting the flow-through. The sample was repassed over the resin at least two more times to ensure that all free His-tag peptides were bound, collecting the flow through each time. After the final flow-through was collected (which contains the purified untagged C99), the resin was eluted using C99 lysis buffer + 500 mM imidazole, collecting the sample in a separate tube. The flow-through sample (containing C99) was then buffer exchanged into NMR buffer (PIPES or imidazole NMR buffer, depending on the experiment) using an Amicon 10 kDa cutoff centrifugal concentrator. When thoroughly buffer exchanged (after at least 3 by 10x dilutions into NMR buffer), the protein concentration was determined by UV₂₈₀ absorbance using the concentrator flow-through as a blank and the UV₂₈₀ nm extinction coefficient (ϵ) of 5,960 units per molar per cm. Typical yields for untagged C99 after thrombin cleavage and repurification were around 2-5 mg of pure protein per liter of M9 cell growth. The protein was then concentrated to 200 μ M and flash frozen in liquid nitrogen in 250 μ l aliquots and stored at -80 °C until further use.

Expression, purification, and thrombin cleavage C99 truncations C55 and C74 (His tag-cleavable)

These expressions and purification were done exactly as described for **C99-NT2** above, however the proteins were concentrated using 3 kDa MW cutoff Amicon filters. Furthermore, due to lack of aromatic residues to contribute to extinction coefficient, protein concentration was determined using Bradford or BCA assays. Typical yields were 2-3 mg/liter of M9 growth.

Expression and purification of Notch-1 TM/JM

His-tagged Notch-1 TM/JM; as previously described by Deatherage *et al.*^{223, 264}) was expressed in the BL21DE3 Star strain of *E. coli* using a pET21b expression vector system. The expression protocol for this construct follows the same steps as the **C-terminally His-tagged I109W C99** expression protocol mentioned above.

Notch-1 TM/JM pellets were removed from -80°C and thawed at room temperature for 30 minutes. The thawed pellet was then resuspended in 10 ml of Notch-1 Lysis buffer per gram of wet cell, followed by the addition of 1 mM PMSF from a 0.1 M stock in EtOH and 20 µg Lysozyme, 2 µg DNase, and 2 µg RNase from a 500x stock. The sample was then tumbled at 4 °C for 1 hour then sonicated on ice at 60 amps, 5 seconds on / 5 seconds off, for a total of 10 minutes. DTT (dithiothreitol) and Empigen™ were then added to the lysate to a final concentration of 1 mM and 3% w/v, respectively. The sample was then tumbled overnight at 4°C to ensure whole cell solubilization. The next day, the solution was transferred to centrifuge tubes and spun at 50,000x g for 20 minutes at 4 °C using a JA25.50 rotor in a Beckman J-20 XP centrifuge.

The following morning, the sample was centrifuged at 50,000x g at 4 °C for 20 minutes, keeping the supernatant and discarding the pellet. The supernatant was then tumbled with 1 ml of pre-equilibrated Nickel NTA resin per 50 ml of lysate for 1 hour at 4 °C. The resin was then spun down in a table-top centrifuge at 500x g for 5 minutes and transferred to a column. The column was first washed with 25 CV of Notch-1 lysis buffer + 3% w/v Empigen + 1 mM DTT, then 25 CV of Notch-1 Lysis buffer + 1.5% w/v Empigen + 1 mM DTT. Once fully drained, the column was then wash/exchanged into 25 CV of Notch-1 Lysis buffer + 0.05% w/v LMPG (14:0 Lyso PG; Avanti 858120) detergent. Then, weakly bound proteins were removed by adding 25 CV of Notch-1 lysis buffer + 0.05% w/v LMPG + 25 mM imidazole + 1 mM DTT, collecting a sample for an SDS-PAGE sample. The remaining weakly bound proteins were washed away using 25 CV of Notch-1 lysis buffer + 0.05% LMPG + 65 mM imidazole + 1 mM DTT, collecting some of the flow-through for an SDS-PAGE sample. Finally, the protein was eluted from the column using 5-10 CV of Notch-1 lysis buffer + 0.2% w/v LMPG + 500 mM imidazole + 1 mM DTT. The eluate was then buffer exchanged into NMR Buffer (PIPES or imidazole NMR buffer, depending on the experiment) using a 50 ml Amicon 10 kDa cutoff centrifugal concentrator. When thoroughly buffer exchanged (after at least 3 cycles of 10x concentration/dilutions into NMR buffer), the protein concentration was determined by UV₂₈₀ absorbance using the concentrator flow-through as a blank and the molar extinction coefficient (ϵ) of 6,990. Typical yields for Notch-1 TM/JM are 5-10 mg of pure protein per liter of M9 cell growth.

The protein was then concentrated to 200 μ M and flash frozen in liquid nitrogen in 250 μ l aliquots and stored at -80 $^{\circ}$ C until further use.

Expression and Purification of KCNQ1-VSD

The sequence encoding human KCNQ1 VSD (residues 100-249) was cloned into a pET16b expression vector as previously described [Peng D, Kim JH, Kroncke BM, Law CL, Xia Y, Droege KD, Van Horn WD, Vanoye CG, Sanders CR (2014). Purification and structural study of the voltage-sensor domain of the human KCNQ1 potassium ion channel *Biochemistry* 53:2032–2042.]. The resulting cloned plasmid encodes the KCNQ1 VSD with the N-terminal hexahistidine tag sequence MGHHHHHHG. This plasmid was then transformed into *E. coli* strain C43(DE3) harboring the rare tRNA-encoding plasmid pRARE from *E. coli* strain RosettaTM(DE3) (Novagen). Individual transformants were cultured overnight in Luria-Bertani medium containing 100 μ g/mL ampicillin and 30 μ g/mL chloramphenicol. 4mL of this starter culture was used to inoculate each liter of M9 minimal medium for protein expression. M9 minimal medium was supplemented with the same antibiotics as in the starter culture, as well as MEM vitamins (Mediatech), and 50 μ M ZnCl₂. To ensure complete ¹⁵N-labeling of KCNQ1 VSD, 1g ¹⁵NH₄Cl was included per liter of M9 minimal medium. Cultures were incubated at 20 $^{\circ}$ C with shaking at 220rpm until the OD₆₀₀ value reached 0.8, upon which expression was induced by the addition of isopropyl β -D-1-thiogalactopyranoside (IPTG) to a final concentration of 1mM. Cultures were harvested 24 hours after induction by centrifugation at 4,000 x g and the cell pellets were stored at -80 $^{\circ}$ C until further use.

Cell pellets were thawed and resuspended in lysis buffer (75mM Tris-HCl, 300mM NaCl, and 1mM Ethylenediaminetetraacetic Acid (EDTA), 5mM Mg(Acetate)₂, 1mM phenylmethylsulfonyl fluoride (PMSF), 0.02mg/ml DNase, 0.02mg/ml RNase, 0.2mg/ml chicken egg white lysozyme) and tumbled for 30 min. The cells were lysed by probe sonication on ice at 4 $^{\circ}$ C for 20 minutes. Inclusion bodies were then isolated by centrifugation of the lysate at 20,000 x g for 20 minutes at 4 $^{\circ}$ C. Inclusion body pellets were resuspended in fresh lysis buffer using a Dounce homogenizer, then the sonication and centrifugation steps were repeated. The refined inclusion body pellet was then resuspended in 10mL buffer A (40mM HEPES, 300mM NaCl, pH 7.5) containing 0.5% (w/v) dodecylphosphocholine (DPC) (Anatrace, Maumee, OH) and 2mM TCEP per 1g of initial cell pellet. Inclusion bodies were fully solubilized by overnight tumbling at 4 $^{\circ}$ C. Next, insoluble debris was removed by centrifugation at 20,000 x g for 20 minutes at 4 $^{\circ}$ C. The supernatant was then incubated with 1mL Superflow Ni(II)-NTA resin (Qiagen, Germantown, MD) per 1L M9 culture for 3 hours at 4 $^{\circ}$ C. The resin was then loaded into a gravity-flow column and washed with 10 column volumes (CV) of buffer A containing 0.5% (w/v) DPC and 2mM TCEP. Nonspecifically bound proteins were washed from the resin with 15CV of buffer A containing 0.5% DPC, 2mM TCEP, and 40mM imidazole. Detergent exchange was then performed by washing with 10CV of buffer A containing 0.2% (w/v) LMPG (lyso-myristoylphosphatidylglycerol) and 2mM TCEP. The KCNQ1 VSD was eluted 0.5CV fractions of buffer A containing 0.2% (w/v) LMPG, 2mM TCEP, and 500mM imidazole until A280 measured less than 0.05. Eluted protein was concentrated

twenty-fold by centrifugation (3700 x g, 4°C) in an Amicon Ultra-15 centrifugal filter cartridge (10,000 Da molecular weight cut-off). The concentrated sample was then clarified of insoluble aggregates by passage through a 0.22µm polyvinylidene difluoride (PVDF) filter. The sample was then purified by size-exclusion chromatography (SEC) using a Superdex 200 Increase 10/300 GL column and Äkta

Pure FPLC with 0.5mL sample injection loop. SEC was carried out in buffer A containing 0.2% (w/v) LMPG and 5mM TCEP at a constant 0.5mL/minute flow rate with 0.5mL fraction collection. Fractions corresponding to peaks on the chromatogram were analyzed by SDS-PAGE, and those showing the isolated 18kDa band corresponding to KCNQ1 VSD were pooled. The pooled fractions were then diluted ten-fold in VSD NMR buffer (50mM PIPES, 100mM NaCl, 0.5 mM EDTA, 1mM TCEP, pH 6.5) and re-concentrated in a centrifugal concentrator as above. This process was repeated a total of four times. Final KCNQ1 VSD concentration was approximated by A280 using an extinction coefficient of 34950M⁻¹cm⁻¹, suggesting a final yield of roughly 3mg protein per liter of culture. Purity was approximated to be greater than 99% by colorimetric scanning of a Coomassie G250-stained SDS-PAGE gel loaded with 2µg purified KCNQ1 VSD.

High-throughput Screening

Hit compound sourcing

Compounds in hit wells were identified using either WaveGuide (BioVIA) or ChemCart softwares. Compounds were then ordered using the WaveGuide system and picked up from the HTS Core upon completion of compound distribution. SAR was conducted by locating analogs of hit compounds using the Structure Similarity Search function in WaveGuide and were distributed by the HTS core. For analogs that were unavailable at the HTS core, commercial sourcing was done using PubChem structure similarity searches and the compounds were purchased from various companies.

Compound Distribution

Compounds were provided by the Vanderbilt University High-Throughput Screening Core using a robotic Echo compound dispensing system. The FDA-approved drug library was acquired from the SelleckChem Company. Solid compounds from SelleckChem were dissolved by the HTS core in DMSO to a final stock concentration of 10 mM, and a 1 µl drop of each compound stock was dispensed per well on 96-well plates. To these pre-dispensed plates, premixed NMR samples were added (see **C99 NMR screening sample preparation**).

Compound Storage

If the compounds were not used the same day of distribution (ideally they are used the same day of distribution), the compounds were frozen at -20 °C in DMSO (or as powers) until the day of use.

Sample preparation and mixing for screening

The preparation of NMR screening samples consisted of final concentrations of 50 μ M C99, 2.5% w/v LMPG, 50 mM buffer imidazole, 5% v/v D₂O, 0.5 mM EDTA, pH 6.5. To ensure that these final conditions were maintained, the individual components of the screening samples were added from stocks in a specific order. For example, to make 10 ml of screening sample in imidazole NMR buffer, the following was added: 1) 10 by 250 μ l frozen stocks of 200 μ M protein were thawed on ice and transferred to a 15 ml conical vial. 2) 1.25 ml of 20% w/v LMPG stock (dissolved in H₂O) was added to the conical vial, which was mixed by vortexing. 3) 1 ml of 10x concentrated imidazole NMR buffer was added to the conical vial and mixed by vortexing. 4) The sample was then diluted to 10 ml by adding 4.75 ml of ddH₂O and 0.5 ml of D₂O and allowed to reach equilibrium for at least 60 minutes. This final pool contained 50 μ M C99, 25 mM imidazole, 100 mM NaCl, 2.5% LMPG, 5% v/v D₂O, 0.5 mM EDTA, pH 6.5. At that point, the samples (199 μ l for each well) were distributed into 96-well plates containing pre-dispensed compounds, thoroughly mixed by pipette, and the complete 200 μ l mixtures were transferred to 3 mm x 4 inch NMR tubes. At this point, each 3 mm NMR tube contained a 200 μ l sample of 50 μ M C99, 50 μ M Compound, 25 mM imidazole, 100 mM NaCl, 2.5% w/v LMPG, 5% v/v D₂O, 0.5% v/v DMSO, 0.5 mM EDTA, pH 6.5. Loaded NMR tubes were cleaned with 100% Ethanol on a kimwipe, securely capped, and transferred to an NMR tube rack compatible with a Bruker SampleJet system.

NMR Spectroscopy

High-throughput NMR Screening of C99

A Bruker Avance III 600 MHz NMR spectrometer equipped with a cryoprobe (CPTCI), and automated sample changer (SampleJet) was used to collect NMR spectra. Sample details are described above. For high-throughput screening data collection, the ¹⁵N-¹H BEST-TROSY (b_trosy3gpplh.2) experiment with 64 scans for each of 96 increments and a relaxation delay of 200ms was run at 318 °K for a total data acquisition time of 35 minutes per sample. To achieve enhanced signal-to-noise, follow-up titrations and control experiments were conducted using the BEST-TROSY pulse program with 200 scans per 96 increments at 318 °K, for a total data acquisition time of 110 minutes per sample. Data was processed using Bruker Topspin 3.6 using a Gaussian window function with a line broadening of -10 and a gaussian max of 0.1 in both dimensions. NMR data was then further processed and analyzed using NMR-FAM SPARKY, plotted using GraphPad Prism 9, and prepared for publication figures using Affinity Designer.

Fitting of NMR Binding Data

2D ¹⁵N-¹H HSQC NMR data used to calculate dissociations constant (K_D) values by first normalizing 2D data using the established formula²⁶⁵ (equation 1):

Equation 1:

$$\delta(1H, 15N) = \sqrt{(1/2 [\delta^2_H + .14 * \delta^2_N])}$$

Where, $\delta(1H,15N)$ is the square root of linear chemical shifts in each respective dimension, δ_H and δ_N with the Nitrogen normalization factor of 0.14.

After 2D normalization, the data was fit to a hyperbolic binding isotherm using one of the following formulas depending of the data:

$$\text{Equation 2: } Y = \frac{B_{max} * X}{(K_D + X)} + NS * X$$

Equation 2 was used for situations where titrations revealed linear shifts at high concentrations of ligand and saturation could not be fully reached. For this equation, Y is the total binding, Bmax is the maximum binding in the same units as Y, X is the added ligand in molar units, K_D is the equilibrium dissociation constant in the same units as X, and NS is a linear term to account for either vehicle or nonspecific verteporfin effects.

$$\text{Equation 3: } Y = \frac{B_{max} * X}{(K_D + X)}$$

Equation 3 was used for fitting situations where chemical shift perturbations saturated during titration and did not have linear shifts due to non-specific effects. For this equation, Y is the total binding, Bmax is the maximum binding in the same units as Y, X is the added ligand in molar units, K_D is the equilibrium dissociation constant in the same units as X. 1D NMR binding curves were generated by directly inputting 1D chemical shift perturbations directly into the proper version of equation 2. Peak height data was first generated using the peak-picking function in NMRFAM Sparky, and peak heights as a function of ligand concentration were used to generate a K_D by addition into Equation 2.

1D ¹H Data Acquisition and Processing Parameters

1D ¹H NMR spectra were collected using the zgesgp pulse program from Bruker with 4 dummy scans (DS), 16 NS and 32768 TD for a total experimental time of 50 seconds. Spectra were typically centered with an offset (O1) of 4.7 PPM, but was adjusted to a low as 4.39 depending on DMSO content of the sample to ensure solvent suppression. Data were processed using a QSINE window function with a sine bell shift SSB of 2. Peak heights and chemical shifts were all calculated manually using the TopSpin 3.6.2 Analyse function. Data were plotted using the TopSpin 3.6.2 Publish feature and graphically enhanced using Affinity Designer.

¹⁵N-¹H CLEANex-HSQC acquisition and processing parameters

These data were collected on either a Bruker Avance 800 MHz or 900 MHz NMR spectrometers both equipped with cryoprobes (CPTCI). The HSQC portion of the experiment was collected using the Bruker fhsqcf3gp pulse program with 16 DS, 256 NS, and 2048 x 128 TD in the 1H F2 and F1 dimensions, respectively. The CLEANEX portion of the experiment was collected using the Bruker fhsqccxf3gp pulse program using the same settings with a 100 ms mixing time. Both sets of data were processed using a gaussian window function with -10 LB and 0.1 GB in both dimensions. If necessary, peak volume was determined using the Analyse function in TopSpin 3.6.2.

Data were then plotted using NMRFAM SPARKY and graphically enhanced using Affinity Designer.

¹H-¹H NOESY acquisition and processing parameters

These data were collected on the more sensitive Bruker Avance 800 MHz and 900 MHz NMR spectrometers both equipped with cryoprobes (CPTCI). A sample was prepared containing 300 μ M C99 and 300 μ M Verteporfin in 2.5% d²⁷-LMPG (deuterated alkyl chains), 50mM d⁴-Imidazole (deuterated imidazole), 100 mM NaCl, 0.5 mM EDTA, 1mM DSS, pH 6.5 in 85% D₂O. The ¹H-¹H NOESY experiment was recorded on the 800 MHz spectrometer with a mixing time of 120ms, relaxation delay of 2 sec, 4k x 1k data acquisition matrix, using the standard Bruker pulse program (noesyphpr). Data was processed and analyzed using TopSpin 3.6 and graphically enhanced using Affinity Designer.

Other Methods

Glutaraldehyde (GA) crosslinking

C-terminally His-tagged C99 was expressed from *E. coli* as mentioned above, and the sample was eluted into a buffer containing 0.1% w/v LMPG, 350 mM Imidazole, 100 mM NaCl, pH 7.8. The protein sample was buffer swapped into GA X-linking buffer containing 0.25% w/v LMPG, 250 mM imidazole, 100 mM NaCl, pH 7.8 and the protein was concentrated to a stock of 300 μ M C99. Protein stocks were either used right away or flash frozen in LN₂ and stored at -80 °C until further use.

On the day of the experiment, fresh glutaraldehyde (from 25% w/v ampoule) was used to prepare serial dilutions and stored on ice. Reaction volumes were set at 50 μ L, containing 30 μ M C99, 25 mM Imidazole, 100 mM NaCl, pH 7.8 and 2.5% w/v LMPG. For a typical GA reaction setup, the following components were added to Eppendorf tubes in this specific order:

5 μ L of 300 μ M C99 was added to the bottom of the tube, followed by 6 μ L of 20% w/w LMPG solution, then the sample was diluted to 50 μ L using 39 μ L of GA X-linking buffer. The sample was mixed by vortex and allowed to sit for at least 30 minutes. After incubation, 1 μ L of Verteporfin stock (typically 10 mM in DMSO) was added to the mixture, vortexed, and allowed to incubate for at least another 30 minutes in the dark. Finally, 1 μ L GA was added from the corresponding stock (depending on the concentration needed) to the side of the Eppendorf tube. After all the samples had GA droplets added to the sides of the corresponding tubes, the drops were plunged to the bottom by centrifugation at 10,000g for 10 seconds and the tubes were mixed by vortex and allowed to react for 30 minutes. After the reaction time was completed, the reactions were quenched using 2 μ L of 1 M Tris/Glycine buffer and allowed to sit for at least 5 more minutes to ensure complete quenching. Then, SDS loading buffer was added directly to the reaction tubes and the samples were visualized using SDS-PAGE and analyzed by densitometry using ImageJ. Data were fit using the following one-phase exponential decay function (equation 4):

Equation 4:

$$Y = (Y_0 - Plateau) * e^{-K*X} + Plateau$$

Where Y starts at Y_0 and decays down to the Plateau (Y_{final}), X is concentration, and K is the rate constant in the reciprocal units of X.

Ion mobility- mass spectrometry (native mass spectrometry)

IM-MS data were collected using a Synapt G2 HDMS IM-Q-ToF mass spectrometer (Waters, Milford, MA), with a direct infusion nESI source set to positive ion mode. The instrument settings were tuned to generate intact C99-verteporfin complex ions while completely dissociating them from detergent LMPG micelles, including appropriately tuned settings for the sampling cone 80 V, trap cell accelerating potential 80 V and the transfer cell accelerating potential 70 V. The trapping cell wave velocity and height were 116 m/s and 0.1 V, respectively. The IMS wave velocity and height were 250 m/s and 15 V, respectively. The transfer cell wave velocity and height were 300 m/s and 10 V. Prior to analysis, C99 in LMPG micelles at a protein concentration of 20 μ M C99 and 100X CMC LMPG or DDMB samples were prepared by incubating 20 μ M C99 with 100X CMC LMPG for 30 minutes, then titrating in DMSO or Verteporfin and incubating in the dark overnight. Verteporfin binding buffer conditions were 200mM Ammonium Acetate at pH 4.5. For all C99-verteporfin LMPG micelles measured at 0 μ M, 10 μ M, 20 μ M, 30 μ M, 40 μ M, 50 μ M, and DMSO verteporfin concentrations, C99 was observed as monomeric and dimeric species, with the monomeric species having a charge state distribution between 9+ - 4+, and the dimeric species having a charge state distribution between 12+ - 8+. These charge state distributions were observed to persist across all verteporfin and DMSO concentrations and were extracted into a text-based format using TWIM extract to compute the relative intensity of each species at a given weight percentage.

γ -Secretase assay

The γ -secretase-dependent proteolysis assays with both substrates (C100-FLAG and HexaHis Notch 1 JM/TM) were performed in a weak zwitterionic detergent (CHAPSO, 3-[(3-cholamidopropyl)dimethylammonio]-2-hydroxy-1-propanesulfonate) solubilized conditions.²⁶⁶⁻²⁶⁷ C100 is C99 with an added N-terminal Met residue. Stock solution of purified γ -secretase²⁶⁸⁻²⁶⁹ was diluted to 30 nM in standard assay buffer containing 50 mM HEPES (pH 7.0), 150 mM NaCl, 0.1 % DOPC (phosphatidylcholine), 0.025% DOPE (phosphatidylethanolamine) and 0.25% CHAPSO) and incubated at 37 °C for 30 min, whereupon stock solution of verteporfin or inhibitor (LY411,575) was added to achieve the desired concentration with 1% final DMSO concentration. Proteolytic reactions were initiated by adding purified substrates (either C100-FLAG²⁶⁶ or HexaHis-Notch 1 JM/TM²⁶⁴) and incubating at 37 °C (16 h for C100Flag and 4 h for HexaHis-Notch 1 JM/TM). Reactions were quenched with SDS, and the cleaved intracellular domain products (AICD-FLAG released from C100-FLAG or truncated intracellular domain (NICD) released from the proteolysis of Hexa-His Notch 1 JM/TM) were visualized by Western blot using specific primary antibodies, anti-FLAG antibody for FLAG tagged AICD and neopeptide-specific anti-V1744 antibody for NICD.^{267, 270-271}

IC₅₀ measurements

Purified γ -secretase was diluted in standard assay buffer to specified concentrations and incubated at 37 °C for 30 minutes, followed by the addition of stock solution of verteporfin in DMSO to achieve various final verteporfin concentrations and 2% final DMSO concentration. Purified C99 FLAG was then added to start the proteolytic reactions, which were incubated for 2 h at 37 °C. The concentrations of A β 40 produced during the proteolysis of C100 FLAG by γ -secretase were determined using a specific sandwich ELISA (Invitrogen). A β 40 concentrations were plotted as a function of verteporfin concentration, and the resultant sigmoidal curves were fitted to Equation 5 to determine IC₅₀ values.^{267, 270}

$$\text{Equation 5: } Y = \text{Min} + \frac{(\text{Max}-\text{Min})}{1 + \left(\frac{X}{\text{IC}_{50}}\right)^{\text{Hill Coefficient}}}$$

Dynamic light scattering

Samples were made according to NMR Sample Conditions. Solutions were first filtered with a 0.2 μm syringe filter then centrifuged at 10,000x g to remove insoluble debris. The solution was then added to the inner chamber of the disposable DLS cuvette. The disposable DLS cuvette was capped and loaded in the DLS instrument. Experiments were carried out at 25 °C. The DLS software (Dynamics 7.5 software; Wyatt Technologies) calculates an apparent hydrodynamic radius (R_h) via the Stokes-Einstein equation (Equation 6):

$$\text{Equation 6: } R_h = \frac{kT}{6\pi\eta D_t}$$

where k is Boltzmann's constant, T is the absolute temperature, η is sample viscosity, and D_t is the diffusion coefficient. The apparent molecular weight of the detergent or verteporfin particles was calculated in the Dynamics software, as based on the measured apparent radius of hydration, using the assumption that the density of the particle was similar to that of a globular protein.

Preparation of protein structures for docking

The full-length structure of C99 in micelles was obtained from the RCSB PDB Database (PDB: 2LP1). The PDB file was relaxed within an implicit membrane in Rosetta 3.13 using RosettaMP protocols.^{272 273 274} Implicit membrane position and thickness was set to span residues A701-V721. 500 relaxed models were generated using the FastRelax mover within the implicit membrane and scored by an all-atom membrane score function. The model with best total score was selected as the representative to be used for docking simulations.

Preparation of verteporfin conformers for docking

The 2D structure of verteporfin was obtained from PubChem (CID: 11980904) and converted to a 3D conformer using CORINA. BCL Conformer Generator was then used to create a conformer library (250 conformers) from this 3D template.²⁷⁵

Local docking of verteporfin to C99

The verteporfin conformer library was docked to the relaxed C99 model within an implicit membrane in Rosetta 3.13 by coupling RosettaLigandDocking and RosettaMP protocols.^{272-274, 276 277 278} Conformers were initially placed between the C99 transmembrane helix and the C-helix to be near perturbed residues identified by ¹⁵N-¹H TROSY experiments. Large conformer moves were sampled by a 1000-step low resolution Monte Carlo search of the binding pocket using the Transform mover. Next, six cycles of the the HighResDocker Mover were used to sample alternate rotamers near the ligand and perform small ligand sampling, repacking the protein-ligand interface every third cycle. Finally, the FinalMinimizer Mover was used to perform in-membrane gradient-based minimization of the pose, refining it to a final output model. 65000 models were generated in this manner and scored within a membrane all-atom score function as during relaxation.

Model evaluation and RMSD analysis Docked models were sorted by their within-membrane interface scores and the best-scoring model was selected as the representative structure. All models were then evaluated against the best scoring model by plotting their interface scores versus their RMSD to the best-scoring model. Plots were generated using the ggplot2 package (version 3.3.2) in R (version 4.0.2).

Appendix

Preliminary Data

Discovery and “SAR by Catalog” optimization of hydroxypyrazole-class compounds that bind C99

As discussed in Chapters 3 and 5 of this thesis, a preliminary single-plate screen led to the discovery that C99 binds VU0410776 (2-phenyl-5-methyl-4*H*-pyrazol-3-one), shown as an insert in **Figure 36A**. It was found that approximately 8 peaks underwent chemical shift perturbations that were in the slow-exchange regime on the NMR timescale, suggesting a tightly bound complex with a slow off-rate. (**Figure 36A**) These resonances mapped back to residues in the C-terminal region of the C99

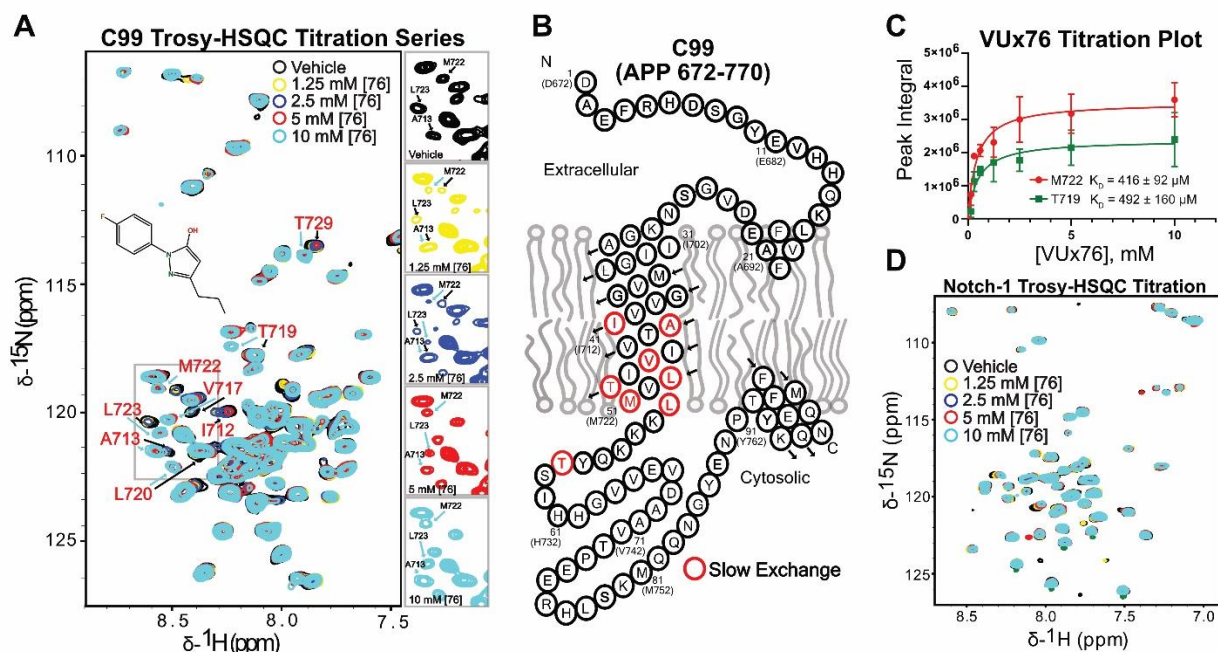


Figure 36. Discovery that VU0410776 is a C99 binder. **A**) Five overlaid ¹⁵N-C99 spectra at varying [VU0410776] concentrations reveals slow exchanging peaks upon compound addition. **B**) Shifting peaks map to C-terminal transmembrane/juxtamembrane region of C99 sequence. **C**) Binding isotherm of the emerging peak integral of the C99 bound-state vs. [VU0410776] concentration. **D**) Notch-1 TM/JM titration with [VU0410776] reveals non-specific, fast-exchange interactions that do not saturate, suggesting VU0410776 does have non-specific interactions with membrane, but prefers C99 over Notch.

transmembrane/juxtamembrane alpha-helix (including residues A713, V717, L720, M722, L723, T729), which is highlighted in **Figure 36B**. Remarkably, C99 was nearly bereft of spectral perturbations at other residues, including those adjacent to the binding site such as G709 or K724. The emergence of bound-state resonances were monitored and plotted using the bound-state peak integral as a function of [VU0410776] concentration, leading us to uncover a K_D of ca. 416 μM for C99. (**Figure 36C**) Finally, we titrated the compound against the Notch-1 TM/JM control and found that there were minor perturbation in 2 Notch residues, however the effects could would not saturate up

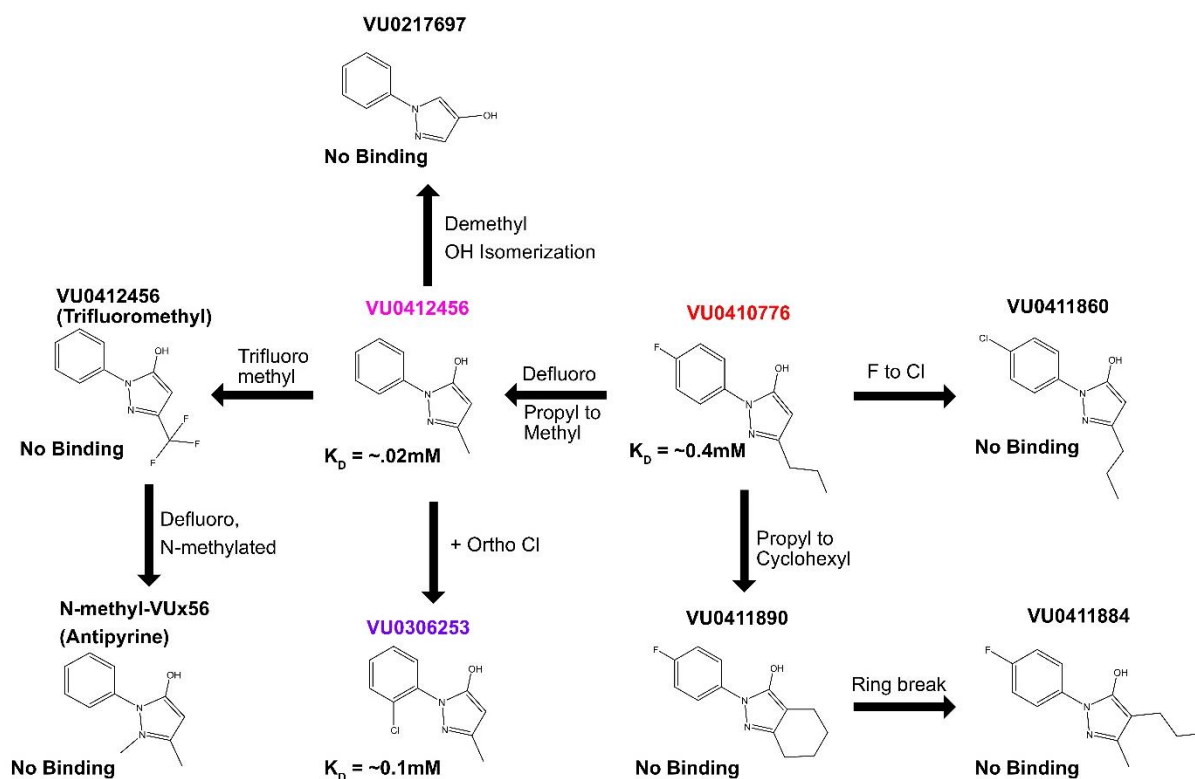


Figure 37. SAR by Catalog optimization of VU0410776 analogs reveals tighter and weaker binding analogs. The right side of this figure shows VU0410776 analogs that revealed no binding, suggesting bulky modifications to the 4- and 5- positions of the hydroxypyrazole ring were not suitable for chemical optimization. Inversely, truncation of the 5-propyl to a 5-methyl group and elimination of the para-fluoro atom increased affinity to C99 by 20-fold (VU0412456). Addition of an ortho-chloro group to VU0412456 partially reduced affinity by 5-fold, indicating a potential region for chemical modification. N-methylation or triflation of the hydroxypyrazole ring, shown on the left, eliminated binding entirely.

to 10 mM [VU0410776], over 20 times higher than the K_D for C99. (**Figure 36D**) Taken together, these data indicate that VU0410776 binds C99 in a specific region of the TM/JM region and exhibits only non-specific interactions with Notch-1, which we hypothesized was because of non-specific membrane interactions.

The next question was whether this compound could be optimized for tighter and more C99-specific binding by testing a series of available VU0410776 analogs, a process known as SAR by Catalog. We sourced approximately 12 VU0410776 analogs that tested various degrees of chemical space while maintaining the key hydroxypyrazole backbone, shown in **Figure 37**. We first tested analogs of VU0410776 that extended or altered the alkyl chains on the 4- and 5- positions of the pyrazole ring. Interestingly, longer or bulkier alkyl chains entirely ablated the affinity of these compounds (VU0411890, VU0411860, and VU0411884) for C99, with no NMR spectral perturbations seen for any of them. This suggested that the face of the hydroxypyrazole class was likely in direct contact with C99 residues. Inversely, truncation of the 5-propyl group to a 5-methyl drastically increased the affinity to C99 from $K_D = 450 \mu\text{M}$ for VU0410776 to $K_D = 20 \mu\text{M}$ for VU0412456, confirming the role of that position for C99 binding (**Figure 37**; pink). At that point, we explored further analogs of VU0412456 and found that an ortho-chloro analog, VU0306253, (**Figure 37**; purple) bound with a modestly reduced affinity for C99 ($\sim 100 \mu\text{M}$ K_D). This indicated to us those substitutions of the phenyl ring were viable candidates for medicinal chemical optimization of this compound, contrary to what we found for the 4- and 5-positions of the hydroxypyrazole ring. Interestingly, isomerization of the 3-hydroxy group to a 4-hydroxy analog, N-methylation of VU0412456, and triflation of the VU0412456 methyl group eliminated C99 binding entirely. We were pleased to see that

the three binding compounds affected the same region of C99 residues, ranging from A713-L723 in the transmembrane helix with some other binding residues seen in the C-loop. As seen in **Figure 38**, VU0412456 bound the same overall position on C99, but also appeared to recruit two more residues, S750 and E758, into the complex. The additional binding energy contributed from those residues could explain why VU0412456 binds 20-times tighter than the parent VU0410776 compound. Furthermore, VU0412456 had virtually no effect on the Notch-1 spectrum at the concentrations tested, suggesting that this compound was a C99-specific binder and would be a good starting point for medicinal chemical optimization.

We decided to pause further SAR and continue using the tightest binding VU0412456 and the VU0410776 parent compounds for further studies. To verify whether

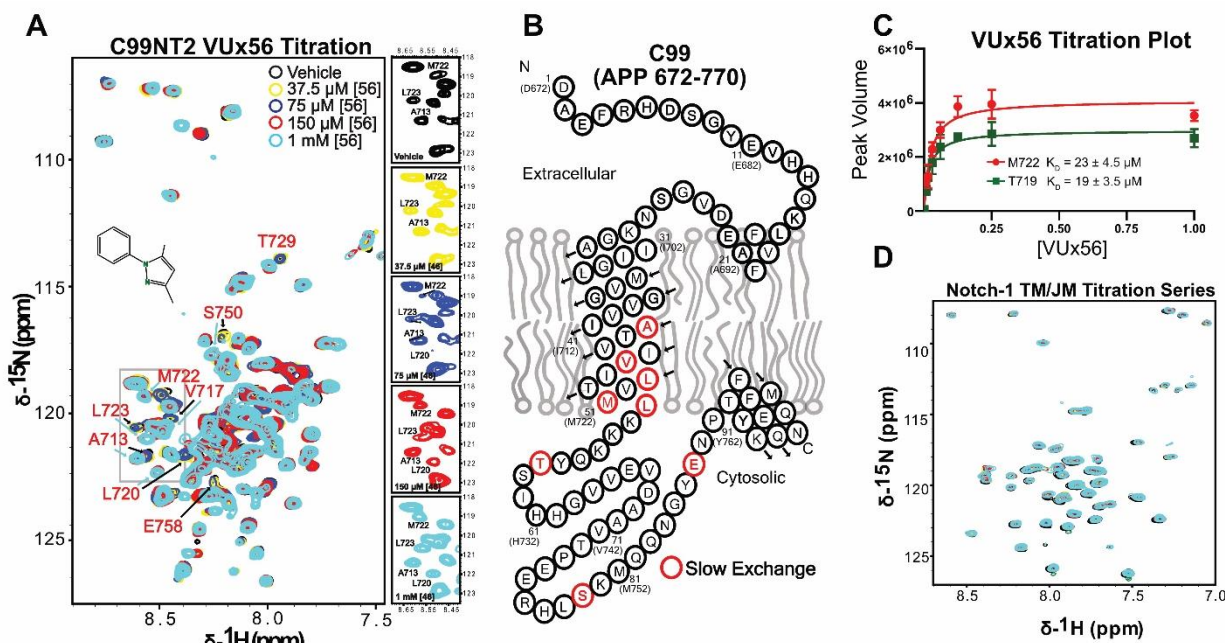


Figure 38. *Discovery that VUx76 analog VU0412456 is a tighter and more specific C99 binder than its parent.* **A)** Five overlaid ^{15}N -C99 spectra at varying [VU0412456] concentrations reveals slow exchanging peaks upon compound addition. **B)** Shifting peaks map to C-terminal transmembrane/juxtamembrane region of C99 sequence, with similar residues as what was seen for the VU0410776 parent. **C)** Binding isotherm of the emerging peak integral of the C99 bound-state vs. [VU0412456] concentration, revealing a K_D of ca. 20 μM . **D)** Notch-1 TM/JM titration with [VU0412456] revealed no spectral perturbations at the concentrations tested, suggesting this compound specifically bound C99.

these interactions were truly direct and not exclusively a consequence of likely detergent interactions, we tested both the parent VU0410776 and optimized VU0412456 hydroxypyrazole analogs against a mutated C99. Specifically, L723, which was directly in the middle of the C99 binding sequence and underwent a large chemical shift perturbation upon titration, was mutated to alanine and titrated with either of the compounds. Remarkably, we found C99 L723A had no affinity for these compounds, confirming the direct interaction between the protein and the compound and confirming the importance of this residue (**Figure 39**).

Discussion and Disclaimer

A major disclaimer about these data must be shared to complete transparency and is the reason I consider this data preliminary. Perhaps the most

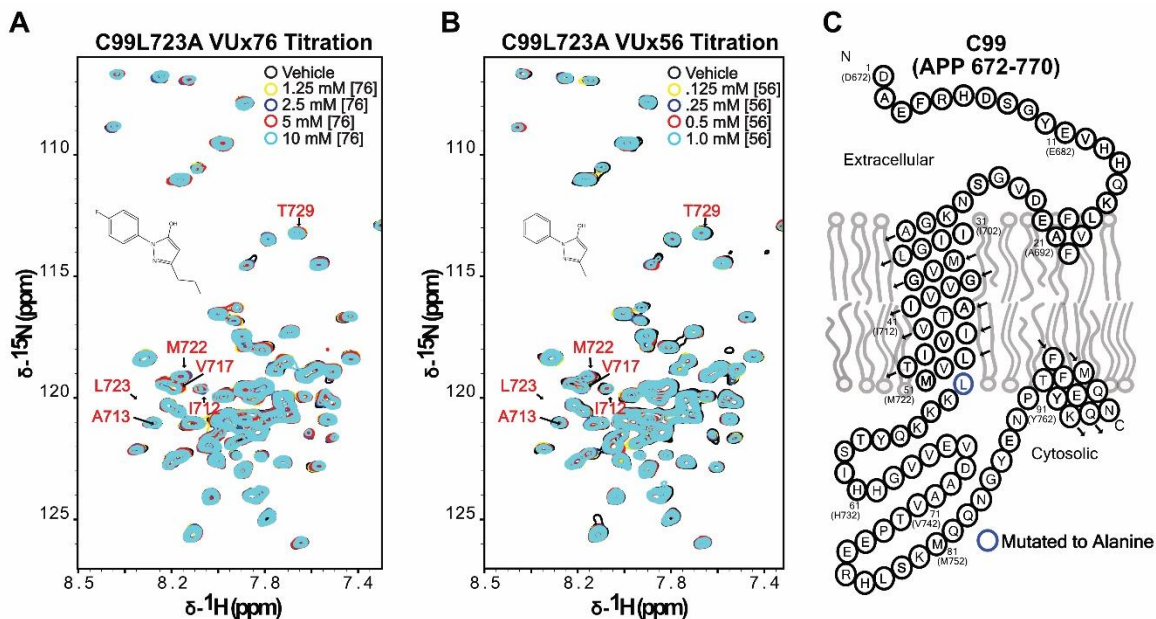


Figure 39. C99 L723A mutant loses all affinity for VUx76 and VUx56 fragments, confirming binding site. **A)** C99 L723A shows only minor, fast-exchanging perturbations in response [VU0410776] titration, reflecting what was seen before for Notch-1. **B)** C99 L723A shows only minor, noisy shifts in response to [VU0412456] titrations, confirming the role that L723 plays in binding. **C)** C99 topology plot highlighting the mutated L723 residue that lies in the middle of the hydroxypyrazole binding site.

puzzling aspect of this class of compounds was the fact I have had trouble reproducing the effects of these compounds from commercial sources. The compounds that were used in the figures shown in this section were all sourced from the Vanderbilt University High Throughput Screening (VUHTS) core, at least originally. VU0410776 was sourced from Hit2Lead.com, and reproducibly bound C99 from their batch over the years (**Figure 36**), which does lend hope that these effects are real. However, VU0412456 was sourced from three different companies and none of them reproduced the shifts in C99 that were shown in the figures above. Interestingly, VU0412456 from the VUHTS core was blue in color, but was yellow / pale yellow from two companies and green from another. Furthermore, ¹H NMR spectra of VU412456 from the HTS core was very slightly different from the commercially sourced equivalent. This suggested to me that the VU412456 compound from the HTS core was likely oxidized or degraded in some way, as the compounds had been sitting in 200 mM DMSO stocks at room temperature for several years since their synthesis. Alternatively, they could have been improperly purified after synthesis and residual metals or byproducts could have been the causative agents in binding. The preliminary SAR I conducted suggests that there really is something about this pharmacophore that interacts with C99, but commercial reproducibility is a major concern that could invalidate all the SAR data. Regardless, these reproducibility issues remain a mystery and are still an ongoing investigation in my research.

Another contraindication for these compounds is that they only bound C99 in LMPG micelles, with only negligible effects observed in DHPC/DMPC bicelles and DDMB micelles (data not shown). This suggested that this class of binders, or whatever the binding agent(s) in the HTS sample was, likely were forming a ternary complex with

C99 and LMPG. Specifically, I hypothesize the negatively charged phosphoglycerol detergent head group played a role in recruiting the binding compounds and stabilizing the complex. This idea could also explain why the binding event was undergoing slow exchange on the NMR timescale despite only having weak K_D values (20-450 μM). Specifically, it is possible that the compounds were 'diffusion-limited', such that they had a very slow binding off-rates due to the combined energetic contributions of the LMPG and C99 binding, leading NMR spectra to reflect slow-exchange. An alternative hypothesis for the slow exchange is that the hydroxypyrazole compounds themselves had nothing to do with the binding, and it was actually a contaminant, biproduct, or degradation product in the DMSO vehicle that was in much lower concentration and was truly a tight binder. Extensive liquid chromatography-mass spectrometry (LC-MS) of these compounds suggested that the degradation hypothesis was likely untrue, as the compounds appeared to be majorly intact (Data not shown). However, the MS data could not rule out the presence of low-abundance impurities in the samples, which are extremely difficult to detect by conventional analytical methods.

Taken together, the discovery of the hydroxypyrazole class of C99 binders has been fascinating but not reached a conclusion. Work is still ongoing to parse out these issues, however it appears that I may have been misled to some degree and these binders may be false positives. If these compounds turn out to be true positives, their discovery would be a monumental advancement for C99 chemical probe development, as they are relatively tight, C99-specific binders. Furthermore, these compounds are primary metabolites of well-studied phenazone NSAID drugs, which have a long history of human use and are tolerable up to millimolar concentrations in human serum. If the

binding turns out to be true, these compounds could be fed right into cellular and animal models of AD to investigate their effects on APP/C99 biology. Considering the region of C99 to which they bind, I hypothesize they would likely be γ -secretase inhibitors and may also have neat properties in perturbing APP/C99 signaling in cells.

REFERENCES

1. Cipriani, G.; Dolciotti, C.; Picchi, L.; Bonuccelli, U., Alzheimer and his disease: a brief history. *Neurol Sci* **2011**, *32* (2), 275-9.
2. Hippus, H.; Neundorfer, G., The discovery of Alzheimer's disease. *Dialogues Clin Neurosci* **2003**, *5* (1), 101-8.
3. Selkoe, D. J.; Hardy, J., The amyloid hypothesis of Alzheimer's disease at 25 years. *EMBO Mol Med* **2016**, *8* (6), 595-608.
4. Mehta, D.; Jackson, R.; Paul, G.; Shi, J.; Sabbagh, M., Why do trials for Alzheimer's disease drugs keep failing? A discontinued drug perspective for 2010-2015. *Expert Opin Investig Drugs* **2017**, *26* (6), 735-739.
5. Panza, F.; Lozupone, M.; Logroscino, G.; Imbimbo, B. P., A critical appraisal of amyloid-beta-targeting therapies for Alzheimer disease. *Nat Rev Neurol* **2019**.
6. Karran, E.; De Strooper, B., The amyloid cascade hypothesis: are we poised for success or failure? *J Neurochem* **2016**, *139* Suppl 2, 237-252.
7. Bekris, L. M.; Yu, C. E.; Bird, T. D.; Tsuang, D. W., Genetics of Alzheimer disease. *J Geriatr Psychiatry Neurol* **2010**, *23* (4), 213-27.
8. Bird, T. D., Early-Onset Familial Alzheimer Disease. In *GeneReviews((R))*, Adam, M. P.; Ardinger, H. H.; Pagon, R. A.; Wallace, S. E.; Bean, L. J. H.; Stephens, K.; Amemiya, A., Eds. Seattle (WA), 1993.
9. Kang, J.; Lemaire, H. G.; Unterbeck, A.; Salbaum, J. M.; Masters, C. L.; Grzeschik, K. H.; Multhaup, G.; Beyreuther, K.; Muller-Hill, B., The precursor of Alzheimer's disease amyloid A4 protein resembles a cell-surface receptor. *Nature* **1987**, *325* (6106), 733-6.
10. Weidemann, A.; Konig, G.; Bunke, D.; Fischer, P.; Salbaum, J. M.; Masters, C. L.; Beyreuther, K., Identification, biogenesis, and localization of precursors of Alzheimer's disease A4 amyloid protein. *Cell* **1989**, *57* (1), 115-26.
11. Goldgaber, D.; Lerman, M. I.; McBride, O. W.; Saffiotti, U.; Gajdusek, D. C., Characterization and chromosomal localization of a cDNA encoding brain amyloid of Alzheimer's disease. *Science* **1987**, *235* (4791), 877-80.
12. Tanzi, R. E.; Gusella, J. F.; Watkins, P. C.; Bruns, G. A.; St George-Hyslop, P.; Van Keuren, M. L.; Patterson, D.; Pagan, S.; Kurnit, D. M.; Neve, R. L., Amyloid beta protein gene: cDNA, mRNA distribution, and genetic linkage near the Alzheimer locus. *Science* **1987**, *235* (4791), 880-4.
13. Pimenova, A. A.; Raj, T.; Goate, A. M., Untangling Genetic Risk for Alzheimer's Disease. *Biol Psychiatry* **2018**, *83* (4), 300-310.
14. Giri, M.; Zhang, M.; Lu, Y., Genes associated with Alzheimer's disease: an overview and current status. *Clin Interv Aging* **2016**, *11*, 665-81.
15. Freudenberg-Hua, Y.; Li, W.; Davies, P., The Role of Genetics in Advancing Precision Medicine for Alzheimer's Disease-A Narrative Review. *Front Med (Lausanne)* **2018**, *5*, 108.
16. Price, J. L.; McKeel, D. W., Jr.; Buckles, V. D.; Roe, C. M.; Xiong, C.; Grundman, M.; Hansen, L. A.; Petersen, R. C.; Parisi, J. E.; Dickson, D. W.; Smith, C. D.; Davis, D. G.; Schmitt, F. A.; Markesbery, W. R.; Kaye, J.; Kurlan, R.; Hulette, C.; Kurland, B. F.; Higdon, R.; Kukull, W.; Morris, J. C., Neuropathology of nondemented aging: presumptive evidence for preclinical Alzheimer disease. *Neurobiol Aging* **2009**, *30* (7), 1026-36.

17. Serrano-Pozo, A.; Qian, J.; Monsell, S. E.; Blacker, D.; Gomez-Isla, T.; Betensky, R. A.; Growdon, J. H.; Johnson, K. A.; Frosch, M. P.; Sperling, R. A.; Hyman, B. T., Mild to moderate Alzheimer dementia with insufficient neuropathological changes. *Ann Neurol* **2014**, *75* (4), 597-601.
18. Kaiser, J., The Alzheimer's gamble. *Science* **2018**, *361* (6405), 838-841.
19. Hardy, J.; Selkoe, D. J., The amyloid hypothesis of Alzheimer's disease: progress and problems on the road to therapeutics. *Science* **2002**, *297* (5580), 353-6.
20. Benilova, I.; Karran, E.; De Strooper, B., The toxic A beta oligomer and Alzheimer's disease: an emperor in need of clothes. *Nature Neuroscience* **2012**, *15* (3), 349-357.
21. Goldgaber, D.; Lerman, M. I.; McBride, W. O.; Saffiotti, U.; Gajdusek, D. C., Isolation, characterization, and chromosomal localization of human brain cDNA clones coding for the precursor of the amyloid of brain in Alzheimer's disease, Down's syndrome and aging. *J Neural Transm Suppl* **1987**, *24*, 23-8.
22. van der Kant, R.; Goldstein, L. S., Cellular functions of the amyloid precursor protein from development to dementia. *Dev Cell* **2015**, *32* (4), 502-15.
23. Zheng, H.; Koo, E. H., Biology and pathophysiology of the amyloid precursor protein. *Molecular Neurodegeneration* **2011**, *6*.
24. Maloney, J. A.; Bainbridge, T.; Gustafson, A.; Zhang, S.; Kyauk, R.; Steiner, P.; van der Brug, M.; Liu, Y.; Ernst, J. A.; Watts, R. J.; Atwal, J. K., Molecular mechanisms of Alzheimer disease protection by the A673T allele of amyloid precursor protein. *J Biol Chem* **2014**, *289* (45), 30990-1000.
25. Benilova, I.; Gallardo, R.; Ungureanu, A. A.; Castillo Cano, V.; Snellinx, A.; Ramakers, M.; Bartic, C.; Rousseau, F.; Schymkowitz, J.; De Strooper, B., The Alzheimer disease protective mutation A2T modulates kinetic and thermodynamic properties of amyloid-beta (Abeta) aggregation. *J Biol Chem* **2014**, *289* (45), 30977-89.
26. Oliver, C.; Holland, A. J., Down's syndrome and Alzheimer's disease: a review. *Psychol Med* **1986**, *16* (2), 307-22.
27. Heston, L. L.; Mastri, A. R., The genetics of Alzheimer's disease: associations with hematologic malignancy and Down's syndrome. *Arch Gen Psychiatry* **1977**, *34* (8), 976-81.
28. Lott, I. T.; Head, E., Dementia in Down syndrome: unique insights for Alzheimer disease research. *Nat Rev Neurol* **2019**.
29. Bugiani, O.; Giaccone, G.; Verga, L.; Pollo, B.; Ghetti, B.; Frangione, B.; Tagliavini, F., Alzheimer patients and Down patients: abnormal presynaptic terminals are related to cerebral preamyloid deposits. *Neurosci Lett* **1990**, *119* (1), 56-9.
30. Doran, E.; Keator, D.; Head, E.; Phelan, M. J.; Kim, R.; Totoiu, M.; Barrio, J. R.; Small, G. W.; Potkin, S. G.; Lott, I. T., Down Syndrome, Partial Trisomy 21, and Absence of Alzheimer's Disease: The Role of APP. *J Alzheimers Dis* **2017**, *56* (2), 459-470.
31. Wiseman, F. K.; Pulford, L. J.; Barkus, C.; Liao, F.; Portelius, E.; Webb, R.; Chavez-Gutierrez, L.; Cleverley, K.; Noy, S.; Sheppard, O.; Collins, T.; Powell, C.; Sarell, C. J.; Rickman, M.; Choong, X.; Tosh, J. L.; Siganporia, C.; Whittaker, H. T.; Stewart, F.; Szaruga, M.; London Down syndrome, c.; Murphy, M. P.; Blennow, K.; de Strooper, B.; Zetterberg, H.; Bannerman, D.; Holtzman, D. M.; Tybulewicz, V. L. J.; Fisher, E. M. C.,

Trisomy of human chromosome 21 enhances amyloid-beta deposition independently of an extra copy of APP. *Brain* **2018**.

32. Sherrington, R.; Rogaev, E. I.; Liang, Y.; Rogaeva, E. A.; Levesque, G.; Ikeda, M.; Chi, H.; Lin, C.; Li, G.; Holman, K.; Tsuda, T.; Mar, L.; Foncin, J. F.; Bruni, A. C.; Montesi, M. P.; Sorbi, S.; Rainero, I.; Pinessi, L.; Nee, L.; Chumakov, I.; Pollen, D.; Brookes, A.; Sanseau, P.; Polinsky, R. J.; Wasco, W.; Da Silva, H. A.; Haines, J. L.; Pericak-Vance, M. A.; Tanzi, R. E.; Roses, A. D.; Fraser, P. E.; Rommens, J. M.; St George-Hyslop, P. H., Cloning of a gene bearing missense mutations in early-onset familial Alzheimer's disease. *Nature* **1995**, *375* (6534), 754-60.

33. Cruts, M.; Van Broeckhoven, C., Molecular genetics of Alzheimer's disease. *Ann Med* **1998**, *30* (6), 560-5.

34. De Strooper, B.; Iwatsubo, T.; Wolfe, M. S., Presenilins and gamma-secretase: structure, function, and role in Alzheimer Disease. *Cold Spring Harb Perspect Med* **2012**, *2* (1), a006304.

35. Wolfe, M. S.; Yankner, B. A., Sorting Out Presenilins in Alzheimer's Disease. *Cell* **2016**, *166* (1), 13-5.

36. Beel, A. J.; Sanders, C. R., Substrate specificity of gamma-secretase and other intramembrane proteases. *Cell Mol Life Sci* **2008**, *65* (9), 1311-34.

37. Carroll, C. M.; Li, Y. M., Physiological and pathological roles of the gamma-secretase complex. *Brain Res Bull* **2016**, *126* (Pt 2), 199-206.

38. Chow, V. W.; Mattson, M. P.; Wong, P. C.; Gleichmann, M., An overview of APP processing enzymes and products. *Neuromolecular Med* **2010**, *12* (1), 1-12.

39. Chasseigneaux, S.; Allinquant, B., Functions of Abeta, sAPPalpha and sAPPbeta : similarities and differences. *J Neurochem* **2012**, *120 Suppl 1*, 99-108.

40. Rice, H. C.; de Malmazet, D.; Schreurs, A.; Frere, S.; Van Molle, I.; Volkov, A. N.; Creemers, E.; Vertkin, I.; Nys, J.; Ranaivoson, F. M.; Comoletti, D.; Savas, J. N.; Remaut, H.; Balschun, D.; Wierda, K. D.; Slutsky, I.; Farrow, K.; De Strooper, B.; de Wit, J., Secreted amyloid-beta precursor protein functions as a GABABR1a ligand to modulate synaptic transmission. *Science* **2019**, *363* (6423).

41. Song, Y. L.; Hustedt, E. J.; Brandon, S.; Sanders, C. R., Competition Between Homodimerization and Cholesterol Binding to the C99 Domain of the Amyloid Precursor Protein. *Biochemistry* **2013**, *52* (30), 5051-5064.

42. Dominguez, L.; Foster, L.; Straub, J. E.; Thirumalai, D., Impact of membrane lipid composition on the structure and stability of the transmembrane domain of amyloid precursor protein. *P Natl Acad Sci USA* **2016**, *113* (36), E5281-E5287.

43. Nadezhdin, K. D.; Bocharova, O. V.; Bocharov, E. V.; Arseniev, A. S., Dimeric structure of transmembrane domain of amyloid precursor protein in micellar environment. *Febs Letters* **2012**, *586* (12), 1687-1692.

44. Nhan, H. S.; Chiang, K.; Koo, E. H., The multifaceted nature of amyloid precursor protein and its proteolytic fragments: friends and foes. *Acta Neuropathol* **2015**, *129* (1), 1-19.

45. Muller, T.; Meyer, H. E.; Egensperger, R.; Marcus, K., The amyloid precursor protein intracellular domain (AICD) as modulator of gene expression, apoptosis, and cytoskeletal dynamics-relevance for Alzheimer's disease. *Prog Neurobiol* **2008**, *85* (4), 393-406.

46. Trillaud-Doppia, E.; Boehm, J., The Amyloid Precursor Protein Intracellular Domain Is an Effector Molecule of Metaplasticity. *Biol Psychiatry* **2018**, *83* (5), 406-415.
47. Hamid, R.; Kilger, E.; Willem, M.; Vassallo, N.; Kostka, M.; Bornhovd, C.; Reichert, A. S.; Kretschmar, H. A.; Haass, C.; Herms, J., Amyloid precursor protein intracellular domain modulates cellular calcium homeostasis and ATP content. *J Neurochem* **2007**, *102* (4), 1264-75.
48. Ward, M. W.; Concannon, C. G.; Whyte, J.; Walsh, C. M.; Corley, B.; Prehn, J. H., The amyloid precursor protein intracellular domain(AICD) disrupts actin dynamics and mitochondrial bioenergetics. *J Neurochem* **2010**, *113* (1), 275-84.
49. von Rotz, R. C.; Kohli, B. M.; Bosset, J.; Meier, M.; Suzuki, T.; Nitsch, R. M.; Konietzko, U., The APP intracellular domain forms nuclear multiprotein complexes and regulates the transcription of its own precursor. *J Cell Sci* **2004**, *117* (Pt 19), 4435-48.
50. Belyaev, N. D.; Nalivaeva, N. N.; Makova, N. Z.; Turner, A. J., Neprilysin gene expression requires binding of the amyloid precursor protein intracellular domain to its promoter: implications for Alzheimer disease. *EMBO Rep* **2009**, *10* (1), 94-100.
51. Ozaki, T.; Li, Y.; Kikuchi, H.; Tomita, T.; Iwatsubo, T.; Nakagawara, A., The intracellular domain of the amyloid precursor protein (AICD) enhances the p53-mediated apoptosis. *Biochem Biophys Res Commun* **2006**, *351* (1), 57-63.
52. Goiran, T.; Duplan, E.; Chami, M.; Bourgeois, A.; El Manaa, W.; Rouland, L.; Dunys, J.; Lauritzen, I.; You, H.; Stambolic, V.; Biferi, M. G.; Barkats, M.; Pimplikar, S. W.; Sergeant, N.; Colin, M.; Morais, V. A.; Pardossi-Piquard, R.; Checler, F.; Alves da Costa, C., beta-Amyloid Precursor Protein Intracellular Domain Controls Mitochondrial Function by Modulating Phosphatase and Tensin Homolog-Induced Kinase 1 Transcription in Cells and in Alzheimer Mice Models. *Biol Psychiatry* **2018**, *83* (5), 416-427.
53. Bauer, C.; Pardossi-Piquard, R.; Dunys, J.; Roy, M.; Checler, F., gamma-Secretase-mediated regulation of neprilysin: influence of cell density and aging and modulation by imatinib. *J Alzheimers Dis* **2011**, *27* (3), 511-20.
54. Ghosal, K.; Stathopoulos, A.; Pimplikar, S. W., APP intracellular domain impairs adult neurogenesis in transgenic mice by inducing neuroinflammation. *PLoS One* **2010**, *5* (7), e11866.
55. Ryan, K. A.; Pimplikar, S. W., Activation of GSK-3 and phosphorylation of CRMP2 in transgenic mice expressing APP intracellular domain. *Journal of Cell Biology* **2005**, *171* (2), 327-335.
56. Heilig, E. A.; Gutti, U.; Tai, T.; Shen, J.; Kelleher, R. J., 3rd, Trans-dominant negative effects of pathogenic PSEN1 mutations on gamma-secretase activity and Abeta production. *J Neurosci* **2013**, *33* (28), 11606-17.
57. Pardossi-Piquard, R.; Checler, F., The physiology of the beta-amyloid precursor protein intracellular domain AICD. *J Neurochem* **2012**, *120 Suppl 1*, 109-24.
58. Ghosal, K.; Fan, Q.; Dawson, H. N.; Pimplikar, S. W., Tau Protein Mediates APP Intracellular Domain (AICD)-Induced Alzheimer's-Like Pathological Features in Mice. *PLoS One* **2016**, *11* (7), e0159435.
59. Hebert, S. S.; Serneels, L.; Tolia, A.; Craessaerts, K.; Derks, C.; Filippov, M. A.; Muller, U.; De Strooper, B., Regulated intramembrane proteolysis of amyloid

- precursor protein and regulation of expression of putative target genes. *EMBO Rep* **2006**, 7 (7), 739-45.
60. Waldron, E.; Isbert, S.; Kern, A.; Jaeger, S.; Martin, A. M.; Hebert, S. S.; Behl, C.; Weggen, S.; De Strooper, B.; Pietrzik, C. U., Increased AICD generation does not result in increased nuclear translocation or activation of target gene transcription. *Exp Cell Res* **2008**, 314 (13), 2419-2433.
61. Wolfe, M. S., Dysfunctional gamma-Secretase in Familial Alzheimer's Disease. *Neurochem Res* **2019**, 44 (1), 5-11.
62. Liu, L.; Ding, L.; Rovere, M.; Wolfe, M. S.; Selkoe, D. J., A cellular complex of BACE1 and gamma-secretase sequentially generates Abeta from its full-length precursor. *J Cell Biol* **2019**.
63. Sun, J.; Roy, S., The physical approximation of APP and BACE-1: A key event in alzheimer's disease pathogenesis. *Dev Neurobiol* **2018**, 78 (3), 340-347.
64. Gregory, G. C.; Halliday, G. M., What is the dominant Abeta species in human brain tissue? A review. *Neurotox Res* **2005**, 7 (1-2), 29-41.
65. Hoshino, M., Fibril formation from the amyloid-beta peptide is governed by a dynamic equilibrium involving association and dissociation of the monomer. *Biophys Rev* **2017**, 9 (1), 9-16.
66. Tu, S.; Okamoto, S.; Lipton, S. A.; Xu, H., Oligomeric Abeta-induced synaptic dysfunction in Alzheimer's disease. *Mol Neurodegener* **2014**, 9, 48.
67. Serra-Batiste, M.; Ninot-Pedrosa, M.; Bayoumi, M.; Gairi, M.; Maglia, G.; Carulla, N., Abeta42 assembles into specific beta-barrel pore-forming oligomers in membrane-mimicking environments. *Proc Natl Acad Sci U S A* **2016**, 113 (39), 10866-71.
68. Lee, J.; Kim, Y. H.; F, T. A.; Gillman, A. L.; Jang, H.; Kagan, B. L.; Nussinov, R.; Yang, J.; Lal, R., Amyloid beta Ion Channels in a Membrane Comprising Brain Total Lipid Extracts. *ACS Chem Neurosci* **2017**, 8 (6), 1348-1357.
69. Jang, H.; Arce, F. T.; Ramachandran, S.; Kagan, B. L.; Lal, R.; Nussinov, R., Disordered amyloidogenic peptides may insert into the membrane and assemble into common cyclic structural motifs. *Chem Soc Rev* **2014**, 43 (19), 6750-6764.
70. Benilova, I.; De Strooper, B., Promiscuous Alzheimer's Amyloid: Yet Another Partner. *Science* **2013**, 341 (6152), 1354-1355.
71. Xia, M.; Cheng, X. F.; Yi, R. F.; Gao, D.; Xiong, J. X., The Binding Receptors of A beta: an Alternative Therapeutic Target for Alzheimer's Disease. *Mol Neurobiol* **2016**, 53 (1), 455-471.
72. Gunther, E. C.; Smith, L. M.; Kostylev, M. A.; Cox, T. O.; Kaufman, A. C.; Lee, S.; Folta-Stogniew, E.; Maynard, G. D.; Um, J. W.; Stagi, M.; Heiss, J. K.; Stoner, A.; Noble, G. P.; Takahashi, H.; Haas, L. T.; Schneekloth, J. S.; Merkel, J.; Teran, C.; Naderi, Z. K.; Supattapone, S.; Strittmatter, S. M., Rescue of Transgenic Alzheimer's Pathophysiology by Polymeric Cellular Prion Protein Antagonists. *Cell Reports* **2019**, 26 (1), 145-+.
73. Ittner, L. M.; Gotz, J., Amyloid-beta and tau - a toxic pas de deux in Alzheimer's disease. *Nat Rev Neurosci* **2011**, 12 (2), 67-72.
74. Ransohoff, R. M., How neuroinflammation contributes to neurodegeneration. *Science* **2016**, 353 (6301), 777-783.
75. Malm, T. M.; Jay, T. R.; Landreth, G. E., The Evolving Biology of Microglia in Alzheimer's Disease. *Neurotherapeutics* **2015**, 12 (1), 81-93.

76. Yang, T.; Li, S. M.; Xu, H. X.; Walsh, D. M.; Selkoe, D. J., Large Soluble Oligomers of Amyloid beta-Protein from Alzheimer Brain Are Far Less Neuroactive Than the Smaller Oligomers to Which They Dissociate. *Journal of Neuroscience* **2017**, *37* (1), 152-163.
77. Brody, D. L.; Jiang, H.; Wildburger, N.; Esparza, T. J., Non-canonical soluble amyloid-beta aggregates and plaque buffering: controversies and future directions for target discovery in Alzheimer's disease. *Alzheimers Res Ther* **2017**, *9*.
78. Marcello, E.; Borroni, B.; Pelucchi, S.; Gardoni, F.; Di Luca, M., ADAM10 as a therapeutic target for brain diseases: from developmental disorders to Alzheimer's disease. *Expert Opin Ther Tar* **2017**, *21* (11), 1017-1026.
79. Deuss, M.; Reiss, K.; Hartmann, D., Part-time alpha-secretases: The functional biology of ADAM 9, 10 and 17. *Current Alzheimer Research* **2008**, *5* (2), 187-201.
80. Peron, R.; Vatanabe, I. P.; Manzine, P. R.; Camins, A.; Cominetti, M. R., Alpha-Secretase ADAM10 Regulation: Insights into Alzheimer's Disease Treatment. *Pharmaceuticals (Basel)* **2018**, *11* (1).
81. Yuan, X. Z.; Sun, S.; Tan, C. C.; Yu, J. T.; Tan, L., The Role of ADAM10 in Alzheimer's Disease. *J Alzheimers Dis* **2017**, *58* (2), 303-322.
82. Matthews, A. L.; Noy, P. J.; Reyat, J. S.; Tomlinson, M. G., Regulation of A disintegrin and metalloproteinase (ADAM) family sheddases ADAM10 and ADAM17: The emerging role of tetraspanins and rhomboids. *Platelets* **2017**, *28* (4), 333-341.
83. Koelsch, G., BACE1 Function and Inhibition: Implications of Intervention in the Amyloid Pathway of Alzheimer's Disease Pathology. *Molecules* **2017**, *22* (10).
84. Edwards, D. R.; Handsley, M. M.; Pennington, C. J., The ADAM metalloproteinases. *Mol Aspects Med* **2008**, *29* (5), 258-89.
85. De Strooper, B.; Annaert, W.; Cupers, P.; Saftig, P.; Craessaerts, K.; Mumm, J. S.; Schroeter, E. H.; Schrijvers, V.; Wolfe, M. S.; Ray, W. J.; Goate, A.; Kopan, R., A presenilin-1-dependent gamma-secretase-like protease mediates release of Notch intracellular domain. *Nature* **1999**, *398* (6727), 518-22.
86. Geling, A.; Steiner, H.; Willem, M.; Bally-Cuif, L.; Haass, C., A gamma-secretase inhibitor blocks Notch signaling in vivo and causes a severe neurogenic phenotype in zebrafish. *Embo Reports* **2002**, *3* (7), 688-694.
87. Fleisher, A. S.; Raman, R.; Siemers, E. R.; Becerra, L.; Clark, C. M.; Dean, R. A.; Farlow, M. R.; Galvin, J. E.; Peskind, E. R.; Quinn, J. F.; Sherzai, A.; Sowell, B.; Aisen, P. S.; Thal, L. J., Phase 2 safety trial targeting amyloid beta production with a gamma-secretase inhibitor in Alzheimer disease. *Arch Neurol-Chicago* **2008**, *65* (8), 1031-1038.
88. Kuruva, C. S.; Reddy, P. H., Amyloid beta modulators and neuroprotection in Alzheimer's disease: a critical appraisal. *Drug Discov Today* **2017**, *22* (2), 223-233.
89. Bursavich, M. G.; Harrison, B. A.; Blain, J. F., Gamma Secretase Modulators: New Alzheimer's Drugs on the Horizon? *J Med Chem* **2016**, *59* (16), 7389-7409.
90. Xia, W. M.; Wong, S. T.; Hanlon, E.; Morin, P., gamma-Secretase Modulator in Alzheimer's Disease: Shifting the End. *Journal of Alzheimers Disease* **2012**, *31* (4), 685-696.

91. Zhou, L.; Brouwers, N.; Benilova, I.; Vandersteen, A.; Mercken, M.; Van Laere, K.; Van Damme, P.; Demedts, D.; Van Leuven, F.; Sleegers, K.; Broersen, K.; Van Broeckhoven, C.; Vandenbergh, R.; De Strooper, B., Amyloid precursor protein mutation E682K at the alternative beta-secretase cleavage beta'-site increases A beta generation. *Embo Molecular Medicine* **2011**, 3 (5), 291-302.
92. Zhang, H.; Ma, Q. L.; Zhang, Y. W.; Xu, H. X., Proteolytic processing of Alzheimer's ss-amyloid precursor protein. *Journal of Neurochemistry* **2012**, 120, 9-21.
93. Willem, M.; Tahirovic, S.; Busche, M. A.; Ovsepian, S. V.; Chafai, M.; Kootar, S.; Hornburg, D.; Evans, L. D. B.; Moore, S.; Daria, A.; Hampel, H.; Muller, V.; Giudici, C.; Nuscher, B.; Wenninger-Weinzierl, A.; Kremmer, E.; Heneka, M. T.; Thal, D. R.; Giedraitis, V.; Lannfelt, L.; Muller, U.; Livesey, F. J.; Meissner, F.; Herms, J.; Konnerth, A.; Marie, H.; Haass, C., eta-Secretase processing of APP inhibits neuronal activity in the hippocampus. *Nature* **2015**, 526 (7573), 443-+.
94. Dunys, J.; Valverde, A.; Checler, F., Are N- and C-terminally truncated A species key pathological triggers in Alzheimer's disease? *Journal of Biological Chemistry* **2018**, 293 (40), 15419-15428.
95. Baranger, K.; Marchalant, Y.; Bonnet, A. E.; Crouzin, N.; Carrete, A.; Paumier, J. M.; Py, N. A.; Bernard, A.; Bauer, C.; Charrat, E.; Moschke, K.; Seiki, M.; Vignes, M.; Lichtenthaler, S. F.; Checler, F.; Khrestchatsky, M.; Rivera, S., MT5-MMP is a new pro-amyloidogenic proteinase that promotes amyloid pathology and cognitive decline in a transgenic mouse model of Alzheimer's disease. *Cellular and Molecular Life Sciences* **2016**, 73 (1), 217-236.
96. Yonemura, Y.; Futai, E.; Yagishita, S.; Kaether, C.; Ishiura, S., Specific combinations of presenilins and Aph1s affect the substrate specificity and activity of gamma-secretase. *Biochem Bioph Res Co* **2016**, 478 (4), 1751-1757.
97. Sannerud, R.; Esselens, C.; Ejsmont, P.; Mattera, R.; Rochin, L.; Tharkeshwar, A. K.; De Baets, G.; De Wever, V.; Habets, R.; Baert, V.; Vermeire, W.; Michiels, C.; Groot, A. J.; Wouters, R.; Dillen, K.; Vints, K.; Baatsen, P.; Munck, S.; Derua, R.; Waelkens, E.; Basi, G. S.; Mercken, M.; Vooijs, M.; Bollen, M.; Schymkowitz, J.; Rousseau, F.; Bonifacino, J. S.; Van Niel, G.; De Strooper, B.; Annaert, W., Restricted Location of PSEN2/gamma-Secretase Determines Substrate Specificity and Generates an Intracellular A beta Pool. *Cell* **2016**, 166 (1), 193-208.
98. Knauer, M. F.; Soreghan, B.; Burdick, D.; Kosmoski, J.; Glabe, C. G., Intracellular accumulation and resistance to degradation of the Alzheimer amyloid A4/beta protein. *Proc Natl Acad Sci U S A* **1992**, 89 (16), 7437-41.
99. Bi, X.; Gall, C. M.; Zhou, J.; Lynch, G., Uptake and pathogenic effects of amyloid beta peptide 1-42 are enhanced by integrin antagonists and blocked by NMDA receptor antagonists. *Neuroscience* **2002**, 112 (4), 827-40.
100. Yang, A. J.; Chandswangbhuvana, D.; Margol, L.; Glabe, C. G., Loss of endosomal/lysosomal membrane impermeability is an early event in amyloid A beta 1-42 pathogenesis. *J Neurosci Res* **1998**, 52 (6), 691-698.
101. Cook, D. G.; Forman, M. S.; Sung, J. C.; Leight, S.; Kolson, D. L.; Iwatsubo, T.; Lee, V. M. Y.; Doms, R. W., Alzheimer's A beta(1-42) is generated in the endoplasmic reticulum/intermediate compartment of NT2N cells. *Nature Medicine* **1997**, 3 (9), 1021-1023.

102. Greenfield, J. P.; Tsai, J.; Gouras, G. K.; Hai, B.; Thinakaran, G.; Checler, F.; Sisodia, S. S.; Greengard, P.; Xu, H. X., Endoplasmic reticulum and trans-Golgi network generate distinct populations of Alzheimer beta-amyloid peptides. *P Natl Acad Sci USA* **1999**, *96* (2), 742-747.
103. Wang, X.; Zhou, X.; Li, G. Y.; Zhang, Y.; Wu, Y. L.; Song, W. H., Modifications and Trafficking of APP in the Pathogenesis of Alzheimer's Disease. *Front Mol Neurosci* **2017**, *10*.
104. Hartmann, T.; Bieger, S. C.; Bruhl, B.; Tienari, P. J.; Ida, N.; Allsop, D.; Roberts, G. W.; Masters, C. L.; Dotti, C. G.; Unsicker, K.; Beyreuther, K., Distinct sites of intracellular production for Alzheimer's disease A beta 40/42 amyloid peptides. *Nature Medicine* **1997**, *3* (9), 1016-1020.
105. Chen, J. X.; Yan, S. S., Role of Mitochondrial Amyloid-beta in Alzheimer's Disease. *Journal of Alzheimers Disease* **2010**, *20*, S569-S578.
106. LaFerla, F. M.; Green, K. N.; Oddo, S., Intracellular amyloid-beta in Alzheimer's disease. *Nat Rev Neurosci* **2007**, *8* (7), 499-509.
107. Pera, M.; Larrea, D.; Guardia-Laguarta, C.; Montesinos, J.; Velasco, K. R.; Agrawal, R. R.; Xu, Y.; Chan, R. B.; Di Paolo, G.; Mehler, M. F.; Perumal, G. S.; Macaluso, F. P.; Freyberg, Z. Z.; Acin-Perez, R.; Enriquez, J. A.; Schon, E. A.; Area-Gomez, E., Increased localization of APP-C99 in mitochondria-associated ER membranes causes mitochondrial dysfunction in Alzheimer disease. *EMBO J* **2017**, *36* (22), 3356-3371.
108. Hu, H.; Tan, C. C.; Tan, L.; Yu, J. T., A Mitocentric View of Alzheimer's Disease. *Mol Neurobiol* **2017**, *54* (8), 6046-6060.
109. Lloret, A.; Fuchsberger, T.; Giraldo, E.; Vina, J., Molecular mechanisms linking amyloid beta toxicity and Tau hyperphosphorylation in Alzheimers disease. *Free Radic Biol Med* **2015**, *83*, 186-91.
110. Zheng, W. H.; Bastianetto, S.; Mennicken, F.; Ma, W.; Kar, S., Amyloid beta peptide induces tau phosphorylation and loss of cholinergic neurons in rat primary septal cultures. *Neuroscience* **2002**, *115* (1), 201-211.
111. Stancu, I. C.; Vasconcelos, B.; Terwel, D.; Dewachter, I., Models of beta-amyloid induced Tau-pathology: the long and "folded" road to understand the mechanism. *Molecular Neurodegeneration* **2014**, *9*.
112. Nisbet, R. M.; Polanco, J. C.; Ittner, L. M.; Gotz, J., Tau aggregation and its interplay with amyloid-beta. *Acta Neuropathologica* **2015**, *129* (2), 207-220.
113. Biffi, A.; Greenberg, S. M., Cerebral Amyloid Angiopathy: A Systematic Review. *J Clin Neurol* **2011**, *7* (1), 1-9.
114. Head, E.; Phelan, M. J.; Doran, E.; Kim, R. C.; Poon, W. W.; Schmitt, F. A.; Lott, I. T., Cerebrovascular pathology in Down syndrome and Alzheimer disease. *Acta Neuropathol Com* **2017**, *5*.
115. Buhimschi, I. A.; Nayeri, U. A.; Zhao, G. M.; Shook, L. L.; Pensalfini, A.; Funai, E. F.; Bernstein, I. M.; Glabe, C. G.; Buhimschi, C. S., Protein misfolding, congophilia, oligomerization, and defective amyloid processing in preeclampsia. *Science Translational Medicine* **2014**, *6* (245).
116. Tanzi, R. E., The genetics of Alzheimer disease. *Cold Spring Harb Perspect Med* **2012**, *2* (10).
117. Reiss, A. B.; Arain, H. A.; Stecker, M. M.; Siegart, N. M.; Kasselmann, L. J., Amyloid toxicity in Alzheimer's disease. *Rev Neurosci* **2018**, *29* (6), 613-627.

118. Carrillo-Mora, P.; Luna, R.; Colin-Barenque, L., Amyloid beta: multiple mechanisms of toxicity and only some protective effects? *Oxid Med Cell Longev* **2014**, *2014*, 795375.
119. Kaden, D.; Harmeier, A.; Weise, C.; Munter, L. M.; Althoff, V.; Rost, B. R.; Hildebrand, P. W.; Schmitz, D.; Schaefer, M.; Lurz, R.; Skodda, S.; Yamamoto, R.; Arlt, S.; Finckh, U.; Multhaup, G., Novel APP/Abeta mutation K16N produces highly toxic heteromeric Abeta oligomers. *EMBO Mol Med* **2012**, *4* (7), 647-59.
120. Mullan, M.; Crawford, F.; Axelman, K.; Houlden, H.; Lilius, L.; Winblad, B.; Lannfelt, L., A pathogenic mutation for probable Alzheimer's disease in the APP gene at the N-terminus of beta-amyloid. *Nat Genet* **1992**, *1* (5), 345-7.
121. Scheuner, D.; Eckman, C.; Jensen, M.; Song, X.; Citron, M.; Suzuki, N.; Bird, T. D.; Hardy, J.; Hutton, M.; Kukull, W.; Larson, E.; Levy-Lahad, E.; Viitanen, M.; Peskind, E.; Poorkaj, P.; Schellenberg, G.; Tanzi, R.; Wasco, W.; Lannfelt, L.; Selkoe, D.; Younkin, S., Secreted amyloid beta-protein similar to that in the senile plaques of Alzheimer's disease is increased in vivo by the presenilin 1 and 2 and APP mutations linked to familial Alzheimer's disease. *Nat Med* **1996**, *2* (8), 864-70.
122. Nilsberth, C.; Westlind-Danielsson, A.; Eckman, C. B.; Condrón, M. M.; Axelman, K.; Forsell, C.; Sten, C.; Luthman, J.; Teplow, D. B.; Younkin, S. G.; Naslund, J.; Lannfelt, L., The 'Arctic' APP mutation (E693G) causes Alzheimer's disease by enhanced Abeta protofibril formation. *Nat Neurosci* **2001**, *4* (9), 887-93.
123. Johnston, J. A.; Cowburn, R. F.; Norgren, S.; Wiehager, B.; Venizelos, N.; Winblad, B.; Vigo-Pelfrey, C.; Schenk, D.; Lannfelt, L.; O'Neill, C., Increased beta-amyloid release and levels of amyloid precursor protein (APP) in fibroblast cell lines from family members with the Swedish Alzheimer's disease APP670/671 mutation. *FEBS Lett* **1994**, *354* (3), 274-8.
124. Citron, M.; Vigo-Pelfrey, C.; Teplow, D. B.; Miller, C.; Schenk, D.; Johnston, J.; Winblad, B.; Venizelos, N.; Lannfelt, L.; Selkoe, D. J., Excessive production of amyloid beta-protein by peripheral cells of symptomatic and presymptomatic patients carrying the Swedish familial Alzheimer disease mutation. *Proc Natl Acad Sci U S A* **1994**, *91* (25), 11993-7.
125. Citron, M.; Oltersdorf, T.; Haass, C.; McConlogue, L.; Hung, A. Y.; Seubert, P.; Vigo-Pelfrey, C.; Lieberburg, I.; Selkoe, D. J., Mutation of the beta-amyloid precursor protein in familial Alzheimer's disease increases beta-protein production. *Nature* **1992**, *360* (6405), 672-4.
126. Cai, X. D.; Golde, T. E.; Younkin, S. G., Release of excess amyloid beta protein from a mutant amyloid beta protein precursor. *Science* **1993**, *259* (5094), 514-6.
127. Grabowski, T. J.; Cho, H. S.; Vonsattel, J. P.; Rebeck, G. W.; Greenberg, S. M., Novel amyloid precursor protein mutation in an Iowa family with dementia and severe cerebral amyloid angiopathy. *Ann Neurol* **2001**, *49* (6), 697-705.
128. Krone, M. G.; Baumketner, A.; Bernstein, S. L.; Wyttenbach, T.; Lazo, N. D.; Teplow, D. B.; Bowers, M. T.; Shea, J. E., Effects of familial Alzheimer's disease mutations on the folding nucleation of the amyloid beta-protein. *J Mol Biol* **2008**, *381* (1), 221-8.
129. Van Nostrand, W. E.; Melchor, J. P.; Romanov, G.; Zeigler, K.; Davis, J., Pathogenic effects of cerebral amyloid angiopathy mutations in the amyloid beta-protein precursor. *Ann N Y Acad Sci* **2002**, *977*, 258-65.

130. Van Nostrand, W. E.; Melchor, J. P.; Cho, H. S.; Greenberg, S. M.; Rebeck, G. W., Pathogenic effects of D23N Iowa mutant amyloid beta -protein. *J Biol Chem* **2001**, *276* (35), 32860-6.
131. Zheng, X.; Liu, D.; Roychaudhuri, R.; Teplow, D. B.; Bowers, M. T., Amyloid beta-Protein Assembly: Differential Effects of the Protective A2T Mutation and Recessive A2V Familial Alzheimer's Disease Mutation. *ACS Chem Neurosci* **2015**, *6* (10), 1732-40.
132. Theuns, J.; Marjaux, E.; Vandenbulcke, M.; Van Laere, K.; Kumar-Singh, S.; Bormans, G.; Brouwers, N.; Van den Broeck, M.; Vennekens, K.; Corsmit, E.; Cruts, M.; De Strooper, B.; Van Broeckhoven, C.; Vandenberghe, R., Alzheimer dementia caused by a novel mutation located in the APP C-terminal intracytosolic fragment. *Hum Mutat* **2006**, *27* (9), 888-96.
133. Herl, L.; Thomas, A. V.; Lill, C. M.; Banks, M.; Deng, A.; Jones, P. B.; Spoelgen, R.; Hyman, B. T.; Berezovska, O., Mutations in amyloid precursor protein affect its interactions with presenilin/gamma-secretase. *Mol Cell Neurosci* **2009**, *41* (2), 166-74.
134. Kwok, J. B.; Li, Q. X.; Hallupp, M.; Whyte, S.; Ames, D.; Beyreuther, K.; Masters, C. L.; Schofield, P. R., Novel Leu723Pro amyloid precursor protein mutation increases amyloid beta42(43) peptide levels and induces apoptosis. *Ann Neurol* **2000**, *47* (2), 249-53.
135. Eckman, C. B.; Mehta, N. D.; Crook, R.; Perez-tur, J.; Prihar, G.; Pfeiffer, E.; Graff-Radford, N.; Hinder, P.; Yager, D.; Zenk, B.; Refolo, L. M.; Prada, C. M.; Younkin, S. G.; Hutton, M.; Hardy, J., A new pathogenic mutation in the APP gene (I716V) increases the relative proportion of A beta 42(43). *Hum Mol Genet* **1997**, *6* (12), 2087-9.
136. De Jonghe, C.; Esselens, C.; Kumar-Singh, S.; Craessaerts, K.; Serneels, S.; Checler, F.; Annaert, W.; Van Broeckhoven, C.; De Strooper, B., Pathogenic APP mutations near the gamma-secretase cleavage site differentially affect Abeta secretion and APP C-terminal fragment stability. *Hum Mol Genet* **2001**, *10* (16), 1665-71.
137. Xu, T. H.; Yan, Y.; Kang, Y.; Jiang, Y.; Melcher, K.; Xu, H. E., Alzheimer's disease-associated mutations increase amyloid precursor protein resistance to gamma-secretase cleavage and the Abeta42/Abeta40 ratio. *Cell Discov* **2016**, *2*, 16026.
138. Yan, Y.; Xu, T. H.; Harikumar, K. G.; Miller, L. J.; Melcher, K.; Xu, H. E., Dimerization of the transmembrane domain of amyloid precursor protein is determined by residues around the gamma-secretase cleavage sites. *J Biol Chem* **2017**, *292* (38), 15826-15837.
139. Zhou, R.; Yang, G.; Guo, X.; Zhou, Q.; Lei, J.; Shi, Y., Recognition of the amyloid precursor protein by human gamma-secretase. *Science* **2019**.
140. Ho, A.; Shen, J., Presenilins in synaptic function and disease. *Trends Mol Med* **2011**, *17* (11), 617-24.
141. Bertram, L.; Tanzi, R. E., The genetics of Alzheimer's disease. *Prog Mol Biol Transl Sci* **2012**, *107*, 79-100.
142. Kelleher, R. J.; Shen, J., gamma-Secretase and Human Disease. *Science* **2010**, *330* (6007), 1055-1056.
143. Wang, B. X.; Yang, W.; Wen, W.; Sun, J.; Su, B.; Liu, B.; Ma, D. L.; Lv, D.; Wen, Y. R.; Qu, T.; Chen, M.; Sun, M. A.; Shen, Y.; Zhang, X., gamma-Secretase Gene Mutations in Familial Acne Inversa. *Science* **2010**, *330* (6007), 1065-1065.

144. Zhou, R.; Yang, G.; Shi, Y., Dominant negative effect of the loss-of-function gamma-secretase mutants on the wild-type enzyme through heterooligomerization. *Proc Natl Acad Sci U S A* **2017**, *114* (48), 12731-12736.
145. Cacquevel, M.; Aeschbach, L.; Houacine, J.; Fraering, P. C., Alzheimer's Disease-Linked Mutations in Presenilin-1 Result in a Drastic Loss of Activity in Purified gamma-Secretase Complexes. *Plos One* **2012**, *7* (4).
146. Xia, D.; Watanabe, H.; Wu, B.; Lee, S. H.; Li, Y.; Tsvetkov, E.; Bolshakov, V. Y.; Shen, J.; Kelleher, R. J., 3rd, Presenilin-1 knockin mice reveal loss-of-function mechanism for familial Alzheimer's disease. *Neuron* **2015**, *85* (5), 967-81.
147. Woodruff, G.; Young, J. E.; Martinez, F. J.; Buen, F.; Gore, A.; Kinaga, J.; Li, Z.; Yuan, S. H.; Zhang, K.; Goldstein, L. S. B., The Presenilin-1 Delta E9 Mutation Results in Reduced gamma-Secretase Activity, but Not Total Loss of PS1 Function, in Isogenic Human Stem Cells. *Cell Reports* **2013**, *5* (4), 974-985.
148. Sun, L.; Zhou, R.; Yang, G.; Shi, Y., Analysis of 138 pathogenic mutations in presenilin-1 on the in vitro production of Abeta42 and Abeta40 peptides by gamma-secretase. *Proc Natl Acad Sci U S A* **2017**, *114* (4), E476-E485.
149. Marinko, J. T.; Huang, H.; Penn, W. D.; Capra, J. A.; Schleich, J. P.; Sanders, C. R., Folding and Misfolding of Human Membrane Proteins in Health and Disease: From Single Molecules to Cellular Proteostasis. *Chem Rev* **2019**.
150. Sanders, C. R.; Myers, J. K., Disease-related misassembly of membrane proteins. *Annu Rev Biophys Biomol Struct* **2004**, *33*, 25-51.
151. Sanders, C. R.; Ismail-Beigi, F.; McEnery, M. W., Mutations of peripheral myelin protein 22 result in defective trafficking through mechanisms which may be common to diseases involving tetraspan membrane proteins. *Biochemistry* **2001**, *40* (32), 9453-9.
152. Doody, R. S.; Aisen, P. S.; Iwatsubo, T., Semagacestat for treatment of Alzheimer's disease. *N Engl J Med* **2013**, *369* (17), 1661.
153. Doody, R. S.; Raman, R.; Farlow, M.; Iwatsubo, T.; Vellas, B.; Joffe, S.; Kieburtz, K.; He, F.; Sun, X.; Thomas, R. G.; Aisen, P. S.; Alzheimer's Disease Cooperative Study Steering, C.; Siemers, E.; Sethuraman, G.; Mohs, R.; Semagacestat Study, G., A phase 3 trial of semagacestat for treatment of Alzheimer's disease. *N Engl J Med* **2013**, *369* (4), 341-50.
154. Coric, V.; van Dyck, C. H.; Salloway, S.; Andreasen, N.; Brody, M.; Richter, R. W.; Soininen, H.; Thein, S.; Shiovitz, T.; Pilcher, G.; Colby, S.; Rollin, L.; Dockens, R.; Pachai, C.; Portelius, E.; Andreasson, U.; Blennow, K.; Soares, H.; Albright, C.; Feldman, H. H.; Berman, R. M., Safety and tolerability of the gamma-secretase inhibitor avagacestat in a phase 2 study of mild to moderate Alzheimer disease. *Arch Neurol* **2012**, *69* (11), 1430-40.
155. Cummings, J., Lessons Learned from Alzheimer Disease: Clinical Trials with Negative Outcomes. *Clin Transl Sci* **2018**, *11* (2), 147-152.
156. Kim, J.; Chakrabarty, P.; Hanna, A.; March, A.; Dickson, D. W.; Borchelt, D. R.; Golde, T.; Janus, C., Normal cognition in transgenic BRI2-Abeta mice. *Mol Neurodegener* **2013**, *8*, 15.
157. Hamm, V.; Heraud, C.; Bott, J. B.; Herbeaux, K.; Strittmatter, C.; Mathis, C.; Goutagny, R., Differential contribution of APP metabolites to early cognitive deficits in a TgCRND8 mouse model of Alzheimer's disease. *Sci Adv* **2017**, *3* (2), e1601068.

158. Devi, L.; Prabhu, B. M.; Galati, D. F.; Avadhani, N. G.; Anandatheerthavarada, H. K., Accumulation of amyloid precursor protein in the mitochondrial import channels of human Alzheimer's disease brain is associated with mitochondrial dysfunction. *J Neurosci* **2006**, *26* (35), 9057-68.
159. Cummings, B. J.; Su, J. H.; Geddes, J. W.; Van Nostrand, W. E.; Wagner, S. L.; Cunningham, D. D.; Cotman, C. W., Aggregation of the amyloid precursor protein within degenerating neurons and dystrophic neurites in Alzheimer's disease. *Neuroscience* **1992**, *48* (4), 763-77.
160. Deyts, C.; Clutter, M.; Herrera, S.; Jovanovic, N.; Goddi, A.; Parent, A. T., Loss of presenilin function is associated with a selective gain of APP function. *Elife* **2016**, *5*.
161. Bourgeois, A.; Lauritzen, I.; Lorivel, T.; Bauer, C.; Checler, F.; Pardossi-Piquard, R., Intraneuronal accumulation of C99 contributes to synaptic alterations, apathy-like behavior, and spatial learning deficits in 3xTgAD and 2xTgAD mice. *Neurobiol Aging* **2018**, *71*, 21-31.
162. Lauritzen, I.; Pardossi-Piquard, R.; Bauer, C.; Brigham, E.; Abraham, J. D.; Ranaldi, S.; Fraser, P.; St-George-Hyslop, P.; Le Thuc, O.; Espin, V.; Chami, L.; Dunys, J.; Checler, F., The beta-secretase-derived C-terminal fragment of betaAPP, C99, but not Abeta, is a key contributor to early intraneuronal lesions in triple-transgenic mouse hippocampus. *J Neurosci* **2012**, *32* (46), 16243-1655a.
163. Mondragon-Rodriguez, S.; Gu, N.; Manseau, F.; Williams, S., Alzheimer's Transgenic Model Is Characterized by Very Early Brain Network Alterations and beta-CTF Fragment Accumulation: Reversal by beta-Secretase Inhibition. *Front Cell Neurosci* **2018**, *12*, 121.
164. Tamayev, R.; Matsuda, S.; Arancio, O.; D'Adamio, L., beta- but not gamma-secretase proteolysis of APP causes synaptic and memory deficits in a mouse model of dementia. *EMBO Mol Med* **2012**, *4* (3), 171-9.
165. Lauritzen, I.; Pardossi-Piquard, R.; Bourgeois, A.; Pagnotta, S.; Biferi, M. G.; Barkats, M.; Lacor, P.; Klein, W.; Bauer, C.; Checler, F., Intraneuronal aggregation of the beta-CTF fragment of APP (C99) induces Abeta-independent lysosomal-autophagic pathology. *Acta Neuropathol* **2016**, *132* (2), 257-76.
166. Chen, H. Y.; Wang, L.; Liu, J. F.; Wang, W. Z.; Yu, C. J., Effect of the beta secretase-1 inhibitor on the amyloid C-terminal fragment of amyloid precursor protein processing in a hyperphosphorylated tau rat model. *Genet Mol Res* **2014**, *13* (3), 6213-27.
167. Jiang, Y.; Mullaney, K. A.; Peterhoff, C. M.; Che, S.; Schmidt, S. D.; Boyer-Boiteau, A.; Ginsberg, S. D.; Cataldo, A. M.; Mathews, P. M.; Nixon, R. A., Alzheimer's-related endosome dysfunction in Down syndrome is Abeta-independent but requires APP and is reversed by BACE-1 inhibition. *Proc Natl Acad Sci U S A* **2010**, *107* (4), 1630-5.
168. Israel, M. A.; Yuan, S. H.; Bardy, C.; Reyna, S. M.; Mu, Y.; Herrera, C.; Hefferan, M. P.; Van Gorp, S.; Nazor, K. L.; Boscolo, F. S.; Carson, C. T.; Laurent, L. C.; Marsala, M.; Gage, F. H.; Remes, A. M.; Koo, E. H.; Goldstein, L. S., Probing sporadic and familial Alzheimer's disease using induced pluripotent stem cells. *Nature* **2012**, *482* (7384), 216-20.
169. Cuccaro, M. L.; Carney, R. M.; Zhang, Y. L.; Bohm, C.; Kunkle, B. W.; Vardarajan, B. N.; Whitehead, P. L.; Cukier, H. N.; Mayeux, R.; St George-Hyslop, P.;

- Pericak-Vance, M. A., SORL1 mutations in early- and late-onset Alzheimer disease. *Neurol-Genet* **2016**, *2* (6).
170. Holtzman, D. M., Apolipoprotein E and Alzheimer's Disease: the influence of apoE on amyloid beta and other amyloidogenic proteins (vol 58, pg 824, 2017). *J Lipid Res* **2018**, *59* (8), 1546-1546.
171. Xu, W.; Tan, L.; Yu, J. T., The Role of PICALM in Alzheimer's Disease. *Mol Neurobiol* **2015**, *52* (1), 399-413.
172. Carmona, S.; Zahs, K.; Wu, E.; Dakin, K.; Bras, J.; Guerreiro, R., The role of TREM2 in Alzheimer's disease and other neurodegenerative disorders. *Lancet Neurol* **2018**, *17* (8), 721-730.
173. Aikawa, T.; Holm, M. L.; Kanekiyo, T., ABCA7 and Pathogenic Pathways of Alzheimer's Disease. *Brain Sci* **2018**, *8* (2).
174. Tan, M. S.; Yu, J. T.; Tan, L., Bridging integrator 1 (BIN1): form, function, and Alzheimer's disease. *Trends in Molecular Medicine* **2013**, *19* (10), 594-603.
175. Lee, M. H.; Siddoway, B.; Kaeser, G. E.; Segota, I.; Rivera, R.; Romanow, W. J.; Liu, C. S.; Park, C.; Kennedy, G.; Long, T.; Chun, J., Somatic APP gene recombination in Alzheimer's disease and normal neurons. *Nature* **2018**, *563* (7733), 639-645.
176. Rohrback, S.; Siddoway, B.; Liu, C. S.; Chun, J., Genomic mosaicism in the developing and adult brain. *Dev Neurobiol* **2018**, *78* (11), 1026-1048.
177. Koyuncu, O. O.; Hogue, I. B.; Enquist, L. W., Virus Infections in the Nervous System. *Cell Host Microbe* **2013**, *13* (4), 379-393.
178. Kumar, A. M.; Borodowsky, I.; Fernandez, B.; Gonzalez, L.; Kumar, M., Human immunodeficiency virus type 1 RNA levels in different regions of human brain: Quantification using real-time reverse transcriptase-polymerase chain reaction. *J Neurovirol* **2007**, *13* (3), 210-224.
179. Bugge, K.; Lindorff-Larsen, K.; Kragelund, B. B., Understanding single-pass transmembrane receptor signaling from a structural viewpoint-what are we missing? *FEBS J* **2016**, *283* (24), 4424-4451.
180. Erickson-Miller, C. L.; DeLorme, E.; Tian, S. S.; Hopson, C. B.; Stark, K.; Giampa, L.; Valoret, E. I.; Duffy, K. J.; Luengo, J. L.; Rosen, J.; Miller, S. G.; Dillon, S. B.; Lamb, P., Discovery and characterization of a selective, nonpeptidyl thrombopoietin receptor agonist. *Exp Hematol* **2005**, *33* (1), 85-93.
181. Kuter, D. J., Biology and chemistry of thrombopoietic agents. *Semin Hematol* **2010**, *47* (3), 243-8.
182. Ma, W.; Yang, L.; He, L., Overview of the detection methods for equilibrium dissociation constant KD of drug-receptor interaction. *J Pharm Anal* **2018**, *8* (3), 147-152.
183. Howarth, F. C.; Singh, J.; Waring, J. J.; Hustler, B. I.; Bailey, M., Effects of monovalent cations, pH and temperature on the dissociation constant (KD) for the fluorescent indicator mag-fura-2 at different excitation wavelengths. *Magnes Res* **1995**, *8* (4), 299-306.
184. Zhang, M.; Huang, R.; Im, S.-C.; Waskell, L.; Ramamoorthy, A., Effects of Membrane Mimetics on Cytochrome P450-Cytochrome b5 Interactions Characterized by NMR Spectroscopy*. *Journal of Biological Chemistry* **2015**, *290* (20), 12705-12718.
185. Freitag, S.; Le Trong, I.; Klumb, L.; Stayton, P. S.; Stenkamp, R. E., Structural studies of the streptavidin binding loop. *Protein Sci* **1997**, *6* (6), 1157-66.

186. General, I. J.; Dragomirova, R.; Meirovitch, H., Absolute free energy of binding of avidin/biotin, revisited. *J Phys Chem B* **2012**, *116* (23), 6628-36.
187. Wacker, D.; Wang, S.; McCorvy, J. D.; Betz, R. M.; Venkatakrishnan, A. J.; Levit, A.; Lansu, K.; Schools, Z. L.; Che, T.; Nichols, D. E.; Shoichet, B. K.; Dror, R. O.; Roth, B. L., Crystal Structure of an LSD-Bound Human Serotonin Receptor. *Cell* **2017**, *168* (3), 377-389 e12.
188. Koutcher, J. A.; Burt, C. T., Principles of nuclear magnetic resonance. *J Nucl Med* **1984**, *25* (1), 101-11.
189. Trabesinger, A., Less room for failure. *Nature Physics* **2011**, *7* (10), 745-745.
190. Darbeau, R. W., Nuclear Magnetic Resonance (NMR) Spectroscopy: A Review and a Look at Its Use as a Probative Tool in Deamination Chemistry. *Applied Spectroscopy Reviews* **2006**, *41* (4), 401-425.
191. Williamson, M. P.; Havel, T. F.; Wüthrich, K., Solution conformation of proteinase inhibitor IIA from bull seminal plasma by ¹H nuclear magnetic resonance and distance geometry. *Journal of Molecular Biology* **1985**, *182* (2), 295-315.
192. Ronconi, L.; Sadler, P. J., Applications of heteronuclear NMR spectroscopy in biological and medicinal inorganic chemistry. *Coord Chem Rev* **2008**, *252* (21), 2239-2277.
193. Erlanson, D. A.; Fesik, S. W.; Hubbard, R. E.; Jahnke, W.; Jhoti, H., Twenty years on: the impact of fragments on drug discovery. *Nat Rev Drug Discov* **2016**, *15* (9), 605-619.
194. Oliver, R. C.; Lipfert, J.; Fox, D. A.; Lo, R. H.; Doniach, S.; Columbus, L., Dependence of micelle size and shape on detergent alkyl chain length and head group. *PLoS One* **2013**, *8* (5), e62488.
195. Castro, M. A.; Hadziselimovic, A.; Sanders, C. R., The vexing complexity of the amyloidogenic pathway. *Protein Sci* **2019**, *28* (7), 1177-1193.
196. van Duijn, C. M.; Hendriks, L.; Cruts, M.; Hardy, J. A.; Hofman, A.; Van Broeckhoven, C., Amyloid precursor protein gene mutation in early-onset Alzheimer's disease. *Lancet* **1991**, *337* (8747), 978.
197. Hardy, J., The discovery of Alzheimer-causing mutations in the APP gene and the formulation of the "amyloid cascade hypothesis". *FEBS J* **2017**, *284* (7), 1040-1044.
198. Chartier-Harlin, M. C.; Crawford, F.; Houlden, H.; Warren, A.; Hughes, D.; Fidani, L.; Goate, A.; Rossor, M.; Roques, P.; Hardy, J.; et al., Early-onset Alzheimer's disease caused by mutations at codon 717 of the beta-amyloid precursor protein gene. *Nature* **1991**, *353* (6347), 844-6.
199. Hardy, J. A.; Higgins, G. A., Alzheimer's disease: the amyloid cascade hypothesis. *Science* **1992**, *256* (5054), 184-5.
200. Hardy, J., Alzheimer's disease: the amyloid cascade hypothesis: an update and reappraisal. *J Alzheimers Dis* **2006**, *9* (3 Suppl), 151-3.
201. Woo, H. N.; Park, J. S.; Gwon, A. R.; Arumugam, T. V.; Jo, D. G., Alzheimer's disease and Notch signaling. *Biochem Biophys Res Commun* **2009**, *390* (4), 1093-7.
202. Guner, G.; Lichtenthaler, S. F., The substrate repertoire of gamma-secretase/presenilin. *Semin Cell Dev Biol* **2020**, *105*, 27-42.

203. Ryeom, S. W., The cautionary tale of side effects of chronic Notch1 inhibition. *J Clin Invest* **2011**, *121* (2), 508-9.
204. Montesinos, J.; Pera, M.; Larrea, D.; Guardia-Laguarta, C.; Agrawal, R. R.; Velasco, K. R.; Yun, T. D.; Stavrovskaya, I. G.; Xu, Y.; Koo, S. Y.; Snead, A. M.; Sproul, A. A.; Area-Gomez, E., The Alzheimer's disease-associated C99 fragment of APP regulates cellular cholesterol trafficking. *EMBO J* **2020**, *39* (20), e103791.
205. Pera, M.; Montesinos, J.; Larrea, D.; Agrawal, R. R.; Velasco, K. R.; Stavrovskaya, I. G.; Yun, T. D.; Area-Gomez, E., MAM and C99, key players in the pathogenesis of Alzheimer's disease. *Int Rev Neurobiol* **2020**, *154*, 235-278.
206. Kukar, T. L.; Ladd, T. B.; Bann, M. A.; Fraering, P. C.; Narlawar, R.; Maharvi, G. M.; Healy, B.; Chapman, R.; Welzel, A. T.; Price, R. W.; Moore, B.; Rangachari, V.; Cusack, B.; Eriksen, J.; Jansen-West, K.; Verbeeck, C.; Yager, D.; Eckman, C.; Ye, W.; Sagi, S.; Cottrell, B. A.; Torpey, J.; Rosenberry, T. L.; Fauq, A.; Wolfe, M. S.; Schmidt, B.; Walsh, D. M.; Koo, E. H.; Golde, T. E., Substrate-targeting gamma-secretase modulators. *Nature* **2008**, *453* (7197), 925-9.
207. Kreft, A.; Harrison, B.; Aschmies, S.; Atchison, K.; Casebier, D.; Cole, D. C.; Diamantidis, G.; Ellingboe, J.; Hauze, D.; Hu, Y.; Hury, D.; Jin, M.; Kubrak, D.; Lu, P.; Lundquist, J.; Mann, C.; Martone, R.; Moore, W.; Oganessian, A.; Porte, A.; Riddell, D. R.; Sonnenberg-Reines, J.; Stock, J. R.; Sun, S. C.; Wagner, E.; Woller, K.; Xu, Z.; Zhou, H.; Steven Jacobsen, J., Discovery of a novel series of Notch-sparing gamma-secretase inhibitors. *Bioorg Med Chem Lett* **2008**, *18* (14), 4232-6.
208. Gillman, K. W.; Starrett, J. E., Jr.; Parker, M. F.; Xie, K.; Bronson, J. J.; Marcin, L. R.; McElhone, K. E.; Bergstrom, C. P.; Mate, R. A.; Williams, R.; Meredith, J. E., Jr.; Burton, C. R.; Barten, D. M.; Toyn, J. H.; Roberts, S. B.; Lentz, K. A.; Houston, J. G.; Zaczek, R.; Albright, C. F.; Decicco, C. P.; Macor, J. E.; Olson, R. E., Discovery and Evaluation of BMS-708163, a Potent, Selective and Orally Bioavailable gamma-Secretase Inhibitor. *ACS Med Chem Lett* **2010**, *1* (3), 120-4.
209. Espeseth, A. S.; Xu, M.; Huang, Q.; Coburn, C. A.; Jones, K. L.; Ferrer, M.; Zuck, P. D.; Strulovici, B.; Price, E. A.; Wu, G.; Wolfe, A. L.; Lineberger, J. E.; Sardana, M.; Tugusheva, K.; Pietrak, B. L.; Crouthamel, M. C.; Lai, M. T.; Dodson, E. C.; Bazzo, R.; Shi, X. P.; Simon, A. J.; Li, Y.; Hazuda, D. J., Compounds that bind APP and inhibit Abeta processing in vitro suggest a novel approach to Alzheimer disease therapeutics. *J Biol Chem* **2005**, *280* (18), 17792-7.
210. Tong, G.; Wang, J. S.; Sverdlov, O.; Huang, S. P.; Slemmon, R.; Croop, R.; Castaneda, L.; Gu, H.; Wong, O.; Li, H.; Berman, R. M.; Smith, C.; Albright, C. F.; Dockens, R. C., Multicenter, randomized, double-blind, placebo-controlled, single-ascending dose study of the oral gamma-secretase inhibitor BMS-708163 (Avagacestat): tolerability profile, pharmacokinetic parameters, and pharmacodynamic markers. *Clin Ther* **2012**, *34* (3), 654-67.
211. Crump, C. J.; Castro, S. V.; Wang, F.; Pozdnyakov, N.; Ballard, T. E.; Sisodia, S. S.; Bales, K. R.; Johnson, D. S.; Li, Y. M., BMS-708,163 targets presenilin and lacks notch-sparing activity. *Biochemistry* **2012**, *51* (37), 7209-11.
212. Beel, A. J.; Barrett, P.; Schnier, P. D.; Hitchcock, S. A.; Bagal, D.; Sanders, C. R.; Jordan, J. B., Nonspecificity of binding of gamma-secretase modulators to the amyloid precursor protein. *Biochemistry* **2009**, *48* (50), 11837-9.

213. Barrett, P. J.; Sanders, C. R.; Kaufman, S. A.; Michelsen, K.; Jordan, J. B., NSAID-based gamma-secretase modulators do not bind to the amyloid-beta polypeptide. *Biochemistry* **2011**, *50* (47), 10328-42.
214. Mekala, S.; Nelson, G.; Li, Y. M., Recent developments of small molecule gamma-secretase modulators for Alzheimer's disease. *RSC Med Chem* **2020**, *11* (9), 1003-1022.
215. Bulic, B.; Ness, J.; Hahn, S.; Rennhack, A.; Jumpertz, T.; Weggen, S., Chemical Biology, Molecular Mechanism and Clinical Perspective of gamma-Secretase Modulators in Alzheimer's Disease. *Curr Neuropharmacol* **2011**, *9* (4), 598-622.
216. Crump, C. J.; Johnson, D. S.; Li, Y. M., Development and mechanism of gamma-secretase modulators for Alzheimer's disease. *Biochemistry* **2013**, *52* (19), 3197-216.
217. Barrett, P. J.; Song, Y.; Van Horn, W. D.; Hustedt, E. J.; Schafer, J. M.; Hadziselimovic, A.; Beel, A. J.; Sanders, C. R., The amyloid precursor protein has a flexible transmembrane domain and binds cholesterol. *Science* **2012**, *336* (6085), 1168-71.
218. Beel, A. J.; Sakakura, M.; Barrett, P. J.; Sanders, C. R., Direct binding of cholesterol to the amyloid precursor protein: An important interaction in lipid-Alzheimer's disease relationships? *Biochim Biophys Acta* **2010**, *1801* (8), 975-82.
219. Li, X.; Song, Y.; Sanders, C. R.; Buxbaum, J. N., Transthyretin Suppresses Amyloid-beta Secretion by Interfering with Processing of the Amyloid-beta Protein Precursor. *J Alzheimers Dis* **2016**, *52* (4), 1263-75.
220. Zhuang, T.; Jap, B. K.; Sanders, C. R., Solution NMR approaches for establishing specificity of weak heterodimerization of membrane proteins. *J Am Chem Soc* **2011**, *133* (50), 20571-80.
221. Farjon, J.; Boisbouvier, J.; Schanda, P.; Pardi, A.; Simorre, J. P.; Brutscher, B., Longitudinal-relaxation-enhanced NMR experiments for the study of nucleic acids in solution. *J Am Chem Soc* **2009**, *131* (24), 8571-7.
222. Lescop, E.; Kern, T.; Brutscher, B., Guidelines for the use of band-selective radiofrequency pulses in hetero-nuclear NMR: example of longitudinal-relaxation-enhanced BEST-type 1H-15N correlation experiments. *J Magn Reson* **2010**, *203* (1), 190-8.
223. Deatherage, C. L.; Lu, Z.; Kroncke, B. M.; Ma, S.; Smith, J. A.; Voehler, M. W.; McFeeters, R. L.; Sanders, C. R., Structural and biochemical differences between the Notch and the amyloid precursor protein transmembrane domains. *Sci Adv* **2017**, *3* (4), e1602794.
224. Stafford, R. E.; Fanni, T.; Dennis, E. A., Interfacial properties and critical micelle concentration of lysophospholipids. *Biochemistry* **1989**, *28* (12), 5113-20.
225. Song, Y.; Mittendorf, K. F.; Lu, Z.; Sanders, C. R., Impact of bilayer lipid composition on the structure and topology of the transmembrane amyloid precursor C99 protein. *J Am Chem Soc* **2014**, *136* (11), 4093-6.
226. Song, Y.; Hustedt, E. J.; Brandon, S.; Sanders, C. R., Competition between homodimerization and cholesterol binding to the C99 domain of the amyloid precursor protein. *Biochemistry* **2013**, *52* (30), 5051-64.

227. Fernandez, M. A.; Biette, K. M.; Dolios, G.; Seth, D.; Wang, R.; Wolfe, M. S., Transmembrane Substrate Determinants for gamma-Secretase Processing of APP CTFbeta. *Biochemistry* **2016**, *55* (40), 5675-5688.
228. Konijnenberg, A.; Yilmaz, D.; Ingolfsson, H. I.; Dimitrova, A.; Marrink, S. J.; Li, Z.; Venien-Bryan, C.; Sobott, F.; Kocer, A., Global structural changes of an ion channel during its gating are followed by ion mobility mass spectrometry. *Proc Natl Acad Sci U S A* **2014**, *111* (48), 17170-5.
229. Konijnenberg, A.; van Dyck, J. F.; Kailing, L. L.; Sobott, F., Extending native mass spectrometry approaches to integral membrane proteins. *Biol Chem* **2015**, *396* (9-10), 991-1002.
230. Bolla, J. R.; Agasid, M. T.; Mehmood, S.; Robinson, C. V., Membrane Protein-Lipid Interactions Probed Using Mass Spectrometry. *Annu Rev Biochem* **2019**, *88*, 85-111.
231. Patrick, J. W.; Laganowsky, A., Generation of Charge-Reduced Ions of Membrane Protein Complexes for Native Ion Mobility Mass Spectrometry Studies. *J Am Soc Mass Spectrom* **2019**, *30* (5), 886-892.
232. Liu, Y.; Cong, X.; Liu, W.; Laganowsky, A., Characterization of Membrane Protein-Lipid Interactions by Mass Spectrometry Ion Mobility Mass Spectrometry. *J Am Soc Mass Spectrom* **2017**, *28* (4), 579-586.
233. Fantin, S. M.; Parson, K. F.; Niu, S.; Liu, J.; Polasky, D. A.; Dixit, S. M.; Ferguson-Miller, S. M.; Ruotolo, B. T., Collision Induced Unfolding Classifies Ligands Bound to the Integral Membrane Translocator Protein. *Anal Chem* **2019**, *91* (24), 15469-15476.
234. Ruotolo, B. T.; Benesch, J. L.; Sandercock, A. M.; Hyung, S. J.; Robinson, C. V., Ion mobility-mass spectrometry analysis of large protein complexes. *Nat Protoc* **2008**, *3* (7), 1139-52.
235. Gupta, K.; Donlan, J. A. C.; Hopper, J. T. S.; Uzdavinyis, P.; Landreh, M.; Struwe, W. B.; Drew, D.; Baldwin, A. J.; Stansfeld, P. J.; Robinson, C. V., The role of interfacial lipids in stabilizing membrane protein oligomers. *Nature* **2017**, *541* (7637), 421-424.
236. Rabuck, J. N.; Hyung, S. J.; Ko, K. S.; Fox, C. C.; Soellner, M. B.; Ruotolo, B. T., Activation state-selective kinase inhibitor assay based on ion mobility-mass spectrometry. *Anal Chem* **2013**, *85* (15), 6995-7002.
237. Hutchison, J. M.; Shih, K. C.; Scheidt, H. A.; Fantin, S. M.; Parson, K. F.; Pantelopulos, G. A.; Harrington, H. R.; Mittendorf, K. F.; Qian, S.; Stein, R. A.; Collier, S. E.; Chambers, M. G.; Katsaras, J.; Voehler, M. W.; Ruotolo, B. T.; Huster, D.; McFeeters, R. L.; Straub, J. E.; Nieh, M. P.; Sanders, C. R., Bicelles Rich in both Sphingolipids and Cholesterol and Their Use in Studies of Membrane Proteins. *J Am Chem Soc* **2020**, *142* (29), 12715-12729.
238. Fantin, S. M.; Parson, K. F.; Yadav, P.; Juliano, B.; Li, G. C.; Sanders, C. R.; Ohi, M. D.; Ruotolo, B. T., Ion mobility-mass spectrometry reveals the role of peripheral myelin protein dimers in peripheral neuropathy. *Proc Natl Acad Sci U S A* **2021**, *118* (17).
239. Haynes, S. E.; Polasky, D. A.; Dixit, S. M.; Majmudar, J. D.; Neeson, K.; Ruotolo, B. T.; Martin, B. R., Variable-Velocity Traveling-Wave Ion Mobility Separation

Enhancing Peak Capacity for Data-Independent Acquisition Proteomics. *Anal Chem* **2017**, *89* (11), 5669-5672.

240. Schmidt-Erfurth, U.; Hasan, T., Mechanisms of action of photodynamic therapy with verteporfin for the treatment of age-related macular degeneration. *Surv Ophthalmol* **2000**, *45* (3), 195-214.

241. Yin, H.; Flynn, A. D., Drugging Membrane Protein Interactions. *Annu Rev Biomed Eng* **2016**, *18*, 51-76.

242. Stasi, R., Eltrombopag for the treatment of idiopathic thrombocytopenic purpura. *Expert Rev Hematol* **2008**, *1* (2), 145-52.

243. Stasi, R., Eltrombopag: the discovery of a second generation thrombopoietin-receptor agonist. *Expert Opin Drug Discov* **2009**, *4* (1), 85-93.

244. Erickson-Miller, C. L.; Delorme, E.; Tian, S. S.; Hopson, C. B.; Landis, A. J.; Valoret, E. I.; Sellers, T. S.; Rosen, J.; Miller, S. G.; Luengo, J. I.; Duffy, K. J.; Jenkins, J. M., Preclinical activity of eltrombopag (SB-497115), an oral, nonpeptide thrombopoietin receptor agonist. *Stem Cells* **2009**, *27* (2), 424-30.

245. Fraering, P. C.; Ye, W.; Strub, J. M.; Dolios, G.; LaVoie, M. J.; Ostaszewski, B. L.; van Dorsselaer, A.; Wang, R.; Selkoe, D. J.; Wolfe, M. S., Purification and characterization of the human gamma-secretase complex. *Biochemistry* **2004**, *43* (30), 9774-89.

246. Osenkowski, P.; Ye, W.; Wang, R.; Wolfe, M. S.; Selkoe, D. J., Direct and potent regulation of gamma-secretase by its lipid microenvironment. *J Biol Chem* **2008**, *283* (33), 22529-40.

247. Holmes, O.; Paturi, S.; Ye, W.; Wolfe, M. S.; Selkoe, D. J., Effects of membrane lipids on the activity and processivity of purified gamma-secretase. *Biochemistry* **2012**, *51* (17), 3565-75.

248. Simutis, F. J.; Sanderson, T. P.; Pilcher, G. D.; Graziano, M. J., Nonclinical Safety Assessment of the gamma-Secretase Inhibitor Avagacestat. *Toxicol Sci* **2018**, *163* (2), 525-542.

249. Konstantinou, E. K.; Notomi, S.; Kosmidou, C.; Brodowska, K.; Al-Moujahed, A.; Nicolaou, F.; Tsoka, P.; Gragoudas, E.; Miller, J. W.; Young, L. H.; Vavvas, D. G., Verteporfin-induced formation of protein cross-linked oligomers and high molecular weight complexes is mediated by light and leads to cell toxicity. *Sci Rep* **2017**, *7*, 46581.

250. Donohue, E.; Tovey, A.; Vogl, A. W.; Arns, S.; Sternberg, E.; Young, R. N.; Roberge, M., Inhibition of autophagosome formation by the benzoporphyrin derivative verteporfin. *J Biol Chem* **2011**, *286* (9), 7290-300.

251. Wang, C.; Zhu, X.; Feng, W.; Yu, Y.; Jeong, K.; Guo, W.; Lu, Y.; Mills, G. B., Verteporfin inhibits YAP function through up-regulating 14-3-3sigma sequestering YAP in the cytoplasm. *Am J Cancer Res* **2016**, *6* (1), 27-37.

252. Feng, J.; Gou, J.; Jia, J.; Yi, T.; Cui, T.; Li, Z., Verteporfin, a suppressor of YAP-TEAD complex, presents promising antitumor properties on ovarian cancer. *Oncotargets Ther* **2016**, *9*, 5371-81.

253. Baell, J. B.; Nissink, J. W. M., Seven Year Itch: Pan-Assay Interference Compounds (PAINS) in 2017-Utility and Limitations. *ACS chemical biology* **2018**, *13* (1), 36-44.

254. Dahlin, J. L.; Walters, M. A., How to Triage PAINS-Full Research. *Assay Drug Dev Technol* **2016**, *14* (3), 168-174.

255. Taylor, K. C.; Kang, P. W.; Hou, P.; Yang, N. D.; Kuenze, G.; Smith, J. A.; Shi, J.; Huang, H.; White, K. M.; Peng, D.; George, A. L.; Meiler, J.; McFeeters, R. L.; Cui, J.; Sanders, C. R., Structure and physiological function of the human KCNQ1 channel voltage sensor intermediate state. *Elife* **2020**, *9*.
256. Castro, M. A.; Parson, K. F.; Beg, I.; Wilkinson, M. C.; Nurmakova, K.; Levesque, I.; Voehler, M. W.; Wolfe, M. S.; Ruotolo, B. T.; Sanders, C. R., Verteporfin is a substrate-selective gamma-secretase inhibitor that binds the amyloid precursor protein transmembrane domain. *J Biol Chem* **2022**, *298* (4), 101792.
257. Jasial, S.; Hu, Y.; Bajorath, J., How Frequently Are Pan-Assay Interference Compounds Active? Large-Scale Analysis of Screening Data Reveals Diverse Activity Profiles, Low Global Hit Frequency, and Many Consistently Inactive Compounds. *J Med Chem* **2017**, *60* (9), 3879-3886.
258. Zhou, H.-X.; Cross, T. A., Influences of membrane mimetic environments on membrane protein structures. *Annu Rev Biophys* **2013**, *42*, 361-392.
259. Mayne, C. G.; Arcario, M. J.; Mahinthichaichan, P.; Baylon, J. L.; Vermaas, J. V.; Navidpour, L.; Wen, P.-C.; Thangapandian, S.; Tajkhorshid, E., The cellular membrane as a mediator for small molecule interaction with membrane proteins. *Biochimica et Biophysica Acta (BBA) - Biomembranes* **2016**, *1858* (10), 2290-2304.
260. Baell, J. B.; Holloway, G. A., New substructure filters for removal of pan assay interference compounds (PAINS) from screening libraries and for their exclusion in bioassays. *J Med Chem* **2010**, *53* (7), 2719-40.
261. Husain, M. A.; Laurent, B.; Plourde, M., APOE and Alzheimer's Disease: From Lipid Transport to Physiopathology and Therapeutics. *Frontiers in Neuroscience* **2021**, *15*.
262. Yamazaki, Y.; Zhao, N.; Caulfield, T. R.; Liu, C.-C.; Bu, G., Apolipoprotein E and Alzheimer disease: pathobiology and targeting strategies. *Nature Reviews Neurology* **2019**, *15* (9), 501-518.
263. Wang, C.; Xiong, M.; Gratuze, M.; Bao, X.; Shi, Y.; Andhey, P. S.; Manis, M.; Schroeder, C.; Yin, Z.; Madore, C.; Butovsky, O.; Artyomov, M.; Ulrich, J. D.; Holtzman, D. M., Selective removal of astrocytic APOE4 strongly protects against tau-mediated neurodegeneration and decreases synaptic phagocytosis by microglia. *Neuron* **2021**, *109* (10), 1657-1674.e7.
264. Deatherage, C. L.; Lu, Z.; Kim, J. H.; Sanders, C. R., Notch Transmembrane Domain: Secondary Structure and Topology. *Biochemistry* **2015**, *54* (23), 3565-8.
265. Williamson, M. P., Using chemical shift perturbation to characterise ligand binding. *Prog Nucl Magn Reson Spectrosc* **2013**, *73*, 1-16.
266. Li, Y. M.; Lai, M. T.; Xu, M.; Huang, Q.; DiMuzio-Mower, J.; Sardana, M. K.; Shi, X. P.; Yin, K. C.; Shafer, J. A.; Gardell, S. J., Presenilin 1 is linked with gamma-secretase activity in the detergent solubilized state. *Proc Natl Acad Sci U S A* **2000**, *97* (11), 6138-43.
267. Bolduc, D. M.; Selkoe, D. J.; Wolfe, M. S., Enzymatic Assays for Studying Intramembrane Proteolysis. *Methods Enzymol* **2017**, *584*, 295-308.
268. Lu, P.; Bai, X. C.; Ma, D.; Xie, T.; Yan, C.; Sun, L.; Yang, G.; Zhao, Y.; Zhou, R.; Scheres, S. H. W.; Shi, Y., Three-dimensional structure of human gamma-secretase. *Nature* **2014**, *512* (7513), 166-170.

269. Bolduc, D. M.; Montagna, D. R.; Seghers, M. C.; Wolfe, M. S.; Selkoe, D. J., The amyloid-beta forming tripeptide cleavage mechanism of gamma-secretase. *Elife* **2016**, *5*.
270. Bolduc, D. M.; Montagna, D. R.; Gu, Y.; Selkoe, D. J.; Wolfe, M. S., Nicastrin functions to sterically hinder gamma-secretase-substrate interactions driven by substrate transmembrane domain. *Proc Natl Acad Sci U S A* **2016**, *113* (5), E509-18.
271. Devkota, S.; Williams, T. D.; Wolfe, M. S., Familial Alzheimer's disease mutations in amyloid protein precursor alter proteolysis by gamma-secretase to increase amyloid beta-peptides of >45 residues. *J Biol Chem* **2021**, 100281.
272. Alford, R. F.; Koehler Leman, J.; Weitzner, B. D.; Duran, A. M.; Tilley, D. C.; Elazar, A.; Gray, J. J., An Integrated Framework Advancing Membrane Protein Modeling and Design. *PLoS Comput Biol* **2015**, *11* (9), e1004398.
273. Alford, R. F.; Fleming, P. J.; Fleming, K. G.; Gray, J. J., Protein Structure Prediction and Design in a Biologically Realistic Implicit Membrane. *Biophys J* **2020**, *118* (8), 2042-2055.
274. Koehler Leman, J.; Mueller, B. K.; Gray, J. J., Expanding the toolkit for membrane protein modeling in Rosetta. *Bioinformatics* **2017**, *33* (5), 754-756.
275. Kothiwale, S.; Mendenhall, J. L.; Meiler, J., BCL::Conf: small molecule conformational sampling using a knowledge based rotamer library. *J Cheminform* **2015**, *7*, 47.
276. Davis, I. W.; Baker, D., RosettaLigand docking with full ligand and receptor flexibility. *J Mol Biol* **2009**, *385* (2), 381-92.
277. Lemmon, G.; Meiler, J., Rosetta Ligand docking with flexible XML protocols. *Methods Mol Biol* **2012**, *819*, 143-55.
278. Combs, S. A.; Deluca, S. L.; Deluca, S. H.; Lemmon, G. H.; Nannemann, D. P.; Nguyen, E. D.; Willis, J. R.; Sheehan, J. H.; Meiler, J., Small-molecule ligand docking into comparative models with Rosetta. *Nat Protoc* **2013**, *8* (7), 1277-98.